SIMULATION AND DESIGN OF NSM STRENGTHENED BEAMS USING MOMENT-ROTATION APPROACH

AHMAD AZIM BIN SHUKRI

FACULTY OF ENGINEERING
UNIVERSITY OF MALAYA
KUALA LUMPUR

2019

SIMULATION AND DESIGN OF NSM STRENGTHENED BEAMS USING MOMENT-ROTATION APPROACH

AHMAD AZIM BIN SHUKRI

THESIS SUBMITTED IN FULFILMENT OF THE REQUIREMENTS FOR THE DEGREE OF DOCTOR OF PHILOSOPHY

FACULTY OF ENGINEERING
UNIVERSITY OF MALAYA
KUALA LUMPUR

2019

UNIVERSITY OF MALAYA

ORIGINAL LITERARY WORK DECLARATION

Name of Candidate: Ahmad Azim Bin Shukri

Matric No: KHA150078

Name of Degree: Doctor of Philosophy

Title of Project Paper/Research Report/Dissertation/Thesis ("this Work"):

Simulation and Design of NSM Strengthened Beams Using Moment-Rotation Approach

Field of Study: Structural Engineering & Materials (Civil Engineering)

I do solemnly and sincerely declare that:

(1) I am the sole author/writer of this Work;
(2) This Work is original;
(3) Any use of any work in which copyright exists was done by way of fair dealing and for permitted purposes and any excerpt or extract from, or reference to or reproduction of any copyright work has been disclosed expressly and sufficiently and the title of the Work and its authorship have been acknowledged in this Work;
(4) I do not have any actual knowledge nor do I ought reasonably to know that the making of this work constitutes an infringement of any copyright work;
(5) I hereby assign all and every rights in the copyright to this Work to the University of Malaya ("UM"), who henceforth shall be owner of the copyright in this Work and that any reproduction or use in any form or by any means whatsoever is prohibited without the written consent of UM having been first had and obtained;
(6) I am fully aware that if in the course of making this Work I have infringed any copyright whether intentionally or otherwise, I may be subject to legal action or any other action as may be determined by UM.

Candidate's Signature Date:

Subscribed and solemnly declared before,

Witness's Signature Date:

Name:

Designation:

SIMULATION AND DESIGN OF NSM STRENGTHENED BEAMS USING MOMENT-ROTATION APPROACH

ABSTRACT

The near surface mounted (NSM) method is a technique for strengthening reinforced concrete (RC) beams which normally utilizes fibre reinforced polymer (FRP) bars or strips placed within grooves made on the soffit of the beams. One particular problem that has consistently been reported on the NSM method is the premature failure by concrete cover separation (CCS), which causes the beam to fail prior to the full potential of the strengthening reinforcement being utilized. Several methods have been proposed to determine the onset of CCS failure for NSM strengthened beams. The application of these methods however was found to be limited by the empirical formulations that were used, which severely affects their accuracy when applied to situations outside of the testing regime that formed the empirical formulations. In light of these problems, this research aims to present a method for the simulation and design of NSM strengthened beams that is less reliant on empirical formulations.

To that end, the moment-rotation (M/θ) approach was extended to allow for the simulation of NSM strengthened beams. The M/θ approach applies the partial interaction theory which helps reduce the reliance on empirical formulations. The global energy balance approach (GEBA) was used in conjunction with the M/θ approach to simulate CCS failure. The M/θ approach was then applied to simulate and study the side-NSM (SNSM) method, which is an NSM-based strengthening method. The differences involved in simulating virgin and precracked SNSM strengthened beams was presented, where the former represents what is usually tested is laboratories and the latter is meant to simulate real world condition. The M/θ approach was also applied to simulate the beams strengthened with hybrid method, which is another NSM-based method; furthermore, it was shown how the M/θ approach can simulate intermediate crack (IC) debonding through the use of single crack analysis. Lastly, a design procedure for the NSM method was proposed using closed form solutions derived from the M/θ approach.

The result of the research is as follows. The M/θ approach for NSM strengthened beams was validated against published experimental results of RC beams strengthened with either of several types of NSM reinforcement, namely CFRP bars, CFRP strips, steel bars and GFRP bars. The validation process shows good correlation for the experimental and actual failure load. The M/θ approach was also validated against experimental results of SNSM strengthened beams and hybrid strengthened beams, where good accuracy was also found. The final part of this research, the design procedure, was validated against published experimental results and achieves good accuracy. The results show that the M/θ approach for NSM strengthened beams is able to simulate not only normal NSM method, but also other NSM-based methods; this versatility is a direct result of the reduced reliance on empirical formulations. Furthermore, the proposed design procedure gives the benefits of the M/θ approach while also being simple enough for design engineers to use.

Keywords: Near-surface mounted; numerical analysis; partial interaction; reinforced concrete; moment-rotation

SIMULASI DAN REKA BENTUK RASUK YANG DIPERKUKUH DENGAN NSM MENGGUNAKAN PENDEKATAN MOMENT-ROTATION

ABSTRAK

Teknik pemasangan dekat (NSM) untuk menguatkan rasuk konkrit bertetulang (RC) biasanya menggunakan polimer bertetulang gentian (FRP) bentuk bar atau jalur yang diletakkan di dalam alur yang dibuat pada permukaan rasuk. Satu masalah tertentu yang telah dilaporkan secara konsisten bagi kaedah NSM adalah kegagalan awal melalui pemisahan penutup konkrit (CCS), yang menyebabkan rasuk gagal sebelum potensi penuh penguatan tetulang digunakan. Beberapa kaedah telah dicadangkan untuk menentukan permulaan kegagalan CCS untuk rasuk yang diperkukuhkan NSM. Penerapan kaedah-kaedah ini bagaimanapun didapati dihadkan oleh formulasi empirikal yang digunakan, yang sangat mempengaruhi ketepatan mereka ketika diterapkan pada situasi di luar rejim pengujian yang membentuk formulasi empirikal. Berdasarkan kepada masalah ini, penyelidikan ini bertujuan membentangkan kaedah untuk simulasi dan reka bentuk rasuk NSM yang diperkuat yang kurang bergantung kepada rumusan empirikal.

Untuk itu, pendekatan putaran momen (M/θ) telah diperluaskan untuk membolehkan simulasi NSM mengukuhkan rasuk. Pendekatan M/θ menggunakan teori interaksi separa yang membantu mengurangkan pergantungan pada formulasi empirikal. Pendekatan keseimbangan tenaga global (GEBA) digunakan dengan pendekatan M/θ untuk mensimulasikan kegagalan CCS. Pendekatan M/θ kemudiannya digunakan untuk mensimulasikan dan mengkaji kaedah sisi-NSM (SNSM), yang merupakan kaedah pengukuhan berasaskan NSM. Perbezaan yang terlibat dalam mensimulasikan rasuk diperkukuh SNSM yang dara dan yang diperbaiki telah dibentangkan, di mana yang sebelum mewakili apa yang biasanya diuji adalah makmal dan yang selepas adalah untuk mensimulasikan keadaan dunia sebenar. Pendekatan M/θ juga digunakan untuk

mensimulasikan rasuk yang diperkuat dengan kaedah hibrid, yang merupakan satu lagi kaedah berasaskan NSM; tambahan pula, ditunjukkan bagaimana pendekatan M/θ dapat mensimulasikan retakan perantaraan (IC) yang disingkirkan melalui penggunaan analisis retak tunggal. Akhir sekali, prosedur reka bentuk untuk kaedah NSM dicadangkan menggunakan penyelesaian bentuk tertutup yang diperoleh daripada pendekatan M/θ.

Hasil penyelidikan adalah seperti berikut. Pendekatan M/θ untuk rasuk yang diperkuat NSM telah disahkan terhadap keputusan ujian eksperimen rasuk RC yang diperkuat dengan mana-mana beberapa jenis tetulang NSM, iaitu bar CFRP, jalur CFRP, bar keluli dan bar GFRP. Proses pengesahan menunjukkan korelasi yang baik untuk beban kegagalan eksperimen dan sebenar. Pendekatan M/θ juga disahkan terhadap keputusan eksperimen bagi rasuk SNSM yang diperkuatkan dan rasuk diperkuat hibrid, di mana ketepatan yang baik telah diperolehi. Bahagian akhir penyelidikan ini, prosedur reka bentuk, telah disahkan terhadap keputusan eksperimen yang diterbitkan dan mencapai ketepatan yang baik. Keputusan menunjukkan bahawa pendekatan M/θ untuk rasuk NSM yang diperkuatkan dapat mensimulasikan bukan sahaja kaedah NSM biasa, tetapi juga kaedah berasaskan NSM yang lain; kebolehan ini adalah hasil langsung dari pergantungan yang dikurangkan pada formulasi empirikal. Selain itu, prosedur reka bentuk yang dicadangkan menggunakan pendekatan M/θ memberikan manfaat sementara juga cukup mudah untuk digunakan oleh jurutera reka bentuk.

Kata kunci: Teknik pemasangan dekat; analisis berangka; interaksi separa; konkrit bertetulang; putaran momen.

ACKNOWLEDGEMENT

I would like to thank my parents, who were supportive throughout my study. I would never be able to repay them, and without them I would undoubtedly not be able to be where I am.

My thanks as well to Prof. Mohd. Zamin Bin Jumaat and Dr. Zainah Binti Ibrahim, who supervised me during my PhD. I would also like to thank Dr. Phillip Visintin of the University of Adelaide, who gave his help on certain matters of the M/θ approach.

Finally, I would like to thank all my fellow postgraduate students in the Department of Civil Engineering for your companionship and help throughout my study. May we all succeed in our respective goals after graduating.

Special thanks to the Department of Civil Engineering and the Faculty of Engineering and to University of Malaya.

TABLE OF CONTENTS

LIST OF FIGURES

LIST OF TABLES

CHAPTER 1 - INTRODUCTION

1.1 Background

The term structural strengthening refers to the application of a strengthening material onto an existing structural member in order to increase their load carrying capacities. Among the reasons that necessitates structural strengthening are mistakes done during construction, increases in load requirement due to an increase in population and loss of strength due to aging of structures. For strengthening RC beams in flexure, in general there are two types of strengthening that can be applied:

1. The externally bonded (EB) method (Barros et al., 2017; Ceroni, Pecce, Matthys, & Taerwe, 2008; Chen, Zhang, Li, Li, & Zhou, 2016; Maalej, 2005; Pesic, 2005; Tam, Si, & Limam, 2016; Toutanji, Zhao, & Zhang, 2006)
2. The near-surface mounted (NSM) method (Badawi & Soudki, 2009; Capozucca, Domizi, & Magagnini, 2016; Capozucca & Magagnini, 2016; Kreit, Al-Mahmoud, Castel, & François, 2011; Pachalla & Prakash, 2017; Seo, Sung, & Feo, 2016).

The EB method was proposed much earlier than the NSM method and in the beginning was done using steel plates attached on the soffit of RC beams. Nowadays however the EB method uses either fibre reinforced polymer (FRP) plates or sheets due to its low weight and high strength. The NSM method is a relatively new method; this type of strengthening involves the making of grooves on the soffit of RC beams, where either FRP bars or strips will be placed into and the grooves are then filled with epoxy adhesive.

The use of grooves allows a much higher bond between NSM reinforcements and the concrete surface of beams compared to the EB method. Despite this, premature failure of

NSM strengthened beams is still possible. Various experimental studies on the NSM method have reported NSM strengthened beams failing through the concrete cover separation (Hosen, Jumaat, Islam, et al., 2015; Reda, Sharaky, Ghanem, Seleem, & Sallam, 2016; Rezazadeh, Barros, & Ramezansefat, 2016; Zhang & Teng, 2014) which causes the NSM strengthened beam to fail well below the design strength. The concrete cover separation failure involves a crack forming near the location of curtailment for the NSM reinforcement, which then propagates horizontally towards higher moment region of the beam, causing the NSM reinforcement to separate from the beam along with the concrete cover. More recently, it was noted by Zhang, Yu, and Chen (2017) that NSM strengthened beams has also been reported to fail by intermediate crack (IC) debonding, albeit very rarely. The IC debonding starts from the maximum moment region of beams and propagates towards the beam ends. The lack of reported IC debonding of NSM strengthened beams was attributed by Zhang et al. (2017) as the result of high bond strength of NSM reinforcements.

Several methods have been introduced to reduce the probability of concrete cover separation, one of them being the side-NSM strengthening method. Among the problem with applying the NSM method is that it requires the RC beam to be considerably wide; a closely spaced arrangement of NSM bars will cause an overlap of stresses, which causes the tensile stress at the concrete-epoxy interface to be magnified and cause concrete split failure (Hassan & Rizkalla, 2004). The ACI 440 guideline, based on the research work of (Hassan & Rizkalla, 2003) states that the minimum clear groove spacing for NSM bars should be greater than twice the depth of the groove to avoid the overlapping of stresses, while the edge distance should be four times the depth of the groove to minimize edge effects. To make the NSM method applicable to beams with small width, side-NSM method was proposed, where the location of the NSM reinforcement was changed from the soffit of the RC beam to the side of the beam at the same level as the tension reinforcement. The side-NSM method also allows strengthening to be applied on beams with walls beneath them (Sharaky, Reda, Ghanem, Seleem, & Sallam, 2017). Another method proposed to reduce concrete cover separation is the hybrid strengthening method (Rahman, Jumaat, Rahman, & Qeshta, 2015). The main purpose of the hybrid method is to reduce the amount of strengthening reinforcement needed by EB and NSM method individually, thus reducing the thickness of the FRP sheet needed as well as reducing the number of NSM grooves needed. The theory is that the reduction of strengthening reinforcement reduces the interfacial stresses, thus reducing the possibility of debonding failures for both EB and NSM strengthening used in the hybrid method.

While both side-NSM method and hybrid strengthening method are able to reduce concrete cover separation to a certain degree, it cannot be fully eliminated. This means concrete cover separation still needs to be taken into consideration, which brings another problem to fore: currently there is a lack of research done on predicting concrete cover separation in NSM strengthened beams. Several methods to predict or simulate CCS have been proposed using the finite element method (Al-Mahmoud, Castel, François, & Tourneur, 2010; Zhang & Teng, 2014) or using the concrete tooth model (De Lorenzis & Nanni, 2003). Recently, Teng, Zhang, and Chen (2016a) proposed a strength model for NSM CFRP strips derived using finite element study while an analytical design approach was proposed by Rezazadeh et al. (2016), which was derived using concrete fracture mechanic. Most of these methods can be highly empirical, such as in terms of predicting crack spacing. Empirical methods that are formulated around a specific shape or material type of NSM reinforcement are only accurate within the regime of testing used to formulate them, which can limit their usage.

In recent years a global energy balance approach (GEBA) has been developed (Achintha & Burgoyne, 2013, 2011; Achintha, 2009; Guan & Burgoyne, 2014) to predict the concrete cover separation failure of RC beams strengthened with externally bonded FRP plates. The GEBA works by applying fracture mechanics of concrete; the energy available in a strengthened beam is determined from the moment-curvature (M/χ) relationship and compared to the energy required for the debonding crack to propagate. Currently the method for using the GEBA was derived for FRP plated RC beams, and there has not been any published research on using the GEBA with NSM strengthened beams.

In light of this, it is proposed that the moment-rotation (M/θ) technique (Haskett, Oehlers, Visintin, & S, 2011; Oehlers, Visintin, Zhang, Chen, & Knight, 2012; Oehlers, Visintin, Haskett, & Sebastian, 2013; Visintin & Oehlers, 2016; Visintin, Oehlers, Muhamad, & Wu, 2013) be applied to derive the required M/χ relationships. The M/θ technique applies the partial interaction theory (Haskett, Oehlers, & Mohamed Ali, 2008; Muhamad, Mohamed Ali, Oehlers, & Griffith, 2012; Visintin et al., 2013) in order to simulate flexural cracking and tension stiffening by directly simulating the slip of reinforcements in the RC beam. This allows the slip of the NSM reinforcement to be directly simulated, which can help reduce the reliance on empirical formulations in simulating many of the mechanics of NSM strengthened RC beams as seen in practice. Minor changes to the GEBA would then be made to apply it on NSM strengthened beams, allowing the concrete cover separation failure mode to be simulated. Additionally, the debonding crack was allowed to propagate up to the point where the beam can no longer accept additional load nor maintain the current load; this is made so that a more accurate failure load can be obtained.

Due to its reduced reliance on empirical formulations, the method proposed in this thesis should be readily applicable to any shape and material of NSM reinforcements, assuming that the material properties of the NSM reinforcements such as stress-strain relationship and bond stress-slip relationship is known. Other methods on the other hand may require extensive structural testing to formulate empirical formulations to account for any changes to the shape and material of NSM reinforcements. As such the combination of M/θ technique and GEBA provides a more versatile method for simulating NSM strengthened RC beams; furthermore, it can help reduce the cost of developing new types of NSM shapes and materials as there would be no need for extensive structural testing purely to derive empirical formulations.

1.2 Problem statement

The NSM method is prone to failing prematurely, with the most common mode of failure being concrete cover separation. Currently there are few research that has been done on the premature debonding failure modes of NSM strengthened beams. Furthermore, the few methods that has been proposed for predicting concrete cover separation thus far are highly empirical, which limits their usage to specific NSM configurations from which they are derived.

1.3 Objective

The objectives of this research include:

- To extend the moment-rotation (M/θ) approach for simulating the behaviour of NSM strengthened RC beams and the propagation of concrete cover separation.
- To apply the extended M/θ approach in studying side-NSM strengthening method.
- To apply the extended M/θ approach in studying hybrid strengthening method.
- To propose a design procedure for NSM strengthened beam using closed form solutions derived using the extended M/θ approach.

1.4 Scope of study

This research presents an extended M/θ approach for simulating NSM strengthened beams and the propagation of concrete cover separation that theoretically should be applicable to any type and shape of NSM reinforcement material, provided that the correct material models are used. The extended M/θ approach is validated against published experimental results of the following types of RC beams:

- RC beams strengthened with NSM carbon FRP (CFRP) bars.
- RC beams strengthened with NSM CFRP strips.
- RC beams strengthened with NSM glass FRP (GFRP) bars.
- RC beams strengthened with NSM steel bars.

After the validation, examples on how the extended M/θ approach can be applied to perform further studies on new NSM-based methods are presented. To recap, the term NSM-based methods will be used in this thesis to collectively refer to strengthening methods where the strengthening reinforcements are placed in grooves that are made on the concrete cover of RC beams. Two NSM-based methods are studied in this thesis, which are the side-NSM (SNSM) method and the hybrid strengthening method (also called the combined externally bonded and NSM (CEBNSM) method). These two NSM-based methods were developed in University of Malaya under the High Impact Research Grant, "Strengthening Structural Elements for Load and Fatigue". Initially it was planned that further studies on these two methods would be performed, yet due to unexpected problems these plans were shelved. Hence, they represent the perfect usage scenario for the extended M/θ approach, which is intended to reduce the need for extensive structural testing in the research and development of NSM-based methods.

While the extended M/θ approach is applicable to most NSM-based methods, the focus of this research is on the presence of strong bond between NSM reinforcements and concrete. Hence, the extended M/θ approach is not applicable to strengthening methods where bond between the strengthening reinforcement and adjacent concrete is negligible or non-existent, such as the unbonded prestressed NSM method and mechanically fastened FRP.

1.5 Thesis structure

This thesis will be presented through a series of published research papers. The thesis structure is as follows:

- Chapter 2 consists of the literature review of the topics on NSM method and the M/θ approach.
- Chapter 3 is composed of one research paper, which presents the method to simulate the behaviour and concrete cover separation failure of NSM strengthened beams.
- Chapter 4 is composed of two research papers. In this chapter, it will be shown how the simulation method presented in chapter 3 can be applied to reliably simulate the behaviour of RC beams strengthened with the SNSM method used to perform further studies on the SNSM method.
- Chapter 5 is composed of two research papers. In this chapter, it will be shown how the simulation method in chapter 3 can be applied to CEBNSM strengthened RC beams. The method to simulate intermediate crack debonding, which is a type of debonding rarely found in NSM strengthened beams, was discussed and further studies were conducted by means of parametric study.
- Chapter 6 presents a design procedure for NSM strengthened beams, which was made using closed form solutions derived using the M/θ approach.
- Chapter 7 present the conclusions of this research and suggestions for future work.

1.6 Research significance

This research extends the M/θ approach to allow for analysis and simulation of NSM strengthening methods. Unlike the moment-curvature approach, the M/θ approach does not use the linear strain profile, although it is still subject to the Euler-Bernoulli theorem of plane sections remaining plane. The M/θ approach applies the partial interaction theory to simulate the slip of reinforcements, which in turn allows the mechanics of tensile cracking, crack widening and tension stiffening to be simulated. Hence, the extended M/θ approach gives a simulation method for NSM strengthened beams that is less reliant on empiricisms, as it does not need empirical means to simulate the mechanics of RC beams.

The extended M/θ approach is a valuable research tool as it allows fast and accurate simulation of NSM strengthened RC beams. Furthermore, the design procedure (which is based on the extended M/θ approach) proposed in this thesis can be used by design engineers to design NSM strengthened beams that is safe from concrete cover separation failures.

CHAPTER 2 - LITERATURE REVIEW

2.1 Strengthening materials

2.1.1 Steel

Among the earliest form of structural strengthening was the use of steel plates attached at the soffit of RC beams with the purpose of improving the flexural capacity of those beams. The use of steel plates however has too many problems. The process of transporting and applying steel in strengthening of structures is made difficult by the high weight of steel. The low strength-weight ratio of steel also causes the overall load of the structure to increase significantly, especially when used to strengthen a long and wide structural member such as bridge girders. Furthermore, the steel plates are vulnerable to corrosion.

These problems inevitably cause the use of steel plates in strengthening of structures to be in decline. However, there are still some research done on the use of steel in strengthening RC beams such as the one performed by Rahman et al. (2015) steel plates and steel bars are used due to the high ductility that steel possesses. Further details on this research will be discussed in later sections of this literature review.

Steel possesses a bilinear tensile stress-strain relationship as shown in Figure 2.1, where f_y, f_h, E_y, E_h, ε_y and ε_u refers to the yield stress, ultimate stress, elastic modulus, strain hardening modulus, yield strain and ultimate strain respectively. The first linear curve is called the elastic region, where steel can return to its original form when released from tensile load. Beyond the elastic region is the second linear curve called the strain hardening region. The deformations experienced by steel in this region is plastic. The strain hardening modulus (E_h) is generally smaller than the elastic modulus (E_y) by several magnitudes. Steel is an important construction material due to its high ducility; the ultimate strain (ε_u) for steel is generally in the region of 0.2 strain.

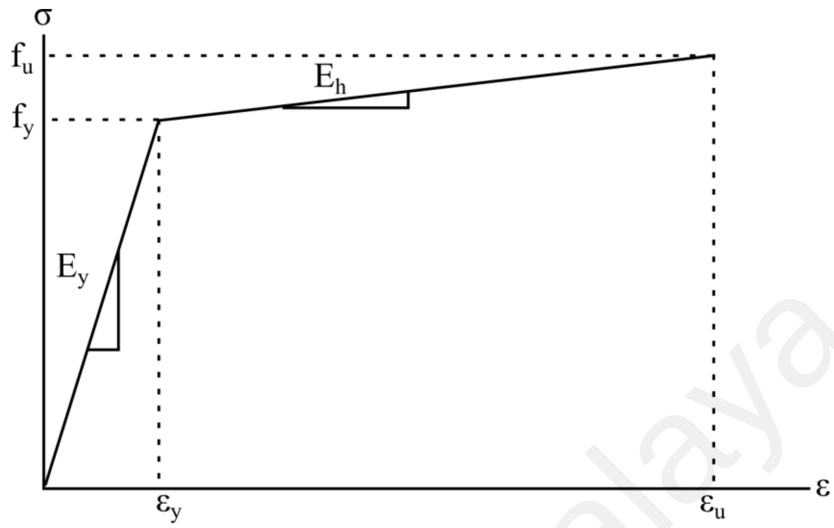

Figure 2.1: Tensile stress-strain relationship of steel.

2.1.2 Fibre reinforced polymers

Due to the problems associated with using steel as a strengthening material, it was clear that another type of strengthening material was needed. The most popular alternative to steel is currently the fibre reinforced polymers (FRP), which are advanced composite polymers that possesses high strength-weight ratio and is non-corrosive. While FRP has been around since 1960s, they are not used in the construction industry until early 2000.

Several advantages of using FRP as strengthening reinforcement are as follows (Zaman, Gutub, & Wafa, 2013):

- FRP has significantly higher ultimate strength at lower density compared to steel.
- FRP has low weight, which make the installation of FRP strengthening much easier compared to steel; they can be moved without the need for heavy lifting

equipment and once the FRP is applied, it can be left without any external support to keep it in place while the epoxy adhesive is drying.

- FRP can be made with a very long length. FRP in sheet from can be manufactured in rolls of 100m length (in Malaysia) whereas steel plates tend to be only 6m long.
- The cost in terms of energy required to produce FRP is a lot lower than steel, making it substantially more environmentally friendly.

There are various types of FRP, with the most popular type for strengthening of RC structures being the carbon FRP (CFRP). CFRP possesses a very high tensile strength and an elastic modulus that is usually almost similar to steel; this makes it highly suitable for strengthening RC structures. Another type of FRP that is regularly used is the glass FRP (GFRP), which possesses a lower tensile strength and elastic modulus compared to CFRP but is significantly more ductile than CFRP. Other types of FRP, such as aramid FRP (AFRP) and basalt FRP (BFRP) have been studied in several researches but as far as the author knows they do not been practically applied for strengthening of RC structures. All types of FRP are brittle, with a linear tensile stress-strain relationship as shown in Figure 2.2 where f_u is the ultimate stress, ε_u is the ultimate strain and E_y is the elastic modulus.

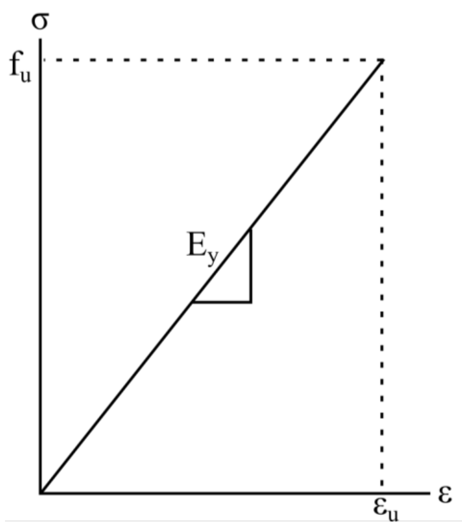

Figure 2.2: Tensile stress-strain relationship of FRP.

FRP is usually applied as strengthening material as a composite; epoxy resin is usually used to create a FRP composite due to its ability to bond well with FRP.

2.2 Strengthening of RC beams

The methods used for strengthening of RC beams in flexure can be divided into two general types:

1. Externally bonded (EB) strengthening.
2. Near-surface mounted (NSM) strengthening.

The EB strengthening method was introduced earlier than the NSM method. As such the amount of research that has been conducted for the EB method is significantly higher compared to the NSM method. The EB method involves placing either FRP sheets or plates on the soffit of the beam using epoxy adhesive, as shown in Figure 2.3(b). This leads to a better understanding of the behaviour of EB strengthened RC beams, allowing guidelines to be made on the design of EB strengthening which leads to a higher amount of real world application. While the EB method is more popular, it is highly susceptible to premature failures. Further discussion on premature failures is available in section 2.3.3 of this literature review.

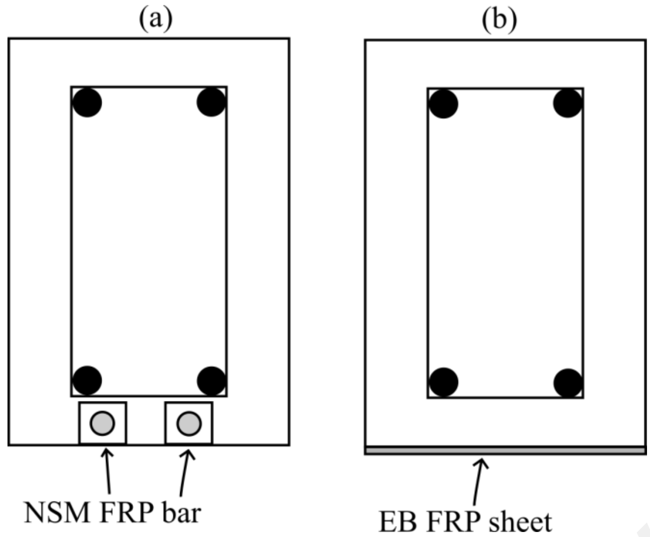

Figure 2.3: Application of NSM and EB strengthening methods on RC beams.

The NSM method on the other hand is a relatively new method for strengthening RC structures. The method involves preparation of grooves on the RC beam and placing the NSM reinforcement within these grooves, as shown in Figure 2.3. Due to the grooves, NSM strengthening is less susceptible to premature failures that is commonly seen in EB strengthened RC beams, although it should be noted that it cannot eliminate premature failures completely.

2.2.1 NSM method

FRP can be manufactured in many different forms. The most common forms used for NSM strengthening are bar and strip forms, as shown in Figure 2.4. NSM FRP bars are more readily available in the market and were noted to be more easily anchored for prestressing (De Lorenzis & Teng, 2007). NSM FRP strips on the other hand maximizes the surface to cross-sectional area, thus this reduces the potential of premature failure (De Lorenzis & Teng, 2007). Several types of surface condition for NSM FRP bars exist, such as spirally wound with fibre tow and ribbed (De Lorenzis, Lundgren, & Rizzo, 2004).

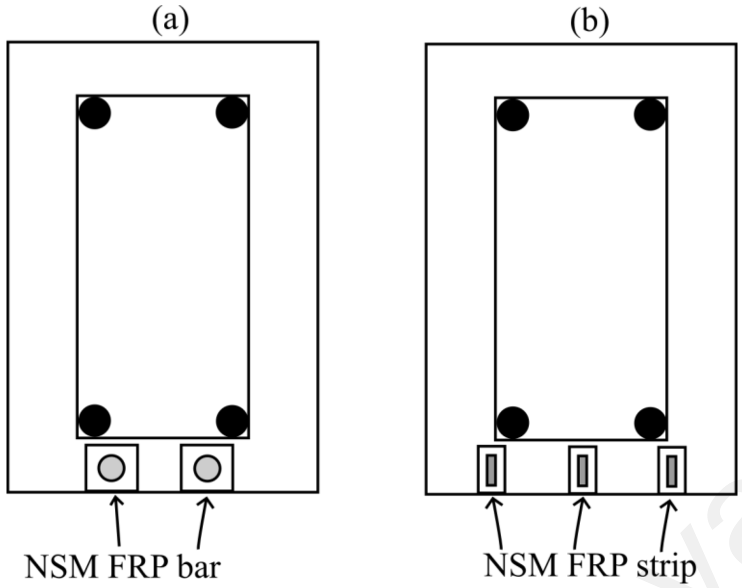

Figure 2.4: NSM FRP bar and strip.

There are many ways to apply NSM strengthening on beams, although a general procedure for NSM strengthening is given below:

1. Grooves of are made at the soffit of the RC beams using any suitable instrument, such as a diamond bladed concrete saw.
2. Hammers and hand chisels can then used to remove the remaining concrete lugs and make the groove surface rougher for better bonding between epoxy and concrete.
3. The grooves are cleaned with a special wire brush and a high-pressure air jet.
4. The grooves are filled with epoxy up to half the groove height, and an FRP bar is placed in the groove.
5. The FRP bar is then pressed lightly to ensure the epoxy was in full contact with the surface of the bar.
6. More epoxy is applied to completely fill the groove and the surface of the epoxy is levelled.

7. A one-week period is usually required to allow the strength of the epoxy to fully develop.

2.2.1.1 Bond behaviour of NSM reinforcement

In flexural strengthening using FRP, the bond behaviour between the FRP and epoxy adhesive is important as the load applied on the FRP is transferred to the epoxy and surrounding concrete through bond stress. Hence many early research on NSM FRP were focused on studying the bond behaviour at the FRP-epoxy interface. De Lorenzis and Nanni (2002) conducted 22 pull-out tests on CFRP and GFRP bars encased in epoxy and concrete. The tested parameters are type of FRP material, bonded length, size of the groove, diameter of the rod and surface condition of the FRP bars. Three types of failure were experienced by the samples, which are cracking of concrete around the groove, splitting of the epoxy adhesive and lastly pull-out failure of the FRP reinforcement.

An important conclusion from the tests is that the surface condition of the FRP bars greatly affects the bond strength. Deformed FRP bars tend to have a better bond performance while sandblasted FRP bars tend to have a very bad bond performance. The depth of the groove was found to affect the failure mode, as when the groove is shallow the failure tends to be due to splitting of epoxy adhesive whereas when the groove is deep enough the failure would occur on the concrete surrounding the groove instead, as shown in Figure 2.5.

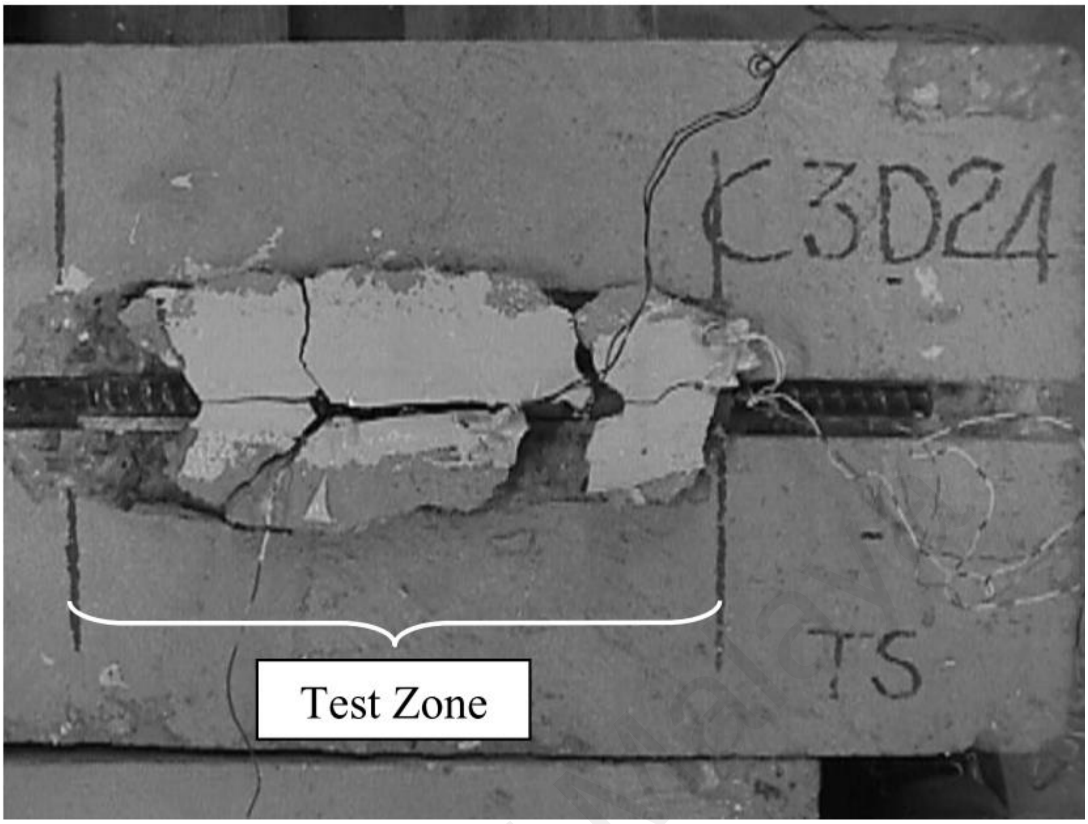

Figure 2.5: Concrete splitting failure of NSM pull-out tests (De Lorenzis and Nanni, 2002).

Hassan and Rizkalla (2004) conducted experimental and analytical work on the bond performance of NSM FRP bars although rather than using pull-out tests, the authors used eight T-beams strengthened with NSM FRP. The parameters tested are types of adhesive and embedment lengths. Using 2D finite element analysis, two equations for bond strength was proposed by the authors with the depth of the groove and the size of the reinforcement being the primary parameters and validated against the test results from the beams. These bond strengths correspond to cracking in either failure in the epoxy-concrete or in the bar-epoxy interfaces. The bond strength equations are as follows:

$$\tau_{e-c} = \frac{f_t \mu}{G_1} \tag{2.2.1}$$

$$\tau_{b-e} = \frac{f_a \mu}{G_2} \tag{2.2.2}$$

Where $\tau_{e\text{-}c}$ is the bond strength for failure in the epoxy-concrete interfaces, $\tau_{b\text{-}e}$ is the bond strength for failure in the bar-concrete interfaces, f_t is the concrete tensile strength, f_a is the epoxy tensile strength, μ is the coefficient of stiffness, G_1 and G_2 are coefficients derived from finite element analysis which can be determined using the design chart as shown in Figure 2.6. The bond model is easy to use, although De Lorenzis and Teng (2007) has raised some questions regarding its accuracy and concluded that the predicted bond strength is much lower than the actual bond strength achieved in pull-out tests.

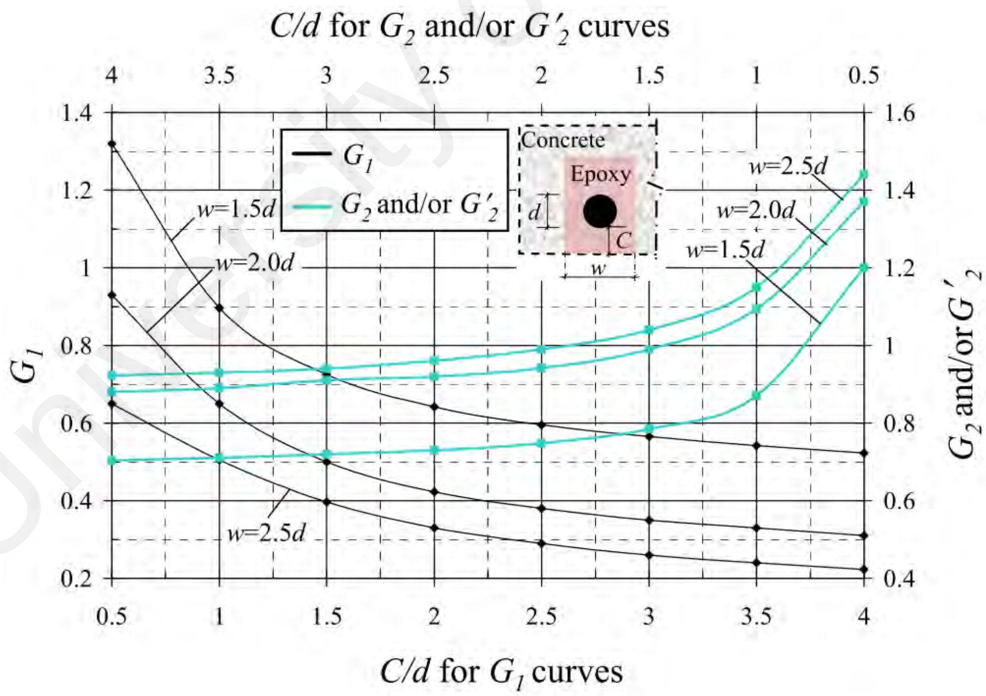

Figure 2.6: Design chart for values of G1 and G2 (Hassan and Rizkalla, 2004).

De Lorenzis (2004) introduced an analytical modelling of bond stress-slip models obtained from experimental pull-out test of FRP bars. The principle bond stress-slip models are different depending on the type of surface condition of the FRP bars. The bond-slip models were found to be reasonably accurate. The details of the models are presented in Figure 2.7.

(

a)

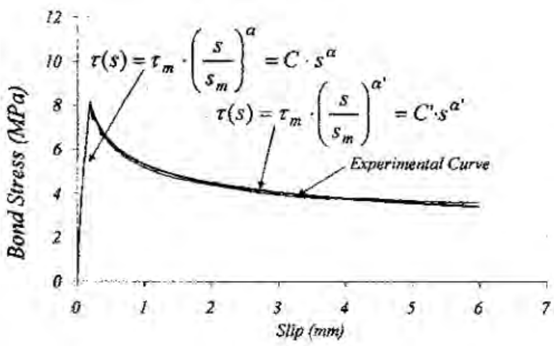

TYPE 1

$\tau(s) = \tau_m \cdot \left(\frac{s}{s_m}\right)^{\alpha} = C \cdot s^{\alpha}$ for $0 \le s \le s_m$

$\tau(s) = \tau_m \cdot \left(\frac{s}{s_m}\right)^{\alpha'} = C' \cdot s^{\alpha'}$ for $s \ge s_m$

Obtained in case of failure at the interf between concrete and groove-filler (smo grooves), and in case of splitting failure CFRP ribbed bars in epoxy and for all bars cement paste.

(

b)

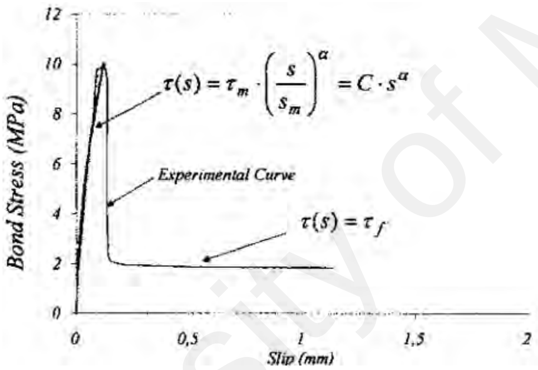

TYPE 2

$\tau(s) = \tau_m \cdot \left(\frac{s}{s_m}\right)^{\alpha} = C \cdot s^{\alpha}$ for $0 \le s \le s_m$

$\tau(s) = \tau_f$ for $s \ge s_m$

Obtained in case of splitting failure for GF ribbed bars and spirally-wound bars in epo and in case of pull-out failure for spirally-wou bars in cement paste.

(

c)

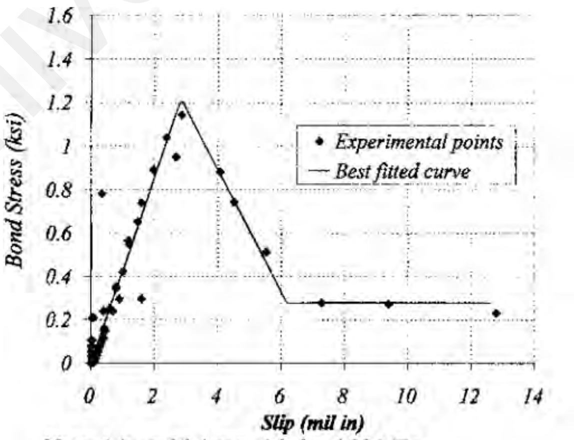

Note: 1 in. = 25.4 mm; 1 ksi = 6.89 MPa

TYPE 3

$\tau(s) = \tau_m \cdot \left(\frac{s}{s_m}\right)^{\alpha} = C \cdot s^{\alpha}$ for $0 \le s \le s_m$

$\tau(s) = \tau_m + p' \cdot (s - s_m)$ for $s_m \le s \le s_f$

$\tau(s) = \tau_f$ for $s \ge s_f$

Obtained for CFRP sandblasted bars in ep (failure by pull-out at the bar-epoxy interface)

Figure 2.7: Principle bond stress-slip models for NSM FRP bars (Lorenzis, 2004).

Cruz and Barros (2004) on the other hand presented the modelling of bond for NSM FRP strips in finite element. The basic model used was similar to the model commonly used for interaction between steel bar and concrete surfaces.

The most recent study on the bond of NSM FRP was done by Zhang et al. (2013) who presented a bond stress-slip model for NSM FRP strips which was derived based on finite element studies. The equations for the bond models are:

$$\tau = A\left(\frac{2B-s}{B}\right)^2 \sin\left(\frac{\pi}{2}\cdot\frac{2B-s}{B}\right), \text{with s} \leq 2\text{B} \quad (2.2.3)$$

$$A = 0.72\gamma^{0.138} f_c^{0.613} \quad (2.2.4)$$

$$B = 0.37\gamma^{0.284} f_c^{0.006} \quad (2.2.5)$$

$$\tau_{max} = 1.15\gamma^{0.138} f_c^{0.613} \quad (2.2.6)$$

Where τ is the bond stress, τ_{max} is the maximum bond stress, s is the slip of the FRP strip, γ is the groove height/width ratio and f_c is the concrete compressive strength. Figure 2.8 shows the bond-slip curves of the proposed model for concrete strength of 30MPa, where h_g/w is the ratio of height/width of the NSM groove.

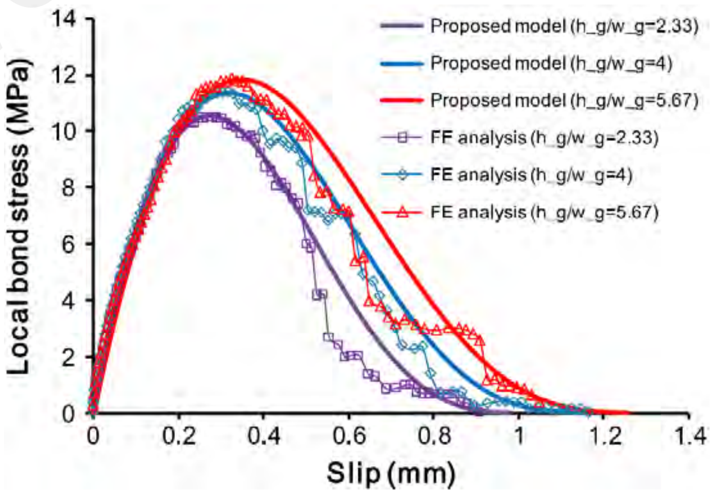

Figure 2.8: Bond stress-slip curves for concrete strength of 30MPa (Zhang et al., 2013)

2.2.1.2 Behaviour of NSM strengthened RC beams

Apart from bond behaviour, there has also been various studies on the performance of NSM strengthened RC beams when compared against other strengthening methods. Note that only the research on flexural strengthening of RC beams using NSM method is presented here, as shear strengthening using NSM method is not the focus of this thesis.

Jung et al. (2005) conducted static loading tests on beam strengthened with EB FRP, NSM FRP bar and NSM FRP strips. The beam strengthened with NSM FRP bar was reported to have failed by debonding at the epoxy-concrete interface which occurred from the cut-off point of the FRP bar, as shown in Figure 2.9, whereas the NSM FRP strip strengthened beam failed by rupture of the FRP strip. Although the NSM FRP bar strengthened beam failed by debonding, the beam was noted to have performed better compared to the beam strengthened with EB FRP. It should also be noted that debonding at the epoxy-concrete interface is rare in more recent published papers. One possibility is that improvements in the epoxy adhesive used in NSM strengthening has mostly eliminate this type of failure, assuming that the NSM strengthening is designed and installed properly.

Figure 2.9: Debonding failure of NSM strengthened RC beam at the epoxy-concrete interfaces (Jung et al., 2005)

Barros and Fortes (2005) conducted monotonic loading tests on beams strengthened with NSM FRP strips with the main parameter tested being the amount of NSM FRP reinforcement used. Nearly all of the beams failed by concrete cover separation while only the beam with the least NSM FRP reinforcement failed by fracture of FRP strip. Quattlebaum et al. (2005) performed monotonic and fatigue loading tests on RC beams strengthened with either EB FRP, NSM FRP strips or what the authors called the power actuated, fastener applied (PAF) strengthening method. As the name implies, PAF strengthening involves short FRP laminates attached on the beam using fasteners. Under monotonic loading, the NSM FRP and PAF strengthened RC beams failed by concrete crushing while the EB FRP was reported to fail by midspan debonding. Under low stress fatigue loading, both the NSM FRP and EB FRP strengthened beams showed high increase in the amount of deflection at the early cycles and negligible increase in deflection in higher cycles. The PAF strengthened RC beam suffered premature failure attributed to improper installation during the low stress fatigue loading test. Under high stress cyclic loading test, the NSM strengthened RC beam failed at a much higher cycle than the EB FRP strengthened beam, although it is outperformed by PAF strengthened beam which lasted the longest.

Barros et al. (2007) conducted flexural and shear monotonic loading tests on beams strengthened with either NSM FRP strips or EB FRP strips or sheets. For the flexural tests, it was found that NSM strengthening provided the highest load carrying capacity and deformation capacity, with the average increase in load carrying capacity by NSM strengthened beams being about 29% higher than the EB strengthened beams. Nearly all strengthened beams failed prematurely, with the NSM strengthened beams failing by concrete cover separation while EB strengthened beams suffered either debonding at epoxy-concrete interface or concrete cover separation.

Ceroni (2010) performed monotonic and cyclic tests on beams strengthened with either NSM FRP bars or EB FRP sheets. The result for monotonic loading shows that the NSM FRP strengthened beams performed better in terms of load carrying and deformation capacity compared to EB FRP strengthened beams for the equivalent amount of FRP reinforcement provided. Most of the beams failed prematurely by concrete cover separation. Under cyclic loading, EB strengthened beams show a reduction of 10% debonding load whereas NSM strengthened beams showed no reduction.

Rasheed, Harrison, Peterman, & Alkhrdaji (2010) studied the use of transverse FRP U-Wraps to control the debonding failure modes of EB and NSM strengthened beams. The NSM strengthened beam show the highest ductility among the tested specimens, although this is due to the stainless-steel bar used as the NSM reinforcement. The NSM strengthened beam failed by concrete crushing, however it is not clear whether the debonding failures were prevented by the U-wraps as the author did not test an NSM strengthened beam without the U-wraps to serve as comparison.

2.2.1.3 Premature failure modes of NSM strengthened RC beams

If the NSM strengthened beam does not fail prematurely, the beam would fail in either fracture of FRP reinforcement or concrete crushing after yield of steel reinforcement. Despite having a high tensile strength, FRP has a very low ductility and would fail earlier than steel reinforcement of the beam. However, it is more common for the beam to fail by concrete crushing, which usually occurs after the formation of concrete wedges. In design based on Eurocode 2, the maximum strain of normal strength concrete is usually taken as 0.0035.

Apart from the failure modes described above, premature failures are also commonly observed in experimental tests on NSM strengthened RC beams. Premature failures, also called debonding failures, refer to failure states that occur before the full potential of the NSM strengthening is realized; ideally, a strengthened beam should fail due to fracture of the NSM reinforcement or concrete crushing after steel yielding.

The NSM method generally suffer only from end debonding type of premature failures. An end debonding refers to debonding that starts from the curtailment location of NSM or EB reinforcements. The end debonding can occur due to three reasons:

- Failure at NSM reinforcement-epoxy interface
- Failure at epoxy-concrete interface.
- Failure at concrete-concrete interface.

The failure at epoxy-concrete interface, as illustrated in Figure 2.10, occurs due to the combination of tensile strength and bond strength of the epoxy being exceeded, causing the is rare in newer published research papers and this author believes that this type of failure can be completely eliminated by proper design and installation of NSM reinforcements, similar to the case of EB strengthened beams (Narayanamurthy, Chen, Cairns, & Oehlers, 2012).

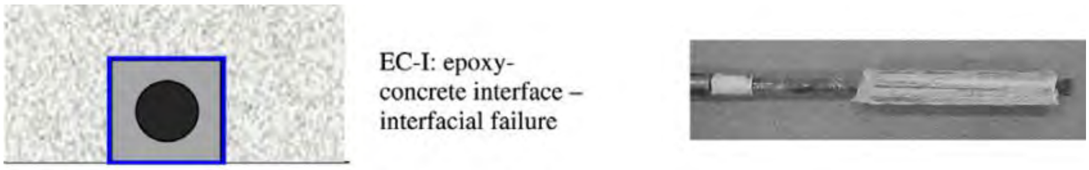

Figure 2.10: Epoxy-concrete interface failure (De Lorenzis 2007).

As for the failure at concrete-concrete interface, Zhang and Teng (2014) described there being two types of failure mode that can happen: the end interfacial debonding and the end cover separation. The failure modes are illustrated in Figure 2.11. The end interfacial debonding failure occurs when a small section of concrete adjacent the NSM reinforcement is separated from the rest of the beam.

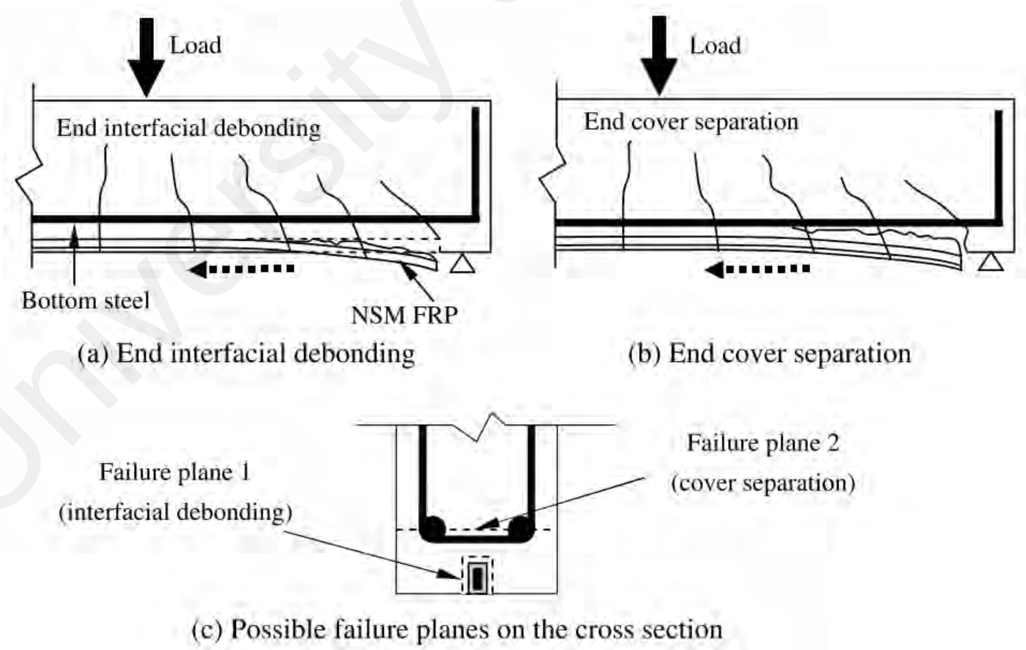

Figure 2.11: End interfacial debonding and end cover separation failure modes (Zhang and Teng, 2014)

The end cover separation, also called the concrete cover separation, occurs when shear cracks form at the cut-off section of the beam and propagates horizontally, causing the NSM reinforcement along with a substantial chunk of the concrete cover to be detached from the beam. The concrete cover separation is far more common than the interfacial debonding, as the radial stresses exerted on the adjacent concrete from the steel reinforcements is significantly high, causing the critical plane to be near the steel reinforcement rather than the NSM reinforcement (Zhang & Teng, 2014).

Currently there is a lack of research done on predicting concrete cover separation in NSM FRP strengthened beam. Zhang and Teng (2014) used a 2D finite element analysis to simulate the concrete cover separation based on these considerations:

- Simulate the tensile and shear behaviour of cracked concrete.
- Simulate the bond stress-slip of steel reinforcement and concrete.
- Simulate the critical debonding plane at the level of steel reinforcement.
- Simulate the radial stresses by steel reinforcements.

From the considerations above, it can be seen that most of the attention was given to the steel reinforcement and not the NSM reinforcement itself. De Lorenzis and Nanni (2003) used the concrete tooth model to predict concrete cover separation. Al-Mahmoud et al. (2010) also applied a method with a similar concept to the concrete tooth model in conjunction with finite element modelling.

Recently, Teng et al. (2016) proposed a strength model for NSM carbon fibre–reinforced polymer (CFRP) strips derived using finite element study while an analytical design approach was proposed by Rezazadeh et al. (2016), which was derived using concrete fracture mechanic.

2.2.2 EB method

The EB method, as mentioned earlier, was introduced much earlier than the NSM method. The amount of research done for the EB method is more wide-ranging compared to the NSM method. Additionally, when the focus of the research community changed from steel plates to FRP plates, it was found that some of the research performed on EB steel plated RC beams are also relevant for EB FRP plates (Smith & Teng, 2002), which hastens the process of making the EB FRP ready for real world application. The EB FRP usually uses FRP plates or sheet as the strengthening reinforcement. It should be noted that since the EB method is not the focus of this research, the discussions on the EB method presented here will be kept brief.

2.2.2.1 Bond behaviour of EB reinforcement

The bond behaviour of EB reinforcement has been exhaustively studied, with more than 253 pull tests conducted in the literature by various researcher (Lu et al., 2005). Figure 2.12 shows a comparison of several bond stress-slip model curves (Lu et al., 2005; Monti et al., 2003; Nakaba et al., 2001; Neubauer & Rostasy, 1999; Savoia et al., 2003); it can be seen that the bond stress-slip models for EB reinforcement tend to be characterized by an ascending and descending curve branches, apart from the model by Neubauer & Rostasy (1999).

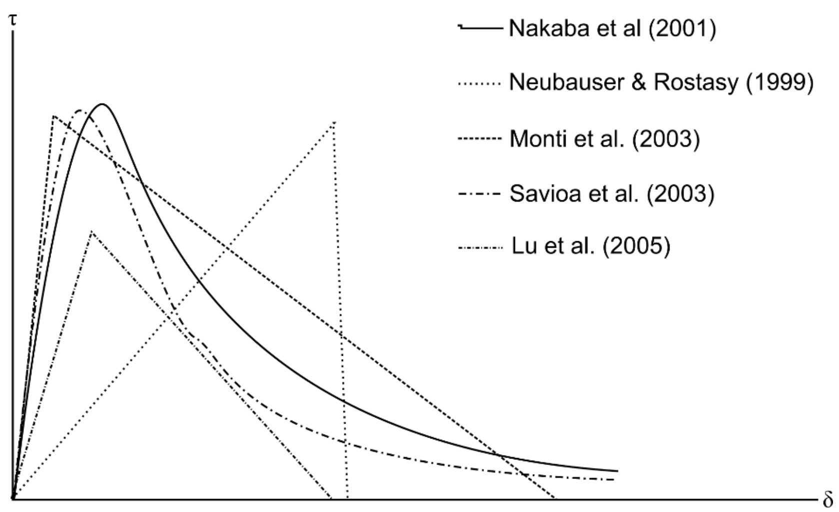

Figure 2.12: Bond stress-slip curves of several existing models

There are in fact several more models not shown in Figure 2.12 and the numerous amount of model available shows the result of extensive research that has been done for the EB method. While not all the models will be presented in detail here, several of them will indeed be discussed. The first is the model of Nakaba et al. (2001), while also featuring an ascending and descending branch, is made of a single curve and the bond stress is determined from a single equation:

$$\tau = \tau_{max}\left(\frac{s}{s_0}\right)\left[3/\left(2+\left(\frac{s}{s_0}\right)\right)^3\right] \tag{2.7}$$

Where,

$$\tau_{max} = 3.5 f_c^{0.19} \tag{2.8}$$

$$s_0 = 0.065 \tag{2.9}$$

Due to its simplicity, the model by Nakaba et al. (2001) is among the most widely used model and is adequately accurate. Another newer model was presented by Lu et al. (2005).

$$\tau = \tau_{max-s}\sqrt{\left(\frac{\delta}{\delta_o}\right)\text{for } \delta \le \delta_o} \tag{2.2.10}$$

$$\tau = \tau_{max-s}\left(\frac{\delta_f - \delta}{\delta_f - \delta_o}\right)\text{for } \delta_o < \delta \ll \delta_f \tag{2.2.11}$$

$$\tau = 0 \text{ for } \delta > \delta_f \tag{2.2.12}$$

Where,

$$B_{\mathrm{w}} = \sqrt{\frac{2.25 - b_{\mathrm{f}}/b_{\mathrm{c}}}{1.25 + b_{\mathrm{f}}/b_{\mathrm{c}}}} \tag{2.2.13}$$

$$\tau_{\max-\mathrm{s}} = 1.5 B_{\mathrm{w}} f_{\mathrm{t}} \tag{2.2.14}$$

$$\delta_{\mathrm{o}} = 0.0195 B_{\mathrm{w}} f_{\mathrm{t}} \tag{2.2.15}$$

$$\delta_{\mathrm{f}} = 2 G_{\mathrm{f}}/\tau_{\max} \tag{2.2.16}$$

$$G_{\mathrm{t}} = 0.308 B_{\mathrm{w}}^2 \sqrt{f_{\mathrm{t}}} \tag{2.2.17}$$

The bond-stress-slip model, derived from a numerical study using finite element models is perhaps more accurate than the one by Nakaba et al., (2001). Note that this is the simplified version of the model proposed by Lu et al. (2005); the original model, which they presented in the same research paper, is more complicated. The simplified model is not only easier to use, but also allows easier quantification of debonding, as will be discussed in the next section.

2.2.2.2 Premature failures of EB strengthened RC beams

The EB method is more prone to premature failures compared to the NSM method. In general, there are three main categories of premature failure mode for EB strengthened RC beams:

- End debonding.
- Critical diagonal crack (CDC) debonding.
- Intermediate crack (IC) debonding.

The end debonding mechanism of the EB method occurs in the same manner as the NSM method and the discussion made on that method also applies here. The IC debonding starts at the tensile crack in high moment area, as shown in Figure 2.13(a) and Figure 2.13(b). The EB reinforcement slips as the tensile crack widens. Referring to the simplified model by Lu et al. (2005), the bond between the FRP sheet and epoxy can in fact be reduced to zero. As such once the slip of EB reinforcement at the crack face reaches the maximum slip sf, the IC debonding will start to occur. The debonded area will grow larger as more load is applied on the beam, progressing towards the support.

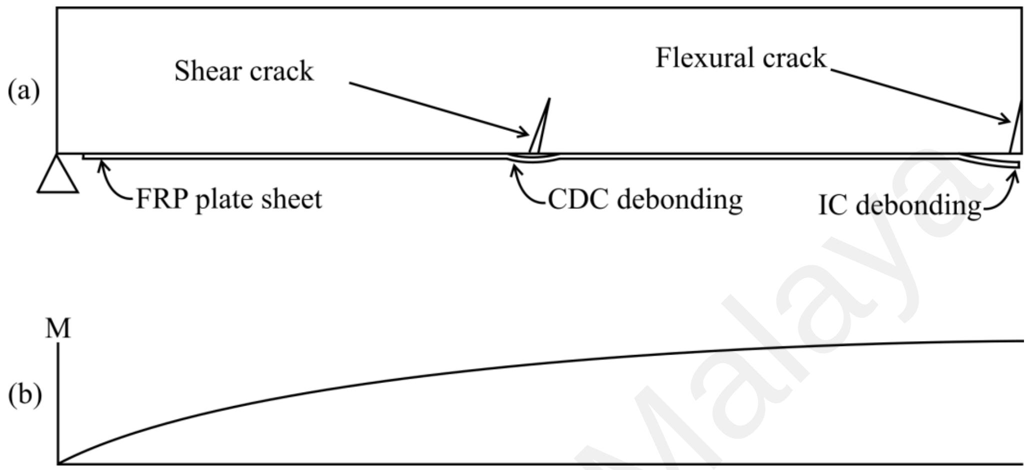

Figure 2.13: IC and CDC debonding failures

The CDC debonding occurs when the strengthened beam forms a shear crack. As this crack widens, the EB reinforcement begins to slip; the CDC debonding then occurs in the same manner as IC debonding. Since the CDC debonding occurs mainly due to shear crack, it can be avoided as long as the shear capacity of the beam is high enough.

2.2.3 NSM-based methods

There exist several new strengthening methods that are based on the NSM method. These methods will be referred to as the NSM methods in this thesis, where the main similarity between these methods is that they involve the FRP reinforcements being places in grooves that are made on the surface of the RC beam. Among them are:

- Prestressed NSM method.
- Partially bonded NSM method.
- side-NSM method.

- hybrid method.

Details on these strengthening methods will be presented in the following sections.

2.2.3.1 Prestressed NSM method

The high strength of FRP makes it suitable for prestressing; when used as a strengthening reinforcement, prestressed NSM FRP is able to give higher serviceability and ultimate load compared to when using prestressed steel. Furthermore, bar or strip shaped FRP used in the NSM method is easier to prestress than FRP sheet or plate (De Lorenzis & Teng, 2007).

Badawi and Soudki (2009) studied the flexural behaviour of prestressed NSM CFRP bars. Higher amount of pre-stressing was reported to increase the serviceability and ultimate load of beams but reduces the ductility. At 60% pre-stressing, the ductility was reduced by 63.9%. All prestressed specimens failed by rupture of FRP bar. An moment-curvature based analytical model was proposed and was found to have good correlation with the experimental results. A finite element model was also proposed by Omran and El-Hacha (2012) for prestressed NSM strengthened RC beams and was found to have good accuracy.

Oudah and El-Hacha (2012b) studied the effect of fatigue loading on prestressed NSM strengthened RC beams. Their study show that anchor slippage was more likely to occur at elevated levels of pre-stressing but does not have a major impact on the bond stress-slip behaviour along the beam. Importantly, it was reported that the prestressed NSM FRP reduces the maximum strain increase of the steel reinforcement while not affecting the strain range increase, hence increasing fatigue life of the beam.

Peng, Zhang, Cai, and Liu (2014) conducted experimental study on RC beams strengthened with prestressed NSM CFRP strips. It was found that two of the specimens failed by concrete cover separation and debonding at the epoxy-concrete interface. It was also reported that while the yield capacity for higher for specimen with prestressed NSM CFRP strip, the ultimate strain of the CFRP was not significantly raised.

Lee, Jung and Chung (2017) performed experimental and numerical study for on RC beams strengthened with prestressed NSM CFRP bars. Anchorage was found to be highly important to limit the prestress losses of NSM CFRP bars. When anchorage was applied, it was found that no slip occurred for NSM CFRP bars. Epoxy adhesive was found to provide better results compared to mortar due to the higher bond strength. The prestressed NSM CFRP bars were also found to increase the cracking capacity of the beams.

2.2.3.2 Partially bonded NSM method

A partially bonded NSM method is nearly identical to the regular NSM method, apart from a section of the NSM reinforcement that is left unbonded, usually at high moment regions of the beam. The use of partially bonded NSM for strengthening of RC beams was first explored by Chahrour & Soudki (2005), who reported that the method when applied in conjunction with end anchorages were able to show better ultimate load and ductility.

The method was explored again by Choi, West, & Soudki (2011). To create the unbonded section, the NSM bar section was placed within a thin plastic tube. The fully bonded beam failed due to rupture of FRP reinforcement whereas all the partially bonded beam failed by concrete crushing. It was reported that the stiffness and ultimate load of the beam reduces as the unbonded length is increased. On the other hand, the ductility of the beam is increased when the unbonded length is increased. An analytical model was proposed, which considers the slip and concrete crushing using empirical methods that is adjusted using results from their experimental work. The proposed model was validated against their own results and correlated well.

The latest research on this method at present was presented by Sharaky et al. (2015). The NSM reinforcements tested were CFRP bar, CFRP strips and GFRP bars. Some of the tested beams were also anchored using a steel tube. Nearly all the beams failed by concrete cover separation, apart from the beam strengthened with CFRP strip which failed through end debonding at the NSM reinforcement-epoxy interface and one of the GFRP strengthened beam which failed at the epoxy-concrete interface. Partially bonded beams were reported to have a better ductility but stiffness and ultimate load compared to fully bonded beams. The authors used an existing analytical model for NSM strengthened beam and reported that while there is some agreement between simulated and experimental result, improvements are needed to make the accuracy acceptable.

2.2.3.3 Side-NSM method

The side-NSM (side-NSM) method was proposed by Hosen et al. (2015) and is a minor modification of the NSM method where the grooves for the FRP reinforcement are made on the sides of the RC beams instead of at the soffit. An example of side-NSM strengthened beam detail in given in Figure 2.14. The purpose of the side-NSM method was to allow NSM strengthening on beams with width that is smaller than the minimum width prescribed by researchers such as described by De Lorenzis and Teng (2007) to avoid premature failure due to overlapping of stresses.

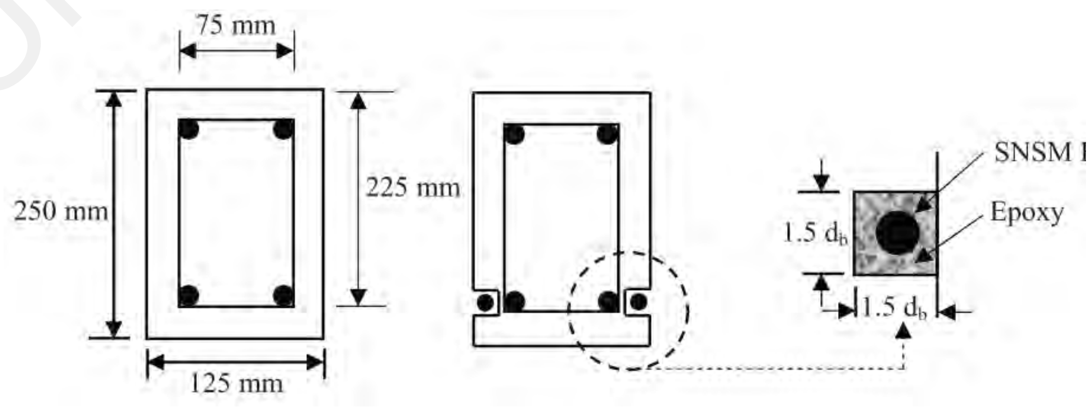

Figure 2.14: Beams details for side-NSM strengthened RC beam (Hosen et al., 2015)

The initial study by Hosen et al. (2015) showed that the side-NSM method provides a higher resistance against concrete cover separation failure, as it avoids the stress overlap between NSM reinforcements that contributes to the concrete cover separation failure. However, it does not eliminate it completely, as shown in from the experimental results where the beams strengthened using 12mm diameter bars as side-NSM reinforcements had failed by concrete cover separation failure, as shown in Figure 2.15.

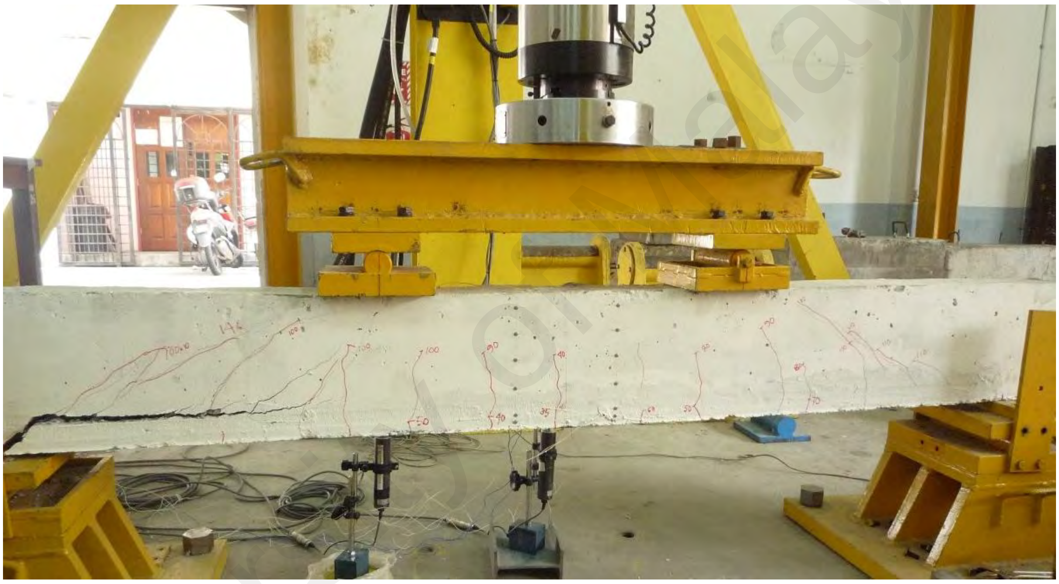

Figure 2.15: Concrete cover separation failure on side-NSM strengthened RC beams (Hosen et al. 2015).

2.2.3.4 Hybrid method

The EB-NSM hybrid, also called the combined externally bonded and near surface mounted (CEBNSM) method is a strengthening method that is a combination between EB method and NSM method as shown in Figure 2.16. Through combining the EB and NSM methods, it is possible to reduce the EB reinforcement thickness by transferring a part of the required total strengthening area of the EB method to NSM reinforcement. This in turn allows the number of NSM reinforcement size and number to be reduced, thus providing sufficient beam width for edge clearance and groove clear spacing requirements of the NSM method.

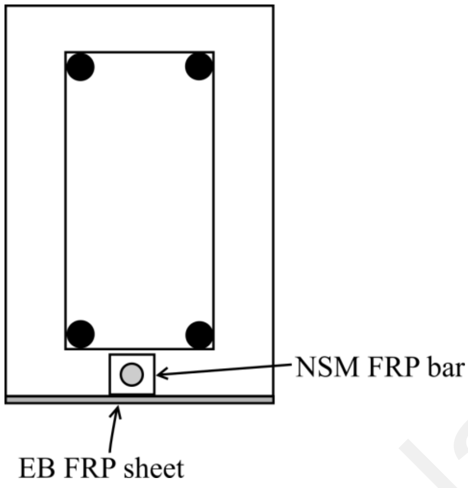

Figure 2.16: EB-NSM hybrid strengthening.

Previous work on EB-NSM hybrid strengthening involved a hybrid between NSM steel bars and EB steel plates, as introduced by Rahman et al. (2015). The use of steel instead of FRP was proposed by Rahman et al. (2015) due to the higher ductility of steel; however, this increase in ductility was not very prominent, as all of the strengthened beams prematurely failed by concrete cover separation.

2.3 Moment-rotation approach

In the moment-rotation (M/θ) approach, two theories are applied to simulate the behaviour of RC beams:

1. Partial interaction theory.
2. Shear friction theory.

Both theories and their application as a standalone theory and as a component of the M/θ approach will be discussed in the following sections. This will be followed by a summary of the work done on the M/θ approach thus far.

2.3.1 Partial interaction theory and applications

In undisturbed sections of an RC beam, that is, areas of the beam where tensile crack has not formed, the tensile reinforcements and the adjacent concrete are extended as one, such that there is strain compatibility between the reinforcements and concrete. In disturbed regions, the partial interaction theory states that where a tensile crack intercepts a reinforcement in RC structural members, infinite strains are theoretically induced in the reinforcing bar that must be relieved by a slip between the steel reinforcement and the concrete. The slip of reinforcement is ultimately responsible for many mechanics of cracked RC beams, such as crack widening and tension stiffening.

The list of research that apply the partial interaction theory will now be presented. Haskett, Oehlers, & Mohamed Ali (2008) applied the partial interaction theory to create a numerical model for the load-slip behaviour of steel reinforcement. This numerical method was used by Haskett, Oehlers, & Mohamed Ali (2008) to simulate load-slip of experimental results of pull-out tests and extract bond stress-slip relationship. The numerical procedure is as given below, along with a graphical representation in Figure 2.17:

1. A strain is fixed at the loaded end Position 0, $\varepsilon(0)$, as shown. Hence the force $P(0)$ from the material properties.
2. Corresponding to this fixed strain $\varepsilon(0)$ and corresponding load $P(0)$ at Position 0, a slip at the loaded end Position 0 is assumed or guessed, i.e. $s(0) = \Delta(0)$ and the following iterative routine is used to find $\Delta(0)$ for $P(0)$.
3. As the segment lengths are made very small, the slip is assumed constant over the segment. Hence the bond stress τ (0) which can be derived from the local bond characteristics is also constant.
4. The bond force acting over the first segment length is $B(0) = \tau(0)\ L_{per}dx$.

5. Hence the load in the reinforcement (plate or reinforcing bar) at the end of the first segment is P(1) = P(0)− B(0).
6. The corresponding strain in the reinforcement (plate or reinforcing bar) is $\varepsilon(1) = P(1)/(AE_p)$ where E/A_p is the axial rigidity of the reinforcement and the corresponding strain in the concrete at the end of the first segment is $\varepsilon_c(1) = -P(1)/(AE)_c$
7. Hence, the slip strain is $ds(0)/dx = \varepsilon(0)-\varepsilon_c(0)$.
8. By integration, the change in slip over the first segment is $\Delta_s(0) = \int(ds(0)/dx)dx$.
9. Therefore, the slip at the beginning of the second segment is $s(1) = s(0)-\Delta s(0)$.
10. The numerical procedure is repeated over the subsequent segments until the known boundary conditions are attained. There are two boundary conditions that can be used to solve the initial guess of $\Delta(0)$. For fully anchored reinforcing bars (or any type of axial reinforcement), the boundary condition is $\delta=ds/dx=0$ and for short reinforcing bars, that is reinforcing bars with bond lengths less than L_{crit}, the boundary condition is $\varepsilon=0$ at the free end.

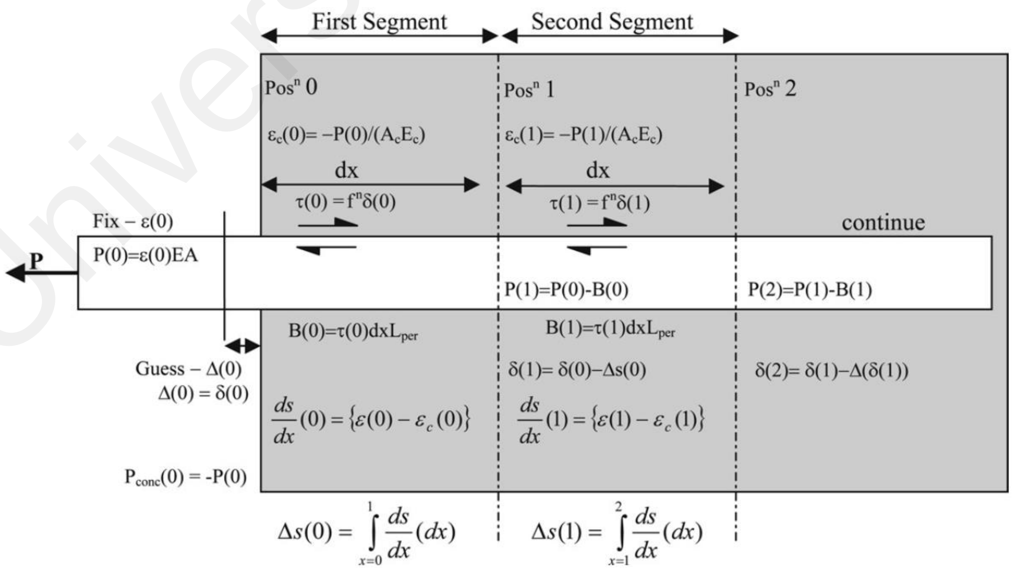

Figure 2.17 Graphical representation of the numerical analysis (Haskett et al., 2008)

Haskett et al. (2008) also found that for corroded steel reinforcement, the values of δ_{max} of the bond stress relationship (τ-δ) was found to decrease, which offsets the increase in bond strength at low levels of corrosion. This finding refutes the conclusion of several researchers who reported that low levels of corrosion is beneficial to the steel reinforcement due to the perceived increase in bond strength (Al-Sulaimani, Kaleemullah, & Basunbul, 1990; A. A. Almusallam, Al-Gahtani, & Aziz, 1996). The research by Haskett, Oehlers, & Mohamed Ali (2008) also concluded that the τ-δ model by CEB model code 90 (CEB-FIP, 1993) is relatively accurate, as the magnitudes of τ_{max} accurately predicts the experimental values. However, Haskett, Oehlers, & Mohamed Ali (2008) did not consider the frictional component of the bond since ignoring it allows mathematical solutions to be developed by other researchers who wish to use the numerical model presented in the paper.

This numerical model was later applied by Muhamad, Mohamed Ali, Oehlers, & Hamid Sheikh (2011) in their research. Closed form solutions for the load-slip relationship of steel reinforcements were proposed, which are based on bond stress-slip models that are either uni-linear descending, bilinear or nonlinear. The closed form solution based on unilinear descending bond for before yield of steel reinforcement is:

$$\delta_{r-el} = \delta_{max}\left(1 - \sqrt{1 - \left(\frac{\varepsilon_{r-el} f_{r-el} A_r}{L_p \tau_{max} \delta_{max}}\right)}\right) \tag{2.18}$$

Where δ_{r-el} is the slip of reinforcement before steel yield, ε_{r-el} is elastic steel strain, f_{r-el} is the elastic steel stress, A_r is the area of steel reinforcement, L_p is the perimeter of the reinforcement, τ_{max} is the maximum bond according to the τ-δ relationship while δ_{max} is the slip corresponding to τ_{max}. The closed form solution based on unilinear descending bond is the simplest but is inaccurate at serviceability. The other closed form solutions are more accurate, but the equations are very complicated and will not be presented here.

2.3.2 Shear friction theory and applications

The term shear friction defines the frictional resistance of concrete-concrete interfaces against sliding. Initially the shear friction theory was used to determine the shear strength by investigating the relationship between the shear stress transference across a cracked concrete interface under various levels of sliding plane confinement (Mattock, 1974). Later, Walraven & Reinhardt (1981) applied the shear friction theory to propose the following relationship:

$$\tau_{cr} = \frac{f_{co}}{30} + (1.8h_{cr}^{-0.8} + (0.234h_{cr}^{-0.707} - 0.2)f_{co}) \cdot \Delta_{wdg} \qquad (2.2.19)$$

Where τ_{cr} is the shear stress transferred across a concrete sliding plane, Δ_{wdg} is the displacement across the sliding plane and h_{cr} is the the crack widening across the sliding planes. In a more recent application of the shear friction theory, Haskett, Oehlers, Mohamed Ali, & Sharma (2011) used the shear capacities proposed by Mattock (1974) and incorporate it into the approach proposed by Walraven & Reinhardt (1981) to create a failure envelope for τ_{cr}–Δ_{wdg} relationship. Haskett, Oehlers, Mohamed Ali, & Sharma (2011) then used their research to show that the shear transfer capacity of initially uncracked planes was greater than that of initially cracked planes and that the crack separation at failure is greater in an initially uncracked plane; the increase in separation at failure was accommodated by the larger normal stress confining the sliding planes for a given displacement.

Chen, Visintin, Oehlers, & Alengaram (2014) used the derived shear friction properties by Haskett, Oehlers, Mohamed Ali, & Sharma (2011) to quantify the shear sliding capacity and shear capacity of non-confined concrete without the need to size factor. This leads to a size-dependent stress-strain model for unconfined concrete:

$$\varepsilon_{axgl} = \left((\varepsilon_{ax})_{pop} - \varepsilon_{mat}\right)\frac{100}{\left(L_{def}\right)_{mem}} + \varepsilon_{mat} \tag{2.2.20}$$

$$\varepsilon_{mat} = \sigma_c/E_c \tag{2.2.21}$$

Where ε_{axgl} is the concrete global axial strain, $(\varepsilon_{ax})_{pop}$ is the axial strain from concrete stress-strain relationship by Popovics (1973) which was used as the reference stress-strain model, ε_{mat} is the material strain of concrete, σ_c is the concrete stress, E_c is the concrete secant modulus and $(L_{def})_{mem}$ is the length of deformation in analysis based on the M/θ approach. It is also shown how to derive a size-dependent stress-strain relationship from a stress-strain relationship obtained using a cylinder/prism compression test:

$$\varepsilon_{axgl} = \left((\varepsilon_{ax})_{pop} - \varepsilon_{mat}\right)\frac{200}{L_{pr}} + \varepsilon_{mat} \tag{2.2.22}$$

Where L_{pr} is the length of cylinder or prism tested.

2.3.3 Current progress on the moment-rotation approach

The M/θ approach in summary is a displacement-based analysis of RC hinges. Partial interaction theory and the shear friction theory are usually applied as components of the M/θ approach. It should be noted that most of the published research refer to the M/θ approach by a number of names. Examples include 'unified approach', 'displacement-based analysis', 'segmental approach', 'partial interaction moment-rotation approach' and lastly 'moment-rotation approach'. While there may be some differences between them, for consistency and brevity, this research uses the term moment-rotation (M/θ) approach as an umbrella term for all these names.

One of the first work on the M/θ approach was presented by Oehlers et al. (2011). The paper presented a ‘unified method’ for simulating the behaviour of FRP plate/sheet strengthened RC beams. The unified method was theoretically generic, although in the paper focus was given on FRP plate/sheet strengthened RC beam and intermediate crack (IC) debonding. No validations were provided in the paper, which makes it difficult to determine the accuracy of what was proposed. It is likely that the accuracy would not be very good, as further research on IC debonding and the M/θ approach proves that there were many aspects that were not accounted for in the paper. The procedure for applying this unified method was also not clear. However, the paper is significant as it presents the fundamental principles on how the partial interaction theory can be used to determine the crack spacing, crack width, tension stiffening and beam deflections. The numerical method proposed by Haskett, Oehlers, & Mohamed Ali (2008), which was based on the partial interaction theory, was used in the research. The shear friction theory was applied to account for the formation of concrete wedges as shown in Figure 2.18.

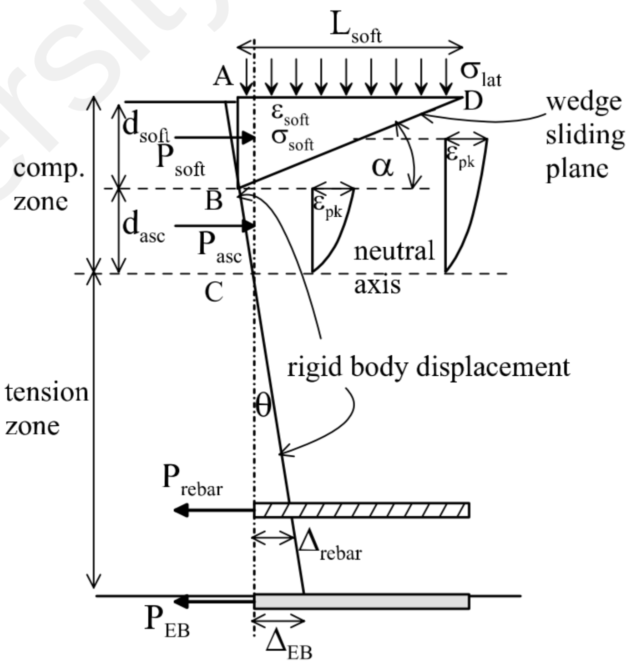

Figure 2.18 Moment/discrete-rotation analysis (Oehlers et al., 2011)

Visintin et al. (2012) further improved the M/θ approach by presenting a method for simulating the full behaviour of plain RC beams with multiple cracks. This is done firstly by applying the shear friction theory for simulating the formation of concrete wedges and the resulting concrete softening; secondly, this paper also introduces the multiple crack analysis for the tension stiffening and M/θ simulation. A single crack analysis based on the partial interaction theory, where only one tensile crack is considered to have formed on the RC beam, was used to determine the primary crack spacing, L_{cr}. Once the primary crack spacing have formed, there will be a symmetry of forces within along the length of the primary cracks as shown in Figure 2.19. Due to the symmetry of forces, only half of L_{cr} needs to be considered; this length of half crack spacing was referred to as the length of deformation, L_{def} as shown in Figure 2.19. While it was not discussed in the paper, it would later be recognized that the multiple crack analysis is better at simulating the effects of tension stiffening compared to the single crack analysis (Oehlers, Visintin, & Lucas, 2015). In cases where the concrete wedge crosses more than one crack, as shown in Figure 2.20, Visintin et al. (2012) stated that the total hinge rotation should be considered, that is, the rotation of the hinge should be the sum of all the rotation at individual tensile cracks that the concrete wedge encompasses. This condition is more likely to happen in deep beams.

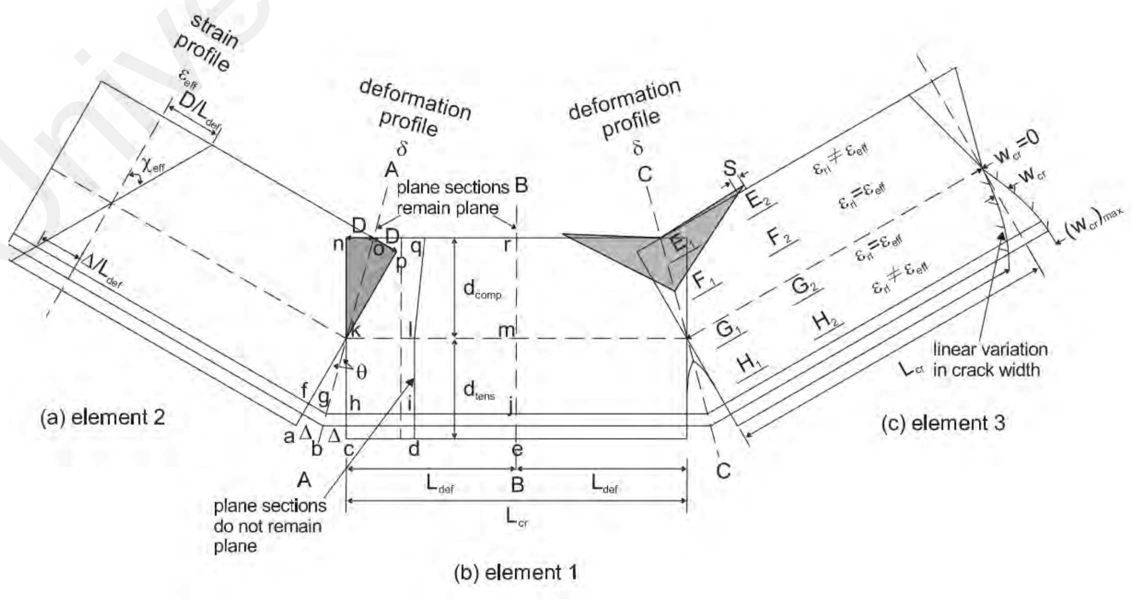

Figure 2.19: Mechanics based beam hinge model in constant moment region (Visintin et al., 2012).

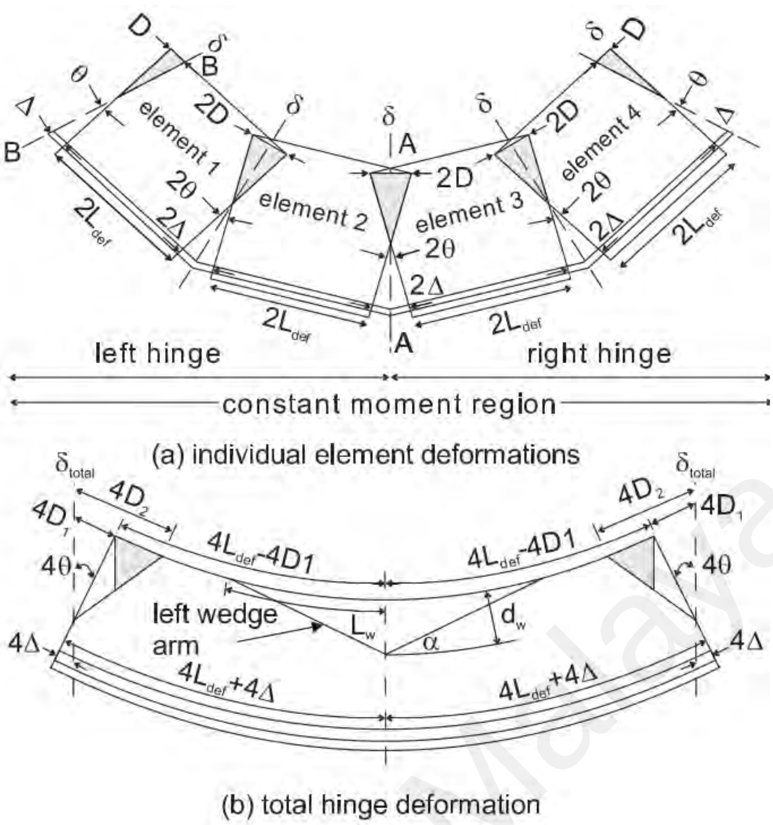

Figure 2.20 Multiple cracks in the hinge region (Visintin et al., 2012)

The multiple crack analysis proved to be an important development for the M/θ approach, as it was then used in several other publications on the simulation of RC beams with some types of EB strengthening. The method served as the basis for the work by Knight et al. (2014) on the simulation of RC beams strengthened with unbonded FRP and steel prestressing tendons. The effect of prestressing was included in the M/θ approach adding a concrete and reinforcement compression strain in the tensile region of the beam:

$$\varepsilon_c = \frac{\delta}{L_{def}} - \varepsilon_{sh} \tag{2.23}$$

$$\varepsilon_r = \frac{\delta}{L_{def}} \tag{2.24}$$

Where ε_c is the concrete compression strain due to prestressing, ε_r is the reinforcement compression strain due to prestressing, δ is the deformation profile between A-A and B-B as shown in Figure 2.21, L_{def} is the length of deformation and ε_{sh} is the strain due to concrete shrinkage. The M/θ procedure for the application of prestressing is given in flowchart form in Figure 2.22, while the full M/θ procedure is given in Figure 2.23.

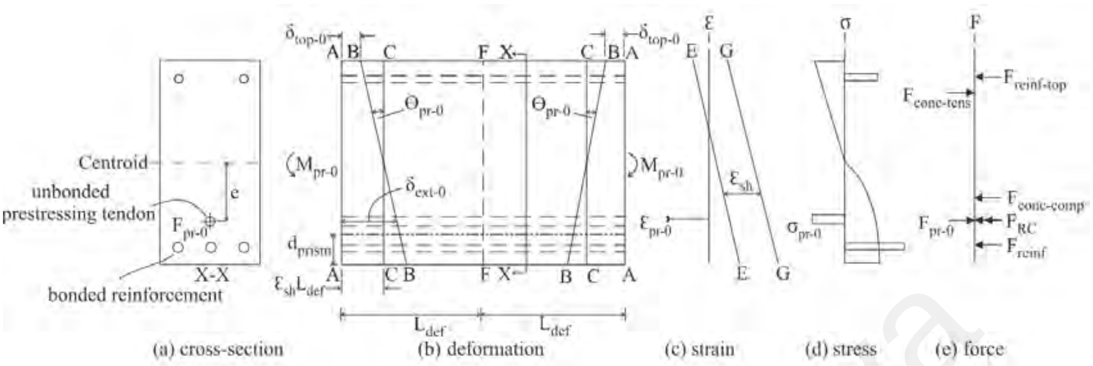

Figure 2.21 Moment analysis of a segment at prestress application (Knight et al., 2014a).

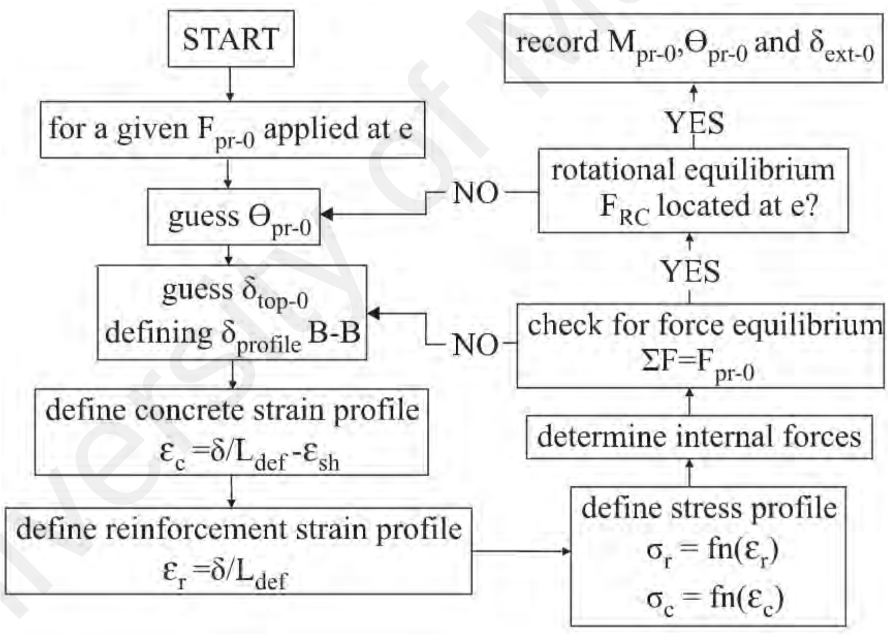

Figure 2.22 M/θ procedure at application of pre-stress (Knight et al., 2014a).

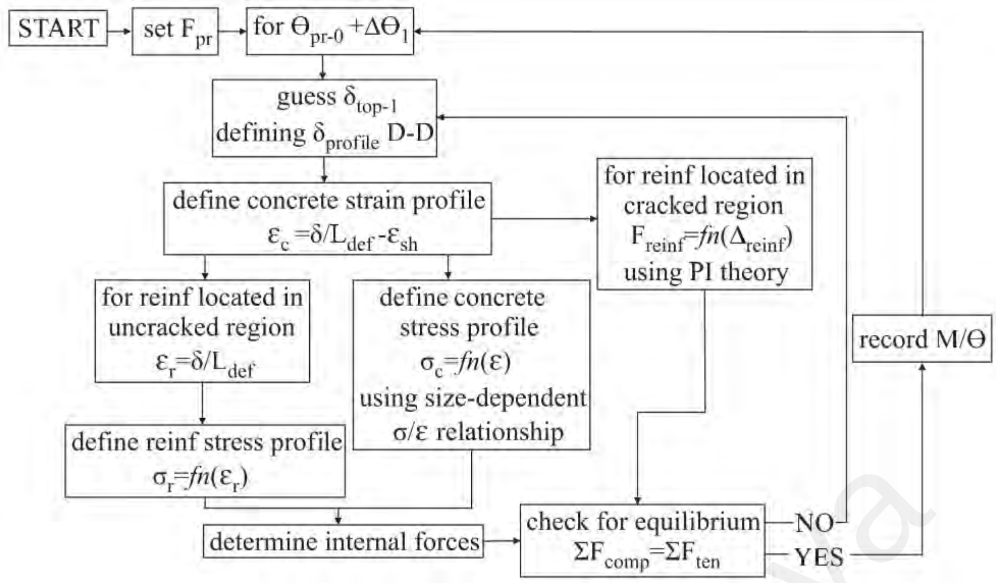

Figure 2.23 Moment-rotation procedure for segment (Knight et al., 2014a).

Knight et al. (2014b) presented a M/θ approach to simulating the behaviour of RC beams strengthened with mechanically fastened RC strips. The mechanically fastened FRP is assumed to slip at the locations where the fasteners are placed. To analyse the force acting on the FRP, the beam shown in Figure 2.24 is given, which is symmetrically loaded and the slip at mid span is zero due to symmetry. A force PFRP-1 is applied over the fastening length L1. The magnitude of moment the M_{app} which induced the applied for PFRP-1 is then assumed. The slip at the next fastener, s_2=L_{b-1}-L_{FRP-1} as shown in Figure 2.24(c); the force acting on at the location of slip, P_{FRP-2}=P_{FRP-1}-P_{F-2}. This is continued until the final fastener, where the boundary condition is $P_{F(n+1)}$=P_{FRP-n}. If the boundary condition is not satisfied, the magnitude of M_{app} is changed. This is continued until a load-slip (P_{FRP}-s) is obtained. The M/θ approach is applied as shown in Figure 2.25, where the P_{FRP}-s relationship is used to determine the force P_{FRP} corresponding to the slip δ_{FRP}.

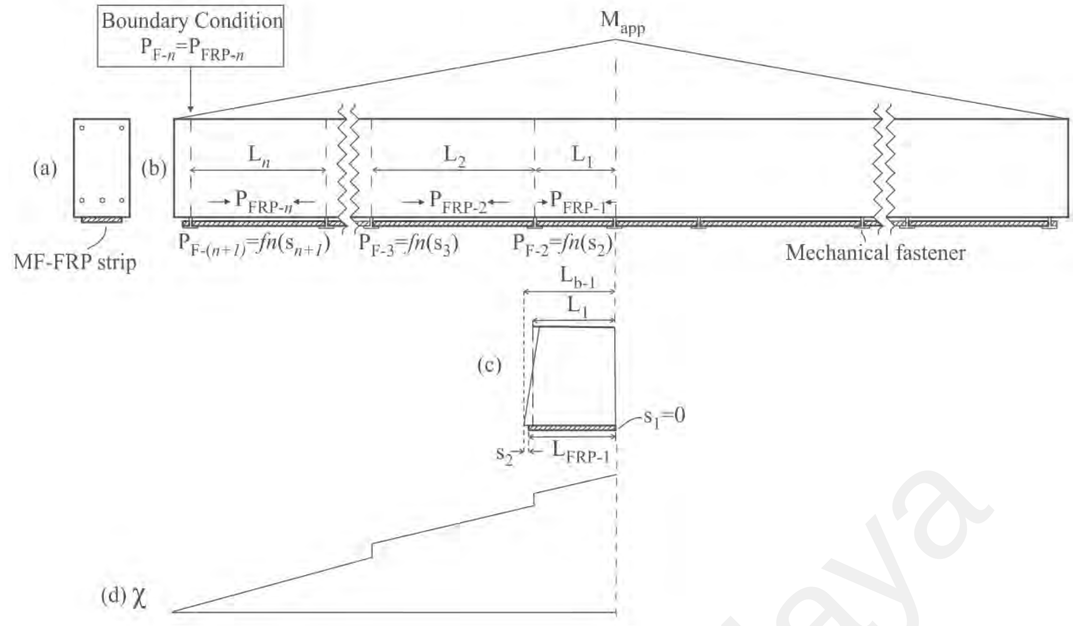

Figure 2.24 Member analysis (Knight et al., 2014b).

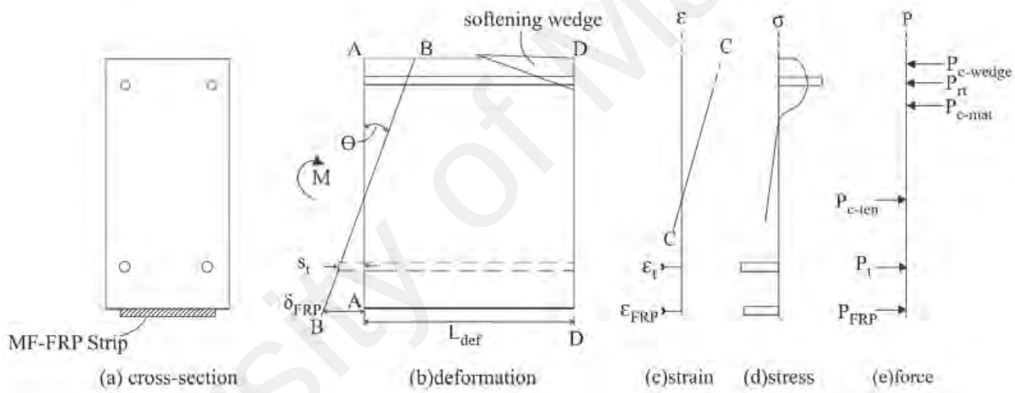

Figure 2.25 Analysis of an MF-FRP RC segment (Knight et al., 2014b).

Oehlers et al. (2015) presented another work on IC debonding. A discussion on single crack analysis and multiple crack analysis is presented. The multiple crack analysis as presented by Visintin et al. (2012) is shown to not limit the force in the FRP plate/sheet; as such the single crack analysis is more accurate in simulating the loss of FRP strength due to IC debonding. A comparison between the multiple crack and single crack analysis are given in Figure 2.26 and Figure 2.27 respectively.

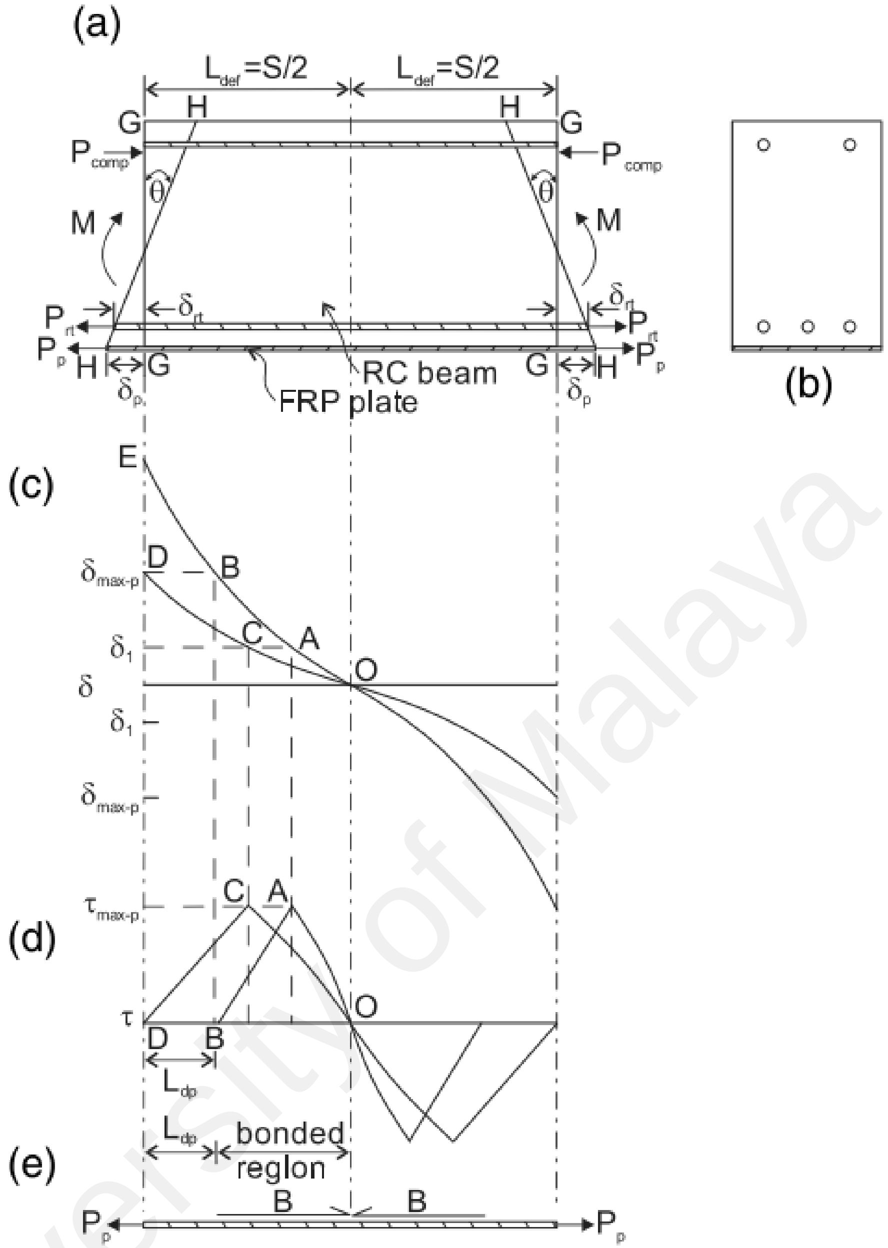

Figure 2.26 Segmental multiple-crack debonding: (a) segment; (b) Section A-A; (c) slip; (d) shear stress; (e) bond force (Oehlers et al., 2015)

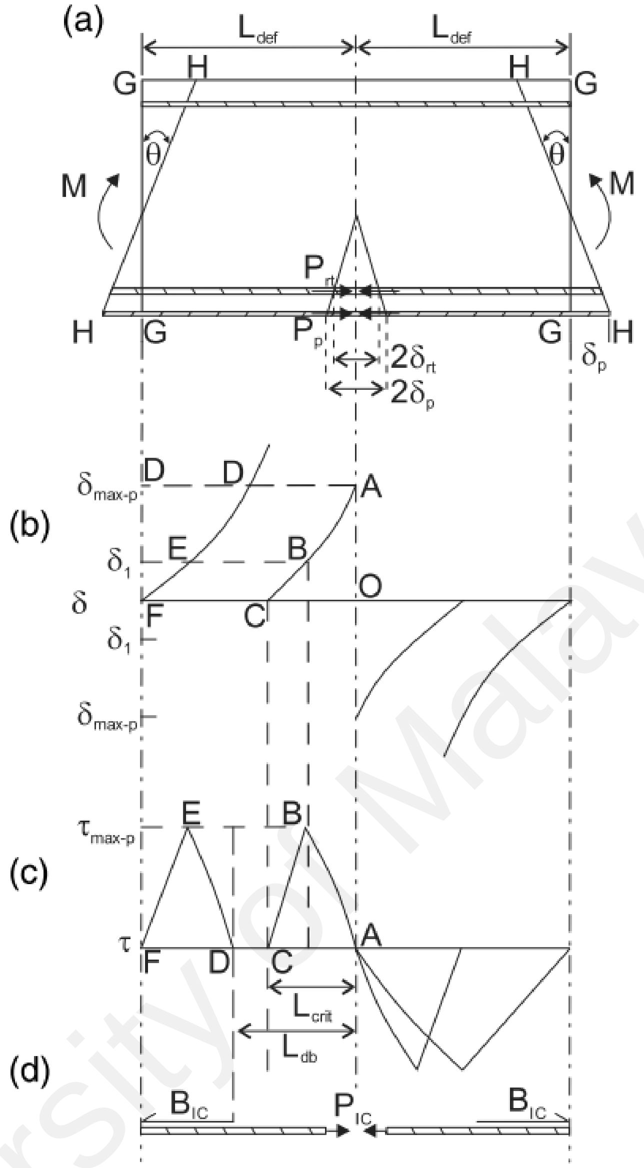

Figure 2.27 Segmental single-crack debonding: (a) segment; (b) slip; (c) shear stress; (d) bond force (Oehlers et al., 2015)

Oehlers et al. (2015) also presented another way to perform partial interaction tension stiffening analysis on beams with multiple layers of reinforcements. Previously the area of adjacent concrete needs to be determined for the steel reinforcements, which can lead to various assumption on how large the area is. As shown in Figure 2.28, Oehlers et al. (2015) presented that the reinforcements can be idealized as a single large reinforcement of area Art, which is the sum of the area of individual reinforcements. While Oehlers et al. (2015) presents much theoretical work, their accuracy cannot be verified as no validations against experimental results were given.

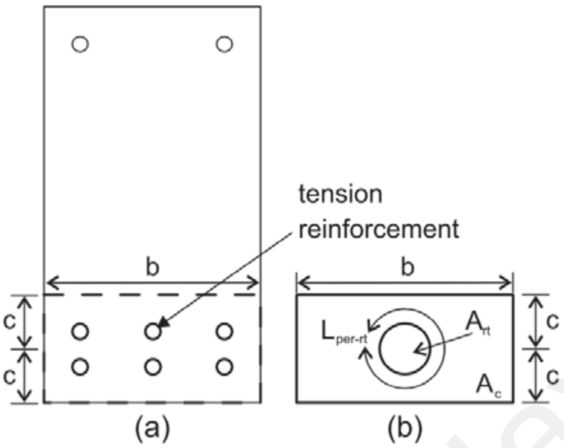

Figure 2.28 Tension-stiffening prism (Deric J. Oehlers et al., 2015).

The M/θ approach was used by Mo, Visintin, Alengaram, & Jumaat (2016) to predict the behaviour of oil palm shell lightweight RC beams. Pull-out test was first applied to obtain the bond stress-slip relationship. The bond stress-slip model proposed by Haskett et al. (2008), which is a modification of the model by CEB model code 90 (CEB-FIP, 1993) was found to give a good representation of the experimental bond stress-slip curve. The prediction of crack spacing using the closed form solution by Muhamad et al. (2012), which is based on the partial interaction theory, was found to predict the experimental crack spacing with deviation between 1-15%. Unfortunately, no comparison of crack spacing predicted using the single crack partial interaction analysis was given. A comparison of experimental moment versus mid-span deflection against simulated results using the multiple crack analysis as proposed by Visintin et al. (2012) was provided. The simulated curve was found to follow the experimental curve reasonably well. A similar comparison using published experimental results of lightweight RC beams using aggregates of either polystyrene, expanded clay, expanded slate or natural aggregates was also provided; the simulated results were accurate at serviceability, but the accuracy is lower after steel yielding. While this paper did not provide any new knowledge for the M/θ approach, it provided various validations against experimental results, which is found to be lacking in many papers on the M/θ approach.

The latest research on M/θ approach was presented by Aydin, Gravina, & Visintin (2018), where the M/θ approach was used to extract the bond stress-slip properties of FRP plates from EB FRP plate strengthened RC beams. A set of published experimental results of EB FRP plate strengthened RC beams was first presented in the paper. A bilinear initial bond stress-slip model was used, as shown in Figure 2.29, where the bond strength τ_{max} and maximum slip δ_{max} were varied until the simulated load versus mid span deflection curve of the strengthened beams matches the experimental load versus mid span deflection curve.

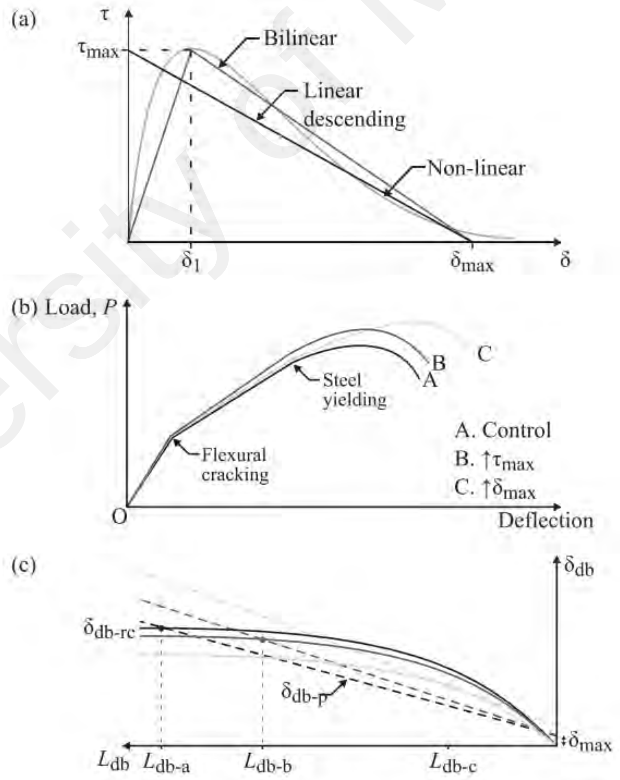

Figure 2.29 Influence of bond characteristics on the load-deflection response (Aydin et al., 2018).

2.4 Global energy balance approach

The global energy balance approach (GEBA) applies the assumption used in fracture mechanics models, which states that interface flaws are inevitable and what matters is whether the flaws can propagate (Hutchinson & Suo, 1991). The first published research paper on GEBA was presented by Achintha and Burgoyne (2008), in which the theory and assumptions for the GEBA were detailed. In the paper, the equation for energy release rate was given as:

$$G_R = \frac{\Delta ER_d}{b_p \delta x} \tag{2.25}$$

Where ΔER_d is the energy available for debonding, b_p is the width of the FRP plate and δx is the horizontal-linear crack extension. The GEBA was later validated against experimental results in Achintha and Burgoyne (2011), where it shows good accuracy for predicting all forms of FRP plate debonding.

The GEBA itself is not complex, although the assumptions it used can be controversial as noted by Achintha and Burgoyne (2013), where these assumptions were discussed in detail. Firstly, it only considers Mode I fracture for the FRP debonding process. The reasoning was that the GEBA was only concerned with the start of the debonding process, such that the effects that come from Mode II such as aggregate interlock were not relevant. This is controversial due to the fact that the shear-lap experiments commonly used to determine the parameters of FRP debonding would result in an estimate of Mode II fracture energy rather than Mode I. Secondly, the fracture energy was regarded as independent of the length of the debonding crack because the strain conditions near the tip of the crack remain unchanged as the crack develops.

The only complexity in using the GEBA lies in how to obtain the ΔER_d, which require the moment-curvature relationship of the RC beam to be determined. Achintha and

Burgoyne (2009) proposed a method based on moment-curvature approach to determine the ΔER_d which uses a modification of Branson's equation (Branson, 1968) for effective second moment of area to indirectly account for tension stiffening effect of cracked RC beam. The modified equation assumes that fully cracked state for RC beam can be reached as it deals with beams that will need to be retrofitted with FRP, whereas the original Branson's equation does not allow fully cracked state as it was intended represent section below the working load and well below the yield of steel reinforcement. The modified equation is as follows:

$$K = \left(\frac{M_{cr}}{M_{app}}\right)^4 \left\{1 - \left(\frac{M_{app} - M_{cr}}{M_y - M_{cr}}\right)^4\right\} \tag{2.26}$$

$$EI_{eq} = \frac{M_{eff}}{\kappa} \tag{2.27}$$

Where K is the extend-of-cracking, M_{cr} is the moment causing first cracking, M_{app} is the externally applied moment, M_y is the moment causing yielding of steel reinforcement, EI_{eq} is the equivalent stiffness for inelastic region, Meff is the effective moment on RC beams and κ is the curvature.

The newest research on GEBA by Guan and Burgoyne (2014) proposed three new moment-curvature models. The first type moment-curvature model, M1 almost similar to the one proposed by Achintha and Burgoyne (2009). The second mode, M2, is also similar to what was proposed by Achintha and Burgoyne (2009) except it uses an effective moment of inertia instead of EI_{eq} for partially cracked section interpolation as shown below:

$$I_{eff} = KI_{un} + (1 - K)I_{fc} \tag{2.28}$$

Where I_{eff} is the effective second moment of area, I_{un} is the second moment of area for uncracking beam and I_{fc} is the second moment of area for fully cracked beam state. The third moment-curvature model, M3, uses interpolation between moment of inertia at the first crack (I_{cr}) and the first yield (I_y) for partially cracked section as shown below:

$$I_{eff} = KI_{cr} + (1 - K)I_y \tag{2.29}$$

All three models were shown to give good accuracy, however the authors stated that considering how critical the moment-curvature relationship is to the FRP debonding prediction, the accuracy of the models are still open to some questions.

2.5 Research gap

Most of the research on the M/θ approach so far have focused strengthening techniques where the bond between strengthening reinforcement and the rest of the RC beam is either weak (i.e. externally bonded FRP sheet/plate) or non-existent (i.e. unbonded prestressed FRP or mechanically fastened FRP). On the other hand, the simulation of strengthening methods with strong bond, such as the NSM method, has yet to be explored.

The first research gap that will be focused on in this research is on extending the M/θ approach to simulate a strong bond strengthening such as NSM. The second research gap is to present a way to simulate concrete cover separation, which tend to be the primary mode of premature failure in NSM strengthened RC beams.

CHAPTER 3 - MOMENT-ROTATION APPROACH FOR SIMULATING THE BEHAVIOUR OF NSM STRENGTHENED RC BEAMS

This chapter presents the research paper “Simulating concrete cover separation in RC beams strengthened with near-surface mounted reinforcements”. In this paper the moment-rotation (M/θ) approach and the global energy balance approach (GEBA) were combined to allow the simulation of the behaviour and concrete cover separation failure of NSM strengthened beams. The proposed method is more versatile compared to existing methods as it requires significantly less empirical formulations when simulating NSM strengthened RC beams as the mechanics of the beam such as crack formation, crack widening and tension stiffening are simulated directly. The M/θ-GEBA method was validated against published experimental results. Comparison between simulated and experimental load-deflection curves shows that the method is able to give good accuracy.

The author had written another paper (Shukri, Darain, & Jumaat, 2015) which is much related to the subject of this chapter, although it could not be compiled with this thesis. The paper, titled “The Tension-Stiffening Contribution of NSM CFRP to the Behavior of Strengthened RC Beams” presents an early idea for the use of M/θ approach for simulating NSM strengthened beams. The paper discusses how the strong bond of NSM strengthening reinforcement exerts an area of influence onto surrounding concrete, hence reducing the available concrete area around the steel reinforcement. This causes the tensile cracking strain to be reached earlier, hence causing the NSM strengthened beam to have a smaller crack spacing compared to non-strengthened beams. Concrete cover separation was not simulated in that paper as GEBA was not used. While that research paper will not be made available here, readers will still able to access the paper if they wish, as the paper was published in an open access journal.

The detail of the research paper contained in this chapter along with the statement of contribution of authors is as follows:

1) Shukri, A. A., & Jumaat, M. Z. (2016). Simulating concrete cover separation in RC beams strengthened with near-surface mounted reinforcements. *Construction and Building Materials*, *122*, 1–11.
    a. Statement of contribution: Ahmad Azim Shukri (author) gathered published experimental results, performed the simulations and wrote the paper, Mohd. Zamin Jumaat (co-author) supervised the research and checked the paper.

3.1 Research paper 1: Simulating Concrete Cover Separation in RC Beams Strengthened with Near-Surface Mounted Reinforcements

Published in *Construction and Building Materials*

Article history:

Received 6 May 2016

Received in revised form 13 June 2016

Accepted 14 June 2016

Construction and Building Materials 122 (2016) 1–11

Contents lists available at ScienceDirect

Construction and Building Materials

journal homepage: www.elsevier.com/locate/conbuildmat

Simulating concrete cover separation in RC beams strengthened with near-surface mounted reinforcements

A.A. Shukri, M.Z. Jumaat *

Department of Civil Engineering, Faculty of Engineering, University of Malaya, 50603 Kuala Lumpur, Malaysia

HIGHLIGHTS

- A method to simulate concrete cover separation for NSM method was presented.
- Combination of global energy balance and moment-rotation approach.
- The simulated results shows good correlation with published experimental results.

ARTICLE INFO

Article history:
Received 6 May 2016
Received in revised form 13 June 2016
Accepted 14 June 2016

Keywords:
Reinforced concrete
Fibre reinforced polymer
Near surface mounted
Partial interaction
Moment-rotation
Fracture

ABSTRACT

The near surface mounted (NSM) technique for strengthening reinforced concrete (RC) beams normally utilizes fibre reinforced polymer (FRP) bars or strips placed within grooves made on the soffit of the beams. For RC beams strengthened with NSM the failure mode would normally be the premature debonding failure by separation of concrete cover. A few methods have been proposed to predict the failure loads. The application of these methods however were found to be limited by the empirical formulations that were used, which severely affects their accuracy when applied to situations outside of the testing regime that formed the empirical formulations. To address this issue, in this paper the moment-rotation technique and the global energy balance technique were combined to predict the failure load. The proposed method is more versatile as it requires significantly less empirical formulations when simulating NSM strengthened RC beams as the mechanics of the beam such as crack formation, crack widening and tension stiffening are simulated directly. The proposed method was validated against published experimental results. Comparison between simulated and experimental load-deflection curves shows that the method is able to give good accuracy.

1. Introduction

Strengthening of structures were normally carried out for various reasons. These include insufficient structural strength of existing structures due to mistakes during construction and reduced structural strength due to aging of structures. In most cases, the material selected to strengthen these structures is usually fibre reinforced polymer (FRP) due to its high strength-to-weight ratio and ease of placement. FRP applied using external bonding with epoxy adhesive [1–4] had been applied in many real-world strengthening cases and were proven effective. Apart from externally bonded FRP, there is another type of FRP application called the near surface mounted (NSM) method which is gaining attention of late.

The application of flexural strengthening using NSM method involves the cutting of grooves in the concrete cover of RC beams [5–9] and placing FRP reinforcement within the grooves, which is then set in place by applying epoxy adhesives. Experimental testing of NSM strengthened RC beams have shown that the NSM method provides better resistance against certain types of debonding failures, which is the main problem affecting externally bonded FRP application. Debonding causes the strengthened RC structural member to fail at a significantly lower load without reaching the full potential of the FRP reinforcements. As the NSM method provides better bonding between the FRP reinforcement and concrete substrate, it reduces the possibility of debonding through intermediate crack debonding and critical diagonal crack debonding.

While there have been much progress on advancing the NSM method, there has been very little study made on predicting the debonding failures of NSM strengthened beams. While intermediate crack debonding and critical diagonal crack debonding is extremely

* Corresponding author.
E-mail addresses: ahmadazimshukri@gmail.com (A.A. Shukri), zamin@um.edu.my (M.Z. Jumaat).

http://dx.doi.org/10.1016/j.conbuildmat.2016.06.048
0950-0618/

rare for NSM strengthened beams, a significant number of published experimental results have reported NSM strengthened beams failing through the concrete cover separation, which is another type of debonding failure mode. The concrete cover separation failure involves a crack forming at the end point of the NSM reinforcement, which tends to propagate horizontally after reaching the shear reinforcement. This causes the concrete cover along with the NSM reinforcement to separate from the beam, thus causing an early failure for the beam.

Currently there is a lack of research done on predicting concrete cover separation in NSM strengthened beam. Zhang and Teng [10] used finite element analysis to simulate the concrete cover separation and introduced a modelling of the radial stresses exerted by steel tension bars onto the surrounding concrete to improve accuracy. De Lorenzis and Nanni [11] used the concrete tooth model to predict concrete cover separation. Al-Mahmoud et al. [12] also applied a method with a similar concept to the concrete tooth model in conjunction with finite element modelling. The most recent method is the model by Teng et al. [13], which is a model formulated from finite element analysis. All of the methods mentioned above can be used to predict concrete cover separation, although the accuracy varies from one model to the other. Most of the models are highly empirical in nature, especially in predicting the crack spacing.

In recent years a global energy balance approach (GEBA) has been developed [14–16] to predict the concrete cover separation failure of RC beams strengthened with externally bonded FRP plates. The GEBA works by applying fracture mechanics of concrete; the energy available in a strengthened beam is determined from the moment-curvature (M/χ) relationship and compared to the energy required for the debonding crack to propagate. Currently the method for using the GEBA was derived for FRP plated RC beams, and there has not been any published research on using the GEBA with NSM strengthened beams.

1.1. Objective

In light of this, it is proposed that the moment-rotation (M/θ) technique [17–23] be applied to derive the required M/χ relationships. The M/θ technique applies the partial interaction theory [24–26] in order to simulate flexural cracking and tension stiffening by directly simulating the slip of reinforcements in the RC beam. This allows the slip of the NSM reinforcement to be directly simulated, which can help reduce the reliance on empirical formu-

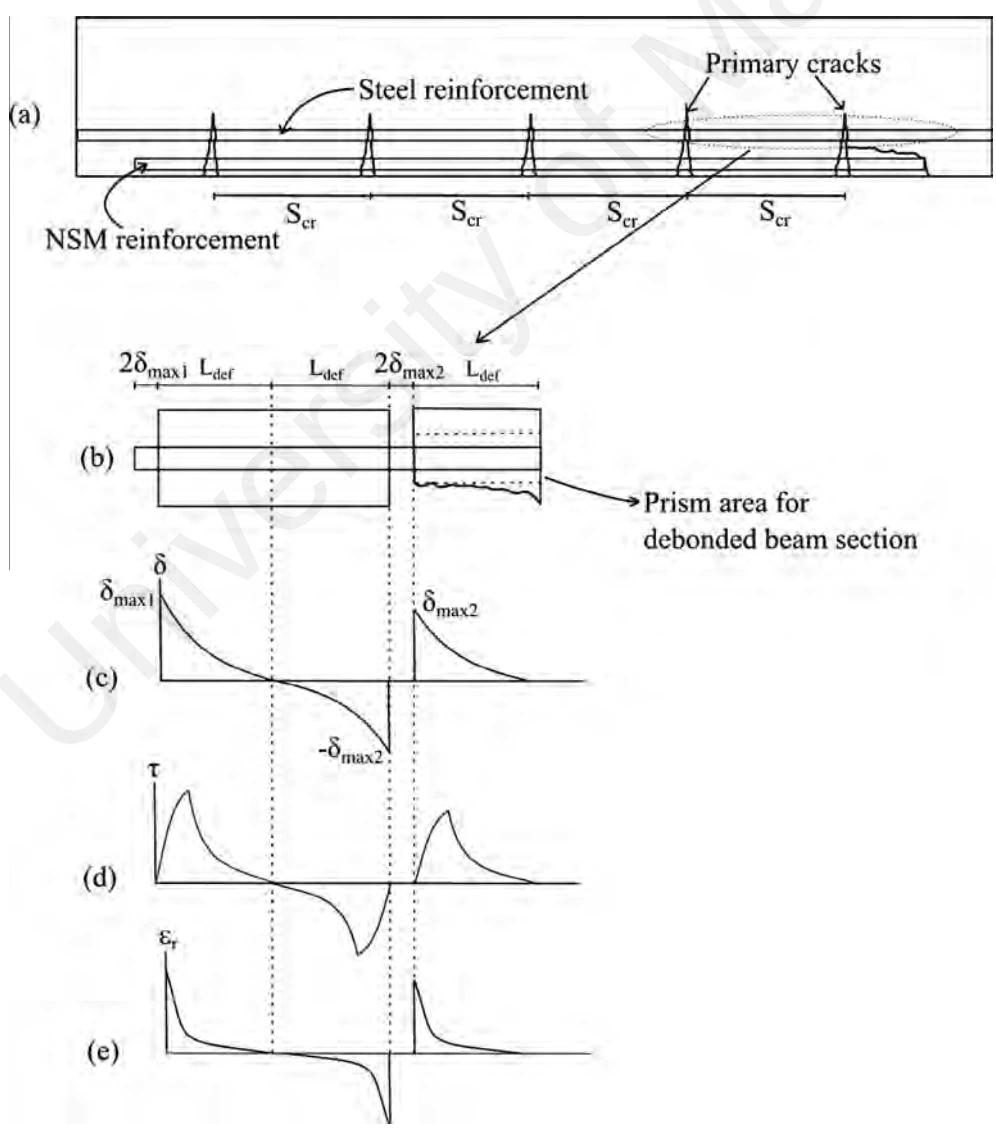

Fig. 1. Tension stiffening simulation for steel reinforcement. (a) NSM strengthened RC beam; (b) Tension stiffening simulation prism; (c) Slip distribution; (d) Bond stress distribution; (e) Steel strain distribution.

lations in simulating many of the mechanics of NSM strengthened RC beams as seen in practice. Minor changes to the GEBA would then be made to apply it on NSM strengthened beams, allowing the concrete cover separation failure mode to be simulated. Additionally, the debonding crack was allowed to propagate up to the point where the beam can no longer accept additional load nor maintain the current load; this is made so that a more accurate failure load can be obtained.

Due to its reduced reliance on empirical formulations, the method proposed in this paper should be readily applicable to any shape and material of NSM reinforcements, assuming that the material properties of the NSM reinforcements such as stress-strain relationship and bond stress-slip relationship is known. Other methods on the other hand may require extensive structural testing to formulate empirical formulations to account for any changes to the shape and material of NSM reinforcements. As such the combination of M/θ technique and GEBA provides a more versatile method for simulating NSM strengthened RC beams; furthermore it can help reduce the cost of developing new types of NSM shapes and materials as there would be no need for extensive structural testing purely to derive empirical formulations.

2. Moment rotation simulation

2.1. Tension stiffening simulation for steel and NSM reinforcements

In an uncracked RC beam, the steel reinforcements and concrete would extend uniformly when load is applied. When flexural cracks have formed on the beam, imperfect bond between the steel reinforcement and concrete would cause the steel to slip from the concrete, such that the steel stress would no longer be uniform along the beam. Similarly, any NSM reinforcement would also slip from the adjacent concrete. The load-slip (P/δ) relationship of the reinforcements can be used to simulate the formation of new flexural cracks as well as the tension stiffening [17,25].

The P/δ of steel and NSM reinforcements can be quantified through a numerical analysis performed on prisms made of a single reinforcement with adjacent concrete as shown in Fig. 1. The

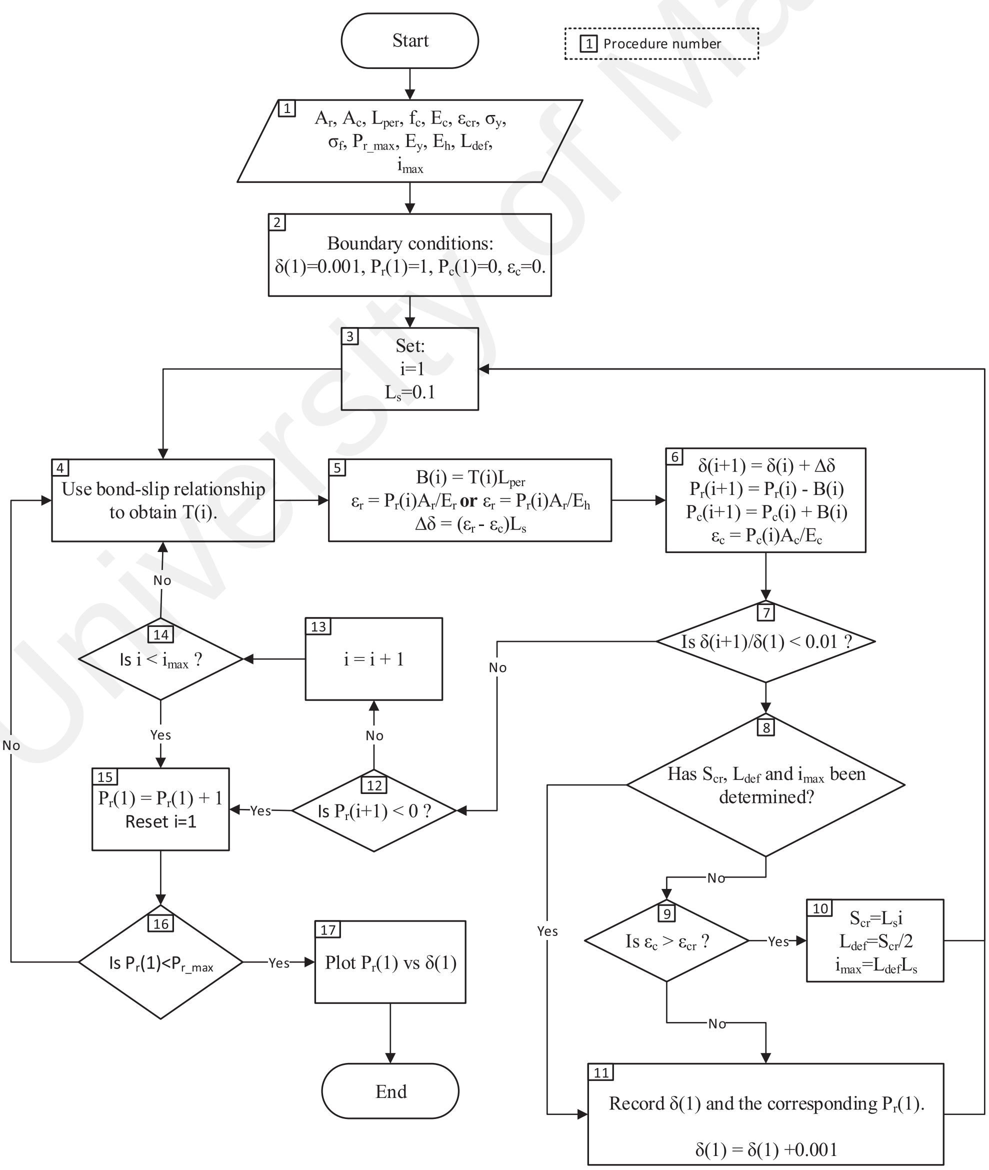

Fig. 2. Tension stiffening analysis procedure to determine the crack spacing and load-slip relationship for steel or NSM reinforcements.

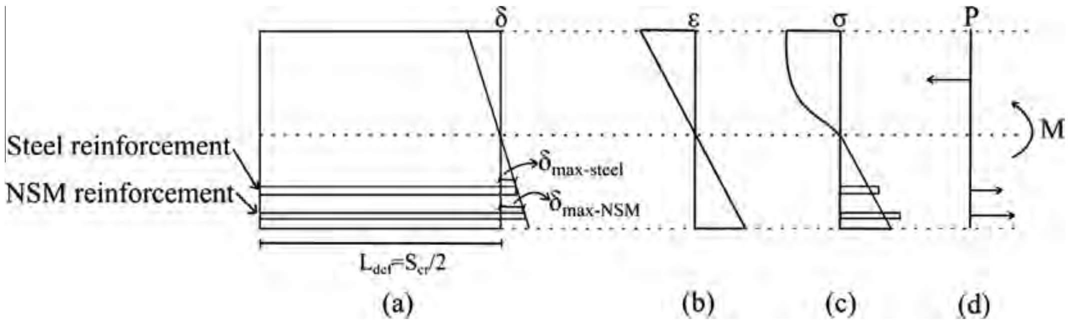

Fig. 3. Moment-rotation analysis of beam section. (a) Beam section of length L_{def} and deformation profile; (b) Strain profile; (c) Stress profile; (d) Forces acting on the beam section.

reinforcement is placed at the middle of the prism, such that when load is applied no moment is induced. The numerical analysis is performed by assuming a value of load for a certain value of slip. The load applied to the steel reinforcement causes strain on the steel reinforcement (ε_r), as shown in Fig. 1(e). The strain is gradually reduced as the bond stress (τ), as shown in Fig. 1(d) transfers the load to the surrounding concrete. As the strain is steel is reduced, it causes the slip to gradually reduce as well, as shown in Fig. 1(c). The assumed load is then adjusted until the slip is reduced to zero.

Additionally, the formation of primary cracks can be predicted using the numerical analysis as new cracks can be assumed to form when the load transferred to the concrete reaches the tensile strength of the concrete, as shown in Fig. 1(a), where S_{cr} is the crack spacing. Due to the formation of the primary cracks, the area of the prism required for the numerical analysis can now be reduced to only L_{def} as shown in Fig. 1(b), where $L_{def} = S_{cr}/2$. Due to the symmetry of forces, the slip would tend to be zero between the flexural cracks, as shown in Fig. 1(c). The numerical analysis for L_{def} can be applied to both steel and NSM reinforcements to obtain a P/δ relationship.

The spacing between cracks, S_{cr}, can be assumed to be identical along beams with a moment gradient [17] applied on it, which is usually the case. As such the simulation of debonded sections would also be done on beam section of length L_{def}. However due to the concrete cover separation, there is less concrete area surrounding the steel reinforcement, as shown in Fig. 1(b). This results in the P/δ relationship of steel reinforcement in the debonded beam section to be slightly stiffer compared to the beam sections that are still strengthened by NSM reinforcements.

The tension stiffening analysis procedure is similar for steel reinforcement, steel reinforcement in the debonded area and NSM reinforcement where the tension stiffening prism is first discretised into small elements of length L_s and the stresses and strains acting on each element is solved numerically. The difference between the three are in the material properties, size of adjacent concrete area and the bond stress-slip model that is to be used. The numerical procedure for the tension stiffening analysis is presented here, along with a flowchart in Fig. 2:

1. The required input data are inserted:
   a. Area of steel/NSM reinforcement, A_r.
   b. Area of adjacent concrete, A_c. It should be noted that steel reinforcements in the debonded section would have a smaller adjacent concrete area compared to steel reinforcements in non-debonded areas, as shown in Fig. 1(b).

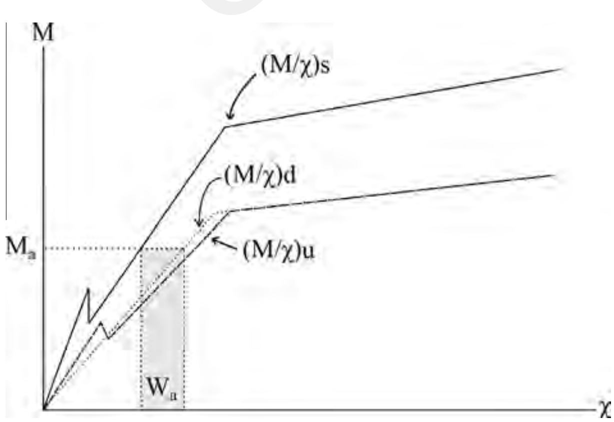

Fig. 4. M/χ of strengthened, unstrengthened and debonded RC beam sections.

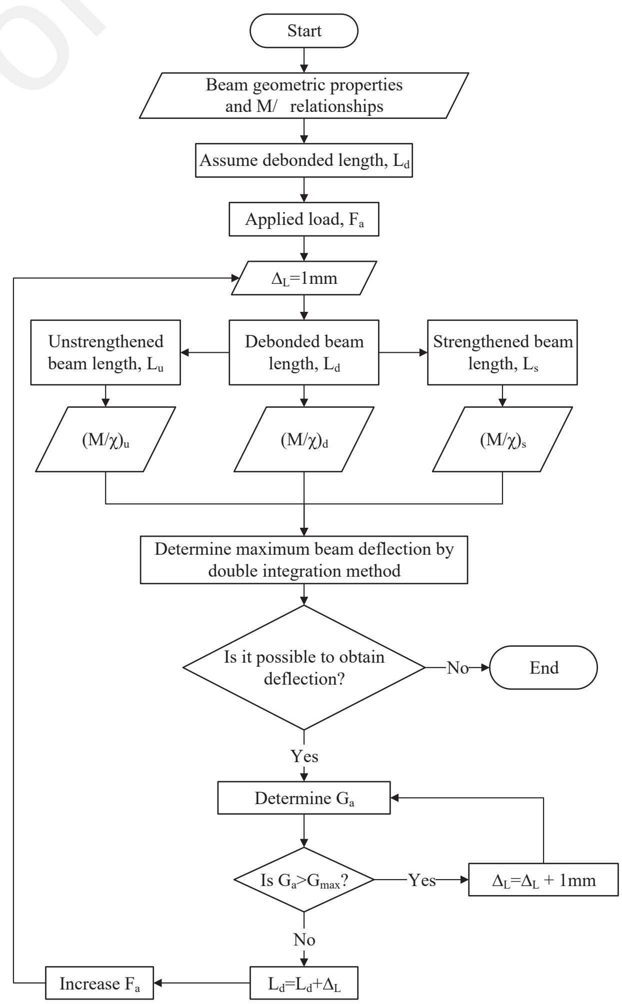

Fig. 5. Flowchart for determining the load-deflection of NSM strengthened beams.

c. Perimeter of steel/NSM reinforcement, L_{per}.
d. Concrete compressive strength, f_c.
e. Concrete elastic modulus, E_c.
f. Concrete cracking strain, $\varepsilon_{cr} = f_t/E_c$.
g. Yield strength of steel/NSM reinforcement (if applicable), σ_y.
h. Ultimate strength of steel/NSM reinforcement, σ_f.
i. Ultimate load of steel/NSM reinforcement, $P_{r\_max} = A_r\sigma_f$
j. Elastic modulus of steel/NSM reinforcement, E_y.
k. Strain hardening modulus of steel/NSM reinforcement (if applicable), E_h.
l. Length of deformation, $L_{def} = S_{cr}/2$.

2. The boundary conditions are used are:
   a. The slip at the crack face, $\delta(1)$=0.001 mm.
   b. Load applied on the adjacent concrete, $P_c(1)$=0 as the concrete-concrete interfaces are not touching at the crack face.
   c. Load applied on steel reinforcement, $P_r(1)$ is assumed to be 1 N.
3. The variable i = 1 is used to determine the location of crack face, and larger values of i is the distance from the crack face. The length of one element, L_s = 0.1 mm.
4. Bond stress, T(i) is determined using the bond stress-slip relationship from CEB-FIP model code for steel reinforcements or using any suitable bond stress-slip model by for NSM reinforcements.
5. The bond force is determined as $B(i) = T(i)L_{per}$. Strain of steel/NSM reinforcement is determined as $\varepsilon_r = P_r(i)A_r/E_r$. The change in slip is then determined as $\Delta\delta = (\varepsilon_r - \varepsilon_c)L_s$.
6. With the value of B(i) and $\Delta\delta$ determined, the values of boundary conditions for the next beam element can be calculated:
   a. $\delta(i+1) = \delta(i) + \Delta\delta$
   b. $P_r(i+1) = P_r(i) - B(i)$

Table 1
Details of NSM strengthened RC beams.

Ref	Beam designation	b (mm)	d (mm)	L (mm)	L_a (mm)	M_{NSM}	N_{NSM}	FM
[22]	A2	125	250	2000	50	CFRP bar	1	CCS
[28]	CRD-NSM	200	300	3000	150	CFRP bar	1	ID
[29]	A9	100	180	2000	0	CFRP bar	1	CCS
[30]	F2C1	160	280	2400	200	CFRP bar	2	CCS
[31]	B21	150	300	1800	50	CFRP bar	2	CC
[32]	B11	150	300	1800	50	CFRP bar	1	CCS
[31]	BS-NP-R	200	400	5000	310	CFRP strip	1	CCS
[33]	NSM S2	120	170	900	50	CFRP strip	2	CCS
[34]	NSM_c_2 1.4 10_1	120	160	2100	100	CFRP strip	2	CDCD
[34]	NSM_c_3 1.4 10_1	120	160	2100	100	CFRP strip	3	CCS
[35]	NSM2	125	250	2000	50	Steel bar	1	F
[35]	NSM3	125	250	2000	50	Steel bar	1	F
[36]	NS8	125	250	2000	50	Steel bar	2	CCS
[36]	NS10	125	250	2000	50	Steel bar	2	CCS
[6]	RW1S	150	200	2000	0	Steel bar	1	CC
[6]	RW1Ø14S	150	200	2000	0	Steel bar	1	CC
[30]	F2G1	160	280	2400	200	GFRP bar	1	CS
[30]	F1G2	160	280	2400	200	GFRP bar	2	ID
[6]	RW1F	150	200	2000	0	GFRP bar	1	F
[5]	B1	150	200	1500		GFRP bar	2	CC

b = width of beam; d = depth of beam; L = length of beam; L_a = distance of NSM to the nearest support; M_{NSM} = material for NSM reinforcement; N_{NSM} = number of NSM reinforcement bar/strip; FM = failure mode; CCS = concrete cover separation; ID = interfacial debonding; CC = concrete crushing; CDCD = critical diagonal crack debonding; F = fracture of NSM reinforcement; CS = concrete splitting.

Table 2
Reinforcement details.

Ref	Beam designation	f_c (N/mm^2)	E_y (N/mm^2)	σ_y (N/mm^2)	E_f (N/mm^2)	σ_f (N/mm^2)
[22]	A2	35.63	200,000	520	165,000	2400
[28]	CRD-NSM	31.3	200,000	426	121,420	1878
[29]	A9	33.6 (cube)	200,000	441	109,000	1020
[30]	F2C1	30.5	200,000	540	170,000	2350
[31]	B21	34.4	200,000	340	170,000	2629
[32]	B11	34.4	200,000	340	170,000	2629
[31]	BS-NP-R	41.5	200,000	438	124,000	2068
[33]	NSM S2	52.2	200,000	788	158,800	2740
[34]	NSM_c_2 1.4 10_1	21 (cube)	200,000	540	171,000	2052
[34]	NSM_c_3 1.4 10_1	21 (cube)	200,000	540	171,000	2052
[35]	8 mm	40 (cube)	200,000	550	200,000	379
[35]	10 mm	41 (cube)	200,000	550	200,000	520
[36]	8 mm × 2	42 (cube)	200,000	550	200,000	379
[36]	10 mm × 2	43 (cube)	200,000	550	200,000	520
[6]	RW1S	36.6	200,000	408	200,000	408
[6]	RW1Ø14S	36.6	200,000	408	200,000	550
[30]	F2G1	30.5	200,000	540	64,000	1350
[30]	F1G2	30.5	200,000	540	64,000	1350
[6]	RW1F	36.6	200,000	408	40,000	743
[5]	B1	45	200,000	500	40,800	760

f_c = concrete strength (cylinder); E_y = steel elastic modulus; σ_y = steel yield strength; E_f = FRP modulus; σ_f = FRP tensile strength.

c. $P_c(i+1) = P_c(i) + B(i)$
d. $\varepsilon_c = P_c(i+1)A_c/E_c$

7. The condition for full-interaction used is the reduction of slip such that $\delta(i+1)/\delta(1) < 0.01$, which represents a 99% reduction from the original slip value at the crack face.
8. If condition in procedure 7 is met, the assumed value of applied load $P_r(1)$ is correct. Another condition is checked, which is whether S_{cr}, L_{def} and i_{max} has been determined.
9. If the condition in procedure 8 is met, then the condition $\varepsilon_c > \varepsilon_{cr}$ is checked.
10. If the condition in procedure 9 is met then a primary crack is considered to have formed. The analysis is now limited to half the length of deformation, L_{def}, by limiting the number of elements in the analysis:
    a. $S_{cr} = L_s i$
    b. $L_{def} = S_{cr}/2$
    a. Maximum number of elements, $i_{max} = L_{def}L_s$.
11. If the condition in either procedure 8 or 9 are not met, the slip $\delta(1)$ and the corresponding $P_r(1)$ is then recorded and a larger value of $\delta(1)$ is set. The analysis is then repeated starting from procedure 2.
12. If the condition in procedure 7 is not met, the location of full-interaction is still not met and another condition is checked, which is $P_r(i+1) < 0$.
13. If the condition in procedure 12 is also not met, the analysis will be repeated for the next beam element and the dummy variable i is increased by 1.
14. If the primary crack has formed, another condition is then checked, which is $i < i_{max}$ since the formation of primary cracks have limited the beam sections that are under partial interaction to the length of deformation, L_{def}. If the primary crack has not formed, then this procedure can be ignored.
15. If the condition in either procedure 12 or 14 are met, the assumed value of applied load $P_r(1)$ is too low and a higher value of $P_r(1)$ is thus assumed.
16. The new $P_r(1)$ is checked whether it reaches or exceeds the ultimate load P_{r_max}. If the condition is not met, procedure 4–15 is repeated.
17. If the condition in procedure 16 is met, the steel/NSM reinforcement has fractured. The recorded values of $\delta(1)$ and $P_r(1)$ are then plotted to obtain the load-slip relationship and the analysis is ended.

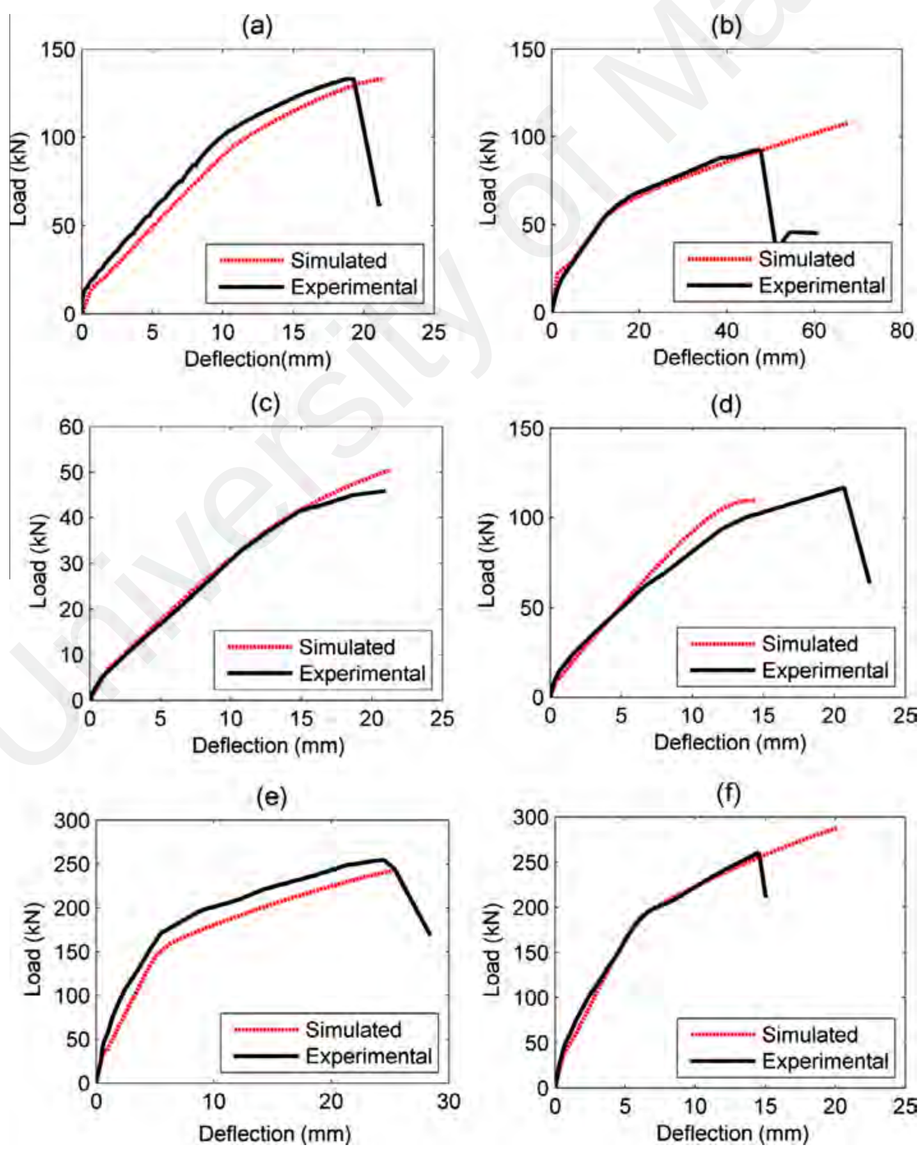

Fig. 6. Comparison of simulated and experimental load-deflection curves for beams strengthened with NSM CFRP bars (a) Beam A2; (b) Beam CRD-NSM; (c) Beam A9; (d) Beam F2C1; (e) Beam B21; (f) Beam B11.

2.2. Moment-rotation of RC beam segment

The M/θ analysis is done by applying a moment M on the beam section of length L_{def}, as shown in Fig. 3. The moment causes a rotation to occur on the beam section, resulting in a deformation profile as shown in Fig. 3(a), with a strain profile as shown in Fig. 3(b). Prior to flexural cracking, the concrete and all reinforcements are extended uniformly in the tensile region of the beam. Hence the stresses of the beam, as shown in Fig. 3(c) can be determined directly from the materials' stress-strain relationships. Once the flexural cracking occur, imperfect bond between the reinforcements and concrete causes the reinforcements to slip from the concrete, such that the strains along the beam section is no longer linear. In this case, the P/δ relationship obtained from then tension stiffening analysis is used to directly obtain the forces acting on the reinforcements, as shown in Fig. 3(d) based on the slip values $\delta_{max\text{-}steel}$ and $\delta_{max\text{-}NSM}$ obtained from the deformation profile in Fig. 3(a).

The stress acting on the concrete is the compression zone can be determined from any suitable concrete stress-strain relationship. However, it has been shown that size of concrete can affect the stress-strain relationship. To obtain an accurate value of stress, the size-dependent stress-strain method as proposed by Chen et al. [27] can be used to adjust the stress-strain relationship to suit the size of the beam section, L_{def}.

The depth of neutral axis is adjusted until the forces acting on the beam are in equilibrium. With the forces in equilibrium, the actual value of the moment M is then determined. The process is then repeated for another value of rotation to obtain the M/θ relationship. The rotation can then be simply be divided by L_{def} to obtain the curvature, χ, hence giving the M/χ relationship.

There are three types of M/χ needed:

1. $(M/\chi)_s$, which is the moment-curvature of the strengthened section of the beam.
2. $(M/\chi)_u$, which is the moment-curvature of the unstrengthened section of the beam.
3. $(M/\chi)_d$, which is the moment-curvature of the debonded section of the beam. The P/δ relationship of the steel reinforcement uses the reduced concrete section area shown in Fig. 1(b) to account for concrete cover separation.

2.3. Simulation of load-deflection and concrete cover separation

Based on the GEBA, it is assumed that there would always be a crack forming at the end of the strengthening reinforcement [14–16]. It was proposed by Achintha and Burgoyne [15] for the initial length of this crack be assumed to be the same as the depth of the concrete cover, c. The energy balance of the beam is then calculated to determine whether there is enough energy for this crack to propagate and cause debonding failure. To determine the available energy, consider Fig. 4, which shows the general shape of M/χ curves obtained using the M/θ analysis.

From Fig. 4, both $(M/\chi)_s$ and $(M/\chi)_u$ have a sharp change in stiffness due to concrete cracking. On the other hand, the debonded sections of the beam already have experienced flexural cracking prior to the debonding. As such the concrete cracking is absent from $(M/\chi)_d$. Additionally, due to the tension stiffening analysis of the steel reinforcement of the debonded section having a smaller concrete area for the beam section length L_{def}, the $(M/\chi)_d$ have a slightly higher stiffness compared to $(M/\chi)_u$.

When the debonding crack propagates, the process is assumed to instantaneously, such that the applied moment, M_a, remains the same as the beam changes from the strengthened condition of $(M/\chi)_s$ to the debonded condition of $(M/\chi)_d$. From the moment M_a, the available energy for crack propagation is the shaded area between $(M/\chi)_s$ and $(M/\chi)_d$.

The energy release rate, Ga is determined as:

$$G_a = \frac{W_a}{b \times \Delta_L}$$

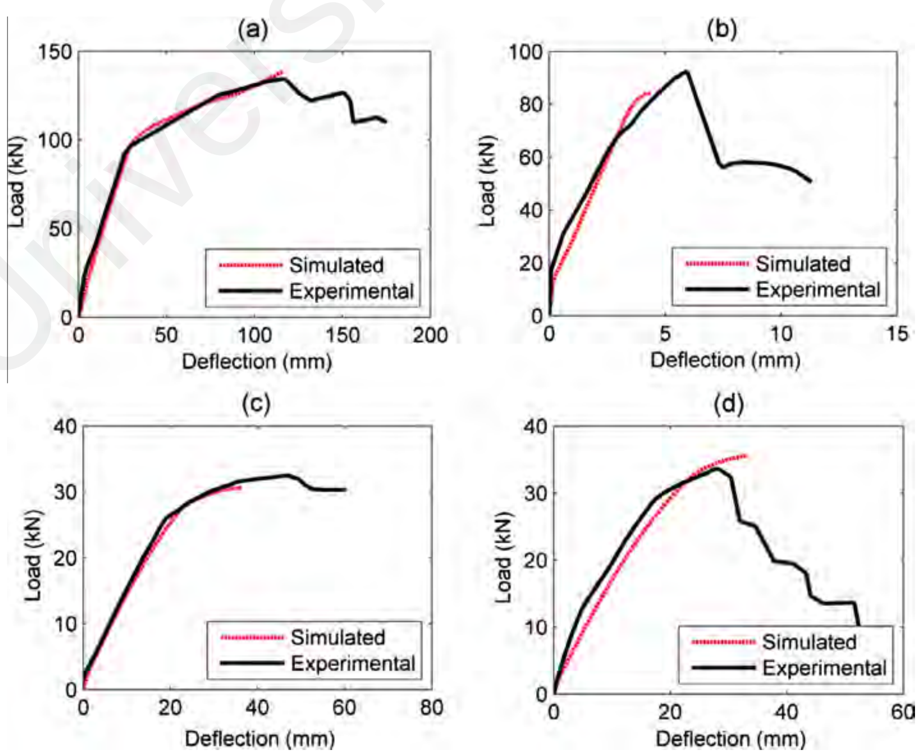

Fig. 7. Comparison of simulated and experimental load-deflection curves for beams strengthened with NSM CFRP strips (a) Beam BS-NP-R; (b) Beam NSM S2; (c) Beam NSM_c_2 × 1.4 × 10_1; (d) Beam NSM_c_3 × 1.4 × 10_1.

where b is the width of debonding crack and Δ_L is the change in debonding crack length. The value of b is taken as the total width of the prism used in the tension stiffening simulation for NSM reinforcement. Further information regarding the size of prism for tension stiffening simulation can be found in [21] and [22].

The process to determine the load-deflection of the beam is presented as a flowchart in Fig. 5. A value of load F_P is set and a debonded length, L_d is assumed in the beginning. Achintha and Burgoyne [15] assumed this length to be equal to the depth of the concrete cover of the beam. The Δ_L is taken as 1 mm. The deflection determined from the $(M/\chi)_s$, $(M/\chi)_d$ and $(M/\chi)_u$ using the double integration method. The $(M/\chi)_s$ and $(M/\chi)_d$ is then used to determine the G_a at the end of the debonded length and this value is compared against the energy required to fracture a unit area of concrete, G_{max}. If $G_a > G_{max}$, the Δ_L is increased by 1 mm. The value of G_a is then calculated again, and this procedure is repeated until the value of Δ_L is large enough such that $G_a < G_{max}$. The new debonded beam length L_d is then determined as $L_d = L_d + \Delta_L$. The whole process is then repeated for a higher applied load, F_a. At some point it is no longer possible to determine the value of deflection as the applied moment Ma is beyond the range of moment in $(M/\chi)_d$. The failure load has then been reached and the beam has suffered debonding failure.

3. Validation of moment rotation simulation

3.1. Beam details

The proposed simulation of NSM strengthened beam was validated a database of 20 NSM strengthened RC beams [22,28–36,6,5]. All the beams are rectangular NSM strengthened RC beams designed to fail by flexure. The details of the beams are given in Table 1. The beams were strengthened with either NSM carbon FRP (CFRP) bars, NSM CFRP strips, NSM steel bars or NSM glass FRP (GFRP) bars to check whether the proposed method is able to correctly simulate the behaviour of beams strengthened with various types of NSM reinforcements. Further details on the reinforcements used on the beams is provided in Table 2.

3.2. Material models

While the M/θ technique is able to simulate the mechanics of RC beams without empirical formulations, the material properties still require empirical models to be simulated. Several material models were used in this research.

The bond stress-slip model by CEB-FIP [37] was used for steel reinforcements. For NSM CFRP bars, NSM GFRP bars and NSM steel

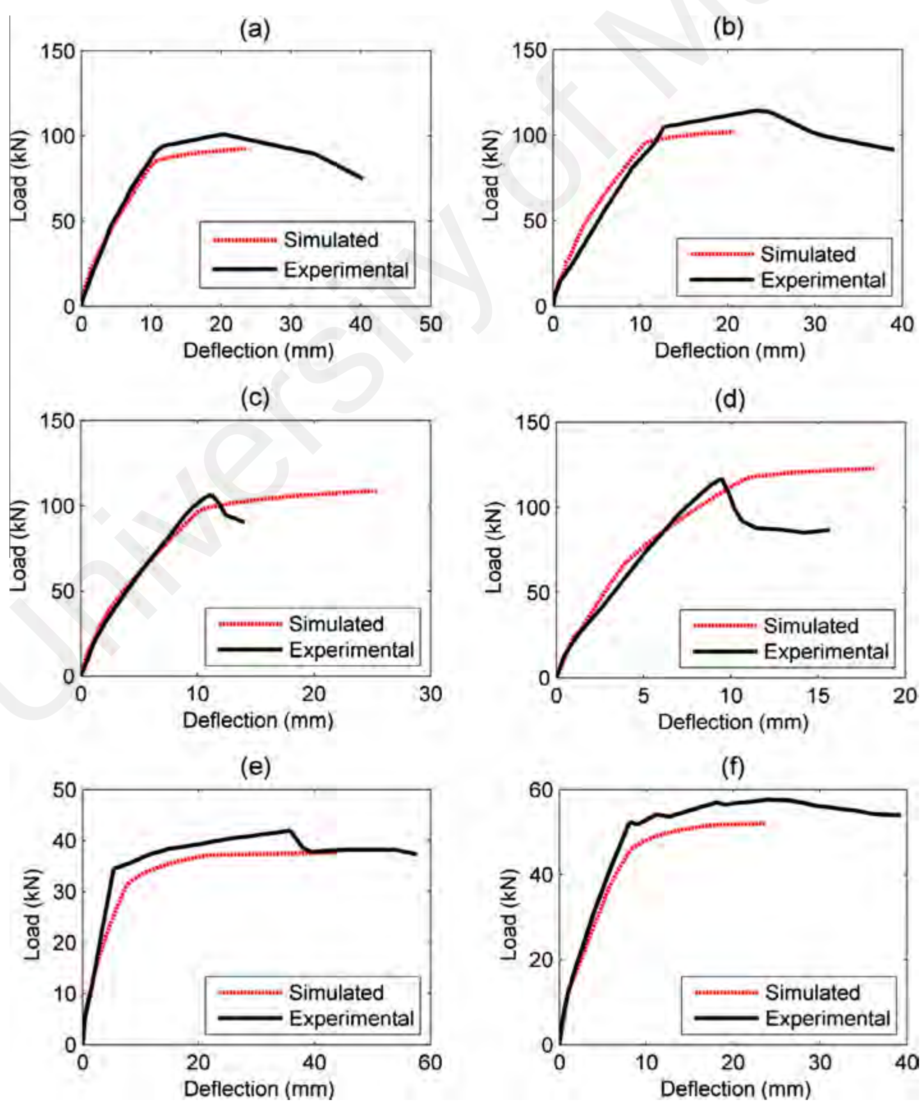

Fig. 8. Comparison of simulated and experimental load-deflection curves for beams strengthened with NSM steel bars (a) Beam NSM2; (b) Beam NSM3; (c) Beam NS8; (d) Beam NS10; (e) Beam RW1S; (f) Beam RW1Ø14S.

bars the bond stress-slip model by De Lorenzis [38] was used. For the CFRP strips, the bond stress-slip model by Zhang et al. [39] was used. The stress-strain model by Popovics [40] was used to create the size-dependent stress-strain relationship for concrete. The fracture energy model by CEB-FIP [37] was used to obtain G_{max}.

3.3. Results and discussion

Comparisons of the simulated and experimental load-deflection for beams strengthened with NSM CFRP bars, NSM CFRP strips, NSM steel bars and NSM GFRP are shown in Figs. 6–9, respectively. It can be seen that the experimental load-deflection curves and the load-deflection curves simulated using the proposed method are in good agreement with each other, which shows that the tension stiffening of the beams were simulated correctly.

A summary of the simulated and experimental load-deflection curves is given in Table 3. The proposed method was able to correctly simulate the failure mode for a large number beams. It should be noted however that the method proposed in this paper does not take into account failures by interfacial debonding and

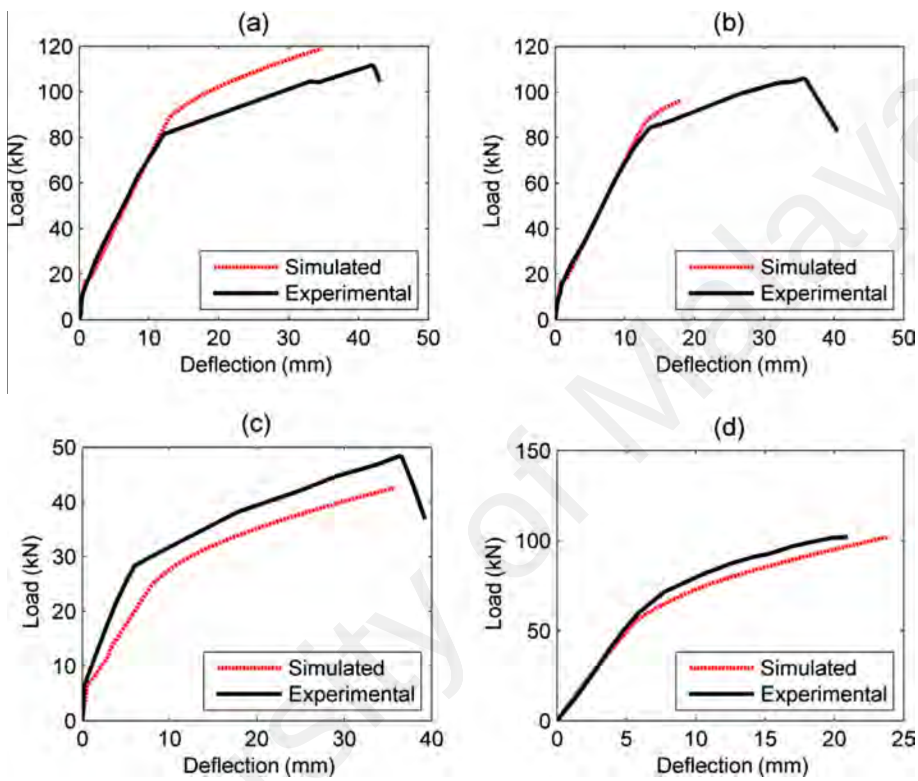

Fig. 9. Comparison of simulated and experimental load-deflection curves for beams strengthened with NSM GFRP bars (a) Beam F2G1; (b) Beam F1G2; (c) Beam RW1F; (d) Beam B1.

Table 3
Summary of simulated and experimental load-deflection curves.

Ref	Beam designation	P_s	P_e	P_s/P_e	δ_s	δ_e	δ_s/δ_e	FM	SFM
[22]	A2	133	133.232	1.00	21.42	19.274	1.11	CCS	CCS
[28]	CRD-NSM	107.8	92.87	1.16	67.59	47.67	1.42	ID	CCS
[29]	A9	50.4	45.7764	1.10	21.23	20.95	1.01	CCS	CCS
[30]	F2C1	109.6	116.796	0.88	14.46	20.68	0.70	CCS	CCS
[31]	B21	288	260.852	1.10	20.17	14.55	1.39	CC	CCS
[32]	B11	243.4	255.266	0.95	25.39	24.41	1.04	CCS	F
[31]	BS-NP-R	138.6	134.67	1.03	116.38	117.39	0.99	CCS	CCS
[33]	NSM S2	84	92.58	0.91	4.38	5.94	0.74	CCS	CCS
[34]	NSM_c_2 1.4 10_1	30.62	32.51	0.94	36.38	47.07	0.77	CDCD	CCS
[34]	NSM_c_3 1.4 10_1	35.6	33.7	1.06	33.2	28.04	1.18	CCS	CCS
[35]	8 mm	92.4	101.05	0.91	23.52	20.27	1.16	F	F
[35]	10 mm	102	114.29	0.89	20.88	23.14	0.90	F	F
[36]	8mmx2	108.6	106.31	1.02	25.4	11.24	2.26	CCS	CCS
[36]	10mmx2	122.6	116.83	1.05	18.18	9.47	1.92	CCS	CCS
[6]	RW1S	38.2	41.97	0.91	45.9	35.79	1.28	CC	F
[6]	RW1Ø14S	52	53.96	0.96	23.63	39.29	0.60	CC	F
[30]	F2G1	118.6	111.84	1.06	34.65	42.12	0.82	CS	F
[30]	F1G2	96	106.19	0.90	17.94	35.8	0.50	ID	CCS
[6]	RW1F	42.6	48.49	0.88	35.86	36.52	0.98	F	F
[5]	B1	102	102.13	1.00	23.86	20.93	1.14	CC	F

P_s = simulated failure load; P_e = experimental failure load; δ_s = simulated failure deflection; δ_e = experimental failure deflection; FM = failure mode; CCS = concrete cover separation; ID = interfacial debonding; CC = concrete crushing; CDCD = critical diagonal crack debonding; F = fracture of NSM reinforcement; CS = concrete splitting; SFM = simulated failure load.

critical diagonal crack debonding and so could not predict these failures, although the study by Oehlers et al. [21] on simulating interfacial debonding and critical diagonal crack debonding for FRP plated RC beams can perhaps be used as a reference for simulating these debonding types on NSM strengthened RC beams. Additionally, the failure mode obtained for several beams was fracture of NSM reinforcement rather than concrete crushing as reported. These beams were strengthened by either NSM steel bars or NSM GFRP bars, which may reflect that the bond stress-slip model chosen to simulate them was not accurate enough, causing the simulated strain in the NSM steel bars and NSM GFRP bars to be higher than it should be.

The simulated and actual failure loads are reasonably close for most of the beams, as illustrated in Fig. 10. The mean of the ratio between the simulated and experimental failure load is 0.9896, with a standard deviation of 0.0862. The comparison of the simulated and experimental failure deflection, as shown in Fig. 11, however, shows a lot of discrepancy. The ratio of the simulated and experimental deflection at failure has a mean of 1.072 with a significantly high standard deviation of 0.4374. The highest discrepancy between simulated and experimental deflection at failure can be observed in load-deflection curves of beams strengthened with NSM steel bars. This problem is attributed to the bond stress-slip model used, which was originally meant for NSM FRP bars. While the bond stress-slip model is able to simulate the tension stiffening with good accuracy, the simulated strain of the NSM steel may not be correct, causing the discrepancy between simulated and experimental deflection at failure.

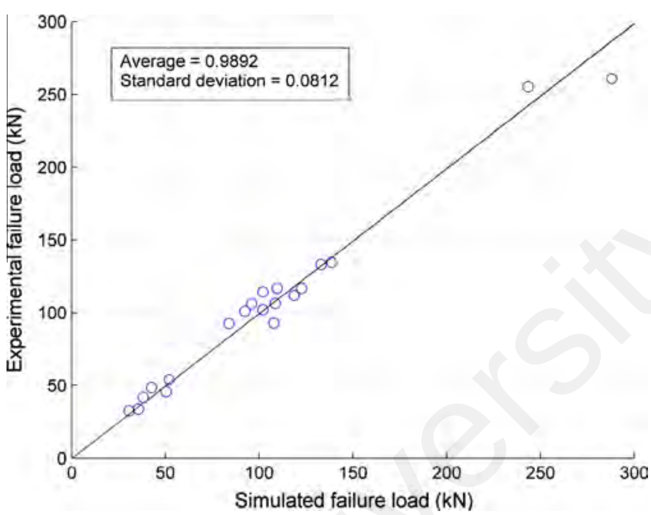

Fig. 10. Comparison of simulated and experimental failure load.

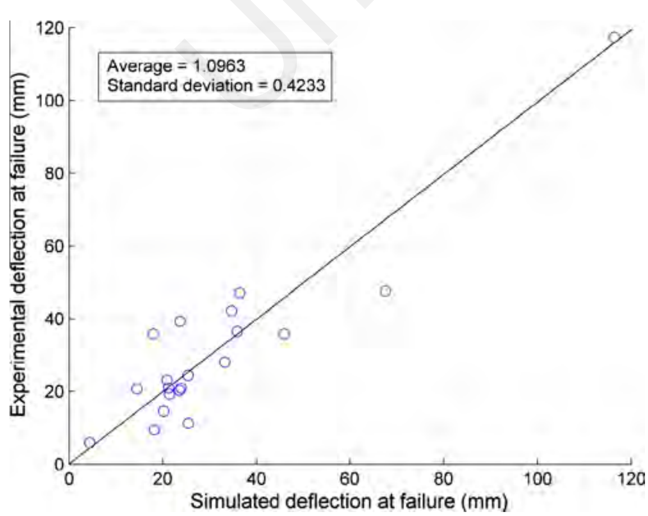

Fig. 11. Comparison of simulated and experimental deflection at failure.

4. Conclusion

From this study, the following conclusions were made:

- The combination of M/θ technique and the GEBA is able to simulate the load-deflection behaviour of NSM strengthened RC beams and simulate the concrete cover separation mode with considerable accuracy and with less reliance on empirical formulations.
- By allowing the debonding crack to propagate up to the point where the beam can no longer accept additional load nor maintain the current load, a more accurate failure load can be obtained.
- As the method presented is less reliant on empirical formulations, it should be possible to apply the same method to other types of FRP materials not used in the validation in this paper; however in cases where new types of FRP materials are used, the bond stress-slip relationship for these material should be studied first in order to ensure good accuracy when using the M/θ technique.

Acknowledgments

Financial support from the University of Malaya, Grand Challenge – SUS (Sustainability Science) Grant, project number GC003A-15SUS is gratefully acknowledged.

Reference

[1] Y.A. Al-Salloum, Influence of edge sharpness on the strength of square concrete columns confined with FRP composite laminates, Compos. Part B Eng. 38 (2007) 640–650.
[2] F. Ceroni, M. Pecce, S. Matthys, L. Taerwe, Debonding strength and anchorage devices for reinforced concrete elements strengthened with FRP sheets, Compos. Part B Eng. 39 (2008) 429–441.
[3] E. Esmaeeli, Ja.O. Barros, Flexural strengthening of RC beams using Hybrid Composite Plate (HCP): experimental and analytical study, Compos. Part B Eng. 79 (2015) 604–620.
[4] I.M.I. Qeshta, P. Shafigh, M.Z. Jumaat, Flexural behaviour of RC beams strengthened with wire mesh-epoxy composite, Constr. Build. Mater. 79 (2015) 104–114.
[5] R. Capozucca, On the strengthening of RC beams with near surface mounted GFRP rods, Compos. Struct. 117 (2014) 143–155.
[6] T.H. Almusallam, H.M Elsanadedy, Y.a Al-Salloum, S.H. Alsayed, Experimental and numerical investigation for the flexural strengthening of RC beams using near-surface mounted steel or GFRP bars, Constr. Build. Mater. 40 (2013) 145–161.
[7] K.M.U. Darain, M.Z. Jumaat, M.A. Hossain, M.A. Hosen, M. Obaydullah, M.N. Huda, et al., Automated serviceability prediction of NSM strengthened structure using a fuzzy logic expert system, Expert Syst. Appl. 42 (2015) 376–389.
[8] A. Hosen, M.Z Jumaat, A.B.M.S. Islam, Inclusion of CFRP-epoxy composite for end anchorage in NSM-epoxy strengthened beams, Adv. Mater. Sci. Eng. (2015).
[9] M.A. Hosen, M.Z. Jumaat, Islam a. BMS. Side Near Surface Mounted (SNSM) technique for flexural enhancement of RC beams, Mater. Des. 83 (2015) 587–597.
[10] S.S. Zhang, J.G. Teng, Finite element analysis of end cover separation in RC beams strengthened in flexure with FRP, Eng. Struct. 75 (2014) 550–560.
[11] Lorenzis L. De, A. Nanni, Proposed design procedure of NSM FRP reinforcement for strengthening of RC beams, in: Proc. 6th Int. Symp. Frp. Reinf. Concr. Struct. Singapore, 2003. 1455–1.
[12] F. Al-Mahmoud, A. Castel, R. François, C. Tourneur, RC beams strengthened with NSM CFRP rods and modeling of peeling-off failure, Compos. Struct. 92 (2010) 1920–1930.
[13] J.G. Teng, S.S. Zhang, J.F. Chen, Strength model for end cover separation failure in RC beams strengthened with near-surface mounted (NSM) FRP strips, Eng. Struct. 110 (2016) 222–232.

[14] G.X. Guan, C.J. Burgoyne, Comparison of moment-curvature models for fiber-reinforced polymer plate-end debonding studies using global energy balance approach, ACI Struct. J. 111 (2014) 27–36.
[15] M. Achintha, C.J. Burgoyne, Fracture mechanics of plate debonding: validation against experiment, Constr. Build. Mater. 25 (2011) 2961–2971.
[16] M. Achintha, C. Burgoyne, Fracture energy of the concrete-FRP interface in strengthened beams, Eng. Fract. Mech. 110 (2013) 38–51.
[17] P. Visintin, D.J. Oehlers, C. Wu, M. Haskett, A mechanics solution for hinges in RC beams with multiple cracks, Eng. Struct. 36 (2012) 61–69.
[18] D.J. Oehlers, P. Visintin, M. Haskett, W.M. Sebastian, Flexural ductility fundamental mechanisms governing all RC members in particular FRP RC, Constr. Build. Mater. 49 (2013) 985–997.
[19] D. Knight, P. Visintin, D.J. Oehlers, M.S. Mohamed Ali, Simulation of RC beams with mechanically fastened FRP strips, Compos. Struct. 114 (2014) 99–106.
[20] D. Knight, P. Visintin, D.J. Oehlers, M.S. Mohamed Ali, Simulating RC beams with unbonded FRP and steel prestressing tendons, Compos. Part B Eng. 60 (2014) 392–399.
[21] D.J. Oehlers, P. Visintin, D. Ph, W. Lucas, D. Ph, Flexural strength and ductility of FRP-plated RC beams: fundamental mechanics incorporating local and global IC debonding, J. Compos. Constr. (2015). 04015046.
[22] A.A. Shukri, K.M.U. Darain, M.Z. Jumaat, The tension-stiffening contribution of NSM CFRP to the behavior of strengthened RC beams, Materials 8 (2015) 4131–4146.
[23] K.H. Mo, P. Visintin, U.J. Alengaram, M.Z. Jumaat, Prediction of the structural behaviour of oil palm shell lightweight concrete beams, Constr. Build. Mater. 102 (2016) 722–732.
[24] A.K. Gupta, S.R. Maestrini, Tension stiffness model for reinforced concrete bars, J. Struct. Eng. 116 (1990) 769–790.
[25] M. Haskett, D.J. Oehlers, M.S. Mohamed Ali, Local and global bond characteristics of steel reinforcing bars, Eng. Struct. 30 (2008) 376–383.
[26] R. Muhamad, M.S. Mohamed Ali, D. Oehlers, Sheikh.A. Hamid, Load-slip relationship of tension reinforcement in reinforced concrete members, Eng. Struct. 33 (2011) 1098–1106.
[27] Y. Chen, P. Visintin, D.J. Oehlers, U.J. Alengaram, Size-dependent stress-strain model for unconfined concrete, J. Struct. Eng. 140 (2014) 04013088.
[28] W. Jung, Y. Park, J. Park, J. Kang, Y. You, Experimental investigation on flexural behavior of RC beams strengthened by NSM CFRP reinforcements, ACI Spec. Publ. (2005) 795–806.
[29] F. Ceroni, Experimental performances of RC beams strengthened with FRP materials, Constr. Build. Mater. 24 (2010) 1547–1559.
[30] I.A. Sharaky, L. Torres, H.E.M. Sallam, Experimental and analytical investigation into the flexural performance of RC beams with partially and fully bonded NSM FRP bars/strips, Compos. Struct. 122 (2015) 113–126.
[31] G. Wu, Z.-Q. Dong, Z.-S. Wu, L.-W. Zhang, Performance and parametric analysis of flexural strengthening for RC beams with NSM-CFRP bars, J. Compos. Constr. 10 (2013) 04013051.
[32] H.Y. Omran, Effects of severe environmental exposure on Rc beams strengthened with prestressed Nsm-Cfrp strips, Proc. 6th Int. Conf. FRP Compos. Civ. Eng. Rome, Italy (2012) 1–8.
[33] J.a.O Barros, S.J.E. Dias, J.L.T. Lima, Efficacy of CFRP-based techniques for the flexural and shear strengthening of concrete beams, Cem. Concr. Compos. 29 (2007) 203–217.
[34] A. Bilotta, F. Ceroni, E. Nigro, M. Pecce, Efficiency of CFRP NSM strips and EBR plates for flexural strengthening of RC beams and loading pattern influence, Compos. Struct. 124 (2015) 163–175.
[35] A. Hosen, M.Z. Jumaat, K. Mahfuz, U. Darain, M. Obaydullah, A.B.M.S. Islam, Flexural strengthening of RC beams with NSM steel bars, Int. Conf. Food, Agric. Biol. (FAB-2014), Kuala Lumpur (2014) 8–13.
[36] A. Hosen, M.Z. Jumaat, A.B.M.S. Islam, M. Kamruzzaman, N. Huda, M.R. Soeb, Eliminating concrete cover separation of NSM strengthened beam by CFRP end anchorage, Struct. Eng. Mech. 56 (2015).
[37] CEB-FIP, CEB-FIP Model Code 1990, Thomas Telford Ltd, London, UK, 1993.
[38] L. De Lorenzis, Anchorage length of near-surface mounted fiber-reinforced polymer rods for concrete strengthening – analytical modeling, ACI Struct. J. 101 (2004) 375–386.
[39] S.S. Zhang, J.G. Teng, T. Yu, Bond–slip model for CFRP strips near-surface mounted to concrete, Eng. Struct. 56 (2013) 945–953.
[40] S. Popovics, A numerical approach to the complete stress-strain curve of concrete, Cem. Concr. Res. 3 (1973) 583–599.

CHAPTER 4 - APPLICATION I: SIDE-NSM METHOD

This chapter presents two research papers. In this chapter, it will be shown how the simulation method presented in chapter 3 can be applied to reliably simulate the behaviour of RC beams strengthened with the SNSM method and used to perform further studies on the SNSM method.

The first paper, “Behaviour of Precracked RC Beams Strengthened Using the Side-NSM Technique” presents a study on SNSM strengthened RC beams, scpecifically the effect of precracking on SNSM strengthened beams’ behaviour. An experimental study involving seven beams was first conducted, followed by a simulation method based on the M/θ approach was then presented and was found to be reasonably accurate and able to simulate the change in stiffness caused by precracking. It should be noted that the credit for the experimental work goes to the second author, Akter Hosen, while this author’s contribution is mostly in the simulation work using M/θ approach.

The second paper, “Parametric Study for Concrete Cover Separation Failure of Retrofitted SNSM Strengthened RC Beams” presents the method to simulate concrete cover separation failure of SNSM strengthened beams using the M/θ approach and GEBA, where the minor differences involved in the simulation process of normal NSM and SNSM strengthened beams were explained. The proposed method was validated and showed good accuracy results using published experimental results. A parametric study on the concrete cover separation failure of SNSM strengthened beams was then conducted using a simulation method based on the moment-rotation (M/θ) approach. Importantly, this parametric study also discusses the differences between virgin and retrofitted SNSM strengthened beams, the former which represents beams tested in labs and the latter representing beams in real world situations. Among the conclusion of the parametric study are:

- SNSM retrofitted strengthened beams was found to have approximately 3 – 4% lower failure load compared to virgin SNSM strengthened beams when concrete cover separation is a factor.
- In cases where concrete cover separation failure did not occur or less pronounced, the failure load was found higher in SNSM retrofitted beams by up to 1% due to approximately 15 – 19% higher flexural stiffness of retrofitted beams than virgin beams due to longer crack spacing of the retrofitted beams.
- There is only a slight difference in failure load of SNSM retrofitted beams compared to virgin SNSM strengthened beams, although the small difference is negligible.
- There is a considerable difference in the flexural stiffness of virgin and retrofitted beams that should not be neglected.
- It was found that retrofitted and virgin beam conditions do not affect the failure mode of the SNSM strengthened beams.

The details of the research papers contained in this chapter along with the statement of contribution of authors is as follows:

1) Shukri, A. A., Hosen, M. A., Muhamad, R., & Jumaat, M. Z. (2016). Behaviour of precracked RC beams strengthened using the side-NSM technique. *Construction and Building Materials*, *123*, 617–626.
    a. Statement of contribution: Ahmad Azim Shukri (author) performed the simulations and wrote the paper, Akter Hosen (co-author) performed the experimental work and checked the paper, Muhamad Rahimah (co-author)

supervised the research and checked the paper, Mohd. Zamin Jumaat (co-author) supervised the research and checked the paper.

2) Shukri, A. A., Shamsudin, M. F., Ibrahim, Z., & Alengaram, U. J. (2018). Parametric study for concrete cover separation failure of retrofitted SNSM strengthened RC beams. *Mechanics of Advanced Materials and Structures*, 1-12.

   a. Statement of contribution: Ahmad Azim Shukri (author) performed the simulations and wrote the paper, Mohd Fazaulnizam Shamsudin (co-author) wrote and checked the paper, Zainah Ibrahim (co-author) supervised the research and checked the paper, U. Johnson Alengaram (co-author) supervised the research and checked the paper.

4.1 Research paper 2: Behaviour of precracked RC beams strengthened using the side-NSM technique

Published in *Construction and Building Materials*

Article history:

Received 24 November 2015

Received in revised form 29 June 2016

Accepted 15 July 2016

Construction and Building Materials 123 (2016) 617–626

Contents lists available at ScienceDirect

Construction and Building Materials

journal homepage: www.elsevier.com/locate/conbuildmat

Behaviour of precracked RC beams strengthened using the side-NSM technique

A.A. Shukri [a], M.A. Hosen [a], R. Muhamad [b], M.Z. Jumaat [a,*]

[a] Department of Civil Engineering, Faculty of Engineering, University of Malaya, 50603 Kuala Lumpur, Malaysia
[b] Department of Engineering, UTM Razak School of Engineering and Advanced Technology, Universiti Teknologi Malaysia, Jalan Sultan Yahya Petra, 54100 Kuala Lumpur, Malaysia

HIGHLIGHTS

- The effect of precracking on beams strengthened using SNSM method was studied.
- Precracked SNSM beams have higher stiffness compared to non-precracked SNSM beams.
- The failure modes of SNSM strengthened RC beams were not affected by precracking.
- A numerical analysis based on the moment-rotation approach was presented.

ARTICLE INFO

Article history:
Received 24 November 2015
Received in revised form 29 June 2016
Accepted 15 July 2016

Keywords:
Near-surface mounted
Numerical analysis
Partial-interaction
Reinforced concrete
Side-NSM

ABSTRACT

The side near-surface mounted (SNSM) method is an alternative method used for applying fibre reinforced polymer (FRP) flexural strengthening on reinforced concrete (RC) beams. The SNSM method places the FRP grooves at the sides of the beam, rather than at the bottom in the normal near surface mounted (NSM) method. This research focuses on studying the performance of precracked RC beams when strengthened with the SNSM method. Six RC beams strengthened with the side-NSM (SNSM) method were tested in flexure. Precracked SNSM strengthened beams have reduced ultimate load by up to 3.3% and higher stiffness by up to 28.4% compared to non-precracked SNSM strengthened beams. The modes of failure for SNSM strengthened beams was identical for the precracked beams and the equivalent non-precracked beams. A simulation method based on the moment-rotation approach was also presented and was found to be reasonably accurate and able to simulate the change in stiffness caused by precracking.

1. Introduction

Research work on the strengthening of reinforced concrete (RC) structures has been given much attention in the past decades, as the deterioration of older RC structures is becoming more prevalent. Many developing countries have begun applying structural strengthening extensively, especially in Bangladesh following the disaster of the collapse of a garment factory, which caused more than a thousand deaths. Rapid repair work using structural strengthening methods would help prevent the loss of life and help reduce cost by allowing the buildings to remain in use.

For many years, the material of choice for structural strengthening has been fibre reinforced polymer (FRP), due to its high strength, light weight and no risk of corrosion. The flexural strengthening of RC beams with FRP is usually done in two ways; either by externally bonding (EB) the FRP reinforcement onto the beam using epoxy adhesive or by cutting a groove into the concrete cover of the beam and placing the FRP reinforcement into the groove, along with epoxy adhesive. The latter method is called the near-surface mounted (NSM) method.

The NSM method possesses several advantages compared to the EB method. The NSM FRP strengthened beams have been confirmed to possess better durability, fatigue resistance and also stress sharing mechanism compared to the EB FRP strengthened beams, as the FRP reinforcement in the NSM method is embedded into the beam [1]. Various research has also been done to determine the effect of NSM FRP on beams [2–11]. In general, it has been found that the NSM FRP technique increases the flexural strength of beams and reduces premature failure by debonding due to better anchoring of the FRP reinforcement. It should be noted however that premature failure by concrete cover separation is still a problem for NSM strengthened beams.

* Corresponding author.
E-mail addresses: ahmadazimshukri@gmail.com (A.A. Shukri), enggakter@gmail.com (M.A. Hosen), rahimah.kl@utm.my (R. Muhamad), zamin@um.edu.my (M.Z. Jumaat).

http://dx.doi.org/10.1016/j.conbuildmat.2016.07.066
0950-0618/

While in both theory and lab tests the NSM method performs well, it does face some problems in its practical usage. The strengthened beam with the NSM method must have a sufficient width in order to provide a necessary edge clearance and clear spacing between the NSM grooves, the lack of which would cause a higher possibility of premature failure by debonding due to overlapping stresses, localized cover separation and beam edge cover separation [4].

In response to this, a simple solution was proposed by Hosen et al. [12], where instead of placing the NSM reinforcements at the soffit of the beam, they are placed at the beams' sides. The authors called this minor modification as the side-NSM (SNSM) method. The method not only solves the problem of overlapping stresses, also found to increase the resistance of the strengthened beam against the concrete cover separation failure, which is the commonly encountered premature failure mode for NSM strengthened beams.

Hosen et al. [12] focused on testing virgin RC beams strengthened with the SNSM method. This paper aims to further the study by performing experimental work on precracked SNSM strengthened RC beams. Thus any changes to the load-deflection behaviour and failure modes of precracked beams strengthened with SNSM can be determined. A method for simulating the SNSM strengthened RC beams will also be presented in this paper.

2. Experimental programme

2.1. Test matrix and specimen configuration

A total of seven test RC beams were cast and tested, where one of the beams served as a control beam and the rest were strengthened with SNSM method. The reinforcement details are given in Table 1. The designation CB is given to the control beam. Non-precracked strengthened specimens were designated as SNC while precracked specimens were designated as PSNC. The designation of 8, 10 and 12 refers to the diameter of the carbon FRP (CFRP) used in strengthening the specimens (8, 10 and 12 mm).

The specimens dimension and reinforcement details of CB and strengthened beam are shown in Fig. 1(a) and (b) respectively. Also, the details of placing the SNSM bar at beam side is shown in Fig. 1(c). The cross-sectional dimensions of the specimens were 125 mm × 250 mm with a clear cover of 27 mm, and the length of the specimens was 2300 mm, with 2000 mm as the effective span and a shear span of 650 mm. The beams were designed as under reinforced beams to initiate failure in flexure in accordance with the ACI code [13].

Table 1
Test matrix.

Beam designation	Strengthening materials				
	Strengthening material	Diameter (mm)	Number	Bonded length (mm)	Pre-cracking load (kN)
CB	Unstrengthened				–
SNC8	CFRP ribbed bar	8	2	1900	–
SNC10		10			–
SNC12		12			–
PSNC8		8			22.5
PSNC10		10			30
PSNC12		12			37.5

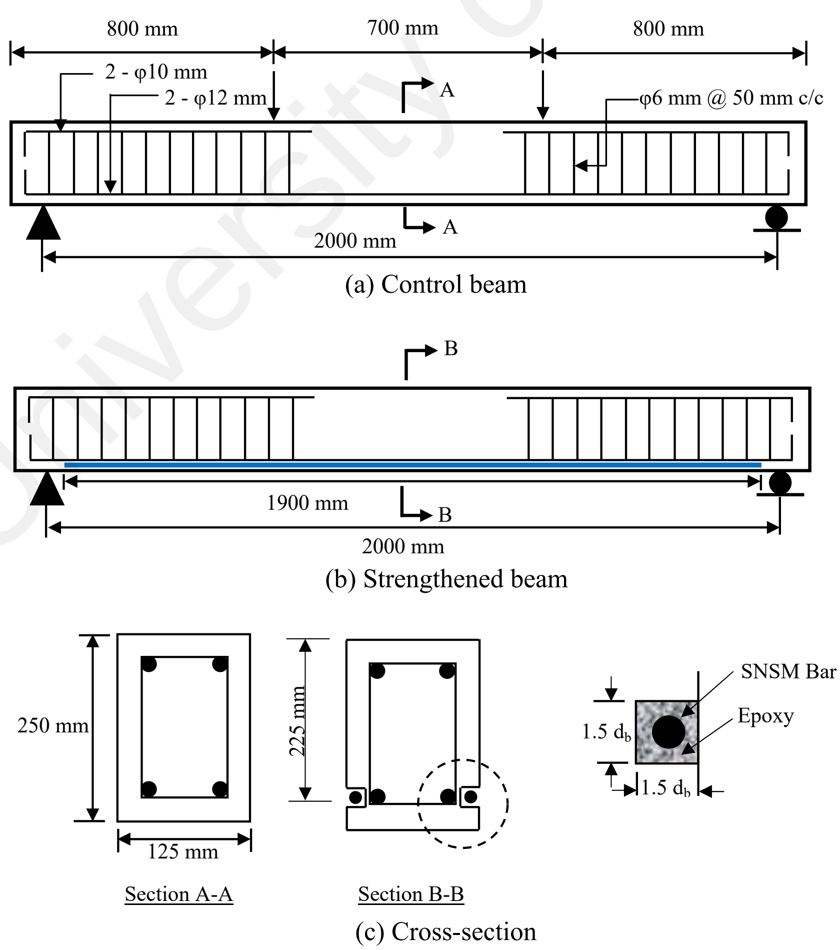

Fig. 1. Specimen design details.

The internal tension reinforcement for all specimens is two deformed steel bars, 12 mm in diameter, which were bent ninety degrees at both ends to fulfil the anchorage criteria. The compression reinforcement was provided by two reinforcement bar with 10 mm diameter deformed bars up to the shear span zone. The shear reinforcement is plain steel bars, 6 mm in diameter, distributed along the length of the specimens but in the unalloyed bending zone; no shear reinforcement was provided to prevent it from influencing crack propagation in the constant moment region.

The process of SNSM strengthening was as follows:

1. Grooves of size 1.5 d_b × 1.5 d_b (where d_b is the diameter of the strengthening bar) were made at the sides of the RC beams using a diamond bladed concrete saw, as shown in Fig. 1(c).
2. A hammer and hand chisel were then used to remove the remaining concrete lugs and to make the groove surface rougher.
3. The grooves were then cleaned with a special wire brush and a high-pressure air jet.
4. The grooves were filled with epoxy up to half the groove height, and a strengthening bar was placed inside each groove.
5. The strengthening bars were then cleaned with acetone to remove any dirt that would interfere with the bonding with the epoxy.
6. The bar was then pressed lightly to ensure the epoxy was in full contact with the surface of the bar.
7. More epoxy was then applied to completely fill the groove and the surface of the epoxy was levelled.
8. A one-week period was given for each specimen to allow the strength of the epoxy to fully develop.

2.2. Material properties

Ordinary Portland Cement (OPC) was used to fabricate the beam, cube and prism specimens. The mix design for the concrete is presented in Table 2. Crushed granite was used as coarse aggregate and the maximum size of the coarse aggregate was 20 mm. Quarry sand was used as fine aggregate. Fresh tap water was used to hydrate the concrete mix during the fabrication and curing of the beam, cube and prism specimens. The 28-day compressive strength, tensile strength and modulus of elasticity of the concrete obtained were 40 MPa, 4.40 MPa and 29.7 GPa, respectively determined using the ASTM C39 [14] and BS EN 12390-22009 [15].

The yield and ultimate strength of all the steel bars were 520 MPa and 570 MPa respectively. The modulus of elasticity for all steel bars was 200 GPa. An epoxy adhesive was used for the

Table 2
Concrete mix design.

Slump (mm)	W/C ratio	Quantity (kg/m^3)			
		Cement	Coarse aggregate	Fine aggregate	Water
45	0.50	420	892	888	224

Table 3
Properties of epoxy adhesive.

Properties	Strength (MPa)
Bond strength	21
Compressive strength	95
Tensile strength	31
Shear strength	19
Modulus of Elasticity	12,800

Fig. 2. Instrumentation and loading setup.

embedment of the SNSM bars to the concrete substrate. The epoxy adhesive has two parts, that is, part A and part B. Part A is white in colour while part B is black. The two parts were mixed in a ratio of 3:1 until a uniform light grey colour was achieved. The density was 1.65 kg/l at 23 °C after mixing. The compressive, tensile and shear strengths, and the modulus of elasticity of the adhesive, as provided by the manufacturer, are as shown in Table 3. The tensile strength and modulus of elasticity of the CFRP bars were 1850 MPa and 124 GPa, respectively.

2.3. Test setup and instrumentation

The beam specimen instrumentation is presented in Fig. 2. Two vertical linear variable differential transducers (LVDT) were used to measure the deflection at mid-span. Several strain gauges were attached to each beam to measure the strain readings. Two 5 mm strain gauges were attached to the CFRP bars, another two 5 mm strain gauges were attached to the steel reinforcement at the mid-span section of the beam and one 30 mm strain gauge was attached to the concrete at the top of the beam. All of the strain gauges were placed in the mid-span section of the beam. Demec gauges were also attached along the depth of the beam at mid-span to measure the transverse strain.

An Instron Universal Testing Machine was used to apply the load for all the specimens under four point bending. All the data were recorded at 10-s intervals.

3. Results and discussion

3.1. Load-deflection behaviour

The load-deflection for all the tested beams are shown in Fig. 3. The precracked and non-precracked beam specimens show a trilinear load-deflection response: (1) the elastic stage, where flexural cracking has not occurred, (2) flexural cracking to steel yielding stage, and (3) steel yielding to failure stage. It was noted that the elastic stage is present in both non-precracked and precracked beams.

A summary of the load-deflection results is given in Table 4. All strengthened beams, precracked and non-precracked, obtained higher ultimate load compared to the control beam, CB. The increase in ultimate is directly proportional to the amount of SNSM reinforcement provided. Precracking seems to affect the yield load (P_y), with PSNC10 and PSNC12 achieving a higher P_y compared to SNC10 and SNC12. However PSNC8 shows a lower P_y compared to SNC8. Due to the contradicting results no conclusion can be drawn on the effect of precracking on the P_y of SNSM strengthened RC beams. From Table 4, it can be seen that precracking negatively

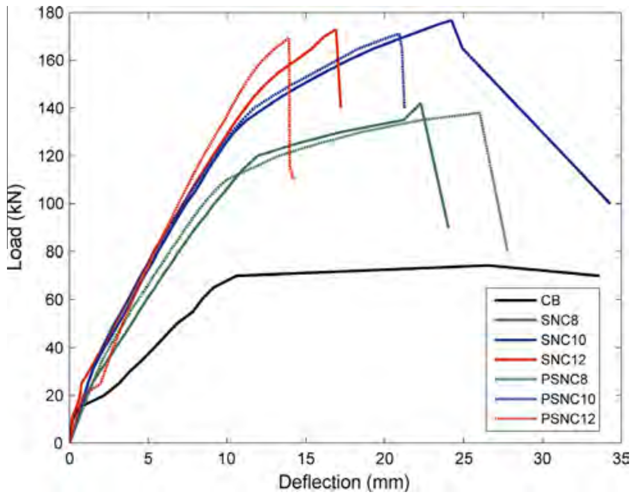

Fig. 3. Experimental load-deflection results.

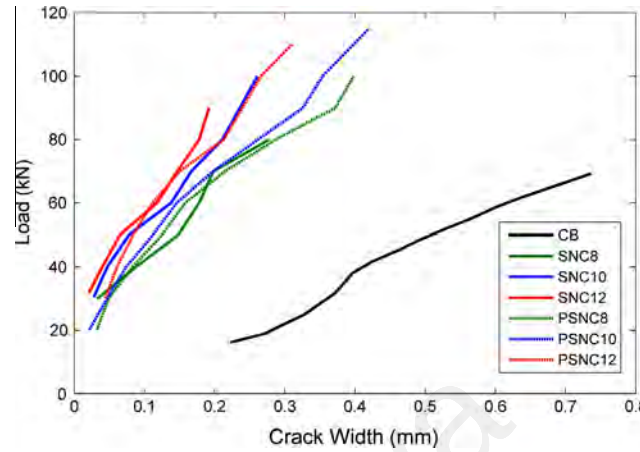

Fig. 4. Crack behaviour of specimens.

effects the ultimate load (P_u) of SNSM strengthened beams. The highest loss in P_u is seen in PSNC10, which has a 3.3% lower ultimate load compared to SNC10.

The recorded mid span deflection at failure (Δ_{max}) for all beams strengthened with SNSM method shows a significant decrease compared to CB. The decrease in maximum mid span deflection is directly proportional to the size of CFRP bar used. The beams strengthened with 12 mm CFRP bars showed a most severe reduction in maximum mid span deflection, with SNC12 and PSNC12 experiencing 49.76% and 58.75% decrease respectively. Precracking was found to cause the Δ_{max} of PSNC10 and PSNC12 to be slightly lower in comparison to SNC10 and SNC12. PSNC8 on the other hand have a slightly higher Δ_{max} compared to SNC8.

The pre-yield stiffness (K_e) of the beams, which were determined by calculating the slope of the load-deflection curve in the elastic region, are also given in Table 4. All of the SNSM strengthened beams show increased K_e compared to the control beam, due to the high stiffness of the CFRP bars compared to the stiffness of steel reinforcements. The increase in K_e is directly proportional to the diameter of CFRP bars used. SNC8, SNC10 and SNC12 show K_e increase of 67.36%, 86% and 90.06% respectively. On the other hand PSNC8, PSNC10 and PSNC12 show K_e increase of 69.17%, 77.59% and 144.15% respectively. The pre-cracked beams show higher K_e compared to the equivalent non-precracked beams, with the exception of PSNC10 which has a K_e value that is less than that of SNC10. The largest gain in K_e caused by precracking is seen in beam PSNC12, which has a 28.4% higher stiffness compared SNC12. This shows that precracked SNSM strengthened beams can have a significantly higher tension stiffening effect compared to non-precracked SNSM strengthened beams.

3.2. Crack width

The load versus crack width results for all the beams are shown in Fig. 4. All of the SNSM strengthened RC beams have significantly smaller crack width compared to the control beam CB. The reduction of crack width is proportional to the size of CFRP bar used; beam SNC12, for example, has a much smaller crack width than SNC8 at the same load level. From Fig. 4, it can be seen that the crack width of precracked SNSM strengthened beams is larger than the equivalent non-precracked SNSM strengthened beams. However the difference in crack width caused by precracking is very slight compared to the difference in crack width caused by the size of CFRP bar used.

3.3. Failure modes

The failure modes of the RC beams are shown in Fig. 5. Beam CB failed by concrete crushing, as shown in Fig. 5(a). The non-precracked beam SNC8 and the precracked specimens PSNC8 failed by rupture of the CFRP bars. Beams SNC10 and PSNC10 also failed by rupture of CFRP ribbed bar. Beam SNC12 and PSNC12 on the other hand experienced premature failure.

The SNSM strengthened beams shows good resistance against the premature failure of concrete cover separation, as beams SNC8, SNC10, PSNC8 and PSNC10 failed through flexure by means of rupture of the CFRP ribbed bar. This resistance against premature failure however is greatly reduced when the size of CFRP bar is increased to above 10 mm, as seen in beams SNC12 and PSNC12 which suffered premature failure. Precracking was found to have no effect to the failure mode of SNSM strengthened beams, as

Table 4
Summary of load-deflection results.

Beam	P_y (kN)	$\%P_y$	P_u (kN)	$\%P_u$	Δ_{max} (mm)	$\%\Delta_{max}$	K_e	$\%K_e$
CB	70	–	74.37	–	33.61	–	6.37	–
SNC8	120	71.43	142.03	90.98	22.27	−33.75	10.66	67.36
SNC10	130	85.71	176.78	137.7	24.03	−28.50	11.85	86
SNC12	140	100	173.02	132.65	16.89	−49.76	12.11	90.06
PSNC8	110.136	57.34	141.54	90.32	25.99	−22.67	10.78	69.17
PSNC10	140.127	100.18	171.13	130.11	20.95	−37.68	11.31	77.59
PSNC12	157.158	124.51	169.41	125.1	13.86	−58.75	15.55	144.15

P_y = yield load; $\%P_y$ = percent change in yield load over the control beam; P_u = ultimate load; $\%P_u$ = percent change in ultimate load over the control beam; Δ_{max} = mid span deflection at failure load; $\%\Delta_{max}$ = percent change in mid span deflection at failure load; K_e = effective pre-yield stiffness; $\%K_e$ = percent change in effective pre-yield stiffness.

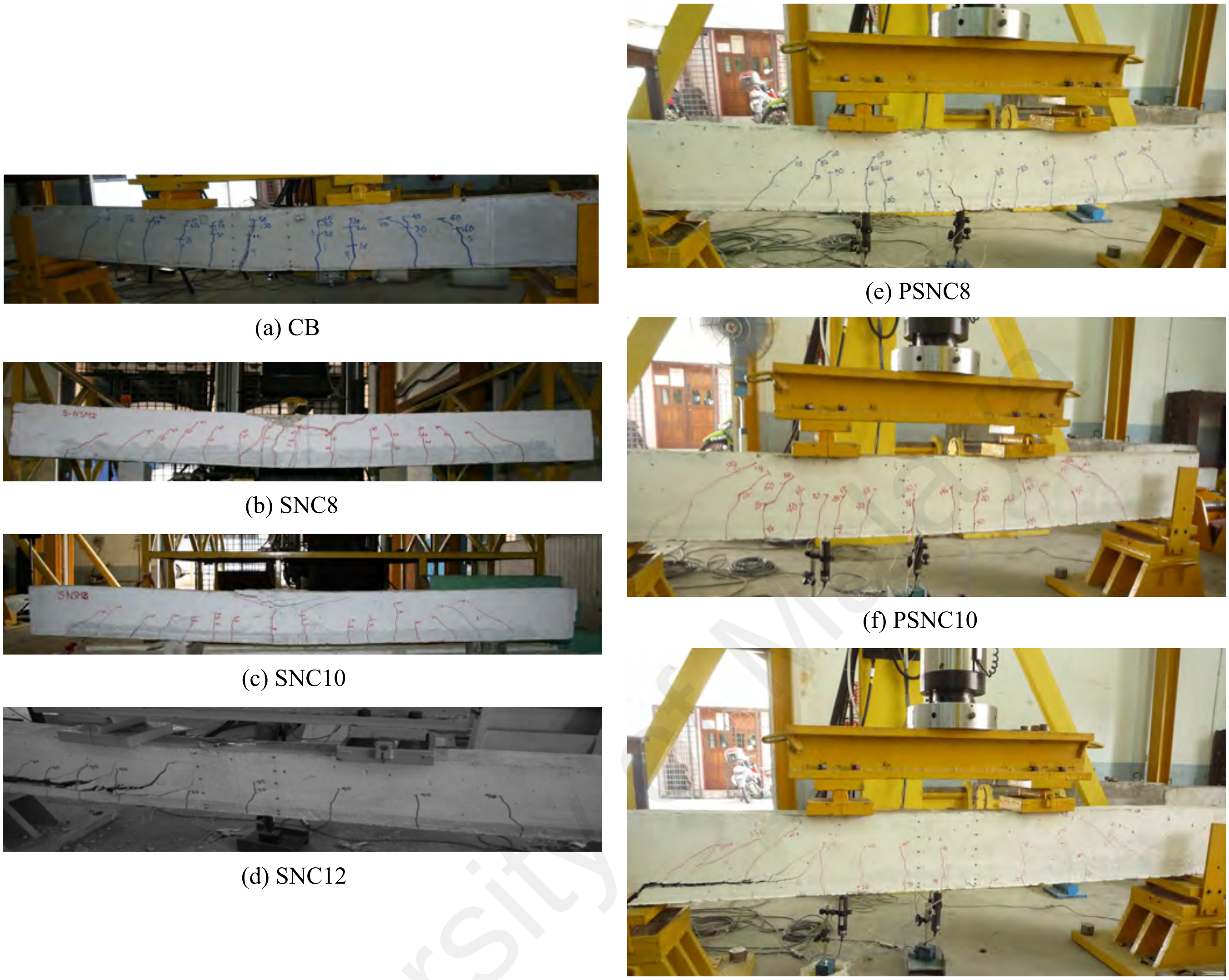

(a) CB (b) SNC8 (c) SNC10 (d) SNC12 (e) PSNC8 (f) PSNC10 (g) PSNC12

Fig. 5. Failure modes of beam specimens.

the precracked beams and the equivalent non-precracked beams experienced the same mode of failure.

The modes of failure in SNC12 and PSNC12 are identical; a crack appears in the bottom soffit of the beam, slightly in front of the ends of the CFRP ribbed bar. As more load was applied to the beams, the crack propagate upwards until it reached the area above the CFRP bars, as shown in Fig. 5(d) and (g). The crack then propagates towards the centre of the beam, causing the whole area of concrete below it to be separated from the beam. The mode of premature failure experienced by SNC12 and PSNC12 is similar to the concrete cover separation that commonly occurs on FRP strengthened beams. However in the case of SNSM strengthening the failure can perhaps be more destructive as while the crack concrete cover separation failure normally stops at the shear link, the crack in the case of SNSM would propagate above the level of the shear link. The amount of concrete cover separated in the case of SNSM would thus be larger than normal NSM or EB strengthening. It is thus recommended that the size of the SNSM reinforcement provided be less than the size of the steel reinforcement bars of the RC beam to prevent premature failure until a better understanding of the premature failure mode in SNSM strengthened beams can be established.

4. Simulation of SNSM strengthened RC beams

4.1. Segmental moment-rotation (M/θ) approach

From the experimental results, it can be seen that the tension stiffening can be affected by precracking, as the precracked SNSM strengthened RC beams were found to have a higher stiffness than non-precracked SNSM strengthened RC beams. This can cause problems in accurately predicting the behaviour of SNSM strengthened RC beams, which is required of the method is to be used in real world application.

Most design codes uses the effective moment of inertia proposed by Branson [16] to simulate the effect of tension stiffening. Branson's equation is empirical in nature, which means it can be highly inaccurate when used outside of the testing regime that formed it. This can be seen when Hosen et al. [12] applied the Branson's equation to predict the load-deflection of non-precracked SNSM strengthened RC beams, where the resulting load-deflection curve either underestimated the yield load or overestimated the tension stiffening.

Hence to accurately simulate the tension stiffening behaviour of SNSM strengthened RC beams, the moment-rotation (M/θ)

approach [17–25] will be extended to allow for SNSM strengthening method. The M/θ approach uses the partial-interaction theory [23–27] to directly incorporate bond-slip relationships, thus allowing it to simulate the mechanics of RC beams such as concrete cracking, crack widening and tension stiffening without empirical formulations to indirectly simulate them. It should be noted that while the approach allows the mechanics of the tension stiffening to be simulated without empiricism, material properties such as stress-strain and bond-slip relationships still require empirical formulations.

4.1.1. Tension stiffening simulation

Prior to flexural cracking, the reinforcements and concrete have perfect bond, such that the reinforcements and concrete deform in unison. Once RC beams are cracked, an imperfect bond exists between the reinforcements and the adjacent concrete, causing the reinforcements to slip from the concrete. This slip is governed by the bond-slip behaviour of the reinforcement, which acts to transfer the load from the reinforcement to the surrounding concrete, hence causing the tension stiffening to occur. From this it can be seen that if the partial interaction behaviour can be simulated, the tension stiffening can be directly accounted for at all load levels until failure without the need for any empirical based formulations.

Simulating the tension stiffening as individual reinforcing bars of area A_r embedded in individual concrete prisms of area A_c as shown in Fig. 6(a) is now a relatively common practice among researchers [23–26]. The reinforcement is located in the middle of the prism, such that when load is applied on the reinforcement, no moment will be induced. Slip of reinforcement is maximum at the location of flexural crack. Bond between the steel reinforcement and concrete gradually transfers the stress from the steel reinforcement to the adjacent concrete. As certain point away from the crack face, the slip and strain of steel reinforcement would be reduced to zero as shown in Fig. 6(b) and (c). On the other hand, concrete strain would be maximum at that point as all the stress has been transferred from the steel reinforcement to the concrete. Assuming more load is applied to the beam, the flexural crack would widen and the concrete cracking strain, ε_{crack} would be reached as illustrated in Fig. 6(d). This causes primary cracks, as shown in Fig. 6(a), to appear. A numerical model based on the process described here was made using Matlab, which allows the hinge length ($L_{cr\text{-}n}$) of the control beam (CB) to be determined. The hinge length of the precracked beams were also determined in this manner, as the precracked beams were assumed to have primary cracks already forming prior to being strengthened using SNSM method.

For non-precracked specimens, the steel reinforcements have to share the available concrete area with the SNSM bars, resulting in a much reduced concrete area as shown in Fig. 7(a). Similar to precracked specimens, the slip and steel strain of the non-precracked beam is gradually reduced to zero the further it gets from the crack face while concrete strain gradually increases as shown in Fig. 7(b)–(d). However due to the reduced concrete area, stress transferred from steel reinforcement to the concrete results in a much higher strain. This causes the resulting hinge length, $L_{cr\text{-}n}$ as shown in Fig. 7(a) to be much shorter than the $L_{cr\text{-}pr}$.

Once the hinge lengths has been determined, the formation of primary cracks means that the numerical analysis can now be reduced to half the length of crack due to the symmetry of forces that occurs [20]. This allows the load-slip relationship of the reinforcements in between primary cracks to be established, which

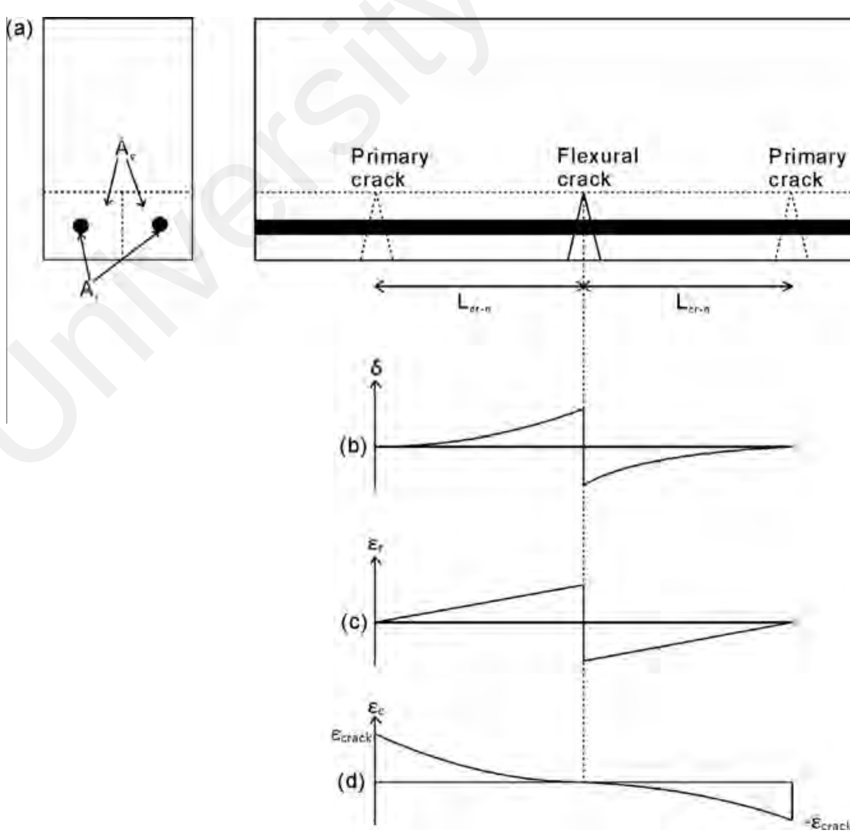

Fig. 6. Determining hinge length of control and precracked beams.

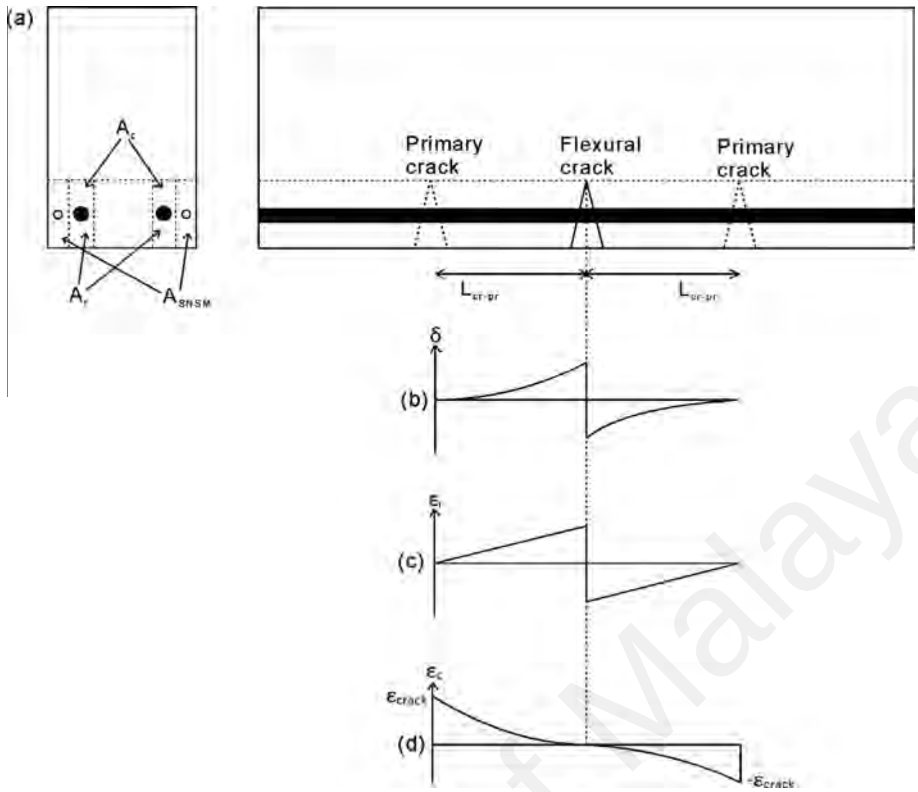

Fig. 7. Determining hinge length of non-precracked beams.

will be used to determine the moment-rotation of the beam segment.

4.1.2. Moment-rotation of beam segment

Once the tensile concrete is cracked, the steel and NSM reinforcements will begin to slip at the same rate, which is referred to as Δ_r in Fig. 8(b). The bond-slip relationship between the reinforcement and the concrete causes the loads acting on the reinforcements to no longer be functions of the strain profile. In this situation, the loads of the reinforcements will be determined from the deformation profile by using the load-slip relationships obtained from the tension stiffening analysis. The depth of neutral axis is then adjusted until equilibrium of forces acting on the beam (Fig. 8(e)) is obtained. Lastly, the moment M for the rotation θ is determined. Once the moment-rotation relationship is obtained, the moment-curvature can be determined simply by dividing the rotation, θ by L_{def}. Using the moment-curvature relationship, the load-deflection of the beam was determined using the double integration method.

4.2. Material models

Several material models were used in the tension stiffening simulation and moment-rotation simulation. The bond-slip model from the CEB-FIP [28] was used to obtain the tension stiffening load-slip relationship of the steel reinforcements. For the SNSM reinforcements, the bond-slip model proposed by Lorenzis [29] was used:

$$\tau = \tau_{max}\left(\frac{\delta}{\delta_{max}}\right)^{\alpha} \text{ for } \delta \leqslant \delta_{max} \quad (1)$$

$$\tau = \tau_{max}\left(\frac{\delta}{\delta_{max}}\right)^{\alpha'} \text{ for } \delta \succ \delta_{max} \quad (2)$$

where τ is the bond stress, τ_{max} is the maximum bond stress, s is the slip and s_m is slip corresponding to τ_{max}. The full list of parameters used for the bond-slip model for NSM FRP bars is provided in Table 5, where the parameters are empirically derived by De Lorenzis [29] for RC beams strengthened with NSM FRP ribbed bars,

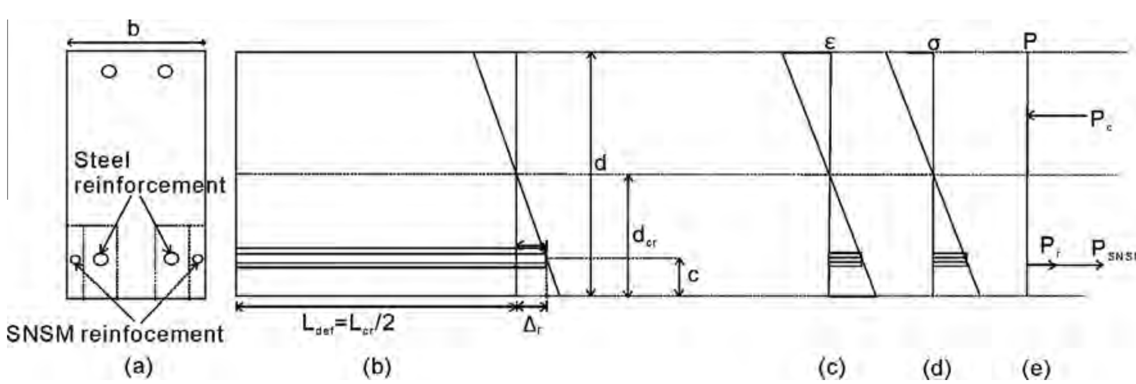

Fig. 8. Segmental M/θ analysis.

Table 5
Parameters for bond-slip of NSM FRP.

Parameter	Value
δ_{max} (mm)	0.162
τ_{max} (mm)	21
α	0.8
α'	−0.66

with the exception of τ_{max} which 21 MPa based on the value of bond strength given by the manufacturer of the epoxy adhesive.

The empirical stress-strain model by Popovics [30] was used to create the size-dependent stress-strain relationship of concrete [27]. A bilinear stress-strain model was adopted for the steel reinforcement, with a strain hardening modulus of 250 MPa.

4.3. Validation of segmental moment-rotation simulation

The segmental moment-rotation simulation was validated against the experimental results. A comparison of the simulated and experimental load-deflection curves is given in Fig. 9. The simulated failure mode of SNC8, SNC10, PSNC8 and PSNC10 is FRP rupture, which is similar to the experimental failure mode. However the moment-rotation approach is currently unable to simulate the concrete cover separation failure, which is the failure mode of SNC12 and PSNC12. Apart from this problem, all the simulated load-deflection curves follows the general shape of the experimental load-deflection curves reasonably well.

A summary of the simulated and experimental load-deflection comparison in given in Table 6. The largest deviation between

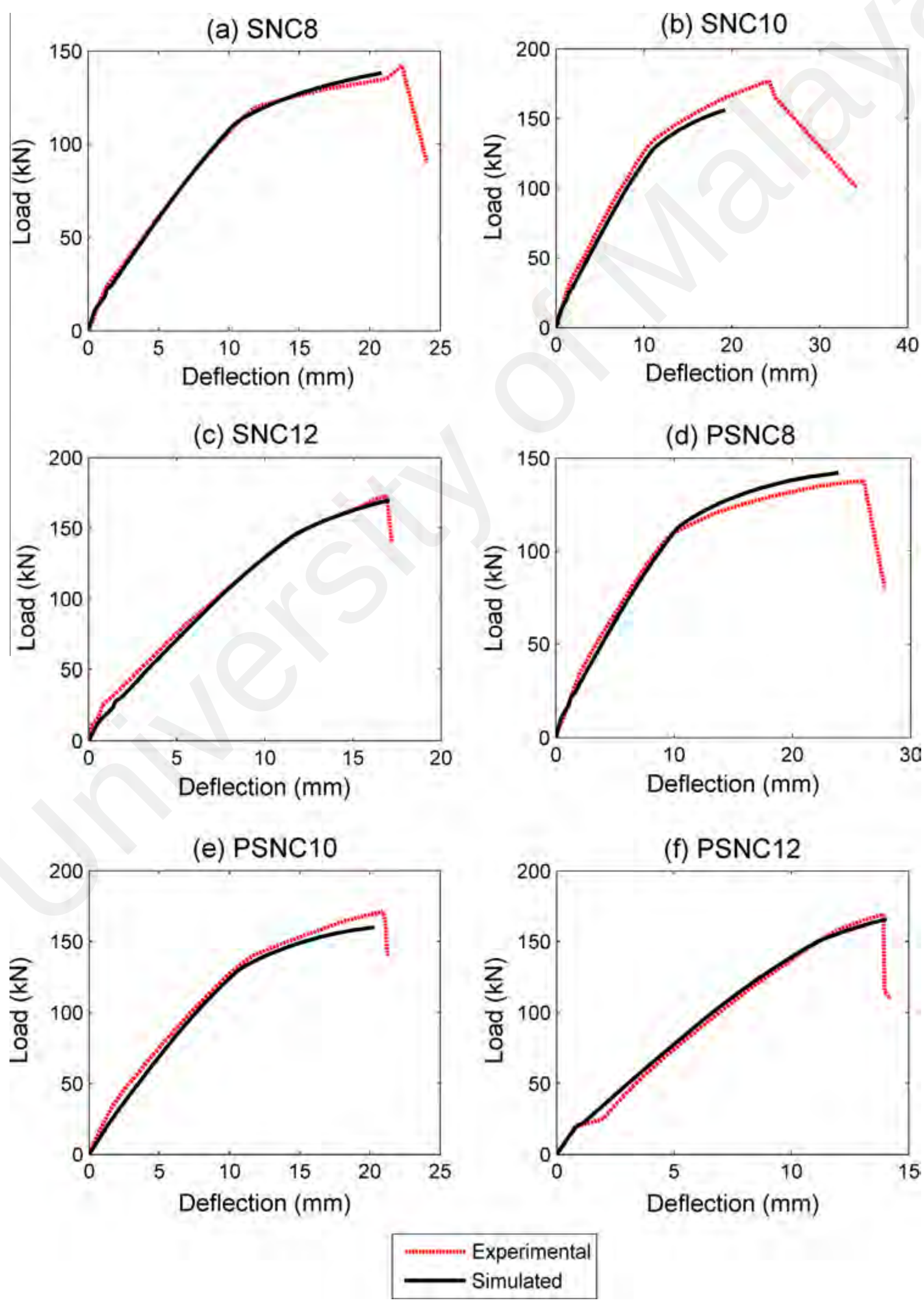

Fig. 9. Comparison of simulated and experimental load-deflection curves.

Table 6
Summary of simulated and experimental results.

Beam	Results	P_y (kN)	P_u (kN)	Δ_{max} (mm)	K_e
SNC8	Simulated	112.32	137.56	20.73	9.67
	Experimental	120.00	142.03	22.27	10.66
	Simulated/Experimental	0.94	0.97	0.93	0.91
SNC10	Simulated	128.40	155.56	19.29	11.34
	Experimental	130.00	176.85	24.03	11.85
	Simulated/Experimental	0.99	0.88	0.80	0.96
SNC12	Simulated	146.62	169.89	16.94	12.77
	Experimental	140.00	173.02	16.89	12.11
	Simulated/Experimental	1.05	0.98	1.00	1.05
PSNC8	Simulated	112.31	142.10	23.79	10.96
	Experimental	110.14	141.54	25.99	10.78
	Simulated/Experimental	1.02	1.00	0.92	1.02
PSNC10	Simulated	133.90	159.94	20.29	12.85
	Experimental	140.13	171.13	20.95	11.31
	Simulated/Experimental	0.96	0.93	0.97	1.14
PSNC12	Simulated	151.13	165.56	13.95	13.82
	Experimental	157.16	169.41	13.86	15.55
	Simulated/Experimental	0.96	0.98	1.01	0.89

P_y = yield load; P_u = ultimate load; Δ_{max} = mid span deflection at failure load; K_e = effective pre-yield stiffness.

the simulated and experimental yield load (P_y) is seen in beam SNC12, which has a deviation of 5%. For ultimate load, the largest deviation is from beam SNC10 which has a deviation of 12%. The reason for this deviation is that the simulated result experiences FRP rupture earlier than the experimental result. The earlier FRP rupture also causes the simulated maximum deflection of beam SNC10 to be considerably high at 20%. However apart from beam SNC10 no other simulated beam results show this amount of deviation. Excluding beam SNC10, the largest deviation for ultimate load is seen in beam PSNC10 at 7% while the largest deviation for maximum deflection values is seen in beam PSNC8 which has a 8% deviation.

For effective stiffness at pre-yield, the largest deviation between simulated and experimental result is from beam PSNC10 with 14% deviation. The large deviation might be caused by the assumption that concrete cracking is assumed to have occurred along the whole length of beam PSNC10 due to the applied precracking. This assumption is not wholly accurate as the applied precracking load is fairly low and thus there should be some areas of the beam that has not experienced concrete cracking. However, the difference in stiffness becomes less apparent at higher applied load and thus the moment-rotation approach used is capable to simulate the change in stiffness due to precracking with acceptable accuracy.

5. Conclusion

An experimental programme was conducted to test the viability of the SNSM method in strengthening precracked RC beams. A mechanics-based moment-rotation approach for simulating the SNSM strengthened beams was also proposed. From the study, the following conclusions were made:

- The ultimate load of SNSM strengthened RC beams is reduced by up to 3.3% due to precracking.
- The stiffness of precracked SNSM strengthened RC beams was found to be higher than the stiffness of non-precracked SNSM strengthened RC beams by up to 28.4%.
- The failure modes of the precracked beams are identical to its equivalent non-precracked beams. It can thus be concluded that the failure modes of SNSM strengthened RC beams are not affected by precracking.
- Both the precracked and non-precracked RC beams strengthened by SNSM using 12 mm CFRP bars failed by concrete cover separation. It is thus recommended that the size of the CFRP bar used in SNSM strengthening method be less than the size of the steel reinforcement bars used in the RC beam.
- The segmental M/θ approach can be used to simulate the behaviour of SNSM strengthened RC beams with acceptable accuracy. Additionally, by changing the amount of concrete area acting on the reinforcements, the M/θ approach allows the difference in stiffness between non-precracked and precracked SNSM strengthened RC beams to be simulated without the need for empirical means.
- Suggestions for future research on SNSM technique includes the application of SNSM on RC beams with high strength concrete as well as the effect of SNSM bond lengths.

Acknowledgement

Financial support from the University of Malaya, Grand Challenge – SUS (Sustainability Science) Grant, project number GC003A-15SUS is gratefully acknowledged.

References

[1] I.A. Sharaky, L. Torres, M. Baena, C. Miàs, An experimental study of different factors affecting the bond of NSM FRP bars in concrete, Compos. Struct. 99 (2013) 350–365.
[2] K.M.U. Darain, S. Shamshirband, M.Z. Jumaat, M. Obaydullah, Adaptive neuro fuzzy prediction of deflection and cracking behavior of NSM strengthened RC beams, Constr. Build. Mater. 98 (2015) 276–285.
[3] J.A. Barros, A. Fortes, Flexural strengthening of concrete beams with CFRP laminates bonded into slits, Cem. Concr. Compos. 27 (4) (2005) 471–480.
[4] L. De Lorenzis, J.G. Teng, Near-surface mounted FRP reinforcement: an emerging technique for strengthening structures, Compos. Part B: Eng. 38 (2) (2006) 119–143.
[5] J.R. Yost, S.P. Gross, D.W. Dinehart, J.J. Mildenberg, Flexural behavior of concrete beams strengthened with near-surface-mounted CFRP strips, ACI Struct. J. 104 (4) (2007).
[6] M. Badawi, K. Soudki, Flexural strengthening of RC beams with prestressed NSM CFRP rods – Experimental and analytical investigation, Constr. Build. Mater. 23 (2009) 3292–3300.
[7] W.C. Tang, R.V. Balendran, A. Nadeem, H.Y. Leung, Flexural strengthening of reinforced lightweight polystyrene aggregate concrete beams with near-surface mounted GFRP bars, Build. Environ. 41 (10) (2006) 1381–1393.
[8] F. Al-Mahmoud, A. Castel, R. François, C. Tourneur, Strengthening of RC members with near-surface mounted CFRP rods, Compos. Struct. 91 (2) (2009) 138–147.
[9] S.M. Soliman, E. El-Salakawy, B. Benmokrane, Flexural behaviour of concrete beams strengthened with near surface mounted fibre reinforced polymer bars, Can. J. Civil Eng. 37 (10) (2010) 1371–1382.
[10] F. Al-Mahmoud, A. Castel, R. François, C. Tourneur, RC beams strengthened with NSM CFRP rods and modeling of peeling-off failure, Compos. Struct. 92 (8) (2010) 1920–1930.
[11] R. Kotynia, Bond between FRP and concrete in reinforced concrete beams strengthened with near surface mounted and externally bonded reinforcement, Constr. Build. Mater. 32 (2012) 41–54.
[12] M.A. Hosen, M.Z. Jumaat, A.B.M.S. Islam, Side Near Surface Mounted (SNSM) technique for flexural enhancement of RC beams, Mater. Des. 83 (2015) 587–597.
[13] ACI 318-11, Building Code Requirements for Structural Concrete and Commentary, ACI Committee 11 (2011) 503.
[14] ASTM C39/C39M-14a, Standard Test Method for Compressive Strength of Cylindrical Concrete Specimens, ASTM Int'l, 2014.
[15] British Standards Institution, Testing Hardened Concrete – Part 5: Flexural Strength of Test Specimens Testing Hardened Concrete, BS EN (2009) 1–14. 12390-22009.
[16] D.E. Branson, Deformation of concrete structures, McGraw, 1977.
[17] J.E. Daniell, D.J. Oehlers, M.C. Griffith, M.S. Mohamed Ali, T. Ozbakkaloglu, The softening rotation of reinforced concrete members, Eng. Struct. 30 (2008) 3159–3166;
R. Muhamad, D. Oehlers, M.M. Ali, Discrete rotation deflection of RC beams at serviceability, Proc. ICE Struct. Build. 164 (2011) 1–14.
[18] D.J. Oehlers, M. Haskett, M.S. Ali, W. Lucas, R. Muhamad, Our obsession with curvature in rc beam modelling, Adv. Struct. Eng. 14 (2011) 391–404.
[19] D. Oehlers, P. Visintin, T. Zhang, Y. Chen, D. Knight, Flexural rigidity of reinforced concrete members using a deformation based analysis, Concr. Aust. (2012) 1–9.

[20] P. Visintin, D.J. Oehlers, C. Wu, M. Haskett, A mechanics solution for hinges in RC beams with multiple cracks, Eng. Struct. 36 (2012) 61–69.
[21] D. Knight, P. Visintin, D.J. Oehlers, M.S. Mohamed Ali, Simulating RC beams with unbonded FRP and steel prestressing tendons, Compos. Part B: Eng. 60 (2014) 392–399.
[22] A.A. Shukri, K.M. Darain, M.Z. Jumaat, The tension-stiffening contribution of NSM CFRP to the behavior of strengthened RC beams, Materials 8 (2015) 4131–4146.
[23] M. Haskett, D.J. Oehlers, M.S. Mohamed Ali, Local and global bond characteristics of steel reinforcing bars, Eng. Struct. 30 (2008) 376–383.
[24] R. Muhamad, M.S. Mohamed Ali, D. Oehlers, A. Hamid Sheikh, Load-slip relationship of tension reinforcement in reinforced concrete members, Eng. Struct. 33 (2011) 1098–1106.
[25] R. Muhamad, M.S. Mohamed Ali, D.J. Oehlers, M. Griffith, The tension stiffening mechanism in reinforced concrete prisms, Adv. Struct. Eng. 15 (2012) 2053–2069.
[26] A.K. Gupta, S.R. Maestrini, Tension stiffness model for reinforced concrete bars, J. Struct. Eng. 116 (1990) 769–790.
[27] Y. Chen, P. Visintin, D.J. Oehlers, U.J. Alengaram, Size dependent stress-strain model for unconfined concrete, J. Struct. Eng. 140 (4) (2013) 04013088.
[28] Comite Euro-International du Beton (CEB-FIP). CEB-FIP model code 1990. Bulletin D'Information No. 213/214 (Concrete Structures), Lausanne, Switzerland; 1993.
[29] L. De Lorenzis, Anchorage length of near-surface mounted fiber-reinforced polymer rods for concrete strengthening – analytical modeling, ACI Struct. J. 101 (2004) 375–386.
[30] S. Popovics, A numerical approach to the complete stress–strain curve of concrete, Cem. Concr. Res. 3 (5) (1973) 583–599.

4.2 Research paper 3: Parametric study for concrete cover separation failure of retrofitted SNSM strengthened RC beams

Published in *Mechanics of Advanced Materials and Structures*

Article history:

Received 2 November 2017

Accepted 24 May 2018

MECHANICS OF ADVANCED MATERIALS AND STRUCTURES
2018, VOL. 0, NO. 0, 1–12
https://doi.org/10.1080/15376494.2018.1482034

Taylor & Francis
Taylor & Francis Group

ORIGINAL ARTICLE

Parametric study for concrete cover separation failure of retrofitted SNSM strengthened RC beams

Ahmad Azim Shukri[a], Mohd Fazaulnizam Shamsudin[b], Zainah Ibrahim[a], and U. Johnson Alengaram[a]

[a]Faculty of Engineering, University of Malaya, Kuala Lumpur, Malaysia; [b]Department of Civil Engineering, University of Nottingham, Nottingham, UK

ABSTRACT
The side near-surface mounted (SNSM) method is a new flexural strengthening method for reinforced concrete (RC) beams which was proposed to allow near-surface mounted (NSM) strengthening to be applied on beams with small width. As a relatively new strengthening method, further studies are needed to determine the effects of strengthening parameters on the flexural performance of RC beams. In response to that, this paper presents a parametric study on the concrete cover separation failure of SNSM strengthened beams using a simulation method based on the moment-rotation (M/θ) approach.

ARTICLE HISTORY
Received 2 November 2017
Accepted 24 May 2018

KEYWORDS
Near-surface mounted; numerical analysis; partial interaction; reinforced concrete; side-NSM

1. Introduction

Reinforced concrete (RC) structures tend to face some degree of strength loss due to aging. To restore the lost strength, or even increase the structural strength beyond the original strength, structural strengthening [1]–[3] can be applied. Among the newer strengthening method is near-surface mounted (NSM) method [4]–[13]. The NSM method consists of NSM reinforcements, which is usually some form of fiber reinforced polymers (FRP) that is placed within a groove made at the soffit of RC beams to strengthen it in flexure.

Among the problems with applying the NSM method is that it requires the RC beam to be considerably wide. A closely spaced arrangement of NSM bars will cause an overlap of stresses, which causes the tensile stress at the concrete-epoxy interface to be magnified and cause concrete split failure [14]. The ACI 440 guideline, based on the research work of [15] states that the minimum clear groove spacing for NSM bars should be greater than twice the depth of the groove to avoid the overlapping of stresses, while the edge distance should be four times the depth of the groove to minimize edge effects. To make the NSM method applicable to beams with small width, a minor modification to the NSM method was introduced. The modified method, named side-NSM (SNSM) method changes the location of the NSM reinforcement from the soffit of the RC beam to the side of the beam at the same level as the tension reinforcement. Additionally, the SNSM method allows strengthening to be applied on beams with walls beneath them [16].

The SNSM method is a relatively new method; there are very limited research that has been done on the SNSM method thus far. Hosen et al. [17] used FRP and steel bars as SNSM reinforcements; it was reported that the FRP bars gives a higher ultimate load but lower ductility while the steel bars is the opposite with lower ultimate load but higher ductility. The newest study on SNSM was done by Sharaky et al. [16] who performed experimental study on GFRP SNSM strengthened beams, where the GFRP bars have ends that are bent into different degrees of inclinations. The bent end conditions for SNSM method was found to be less beneficial compared to bottom NSM, which have good confinement due to the bent ends being encased in concrete.

Shukri et al. [18] studied the behavior of SNSM strengthened RC beams that has been applied a precracking load. The precracking loads were used to induce flexural cracks on beams prior to strengthening them with the SNSM method. The purpose was to simulate the condition of actual beams which would have flexural cracks due to service load prior to being retrofitted. For the sake of brevity, beams that are applied precracking load prior to being strengthened will be referred to as retrofitted beams for the rest of this paper. Shukri et al. [18] reported that SNSM retrofitted beams have a slight decrease in ultimate load of up to 3.3% compared to virgin SNSM strengthened beams. Importantly, it was found that the SNSM retrofitted beams have a higher flexural stiffness than SNSM strengthened beams without pre-existing flexural cracks. To study this occurrence, Shukri et al. [18] performed an analysis using the moment rotation (M/θ) approach; further detail on the M/θ will be given later. From the analysis, it was found that the retrofitted beams have a longer crack spacing compared to virgin strengthened beams due to the larger concrete area adjacent to the steel reinforcement when the flexural cracks formed. The longer crack spacing causes the resulting curvature to be smaller compared to virgin strengthened beams at the same value of moment.

One important characteristic of the SNSM method that can be determined from the experimental works that has been done so far is that concrete cover separation is the sole mode of premature failure. Premature failures refer to failure modes for

CONTACT Zainah Ibrahim zainah@um.edu.my Department of Civil Engineering, Faculty of Engineering, University of Malaya, Kuala Lumpur 50603, Malaysia.
Color versions of one or more of the figures in the article can be found online at www.tandfonline.com/umcm.

strengthened RC beams that occur prior to the rupture of the strengthening reinforcements. The concrete cover separation [19]–[21], also called end debonding or end cover separation, is the failure mode commonly reported in experimental works on NSM strengthened RC beams. The debonding crack forms near the curtailment location of NSM reinforcement, which then propagates upwards until it reaches the shear link of the NSM strengthened beam. The crack then propagates horizontally, causing the NSM reinforcement to be debonded along with the concrete cover of the beam.

It is clear that there need to be a study done on the concrete cover separation failure of SNSM strengthened RC beams. Additionally, the parametric study should involve SNSM retrofitted RC beams so that the study is relatable to actual beams. To this end, this paper aims to study the effect of several selected parameters on the concrete cover separation failure of retrofitted and virgin SNSM strengthened RC beams by using the M/θ approach. The M/θ approach [18], [22]–[36] is a relatively new simulation method. The main characteristic of this approach is the application of the partial interaction theory [37]–[39], which to summarize states that where a tensile crack intercepts a reinforcing bar, infinite strains are theoretically induced in the reinforcing bar that must be relieved by a slip between the steel reinforcement and the concrete. By applying a numerical solution to simulate the slip of steel reinforcement, various mechanics of RC beams, such as the formation of flexural cracks, widening of flexural cracks and tension stiffening can be accounted for. The advantage that the M/θ approach has over conventional moment-curvature (M/χ) approach is the fact that it can readily simulate these mechanics without resorting to empirical formulations, such as the use of Branson's equation to simulate tension stiffening. It should be noted that while the M/θ approach can directly simulate mechanics of RC beams, empirical formulations in terms of material models are still needed, such as stress–strain models and bond stress-slip models.

Previously Shukri et al. [18] extended the M/θ approach to simulate the behavior of SNSM strengthened RC beams. The simulated load–deflection curve could follow the general shape of the experimental load–deflection curve well. The proposed method however was not suitable for parametric study as it could not simulate concrete cover separation, which is a type of debonding found to occur on SNSM strengthened beams tested. This paper will further extend the existing M/θ approach to allow it to simulate concrete cover separation of SNSM strengthened RC beams. In the initial sections of this paper, the fundamental mechanics of the M/θ approach will first be presented. A numerical tension stiffening simulation will then be presented, followed by the M/θ simulation. The method used to simulate the effect of concrete cover separation on SNSM strengthened RC beams will then be shown, along with the difference involved when applying the method on virgin and retrofitted beams. The proposed method is then validated against published experimental results. Parametric study would then be done on several selected parameters.

2. Tension stiffening simulation

In undisturbed regions of an SNSM strengthened RC beam, which remains without any flexural cracks, there exists perfect bonding between the steel and SNSM reinforcements and the concrete adjacent to them, where there is strain compatibility between the reinforcements and the adjacent concrete and no slip of reinforcement occurs. Once flexural cracks form, partial interaction causes both the steel and SNSM reinforcement begins to slip from the concrete. Consider the tension stiffening prism in Figure 1(b), which is made up of the steel reinforcement and the adjacent concrete. The load applied on the beam causes the pullout force P_r, which in turn causes the steel reinforcement and SNSM reinforcement to slip by an amount δ_r; the steel reinforcement and SNSM reinforcement will have the same amount of slip as both have the same height from beam soffit. Due to the bond that exists between steel/SNSM reinforcement and concrete, the pullout force is gradually transferred from and onto the adjacent concrete. As the pullout force is reduced, the slip also gradually drops further away from the crack face as shown in Figure 1(c).

As the load applied on the beam is increased, the amount of load transferred to the concrete will also become higher; this causes the steel reinforcement strain, ε_r to decrease while the concrete strain, ε_c increases as shown in Figure 1(d) and (e), respectively. Once the concrete strain reaches the concrete cracking strain, ε_{cr}, a primary crack will form. The mechanism described here will continue until there are primary cracks along the length of the beam with a crack spacing of S_{cr} as shown in Figure 1(a); the value of S_{cr} here represents the minimum crack spacing, although when moment gradient is present on the beam, which tends to be the case, it is more likely and conservative to take the spacing as S_{cr} [24]. With the formation of primary cracks, the loading of each RC beam segment becomes symmetric, as shown in Figure 1(f). As such only the half-length of the RC section, L_{def}, needs to be considered [24]. The distribution of slip within beam section of length S_{cr} is as shown in Figure 1(g), while the strain of reinforcement and strain of concrete is shown in Figure 1(h) and (i), respectively; the symmetry seen in these three figures reflect the symmetry of forces acting on the beam section.

To consider the effects of concrete cover separation on SNSM strengthened beams, consider the comparison of tension stiffening prism size in the strengthened section of the beam and the debonded section of the beam is given in Figure 2(b) and (c) respectively. When concrete cover separation occurs, as shown in Figure 2(a), the SNSM reinforcement in the debonded section no longer contributes to the beam and only the tensile steel reinforcement needs to be considered. Since the SNSM is applied on the side of the beam, the tension stiffening prism of the tensile steel reinforcement is not affected, as shown in Figure 2(c). This contrasts with NSM strengthened beams, where the steel reinforcements will have a reduced tension stiffening prism size when concrete cover separation occurs [32].

For analysis purpose, the tension stiffening prism's depth can be taken as $2c$, where c is the distance from beam soffit to center of the steel reinforcement [29], [40]. The width of the prism for SNSM reinforcement is taken as the groove width, while for steel reinforcement the width is the sum of the diameters of steel reinforcement and shear link and two times of any remaining width of the concrete cover that is not part of the SNSM groove.

A numerical tension stiffening simulation based on the partial interaction theory has been applied by many researchers to simulate the slip of steel reinforcement [32], [35], [37]–[39], which will serve as the basis for the numerical procedure

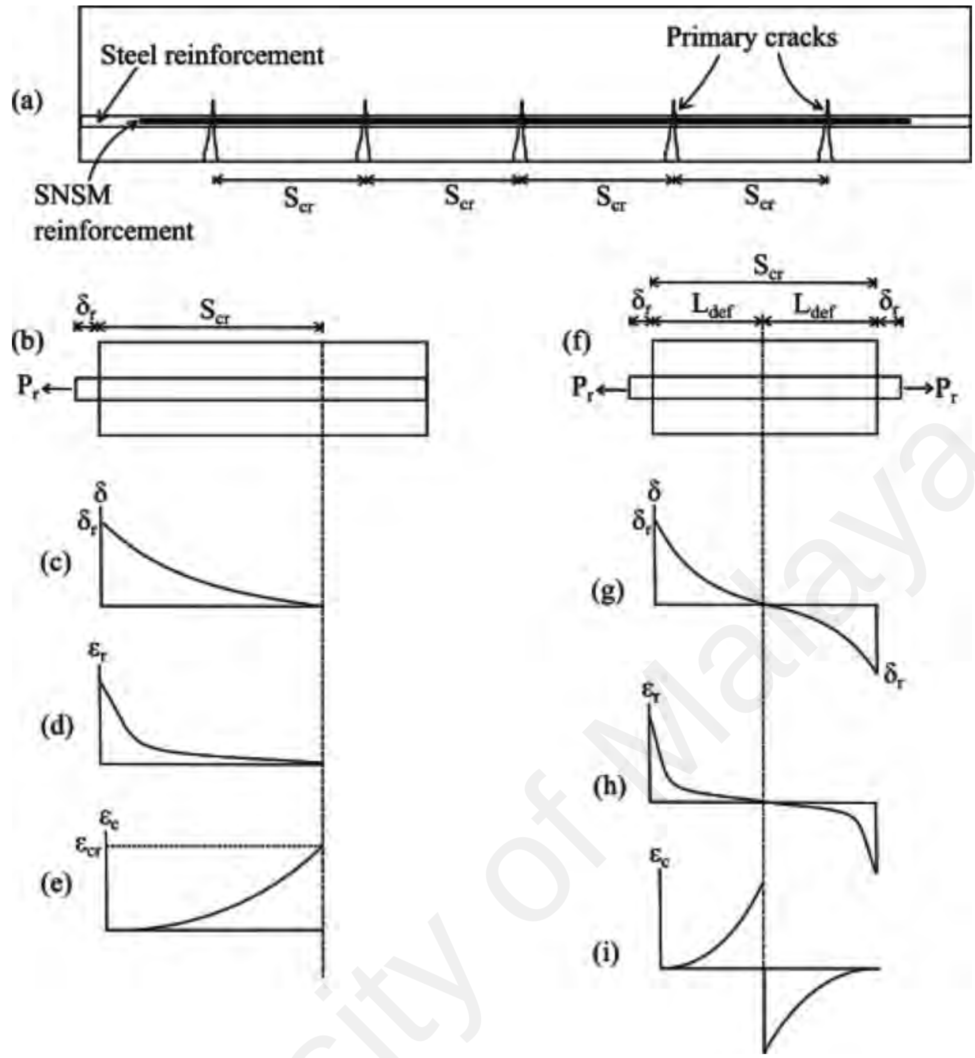

Figure 1. Formation of primary cracks: (a) SNSM strengthened RC beam; (b) tension stiffening prism with variable length; (c) distribution of reinforcement slip; (d) distribution of reinforcement strain; (e) distribution of concrete strain; (f) tension stiffening prism of length S_{cr}; (g) distribution of reinforcement slip; (h) distribution of reinforcement strain; and (i) distribution of concrete strain.

presented here. The numerical analysis firstly determines the length of primary crack spacing, S_{cr}. The analysis is then reduced to half the crack spacing, L_{def} which ends with a load-slip relationship for the steel reinforcement and the SNSM reinforcement each. It should be noted that the numerical procedure is the same for either SNSM or steel reinforcement, but the crack spacing S_{cr} is controlled by the steel reinforcement; hence the numerical tensions stiffening simulation should be performed on the steel reinforcement first so that S_{cr} and L_{def} can be determined. The numerical procedure is similar to the one used by Shukri and Jumaat [32]; the procedure is reproduced here for readers' easy reference and is explained below:

1. The tension stiffening prism is made up of concrete area Ac and steel reinforcement area A_r. The prism is then divided into elements of length L_s; in this paper the Ls is taken to be 0.1 mm, which is small enough such that the stresses and strains acting along each element can be considered constant.
2. At the location of crack, an initial value of slip, $\delta(1)$ is set. The load acting on the concrete, $P_c(1)$ is zero as the concrete-concrete interface is not touching. The load acting on the steel reinforcement, $P_r(1)$ is assumed.
3. The bond force acting on the steel reinforcement is $B(1) = \tau(1)L_{per}L_s$, where $\tau(1)$ is determined using any proper bond stress-slip model while L_{per} is the circumferential perimeter of the reinforcement. The strain of steel reinforcement is $\varepsilon_r = P_r(1)A_r/E_r$ where E_r is the reinforcement's elastic modulus. The change in slip from this prism element to the next is $\Delta\delta(1) = (\varepsilon_r(1) - \varepsilon_c(1))L_s$.
4. The slip in the next prism element is $\delta(2) = \delta(1) - \Delta\delta(1)$. The forces acting on the reinforcement and concrete are $P_r(2) = P_r(1)–B(1)$ and $P_c(2) = P_c(1)+B(1)$, respectively. The concrete strain is $\varepsilon_c = P_c(i+1)A_c/E_c$ where E_c is the concrete modulus. This procedure is repeated for the next prism element as well.
5. Steps 2–4 are repeated with different values of assumed $P_r(1)$ until the initial slip $\delta(1)$ can be reduced to 1% of its value by $\delta(n)$, where n refers to number of prism elements required
6. Steps 2–5 are continued until $\varepsilon_c \geq \varepsilon_{ct}$, where ε_{ct} is the concrete cracking strain. The primary crack length S_{cr} can be determined from the total length of prism elements from $\delta(1)$ to $\delta(n)$.

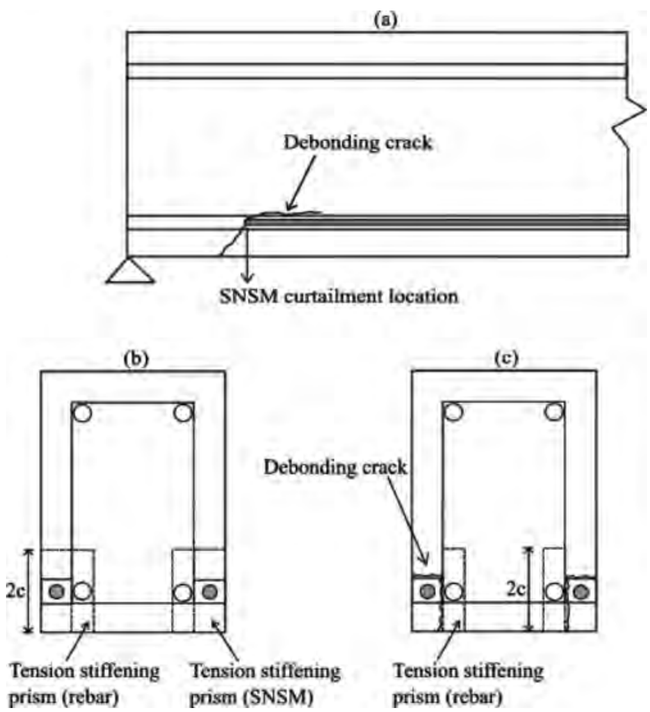

Figure 2. Concrete cover separation on SNSM strengthened RC beams: (a) side view of debonded SNSM strengthened beam; (b) SNSM strengthened beam cross-section prior to debonding; and (c) SNSM strengthened beam cross-section prior to debonding.

7. With the formation of primary crack, steps 1–5 are then repeated with total prism element length n limited to $L_{def} = S_{cr}/2$. The steps are repeated and the values are recorded until a load-slip (P_r/δ) relationship for the steel reinforcement is obtained.
8. Step 7 is then repeated with the SNSM reinforcement to obtain the (P_r/δ) relationship for the SNSM reinforcement. Note that S_{cr} is controlled by steel reinforcement and not the SNSM reinforcement, so procedure 6 does not need to be repeated with the SNSM reinforcement.

3. Moment-rotation simulation

With the load-slip relationship of the steel reinforcement and SNSM reinforcement determined, the M/θ simulation can now be performed. Consider Figure 3, where a beam section of length L_{def} is rotated by θ degree due to moment M. While the RC beam is uncracked, the forces that causes deformation on the beam as shown in Figure 3(a) is to be determined using the stress–strain relationships of each material. The depth of neutral axis d_{na} is then adjusted until equilibrium of forces is achieved; the actual value of moment M which causes rotation θ is then determined. To take into account the formation of concrete wedges and the resulting concrete softening, the stress–strain model for concrete presented by Popovics [41] was used. As the stress–strain of concrete is size dependent, the concrete stress–strain is commonly adjusted for size [22, 33, 42–44] with the size-dependent stress–strain method by Chen et al. [42].

When flexural cracking occurs, slip of reinforcements occur such that the strains of both the SNSM reinforcements and steel reinforcements are no longer constant along length L_{def}. The forces acting on the steel reinforcement and SNSM reinforcements is thus determined using the load-slip relationship obtained from the tension stiffening analysis, where the slip δ_r is determined from the deformation profile in Figure 3(a). Note that the value of slip δ_r applies to both SNSM reinforcements and steel reinforcements, as both have the same value of slip. The d_{na} was again adjusted until equilibrium of forces was obtained, after which the value of M was determined. The whole process was repeated for different values of θ in order to obtain a M/θ relationship. From there to obtain the M/χ relationship is only a matter of dividing the θ with L_{def}. Two types of M/χ are needed to simulate the whole SNSM strengthened RC beam:

1. The moment-curvature of the strengthened section of the beam, $(M/\chi)_s$
2. The moment-curvature of the debonded/unstrengthened section of the beam, $(M/\chi)_u$

4. Determining load–deflection relationship and simulating concrete cover separation

The procedure to determine the load–deflection of the SNSM strengthened beam will be presented here. To take into account the occurrence of concrete cover separation failure, the global energy balance approach (GEBA) [45–48] will be used in conjunction with the M/θ approach. The fundamental principle for GEBA is that it assumes that debonding cracks will always occur on strengthened RC beams; it is then only a matter of determining whether there is enough strain energy for this debonding crack to propagate to cause failure for the SNSM strengthened RC beam. The bending strain energy can be obtained using the M/χ of the strengthened and debonded state of beam at the location of SNSM curtailment as shown in Figure 4. With assumption that moment remains constant due to sudden process in debonding propagation, the strain energy released during debonding is thus the area W_a in Figure 4.

From the value of W_a, the energy release rate (G_a) is then determined as:

$$G_a = \frac{W_a}{b \times \Delta_L} \tag{1}$$

where b is the width of debonding crack, which is taken as two times the width of the SNSM groove and Δ_L is the change in debonding crack length, which is taken as 1 mm for gradual propagation of the debonding crack. The value of G_a is then compared against the fracture strength of concrete, G_{max}. When $G_a > G_{max}$, the debonding crack will progress toward the center of the beam. The load at which this occurs will be referred to as the debonding load, P_d in this manuscript. However this does not mean that the beam has completely failed but rather that the debonding crack has progressed by the length Δ_L. Shukri and Jumaat [32] proposed a procedure for gradual propagation of the debonding crack, which will be used in this manuscript.

A value of load F_P is set and a debonded length, L_d is assumed to have already formed on at the location of curtailment. When applying the GEBA on beams strengthened with FRP sheet [48] or NSM [32] it is assumed that the shear crack that causes the debonding propagates at an angle of 45° to the beam axis until it reaches the shear link, which means the length of L_d is equal to the concrete cover's depth as shown in Figure 5(a) and Figure 5(b). This assumption does not apply to SNSM strengthened

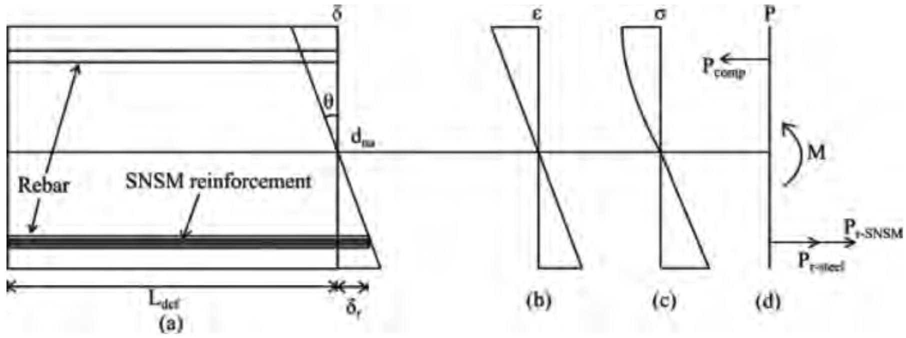

Figure 3. Moment-rotation analysis: (a) beam segment and deformation profile; (b) strain profile; (c) stress profile; and (d) force profile.

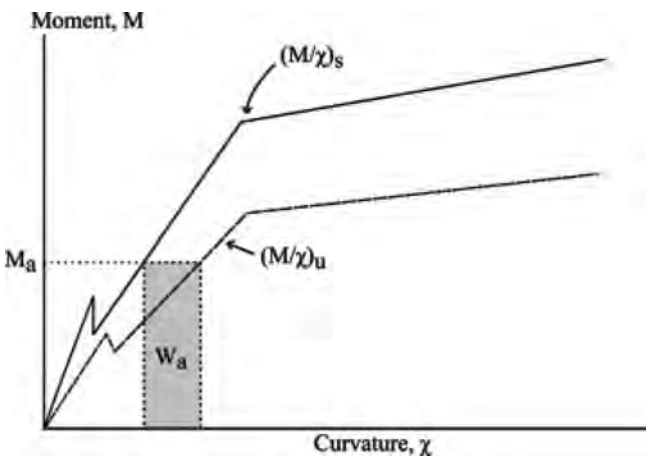

Figure 4. Difference in M/χ at location of SNSM curtailment before and after propagation of debonding crack.

beams since the shear link is not above the SNSM reinforcement, but at its side. From the experimental studies on SNSM strengthened beams [16–18], it was noted that the shear crack starts to propagate horizontally as it reaches the SNSM reinforcement, such that $L_d = 0$ as shown in Figure 5(c).

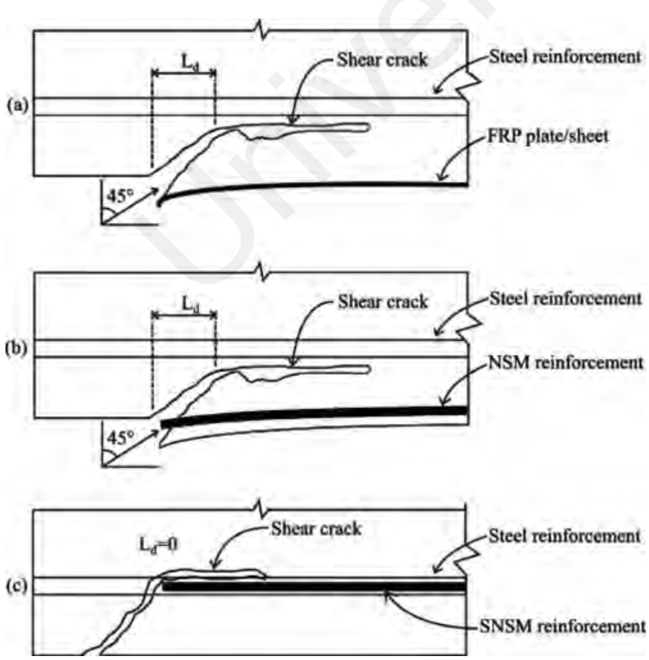

Figure 5. Initial debonded length for different strengthening methods: (a) FRP sheet or plate; (b) NSM reinforcement; and (c) SNSM reinforcement.

In this paper, the change in debonding crack length, Δ_L is taken as 1 mm in the beginning. An initial load, F_a is applied on the simulated beam. The applied moment, M_a is then determined and the commonly used double integration method is then used to determine the deflection by using $(M/\chi)_s$, and $(M/\chi)_u$ for the strengthened and nonstrengthened sections of the beam respectively. The value of G_a at the end of the location of SNSM curtailment is then determined; if $G_a > G_{max}$, the Δ_L is increased by 1 mm. The value of G_a is then calculated again, and this process is repeated until $G_a < G_{max}$. The debonded length L_d is then increased by Δ_L and the applied load F_a is increased and the whole procedure is repeated. At some value of M_a it will no longer possible to determine the value of deflection as the applied moment M_a is beyond the range of moment in $(M/\chi)_u$. The failure load has then been reached and the beam has experienced debonding failure. Alternatively, if this does not occur and the applied M_a exceeds the range of $(M/\chi)_s$ instead, then the beam does not fail by concrete cover separation. The procedure to obtain the load–deflection relationship of SNSM beam discussed here is also shown as a flowchart in Figure 6.

5. Simulating SNSM retrofitted RC beams

The differences involved when simulating SNSM retrofitted RC beam will be presented here. To reiterate, retrofitted RC beams refer to RC beams that have been in service prior to being strengthened; a strengthened virgin beam on the other hand is not. While most lab work focuses on strengthened virgin beams, their results may not be identical to real world results. When a beam needs to be retrofitted or strengthened, there will already be primary cracks already present on the beams. The primary crack spacing of these beams, $S_{cr\text{-}s}$, is likely to be smaller than the primary crack spacing of strengthened virgin beams, $S_{cr\text{-}v}$ as shown in Figure 7.

For SNSM strengthened beams, Shukri et al. [18] showed that the difference in crack spacing is due to the change in tension stiffening prism size. Prior to being retrofitted, the tension stiffening prism is taken to be 2 *c* times the width of the beam divided between the number of steel reinforcements. The tension stiffening prism size is thus larger compared to the size for strengthened RC beam, as shown in **Figure 7(a)**. When the beam is retrofitted, the beam will have the tension stiffening prism size reduced, but the primary cracks will have occurred and the crack spacing will be $S_{cr\text{-}v}$. The combination of a smaller tension stiffening prism and longer crack spacing causes the curvature of a retrofitted beam to be smaller compared to the

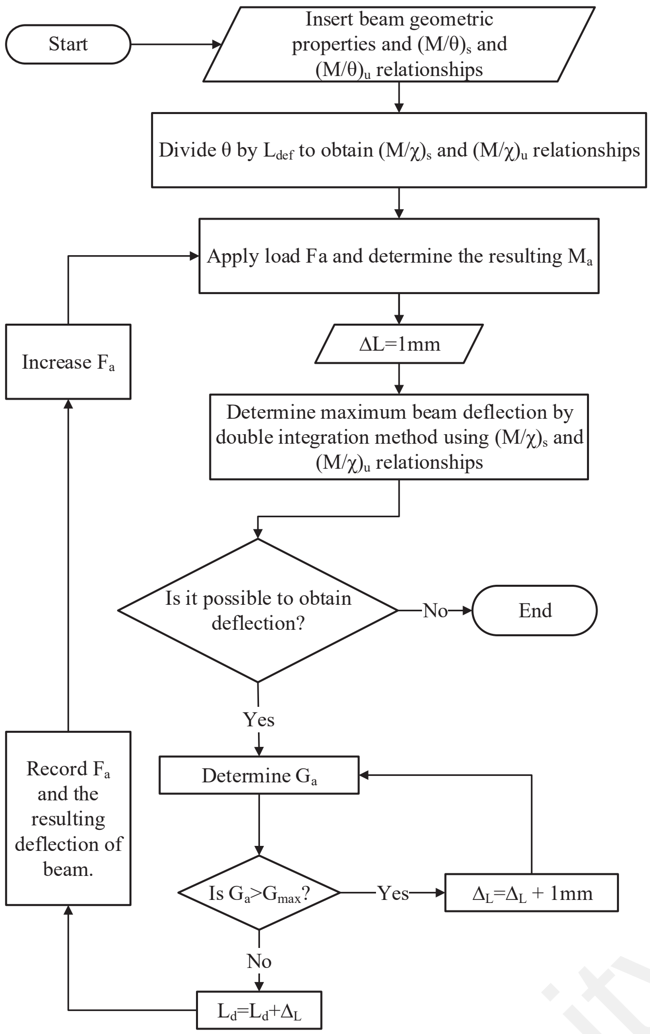

Figure 6. Flowchart for determining the load–deflection of NSM strengthened beams.

curvature of a virgin beam for a similar value of moment. This results in the flexural stiffness of retrofitted beams to be higher than strengthened virgin beams.

While a retrofitted beam may have some existing primary cracks, the low moment regions of the beam may still be undisturbed, as shown in Figure 7(c). If load is applied such that primary cracks appear on these low moment regions after being retrofitted, the crack spacing will be $S_{cr\text{-}v}$ corresponding to the crack spacing for the smaller tension stiffening prism for strengthened RC beam as shown in Figure 7(b). For simplicity, the behavior of an SNSM retrofitted beam can simply be determined by using the crack spacing of $S_{cr\text{-}s}$ for the entirety of the beam with good correlation between simulated and experimental results [18]. When applying GEBA on SNSM retrofitted beam, however, it is more conservative and accurate to use $S_{cr\text{-}v}$ for the regions near the end of the SNSM reinforcement.

To summarize, GEBA procedure for SNSM retrofitted beam as discussed in the previous section is still applicable here, with one change: when calculating the G_a, the rotation, θ for $(M/\theta)_s$ and $(M/\theta)_u$ are divided by $L_{def\text{-}v}$ instead of $L_{def\text{-}s}$ to obtain $(M/\chi)_s$ and $(M/\chi)_u$, respectively. $L_{def\text{-}v}$ and $L_{def\text{-}s}$ are half of the primary crack spacing $S_{cr\text{-}v}$ and $S_{cr\text{-}s}$, respectively.

Table 1. Details of SNSM strengthened RC beams.

Beam designation	d_n (mm)	P_{cr} (kN)
SNC8	8	—
SNC10	10	—
SNC12	12	—
PSNC8	8	22.5
PSNC10	10	30
PSNC12	12	37.5

Note: M_{snsm} = material for SNSM reinforcement; d_n = diameter of SNSM reinforcement; P_{cr} = precracking load.

6. Validation using experimental results

The experimental results by Shukri et al. [18] will be used to validate the proposed method. The load versus mid-span deflection results of six SNSM strengthened RC beams are available, with three of the beams applied precracking loads (P_{cr}) of 22.5, 30, and 37.5 kN each. The purpose of these precracking loads is only to induce flexural cracks in order to simulate the condition of retrofitted beams as seen in practice. The different values of precracking loads correspond to the different flexural rigidity of the beams due to the different sizes of steel reinforcement used. After the precracking load was applied, the beams were unloaded, strengthened using SNSM method and applied load again up to failure. All the beams used carbon FRP (CFRP) bars as SNSM reinforcement. The SNSM CFRP reinforcements had a diameter of either 8, 10, or 12 mm. The further details on the beams are available in Table 1. In Table 2, the material properties of the concrete, steel reinforcement and FRP bars are given.

The beams have a dimension of 125 mm × 250 mm with a clear cover of 27 mm; the length of the beams was 2300 with 2000 mm as the effective span and a shear span of 650 mm. The SNSM reinforcements have a bonded length of 1900 mm. Two steel reinforcements with 12 mm diameter were used as tensile reinforcement. Two steel reinforcements with 10 mm diameter deformed bars were used as compression reinforcement up to the shear span zone. Shear reinforcement was provided through 6 mm diameter bars, distributed along the length of the specimens except in the constant moment region to prevent it from influencing crack propagation.

7. Material models

Several material models were used in this study. It should be noted that the models used in the M/θ approach are intended to act as input for the analysis, they may be refined or changed in order to produce results that are more accurate [23]. Only a general information about the material models are given here to keep the paper short; more information about the models can be obtained using the reference given.

For the steel reinforcements a bilinear stress–strain model with strain hardening was used, the CFRP bars used a linear

Table 2. Material properties.

f_c (MPa)	E_y (MPa)	σ_y (MPa)	σ_u (MPa)	E_f (MPa)	σ_f (MPa)
40	200,000	520	570	124,000	1850

Note: f_c = concrete strength (cylinder); E_y = steel elastic modulus; σ_y = steel yield strength;; σ_u = steel ultimate strength; E_f = FRP modulus; σ_f = FRP tensile strength.

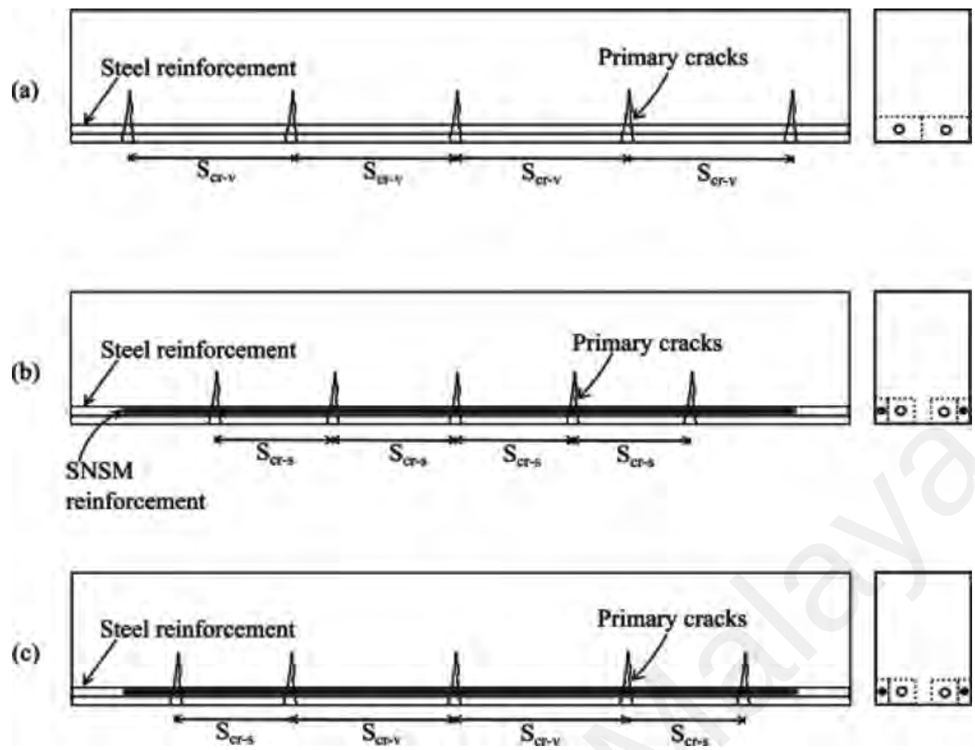

Figure 7. Comparison of primary crack spacing: (a) Virgin RC beam; (b) Virgin SNSM strengthened RC beam; and (c) SNSM retrofitted RC beam.

stress–strain model. The bond-slip model by CEB-FIP [49] for the steel reinforcement was used in the tension stiffening simulation. For the SNSM reinforcements, the bond-slip model by De Lorenzis [50] which was derived for NSM reinforcements is used. The maximum bond stress, τ_{max} was obtained using the bond strength model by Hassan and Rizkalla [14]. Popovics' [41] concrete compressive stress–strain model was used. The concrete stress–strain model was adjusted for size using the size-dependent stress–strain method proposed by Chen et al. [42].

8. Comparison against published experimental results

The comparison of simulated and experimental load versus mid deflection curves for beams SNC8, SNC10, PSNC8, and PSNC10 are given in Figure 8. All the beams were reported to have failed by FRP rupture instead of concrete cover separation. Their inclusion in this study is to determine whether the method proposed in this paper can accurately simulate their behavior. The simulated curve was able to follow the shape of the experimental curve well. The simulated failure loads and deflections at failure are also adequately accurate.

The comparison of load versus mid-span deflection for beams SNC12 and PSNC12 is shown in Figure 9. The beams were reported to have failed by concrete cover separation. From Figure 9, it can be seen that the simulated curve was able to predict the failure load and failure deflection accurately. Figure 9 also includes the simulated curves without GEBA, which means that these curves could not simulate concrete cover separation failure. It can be seen that without the use of GEBA, the simulated result overpredicts the failure load of the beams by a considerable degree.

9. Parametric study

Using the proposed method, parametric studies were conducted to determine the effects of several parameters on the overall behavior of SNSM strengthened RC beams. The detail for the parametric study is given in Table 3. The parameters tested are concrete strength (f_c), elastic modulus of SNSM reinforcement ($E_{r\text{-}snsm}$), bond strength of epoxy adhesive (τ_{max}), and location of SNSM curtailment which is given in term of the distance of the SNSM reinforcement's end to the beam's support (L_a). This parametric study also includes comparison of results between retrofitted and virgin SNSM strengthened RC beams in order to study the difference in behavior between the two beam conditions. The geometric and material properties of beam SNC12 and PSNC12 are used as the reference for this parametric study, where beam SNC12 represents virgin SNSM strengthened beam and PSNC12 represents SNSM retrofitted beams.

The result of the parametric study is given in **Table 3**. The debond load, P_d is the load at which the energy release rate G_a is found to be greater than G_{max}, causing the debonding crack to start propagating horizontally toward the center of the beam. This does not mean the beam would immediately fail, as the debonding crack's propagation can be a gradual process. As can be seen in **Table 3**, for most beams there are considerable difference in the values of P_d before the beams finally fail at the failure load, P_f. Nearly all the beams failed due to concrete cover separation, although it was found that beams with low values of $E_{r\text{-}snsm}$ and $\tau_{max\text{-}snsm}$ failed due to concrete crushing instead. Also presented in **Table 3** are the pre-yield stiffness, K_e of the beams, which were determined by calculating the slope of the load–deflection curve in the elastic region. The retrofitted beams consistently have a higher K_e than the virgin beams, which agrees

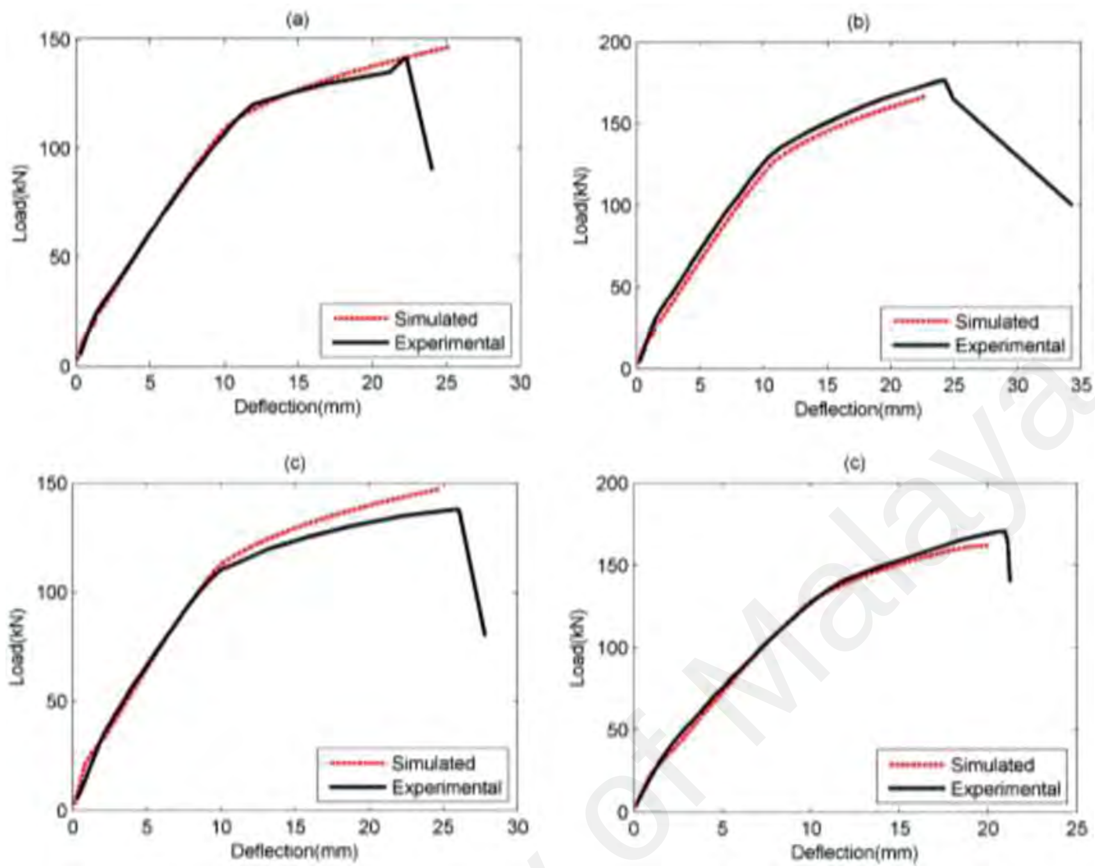

Figure 8. Load versus mid-span deflection curves (a) SNC8; (b) SNC10; (c) PSNC8; and (d) PSNC10.

Table 3. List of parameters tested and summary of simulated results.

Parameter tested	Beam condition	P_d (N/mm^2)	P_f (N/mm^2)	K_e	FM
$f_c = 30$ N/mm^2	Virgin	144.2	150.2	12.1	CCS
$f_c = 40$ N/mm^2	Virgin	163.4	169.4	12.9	CCS
$f_c = 50$ N/mm^2	Virgin	179.0	184.8	12.9	CCS
$f_c = 30$ N/mm^2	Retrofitted	141.2	147.0	13.9	CCS
$f_c = 40$ N/mm^2	Retrofitted	157.2	163.0	15.4	CCS
$f_c = 50$ N/mm^2	Retrofitted	174.2	179.8	15.1	CCS
$E_{r\text{-snsm}} = 62$ kN/mm^2	Virgin	—	155.4	11.0	CC
$E_{r\text{-snsm}} = 124$ kN/mm^2	Virgin	163.4	169.4	12.9	CCS
$E_{r\text{-snsm}} = 186$ kN/mm^2	Virgin	153.4	159.8	14.6	CCS
$E_{r\text{-snsm}} = 62$ kN/mm^2	Retrofitted	—	158.2	12.9	CC
$E_{r\text{-snsm}} = 124$ kN/mm^2	Retrofitted	157.2	163.0	15.4	CCS
$E_{r\text{-snsm}} = 186$ kN/mm^2	Retrofitted	148.0	154.0	17.3	CCS
$\tau_{max} = 9.4$ N/mm^2	Virgin	—	175.6	11.4	CC
$\tau_{max} = 18.8$ N/mm^2	Virgin	163.4	169.4	12.9	CCS
$\tau_{max} = 28.2$ N/mm^2	Virgin	156.0	162.2	14.1	CCS
$\tau_{max} = 9.4$ N/mm^2	Retrofitted	171.8	175.8	13.4	CC
$\tau_{max} = 18.8$ N/mm^2	Retrofitted	157.2	163.0	15.4	CCS
$\tau_{max} = 28.2$ N/mm^2	Retrofitted	150.0	156.0	16.8	CCS
$L_a = 50$ mm	Virgin	163.4	169.4	12.9	CCS
$L_a = 100$ mm	Virgin	81.6	92.2	12.9	CCS
$L_a = 150$ mm	Virgin	54.4	67.8	12.9	CCS
$L_a = 50$ mm	Retrofitted	157.2	163.0	15.4	CCS
$L_a = 100$ mm	Retrofitted	88.6	88.6	15.3	CCS
$L_a = 150$ mm	Retrofitted	52.4	64.8	15.2	CCS

Note: L_a = location of SNSM curtailment; P_d = debond load; K_e = effective pre-yield stiffness; $P_{f\text{-}n}$ = normalizing failure load; FM = failure mode; CCS = concrete cover separation; CC = concrete crushing.

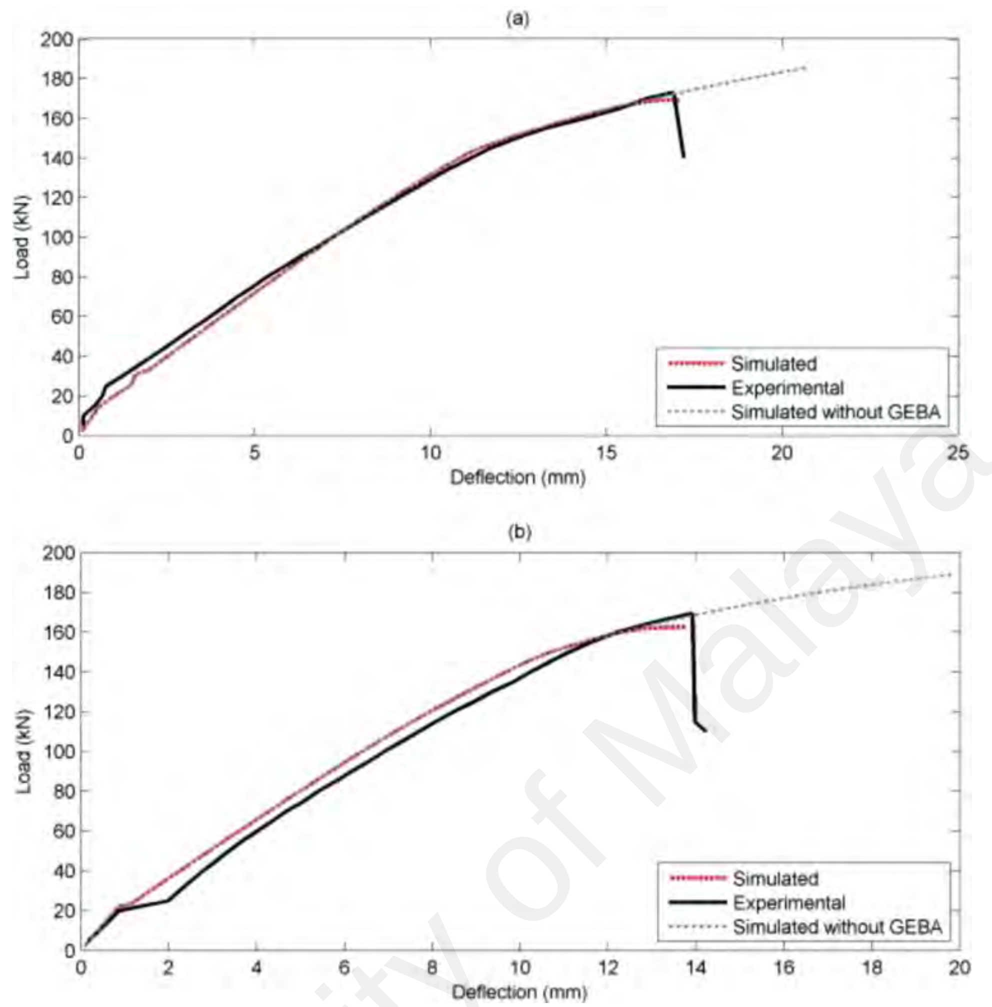

Figure 9. Load versus mid-span deflection curves (a) SNC12 and (b) PSNC12.

with that was reported by Shukri et al. [18] in their experimental study.

10. Discussion on the parametric study

The values of P_f given in **Table 3** is shown in graph form in **Figure 10** to observe the trend of the values of P_f with respect to the parameter tested. The simulated beams which failed by concrete crushing are labelled with 'cc' in Figure 10, while unlabeled ones are simulated to have failed by concrete cover separation. The effect of f_c on P_f is given in **Figure 10(a)**. The values of P_f were found to increase when f_c is increased. The P_f for all retrofitted beams were found to be lower compared to the virgin beams by about 3–4%. At $f_c = 50$ N/mm^2 the effects of concrete cover separation are less pronounced as the higher strength of concrete increases the fracture strength, which in turn reduces propagation of debonding crack. Where the debonding is less pronounced, it can be seen that retrofitted beams have a higher P_f than the virgin beam by about 1% due to the higher stiffness, K_e of the retrofitted beam.

The effect of $E_{r\text{-}snsm}$ of SNSM reinforcement on P_f is given in Figure 10(b). At $E_{r\text{-}snsm}$ of 62 kN/mm^2, it was found that both the virgin and retrofitted beams failed through concrete crushing rather than concrete cover separation. The low $E_{r\text{-}snsm}$ causes the value of W_a to be smaller, which reduces the energy release rate G_a, hence reducing the probability of concrete cover separation. Increasing the $E_{r\text{-}snsm}$ to 124 kN/mm^2 caused the beams to fail by concrete cover separation, due to the larger W_a; despite this premature failure, it was found that the higher $E_{r\text{-}snsm}$ caused the P_f to be much higher than beams with $E_{r\text{-}snsm}$ of 62 kN/mm^2. Increasing the $E_{r\text{-}snsm}$ to 186 kN/mm^2 caused the P_f to drop, as the larger W_a caused the concrete cover separation to occur at a lower debonding load, P_d, than the beams with $E_{r\text{-}snsm}$ of 124 kN/mm^2. A comparison of P_d is given in Table 3. From parametric study, it was found that the beams with $E_{r\text{-}snsm}$ of 124 kN/mm^2 gave the highest P_f. It can also be observed from **Figure 10(b)** that when the beams do not fail by concrete cover separation, the retrofitted beams will have a higher P_f compared to virgin beams. This attribute to higher flexural stiffness of the retrofitted beams. However, when concrete cover separation occurs as in the case when $E_{r\text{-}snsm}$ were 124 and 186 kN/mm^2, the retrofitted beams will have a lower P_f compared to virgin beams. The P_f of retrofitted beams was found to be 4% lower than virgin beams; it was also noted that when $E_{r\text{-}snsm}$ was 62 kN/mm^2, the P_f of the retrofitted beam was 2% higher than the virgin beam.

Figure 10(c) shows the effect of τ_{max} on the P_f of SNSM strengthened beams, where it can be seen that P_f decreases when

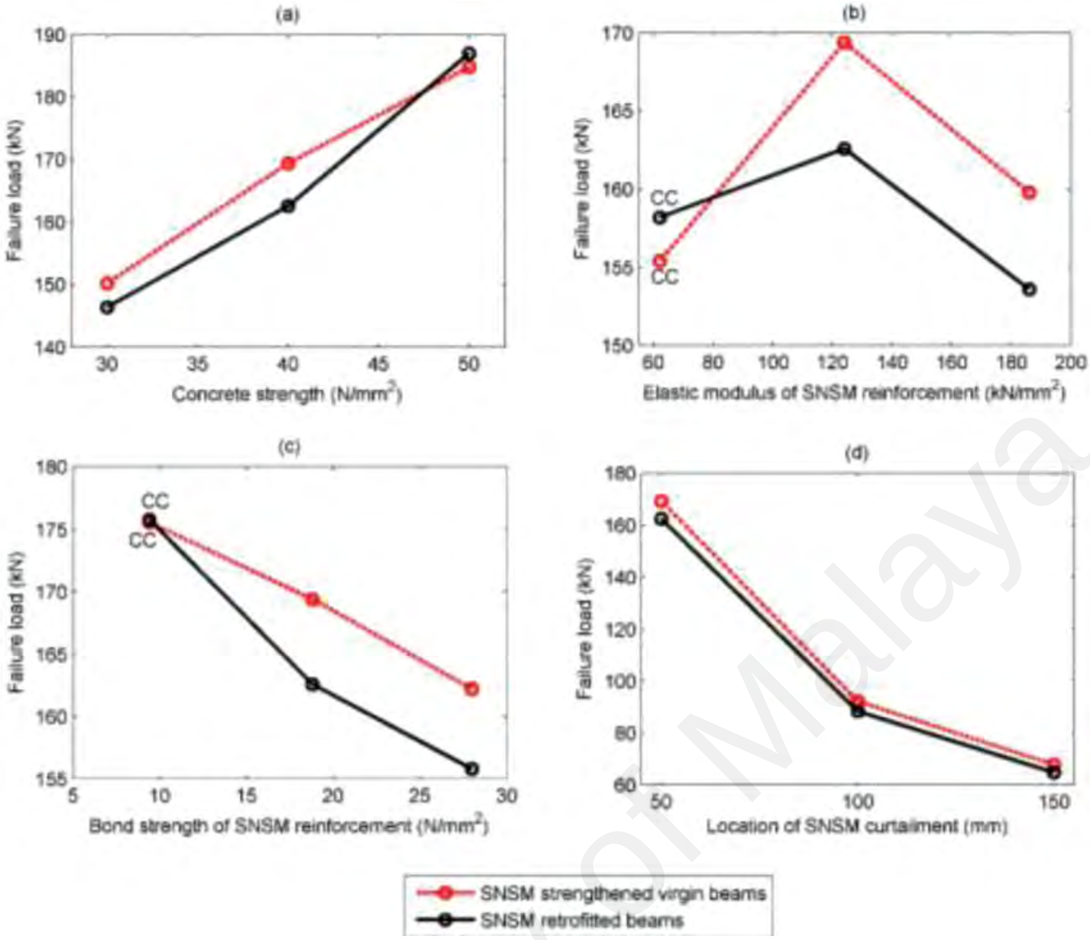

Figure 10. Simulated failure loads of beams in the parametric study (a) concrete strength; (b) elastic modulus of SNSM reinforcement; (c) bond strength of epoxy adhesive; and (d) location of SNSM curtailment.

the τ_{max} is increased. This is again related to the value of W_a and G_a, which increases when higher values of τ_{max} are used, thus causing concrete cover separation to occur at a lower P_d and reducing the P_f. It was found that when τ_{max} was 5 N/mm^2, concrete cover separation did not occur and the P_f of virgin and retrofitted beams were nearly identical. At higher τ_{max}, where concrete cover separation occurs, the P_f for retrofitted beams are significantly lower than virgin beams. The difference in P_f between retrofitted and virgin beams was found to be about 0–4%.

The relationship between L_a and P_f is shown in Figure 10(d). P_f was found to decrease with increasing L_a. A larger L_a results in a larger moment acting around the end of the SNSM reinforcement; this causes a larger W_a and G_a, which then results in a lower P_d and P_f. From Figure 10(d), it can be seen that the retrofitted beams always have a lower P_f compared to virgin beams. However, the difference in P_f due to beam condition was less pronounced when compared to the difference in P_f caused by different values of L_a. The P_f for retrofitted beams were found to be 4% less than virgin beams.

From the result of K_e in Table 3, the retrofitted beams were found to have a higher K_e compared to virgin beams in all cases by about 15–19%. This finding is consistent with what was previously reported in the experimental study performed by Shukri et al. [18].

11. Conclusion

A method to simulate the behavior of SNSM strengthened RC beams was presented; this method allows the simulation of concrete cover separation, which is the primary mode of premature failure for SNSM strengthened beams. It is also shown how the concrete cover separation failure of SNSM retrofitted RC beams can be simulated. Several conclusions can be made from the study:

- The proposed method was validated and showed good accuracy results using published experimental results.
- SNSM retrofitted strengthened beams was found to have approximately 3–4% lower failure load compared to virgin SNSM strengthened beams when concrete cover separation is a factor.
- In cases where concrete cover separation failure did not occur or less pronounced, the failure load was found higher in SNSM retrofitted beams by up to 1% due to approximately 15–19% higher flexural stiffness of retrofitted beams than virgin beams due to longer crack spacing of the retrofitted beams.
- There is only a slight difference in failure load of SNSM retrofitted beams compared to virgin SNSM strengthened beams, although the small difference is negligible.
- There is a considerable difference in the flexural stiffness of virgin and retrofitted beams that should not be neglected.

- It was found that retrofitted and virgin beam conditions do not affect the failure mode of the SNSM strengthened beams.
- While the current proposed method is complicated for general design usage, it is recommended that this method undergo further analysis using similar parametric studies shown to produce simpler design procedures.

Conflict of Interest

The authors declare that they have no conflict of interest.

Funding

This study was supported by the University of Malaya, Grand Challenge - SUS (Sustainability Science) Grant, project number GC003A-15SUS.

References

[1] R. A. Hawileh, M. Z. Naser, and J. A. Abdalla, Finite element simulation of reinforced concrete beams externally strengthened with short-length CFRP plates, Compos. Part B Eng., vol. 45, no. 1, pp. 1722–1730, 2013. doi:10.1016/j.compositesb.2012.09.032.

[2] R. Hawileh, J. A. Abdalla, M. Z. Naser, and M. Tanarslan, Finite element modeling of shear deficient RC beams strengthened with NSM CFRP rods under cyclic loading, Am. Concr. Institute, ACI Spec. Publ., vol. 2015–Janua, no. SP 301, pp. 69–85, 2015.

[3] R. A. Hawileh, H. A. Rasheed, J. A. Abdalla, and A. K. Al-Tamimi, Behavior of reinforced concrete beams strengthened with externally bonded hybrid fiber reinforced polymer systems, Mater. Des., vol. 53, pp. 972–982, 2014. doi:10.1016/j.matdes.2013.07.087.

[4] A. Bilotta, et al., Bond efficiency of EBR and NSM FRP systems for strengthening concrete members, J. Compos. Constr., vol. 15, no. 5, pp. 757–772, 2011. doi:10.1061/(ASCE)CC.1943-5614.0000204.

[5] F. Ceroni, M. Pecce, A. Bilotta, and E. Nigro, Bond behavior of FRP NSM systems in concrete elements, Compos. Part B Eng., vol. 43, no. 2, pp. 99–109, Mar. 2012. doi:10.1016/j.compositesb.2011.10.017.

[6] G. Wu, Z.-Q. Dong, Z.-S. Wu, and L.-W. Zhang, Performance and parametric analysis of flexural strengthening for RC beams with NSM-CFRP bars, J. Compos. Constr., vol. 18, no. 4, p. 4013051, 2013. doi:10.1061/(ASCE)CC.1943-5614.0000451.

[7] A. Bilotta, F. Ceroni, E. Nigro, and M. Pecce, Efficiency of CFRP NSM strips and EBR plates for flexural strengthening of RC beams and loading pattern influence, Compos. Struct., vol. 124, pp. 163–175, 2015. doi:10.1016/j.compstruct.2014.12.046.

[8] L. De Lorenzis and J. G. Teng, Near-surface mounted FRP reinforcement: An emerging technique for strengthening structures, Compos. Part B Eng., vol. 38, no. 2, pp. 119–143, Mar. 2007. doi:10.1016/j.compositesb.2006.08.003.

[9] J. Teng, L. De Lorenzis, and B. Wang, Debonding failures of RC beams strengthened with near surface mounted CFRP strips, J. Compos. Constr., no. April, pp. 92–106, 2006. doi:10.1061/(ASCE)1090-0268(2006)10:2(92).

[10] J. G. Teng, S. S. Zhang, and J. F. Chen, Strength model for end cover separation failure in RC beams strengthened with near-surface mounted (NSM) FRP strips, Eng. Struct., vol. 110, pp. 222–232, 2016. doi:10.1016/j.engstruct.2015.11.049.

[11] S. B. Singh, A. L. Reddy, and C. P. Khatri, Experimental and parametric investigation of response of NSM CFRP-strengthened RC beams, J. Compos. Constr., vol. 18, no. 1, p. 4013021, 2014. doi:10.1061/(ASCE)CC.1943-5614.0000411.

[12] G. M. Dalfré and J. A. O. Barros, Flexural strengthening of RC continuous slab strips using NSM CFRP laminates, Adv. Struct. Eng., vol. 14, no. 6, pp. 1223–1245, 2011. doi:10.1260/1369-4332.14.6.1223.

[13] R. A. Hawileh, Nonlinear finite element modeling of RC beams strengthened with NSM FRP rods, Constr. Build. Mater., vol. 27, no. 1, pp. 461–471, Feb. 2012. doi:10.1016/j.conbuildmat.2011.07.018.

[14] T. K. Hassan and S. H. Rizkalla, Bond mechanism of near-surface-mounted fiber-reinforced polymer bars for flexural strengthening of concrete structures, ACI Struct. J., vol. 101, no. 6, pp. 830–839, 2004.

[15] T. Hassan and S. Rizkalla, Investigation of bond in concrete structures strengthened with near surface mounted carbon fiber reinforced polymer strips, J. Compos. Constr., vol. 7, no. 3, pp. 248–257, 2003. doi:10.1061/(ASCE)1090-0268(2003)7:3(248).

[16] I. A. Sharaky, R. M. Reda, M. Ghanem, M. H. Seleem, and H. E. M. Sallam, Experimental and numerical study of RC beams strengthened with bottom and side NSM GFRP bars having different end conditions, Constr. Build. Mater., vol. 149, pp. 882–903, 2017. doi:10.1016/j.conbuildmat.2017.05.192.

[17] M. A. Hosen, M. Z. Jumaat, and A. B. M. S. Islam, Side near surface mounted (SNSM) technique for flexural enhancement of RC beams, Mater. Des., vol. 83, pp. 587–597, 2015. doi:10.1016/j.matdes.2015.06.035.

[18] A. A. Shukri, M. A. Hosen, R. Muhamad, and M. Z. Jumaat, Behaviour of precracked RC beams strengthened using the side-NSM technique, Constr. Build. Mater., vol. 123, pp. 617–626, 2016. doi:10.1016/j.conbuildmat.2016.07.066.

[19] J. G. Teng, S. S. Zhang, and J. F. Chen, Strength model for end cover separation failure in RC beams strengthened with near-surface mounted (NSM) FRP strips, Eng. Struct., vol. 110, pp. 222–232, 2016. doi:10.1016/j.engstruct.2015.11.049.

[20] S. S. Zhang and J. G. Teng, Finite element analysis of end cover separation in RC beams strengthened in flexure with FRP, Eng. Struct., vol. 75, no. 6, pp. 550–560, 2014. doi:10.1016/j.engstruct.2014.06.031.

[21] M. Rezazadeh, J. A. O. Barros, and H. Ramezansefat, End concrete cover separation in RC structures strengthened in flexure with NSM FRP: Analytical design approach, Eng. Struct., vol. 128, pp. 415–427, 2016. doi:10.1016/j.engstruct.2016.09.062.

[22] K. H. Mo, P. Visintin, U. J. Alengaram, and M. Z. Jumaat, Prediction of the structural behaviour of oil palm shell lightweight concrete beams, Constr. Build. Mater., vol. 102, pp. 722–732, 2016. doi:10.1016/j.conbuildmat.2015.10.184.

[23] D. Knight, P. Visintin, D. J. Oehlers, and M. S. Mohamed Ali, Short-term partial-interaction behavior of RC beams with prestressed FRP and steel, J. Compos. Constr., vol. 18, no. 1, p. 4013029, 2014. doi:10.1061/(ASCE)CC.1943-5614.0000408.

[24] P. Visintin, D. J. Oehlers, C. Wu, and M. Haskett, A mechanics solution for hinges in RC beams with multiple cracks, Eng. Struct., vol. 36, pp. 61–69, Mar. 2012. doi:10.1016/j.engstruct.2011.11.028.

[25] A. A. Shukri, P. Visintin, D. J. Oehlers, and M. Z. Jumaat, Mechanics model for simulating RC hinges under reversed cyclic loading, Materials (Basel)., vol. 9, no. 4, p. 305, 2016. doi:10.3390/ma9040305.

[26] D. Knight, P. Visintin, D. J. Oehlers, and M. S. Mohamed Ali, Simulating RC beams with unbonded FRP and steel prestressing tendons, Compos. Part B Eng., vol. 60, pp. 392–399, Apr. 2014. doi:10.1016/j.compositesb.2013.12.039.

[27] P. Visintin, D. J. Oehlers, C. Wu, and M. C. Griffith, The reinforcement contribution to the cyclic behaviour of reinforced concrete beam hinges, Earthq. Eng. Struct. Dyn., vol. 41, pp. 1591–1608, 2012. doi:10.1002/eqe.1189.

[28] P. Visintin, D. Oehlers, and M. Haskett, Partial-interaction time dependent behaviour of reinforced concrete beams, Eng. Struct., vol. 49, pp. 408–420, Apr. 2013. doi:10.1016/j.engstruct.2012.11.025.

[29] P. Visintin, D. J. Oehlers, R. Muhamad, and C. Wu, Partial-interaction short term serviceability deflection of RC beams, Eng. Struct., vol. 56, pp. 993–1006, Nov. 2013. doi:10.1016/j.engstruct.2013.06.021.

[30] K. M. ud Darain et al., Strengthening of RC beams using externally bonded reinforcement combined with near-surface mounted technique, Polymers (Basel), vol. 8, no. 7, p. 261, 2016. doi:10.3390/polym8070261.

[31] A. A. Shukri, K. M. ud Darain, and M. Z. Jumaat, The tension-stiffening contribution of NSM CFRP to the behavior of strengthened RC beams, Materials (Basel), vol. 8, no. 7, pp. 4131–4146, 2015. doi:10.3390/ma8074131.

[32] A. A. Shukri and M. Z. Jumaat, Simulating concrete cover separation in RC beams strengthened with near-surface mounted

reinforcements, Constr. Build. Mater., vol. 122, pp. 1–11, 2016. doi:10.1016/j.conbuildmat.2016.06.048.

[33] D. J. Oehlers, P. Visintin, and W. Lucas, Flexural strength and ductility of FRP-plated RC beams: Fundamental mechanics incorporating local and global IC debonding, J. Compos. Constr., vol. 20, no. 2, p. 4015046, 2015. doi:10.1061/(ASCE)CC.1943-5614.0000610.

[34] D. J. Oehlers, P. Visintin, M. Haskett, and W. M. Sebastian, Flexural ductility fundamental mechanisms governing all RC members in particular FRP RC, Constr. Build. Mater., vol. 49, pp. 985–997, Dec. 2013. doi:10.1016/j.conbuildmat.2013.02.018.

[35] R. Muhamad, M. S. Mohamed Ali, D. J. Oehlers, and M. Griffith, The tension stiffening mechanism in reinforced concrete prisms, Adv. Struct. Eng., vol. 15, no. 12, pp. 2053–2069, 2012. doi:10.1260/1369-4332.15.12.2053.

[36] D. J. Oehlers, M. Haskett, M. S. Ali, W. Lucas, and R. Muhamad, Our obsession with curvature in RC beam modelling, Adv. Struct. Eng., vol. 14, no. 3, pp. 391–404, Jun. 2011. doi:10.1260/1369-4332.14.3.391.

[37] A. K. Gupta and S. R. Maestrini, Tension stiffness model for reinforced concrete bars, J. Struct. Eng., vol. 116, no. 3, pp. 769–790, 1990. doi:10.1061/(ASCE)0733-9445(1990)116:3(769).

[38] M. Haskett, D. J. Oehlers, and M. S. Mohamed Ali, Local and global bond characteristics of steel reinforcing bars, Eng. Struct., vol. 30, no. 2, pp. 376–383, Feb. 2008. doi:10.1016/j.engstruct.2007.04.007.

[39] R. Muhamad, M. S. Mohamed Ali, D. Oehlers, and A. Hamid Sheikh, Load-slip relationship of tension reinforcement in reinforced concrete members, Eng. Struct., vol. 33, no. 4, pp. 1098–1106, Apr. 2011. doi:10.1016/j.engstruct.2010.12.022.

[40] R. Muhamad, D. J. Oehlers, and M. M. Ali, Discrete rotation deflection of RC beams at serviceability, Proc ICE Struct Build., vol. 164, pp. 1–14, 2011.

[41] S. Popovics, A numerical approach to the complete stress-strain curve of concrete, Cem. Concr. Res., vol. 3, no. 5, pp. 583–599, 1973. doi:10.1016/0008-8846(73)90096-3.

[42] Y. Chen, P. Visintin, D. Oehlers, and U. J. Alengaram, Size-dependent stress-strain model for unconfined concrete, J. Struct. Eng., vol. 140, no. 4, p. 4013088, 2014. doi:10.1061/(ASCE)ST.1943-541X.0000869.

[43] D. Knight, P. Visintin, D. J. Oehlers, and M. S. Mohamed Ali, Simulation of RC beams with mechanically fastened FRP strips, Compos. Struct., vol. 114, pp. 99–106, Aug. 2014. doi:10.1016/j.compstruct.2014.04.012.

[44] D. Oehlers, P. Visintin, T. Zhang, Y. Chen, and D. Knight, Flexural rigidity of reinforced concrete members using a deformation based analysis, Concr. Aust., vol. 38, no. 4, pp. 50–56, 2012.

[45] P. Achintha and C. Burgoyne, Moment-curvature and strain energy of beams with external fiber-reinforced polymer reinforcement, ACI Struct. J., vol. 106, no. 1, pp. 21–29, 2009.

[46] G. X. Guan and C. J. Burgoyne, Comparison of moment-curvature models for fiber- reinforced polymer plate-end debonding studies using global energy balance approach, ACI Struct. J., vol. 111, no. 1, pp. 27–36, 2014.

[47] M. Achintha and C. Burgoyne, Fracture energy of the concrete-FRP interface in strengthened beams, Eng. Fract. Mech., vol. 110, pp. 38–51, Sep. 2013. doi:10.1016/j.engfracmech.2013.07.016.

[48] M. Achintha and C. J. Burgoyne, Fracture mechanics of plate debonding: Validation against experiment, Constr. Build. Mater., vol. 25, no. 6, pp. 2961–2971, Jun. 2011. doi:10.1016/j.conbuildmat.2010.11.103.

[49] CEB-FIP, CEB-FIP Model Code 1990. London, UK: Thomas Telford Ltd., 1993.

[50] L. De Lorenzis, Anchorage length of near-surface mounted fiber-reinforced polymer rods for concrete strengthening – Analytical modeling, ACI Struct. J., vol. 101, no. 3, pp. 375–386, 2004.

CHAPTER 5 - APPLICATION II: HYBRID STRENGTHENING METHOD

In this chapter two research papers are presented. In this chapter, it will be shown how the simulation method in chapter 3 can be applied to hybrid strengthened RC beams. The method to simulate intermediate crack debonding, which was found to affect hybrid strengthened beams due to the use of EB FRP sheets, was presented and further studies were conducted by means of parametric study.

The first paper, “Strengthening of RC Beams Using Externally Bonded Reinforcement Combined with Near-Surface Mounted Technique” presents a study on hybrid strengthening method using NSM CFRP bars and CFRP sheets. An experimental study was first conducted, followed by a simulation method based on the M/θ approach which was found to be reasonably accurate, although in this paper the intermediate crack (IC) debonding was incorrectly simulated. It should be noted that the credit for the experimental work and the discussions on the experimental results goes entirely to the first author, Kh Mahfuz ud Darain and the other co-authors, while this author’s contribution is mostly in the simulation work using M/θ approach.

The second paper, “Simulating IC Debonding on RC Beams Strengthened with Hybrid Methods” presents a better way to simulate IC debonding using the M/θ approach with the single crack analysis method. Comparison against the experimental and simulated results from the previous paper shows that the new simulation method, which was based on the single crack analysis method, was able to simulate IC debonding failure correctly and gives good correlation against experimental results. A parametric analysis was then conducted using the improved method, from which the following conclusions were made:

- Higher elastic modulus of NSM FRP bar increases the rigidity and maximum load of the hybrid strengthened beam while decreasing the length of IC debonding.
- Higher elastic modulus of FRP sheet on the other hand increases the length of IC debonding; as such while the rigidity and maximum load of the hybrid strengthened beam still increase, the amount is less significant compared to increasing the elastic modulus of NSM FRP bar.
- Higher bond strength of NSM FRP bar and FRP sheet slightly increases the rigidity and maximum load of hybrid strengthened beams.

The details of the research papers contained in this chapter along with the statement of contribution of authors is as follows:

1) Darain, K. M. ud, Jumaat, M., Shukri, A. A., Obaydullah, M., Huda, M., Hosen, M., & Hoque, N. (2016). Strengthening of RC Beams Using Externally Bonded Reinforcement Combined with Near-Surface Mounted Technique. *Polymers*, *8*(7), 261.
    a. Statement of contribution: Kh Mahfuz ud Darain (author) performed experimental work and wrote the paper, Mohd. Zamin Jumaat (co-author) supervised the research and checked the paper, Ahmad Azim Shukri (co-author) performed the simulations and wrote the paper, M. Obaydulah (co-author) performed the experimental work, Md. Nazmul Huda (co-author) performed the experimental work, Md. Akter Hosen (co-author) performed experimental work and wrote the paper, Nusrat Hoque (co-author) provided suggestions on improving the paper.
2) Shukri, A. A., Shamsudin, M.F., Ibrahim, I., Alengaram, U.J., Hashim, H. (2017). Simulating intermediate crack debonding on RC beams strengthened with hybrid methods, *Latin American Journal of Solids and Structures*.

a. Statement of contribution: Ahmad Azim Shukri (author) performed the simulations and wrote the paper, Mohd Fazaulnizam Shamsudin (co-author) wrote and checked the paper, Zainah Ibrahim (co-author) supervised the research and checked the paper, U. Johnson Alengaram (co-author) supervised the research and checked the paper, Huzaifa Hashim (co-author) checked the paper.

5.1 Research paper 4: Strengthening of RC beams using externally bonded reinforcement combined with near-surface mounted technique

Published in *Polymers*

Article history:

Received 21 May 2016

Accepted 11 July 2016

polymers

MDPI

Article

Strengthening of RC Beams Using Externally Bonded Reinforcement Combined with Near-Surface Mounted Technique

Kh Mahfuz ud Darain [1,2,*], Mohd Zamin Jumaat [1,*], Ahmad Azim Shukri [1], M. Obaydullah [1], Md. Nazmul Huda [1], Md. Akter Hosen [1] and Nusrat Hoque [1]

1. Centre for Innovative Construction Technology (CICT), Department of Civil Engineering, Faculty of Engineering, University of Malaya, 50603 Kuala Lumpur, Malaysia; ahmadazimshukri@gmail.com (A.A.S.); md_obaydullah@yahoo.com (M.O.); nazmulhuda.128@gmail.com (M.N.H.); enggakter@gmail.com (M.A.H.); nusrat_hoque@yahoo.com (N.H.)
2. Architecture Discipline, Science, Engineering and Technology School, Khulna University, 9208 Khulna, Bangladesh

* Correspondence: khmahfuz@gmail.com (K.M.D.); zamin@um.edu.my (M.Z.J.); Tel.: +60-182-849-027 (K.M.D.); +60-193-129-194 (M.Z.J.)

Academic Editors: Masoud Motavalli and Alper Ilki
Received: 21 May 2016; Accepted: 11 July 2016; Published: 19 July 2016

Abstract: This study investigates the flexural behaviour of reinforced concrete (RC) beams strengthened through the combined externally bonded and near-surface mounted (CEBNSM) technique. The externally bonded reinforcement (EBR) and near-surface mounted (NSM) techniques are popular strengthening solutions, although these methods often demonstrate premature debonding failure. The proposed CEBNSM technique increases the bond area of the concrete–carbon fibre reinforced polymer (CFRP) interface, which can delay the debonding failure. This technique is appropriate when any structure has a narrow cross-sectional width or is in need of additional flexural capacity that an individual technique or material cannot attain. An experimental test matrix was designed with one control and five strengthened RC beams to verify the performance of the proposed technique. The strengthening materials were CFRP bar as NSM reinforcement combined with CFRP fabric as EBR material. The test variables were the diameter of the NSM bars (8 and 10 mm), the thickness of the CFRP fabrics (one and two layers) and the U-wrap anchorage. The strengthened beams showed enhancement of ultimate load capacity, stiffness, cracking behaviour, and strain compatibility. The ultimate capacity of the CEBNSM-strengthened beams increased from 71% to 105% compared to that of the control beam. A simulation method based on the moment-rotation approach was also presented to predict the behaviour of CEBNSM-strengthened RC beams.

Keywords: CEBNSM; CFRP; externally bonded; near surface mounted; moment-rotation analysis

1. Introduction

Throughout the world, the growing interest in the sustainability of construction encourages the engineering community to develop policies that discourage new construction rather than extend the design life of existing structures [1]. Structural strengthening allows existing underperforming structures to survive against additional service load requirement, design, or construction error and structural deterioration due to age or the surrounding environment [2–4]. In the past decade, fibre-reinforced polymer (FRP) has substituted conventional strengthening materials such as steel and concrete because of its high strength-to-weight ratio, resistance to corrosion, and low density [5–10]. The externally bonded reinforcement (EBR) and near-surface mounted (NSM) strengthening techniques are gaining popularity. The EBR technique consists of one or multiple FRP laminates that are bonded on the tension side of the strengthened member [11]. Meanwhile, the NSM technique involves the insertion of FRP strips or rods into pre-cut grooves in concrete covers and then filling up with epoxy adhesives [12]. The NSM technique is a contemporary technique that offers a high level of strengthening efficacy, is less prone to premature debonding failure, and enhances protection against fire, mechanical damage, the effects of aging, and acts of vandalism. The technique also demonstrates better durability, stress-sharing mechanisms, and fatigue performance, given that the reinforcement is located inside [13].

The problem faced with the EBR method is normally in the form of premature debonding due to high interfacial shear stresses between the FRP and the concrete substrate at the sheet of FRP curtailment location [14–16]. The thickness of FRP composite plays an important role regarding this issue, where the reduction of plate thickness drives down the magnitude of stress concentration at the plate ends [17]. For a fixed FRP ratio, the debonding potential has been reported to increase significantly with increasing FRP thickness [18]. Oehlers [19] proposed a formula based on the interaction between flexural and shear capacities of the beam where the de-bonding failure moment is inversely proportional to FRP sheet thickness.

In the NSM method, often, the width of the beam may not be wide enough to provide necessary edge clearance and clear spacing between two adjacent NSM grooves. The American Concrete Institute (ACI) proposed a minimum edge clearance and clear spacing between two adjacent NSM grooves supported by the research of De Lorenzis, Blaschko, and Parretti, and Nanni [20–22]. This strengthening technique necessitates more concrete cover to allocate enough space for cutting grooves without any possibility of damaging the steel. However, lots of existing structures have less concrete cover due to faulty construction or for a number other reasons, posing a major challenge to this technique [23]. Recently, for retrofitting of reinforced concrete (RC) members with deteriorated cover concrete, the effectiveness of a new strengthening technique (Inhibiting-Repairing-Strengthening, IRS) was experimentally evaluated [24–26]. It consists of the installation of an innovative composite system—made of inorganic matrix and stainless steel strip/fabric—in the thickness of the cover concrete during the repairing/restoring of the same.

With regard to these limitations, a hybrid strengthening method between the EB and NSM method is proposed. The strengthening method—which will be called the combined externally bonded and near-surface mounted (CEBNSM) technique—offers a prudent and optimum combination of NSM and EBR techniques, which perform to complement each other and get rid of their limitations reciprocally. Previous work on similar hybrid strengthening involved a hybrid between NSM steel bars and EB steel plates, as introduced by Rahman, et al. [27]. The use of steel instead of FRP was proposed by Rahman, et al. [27] due to the higher ductility of steel; however, this increase in ductility was not very prominent, as all of the strengthened beams prematurely failed by concrete cover separation.

This study proposes the development of another type of CEBNSM strengthening technique involving the use of EB FRP sheets with NSM FRP bars or NSM steel bars, with the aim of developing a cost-effective strengthening solution which will delay or avoid the debonding failure seen in the previous study. It is identified that the drop in Carbon Fiber Reinforced Polymer (CFRP) fabric thickness diminishes the degree of stress concentration at the fabric edge [27,28]. Through combination, it is possible to reduce the CFRP fabric thickness by transferring a part of the required total strengthening area of CFRP fabric material from EBR to NSM technique. Consequently, the NSM bar or strip size can also be reduced through sharing with EBR strengthening material, and thus provide sufficient space for edge clearance and groove clear spacing [29,30], which can help reduce the possibility of concrete cover separation failure. Moreover, the NSM groove itself creates more contact surface area between the FRP composite and the concrete substrate at the cross-section. As stress is equal to the load divided by the corresponding surface area, an increase in surface area will decrease interfacial stress, further reducing the possibility of concrete cover separation. The addition of adhesive in the NSM grooves to the CEBNSM system also improves bond performance between the strengthening CFRP fabric and the concrete substrate.

The experimental results for six beams are presented in this study, where five of the beams are strengthened with CEBNSM technique. The experimental load, deflection, crack spacing, crack width and strain values of the strengthened beams were analysed to evaluate the serviceability behaviour, ductility, and flexural performance of the proposed CEBNSM technique. A simulation method based on the moment-rotation approach was also presented to predict the behaviour of the CEBNSM-strengthened reinforced concrete beam.

2. Materials and Methods

2.1. Test Matrix

The experimental program was designed with six RC beams. Of those beams, one was assigned as the control specimen, and the remaining beams were strengthened with the CEBNSM strengthening technique. The main testing variables were the diameter of the slotted reinforcement (8 and 10 mm), the thickness of the external CFRP fabrics (one and two layers), and the anchorage at the curtailment location. The length of the CFRP fabric was also varied. For the single-ply condition, a 2900 mm-long CFRP fabric was bonded at the beam soffit. However, for the double-ply condition, the second layer was 2600 mm to avoid end peeling failure due to the increased normal stress developed at the curtailment end of the CFRP fabric [10,31]. The detailed test matrix is shown in Table 1. The beam notation is explained as follows, using "CBC10P2A" as an example. Specifically, C denotes the combination technique, BC denotes the bar as CFRP NSM reinforcement, 8 and 10 denotes the 8 or 10 mm diameter NSM bar, P1 and P2 denote the single-ply or double-ply of CFRP fabric through the EBR technique, and A denotes the anchorage.

Table 1. Test matrix of the experimental program.

Serial. No.	Notation	Description	Strengthening details
1	CB	Control RC beam	Without strengthening
2	CBC8P1	8 mm ϕ NSM CFRP bar and 1 ply of EBR CFRP fabric	CFRP bar: 1–8 mm ϕ (L = 2900 mm) CFRP fabric: 2900 × 125 × 0.17 mm^3
3	CBC8P2	8 mm ϕ NSM CFRP bar and 2 ply of EBR CFRP fabric	CFRP bar: 1–8 mm ϕ (L = 2900 mm) CFRP 1st fabric: 2900 × 125 × 0.17 mm^3 CFRP 2nd fabric: 2600 × 125 × 0.17 mm^3
4	CBC10P1	10 mm ϕ NSM CFRP bar and 1 ply of EBR CFRP fabric	CFRP bar: 1–10 mm ϕ (L = 2900 mm) CFRP fabric: 2900 × 125 × 0.17 mm^3
5	CBC10P2	10 mm ϕ NSM CFRP bar and 2 ply of EBR CFRP fabric	CFRP bar: 1–10 mm ϕ (L = 2900 mm) CFRP 1st fabric: 2900 × 125 × 0.17 mm^3 CFRP 2nd fabric: 2600 × 125 × 0.17 mm^3
6	CBC10P2A	NSM CFRP bar, EB 2 ply CFRP fabric and 2 ply U-wrap end anchorage	CFRP bar: 1–10 mm ϕ (2900 mm) CFRP fabric: 2900 × 125 × 0.34 mm^3 CFRP U-wrap anchorage: 2 ply (625 × 125 × 0.34 mm^3)

2.2. Specimens and Materials

In this experimental program, the dimension of the rectangular RC beams was 3300 mm × 250 mm × 125 mm with a clear span of 3.0 m (Figure 1). The steel ratio ($\rho = As/bd$) was 0.0085 to constitute an under-reinforced RC beam. Two 12 and 10 mm diameter deformed bars were used as the bottom and top reinforcements, respectively, having an 8 mm diameter stirrup with a 90 mm spacing. The top reinforcement and the shear reinforcement were discontinued. They were avoided in the maximum moment region to assure flexural failure.

Polymers **2016**, *8*, 261 4 of 23

compressive and flexural strengths—were evaluated 28 days after concrete casting, based on the cube (100 mm × 100 mm) and prism (500 mm × 100 mm × 100 mm) specimens, according to [32,33]. The mechanical properties of concrete are listed in Table 2.

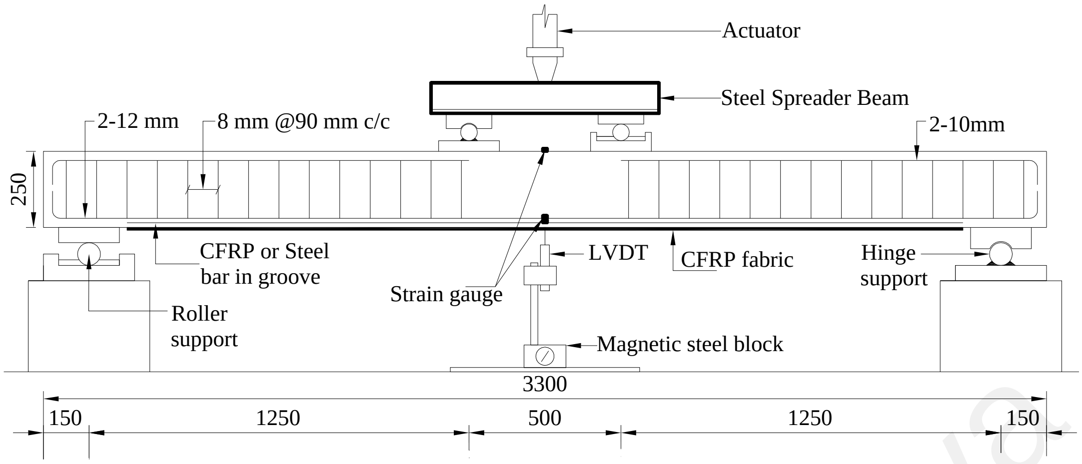

Figure 1. Beam details and test setup (all dimensions are in mm). CFRP: carbon fibre reinforced polymer; LVDT: linear variable differential transducer.

Figure 1. Beam details and test setup (all dimensions are in mm). CFRP: carbon fibre reinforced polymer; LVDT: linear variable differential transducer.

Ready-mix concrete was used for concrete casting. During casting, the same concrete batch was used for the six beams to maintain the same concrete properties. The coarse and fine aggregates were from crushed stone and quarry sand, respectively. The mechanical properties—such as compressive and flexural strengths—were evaluated 28 days after concrete casting, based on the cube (100 mm × 100 mm) and prism (500 mm × 100 mm × 100 mm) specimens, according to [32,33]. The mechanical properties of concrete are listed in Table 2.

The mechanical properties of the steel bar were checked in the laboratory following the [34] guidelines to confirm the specifications given by the suppliers. Either 8 mm or 10 mm diameter CFRP strengthening bar—which was spirally wound with a fibre tow—was placed at the groove, which had a density of 1.65 g/mm^2. A unidirectional, woven CFRP fabric (SikaWrap®-301C) with a thickness of 0.17 mm was used as external strengthening material at the beam soffit. A two-part epoxy (Sikadur® 30) was used as the adhesive filler to fix the CFRP bar inside the groove. The CFRP fabric was also soaked with epoxy resin (Sikadur® 330) for proper bonding with the concrete substrate. These resins are available with a two-part adhesive based on a combination of epoxy resins and filler. Table 2 presents the properties of concrete, internal steel, strengthening steel, CFRP bar, CFRP fabric, and epoxy.

Table 2. Material properties of strengthened specimens.

Material	Mechanical property	Result
Concrete	Compressive strength (MPa)	50.1
	Flexure strength (MPa)	5.5
	Elastic modulus (GPa)	33.26
Steel 12 mm ϕ (Internal bottom reinforcement)	Yield stress (MPa)	529
	Ultimate strength (MPa)	587
	Elastic modulus (GPa)	200
	Elongation (%)	21
Steel 10 mm ϕ (Internal top reinforcement)	Yield stress (MPa)	521
	Ultimate strength (MPa)	578
	Elastic modulus (GPa)	200
	Elongation (%)	20
Steel 8 mm ϕ (Internal shear reinforcement)	Yield stress (MPa)	380
	Ultimate strength (MPa)	450
	Elastic modulus (GPa)	200
	Elongation (%)	29

Table 2. Material properties of strengthened specimens.

Material	Mechanical property	Result
Concrete	Compressive strength (MPa)	50.1
	Flexure strength (MPa)	5.5
	Elastic modulus (GPa)	33.26
Steel 12 mm ϕ (Internal bottom reinforcement)	Yield stress (MPa)	529
	Ultimate strength (MPa)	587
	Elastic modulus (GPa)	200
	Elongation (%)	21
Steel 10 mm ϕ (Internal top reinforcement)	Yield stress (MPa)	521
	Ultimate strength (MPa)	578
	Elastic modulus (GPa)	200
	Elongation (%)	20
Steel 8 mm ϕ (Internal shear reinforcement)	Yield stress (MPa)	380
	Ultimate strength (MPa)	450
	Elastic modulus (GPa)	200
	Elongation (%)	29

Polymers **2016**, *8*, 261 5 of 23

Table 2. *Cont.*

Material	Mechanical property	Result
CFRP bar-12 mm ϕ	Ultimate strength (MPa)	2,400
	Elastic modulus (GPa)	165
	Ultimate strain (%)	1.6
CFRP Fabric (SikaWrap-301C) [35]	Ultimate strength (MPa)	4,900
	Elastic modulus (GPa)	230
	Ultimate strain (%)	2.1
Epoxy (Sikadur®) 30 [36]	Compressive strength	70–80 MPa (15 °C); 85–95 MPa (35 °C)
	Tensile strength	14–17 MPa (15 °C); 16–19 MPa (35 °C)
	Shear strength	24–27 MPa (15 °C); 26–31 MPa (35 °C)
Epoxy (Sikadur®) 330 [37]	Tensile strength (MPa)	30
	Elastic modulus-Flexural (MPa)	3,800
	Elastic modulus-Tensile (MPa)	4,500

2.3. Specimen Design and Preparation

The specimen preparation and strengthening processes are illustrated in Figure 2. A superior quality diamond-bladed concrete saw was used to create 16 mm × 16 mm and 24 mm × 24 mm grooves at the tension region of the RC beam to accommodate the 8 and 10 mm diameter CFRP bars. The groove dimension of the bar diameter was set as two times the diameter of the CFRP bar, as suggested by [23] for the optimal groove size. After using the cutter, the concrete lugs were manually taken out with a hand chisel and a hammer. The remaining rough concrete surface was cleaned using a high-pressure air jet. Acetone was applied on the surface to remove any fine dust particle and any oily substance present in the groove to make a good bonding surface for strengthening. Masking tape was affixed along the ridge of the groove line to ensure the proper placement of epoxy inside the groove and neat finishing of the epoxy surface. Then, approximately two-thirds of the groove was filled with epoxy (Sikadur® 30), which was prepared according to the directions of the manufacturers. The NSM CFRP bar was properly cleaned and gently pressed inside the groove until surrounded by an equal amount of epoxy. Then, a spatula was used to level the surface and clean the area. The whole preparation was left for standard curing time, as prescribed by the manufacturer.

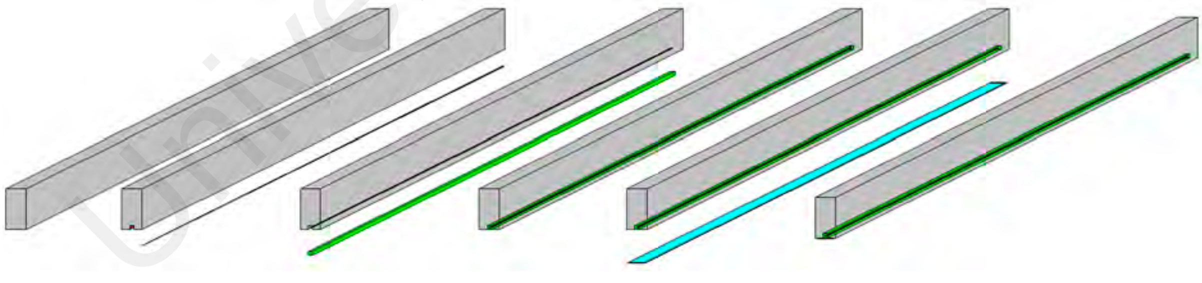

Figure 2. Sequence of specimen preparation and strengthening. Epoxy and CFRP fabric are colored green and light blue respectively.

After the curing period, the remaining cement laitance and loose materials were removed from the concrete surface with the help of an abrader to ensure superior bonding of the concrete–CFRP assemblage. Then, the surface was cleaned with a brush and a high-pressure air jet. Finally, acetone was used on the concrete surface before the wet layup process. Following the instructions of the manufacturers, a layer of epoxy was spread on the surface and then the CFRP fabric was laid over it. A recommended roller was pressed firmly on the fabric layer until the adhesive was squeezed out through the tiny pores of the CFRP fibre. Before the test, the sample was left for standard curing time.

Using suitable support conditions, the test was conducted using a 500 kN load-carrying capacity Instron universal testing machine under a four-point bending load (Figure 1). Deflection was measured using the linear variable differential transducer (LVDT), which was placed at the centre of the maximum moment region. The 5 mm strain gauges were affixed at the centre of the internal steel bars. For measurement of the strain value of the strengthened CFRP and steel bars, the 5 mm-long strain gauges were planted at the central point, which were 500 and 1250 mm away from the centre of the strengthening bar. In the case of the CFRP fabric, 30 mm-long special strain gauges were installed at the central point, which was 250, 500, 1,250, and 1400 mm away from the centre point of the CFRP fabric. The 30 mm-long strain gauges were positioned at the uppermost surface of the concrete beam to measure concrete compressive strain. Transverse strains along the mid-span depth of the beams were measured using Demec points. Micro-cracks along the side of the concrete surface were measured using a DinoLite digital microscope.

3. Results and Discussion

The experimental results of the CEBNSM-strengthened RC beams are arranged in Table 3. These beams were strengthened with the CFRP bar inside the NSM groove and the CFRP fabric bonded at the beam soffit. The main test variables were the bar diameter (8 and 10 mm), the thickness of the CFRP fabric layer (one and two layer), the anchorage (with and without) at the cut-off zone of the EBR CFRP fabric layer (one and two layer), and the anchorage (with and without) at the cut-off point of the EBR CFRP fabric. Results are expressed in terms of their first crack load-carrying capacity, yield load-carrying capacity, and ultimate load-carrying capacity.

Table 3. Summary of the experimental test results.

Beam ID	P_{cr} (kN)	Δ_{cr} (mm)	P_y (kN)	Δ_y (mm)	P_u (kN)	Δ_u (mm)	Failure modes
CB	5	0.5	36	15.0	39	34.3	FFC
CBC8P1	11	1.5	50	14.9	71	39.7	FFF
CBC8P2	13	1.9	55	15.2	77	31.3	FFF
CBC10P1	13	1.6	54	16.6	82	43.3	FFF
CBC10P2	15	2.3	69	23.7	87	42.7	CFD
CBC10P2A	16	2.8	80	24.7	105	47.9	FFC

P_{cr} = first crack load; P_y = yield load; P_u = ultimate load; Δ_{cr} = deflection at 1st crack; Δ_y = deflection at yield of steel; Δ_u = mid-span deflection at failure load; FFC = flexural failure (concrete crushing after steel yielding); FFF = flexure failure due to FRP rupture; CFD = CFRP fabric delamination.

3.1. Load-Carrying Capacity

Table 3 provides the results obtained from the experimental tests carried out on one control beam and five CEBNSM-strengthened RC beams. The addition of the strengthening material to the RC beams caused superior load-carrying capacity, reduced ultimate deflection, and reduced the possibility of the debonding problem. The ultimate load-carrying capacity increased by 82%, 97%, 110%, 124%, and 170% for the CBC8P1-, CBC8P2-, CBC10P1-, CBC10P2-, and CBC10P2A-strengthened beams, respectively, compared with the control beam. The corresponding first crack load-carrying capacity and yield load-carrying capacity of the beams significantly improved after strengthening. The yield point was determined by the stiffness variation in the load–deflection curve, as well as the internal steel yielding point from the corresponding load–steel strain diagram. The average increment of the ultimate load-carrying capacity was 116.5%, compared to that of the control beam. This enhanced ultimate load-carrying capacity shows the superior performance of the strengthened beams compared with that of the control beam.

The percentile increment of the first crack load-carrying capacity, yield load-carrying capacity, and ultimate load-carrying capacity are illustrated in Figure 3. The first crack load-carrying capacity, yield load-carrying capacity, and ultimate load-carrying capacity were significantly improved by the CEBNSM technique. Among these three load states, the first crack load-carrying capacity was

CEBNSM technique. Among these three load states, the first crack load-carrying capacity was significantly improved for all CEBNSM-strengthened beams. The range of the first crack load-carrying capacity improvement was 118% to 230% compared with that of the control beam. This serviceability improvement is one of the positive features of this technique, given that the early first crack load welcomes various environmental agents, which would aggravate the cracking condition and eventually be responsible for further deterioration. The range of the yield load-carrying capacity improvement is lower than that of the first crack load and the ultimate load. This range was 38% to 120% compared with that of the control beam. Figure 3 shows that the average yield load-carrying capacity of the CEBNSM-strengthened beams was approximately 73% of their ultimate load-carrying capacity.

The average increment of the yield load-carrying capacity is 70% compared with that of the control beam, and its trend shows the lowest gain compared with the corresponding first crack load-carrying capacity and ultimate load-carrying capacity of the strengthened beams. The percentage increment of the ultimate load-carrying capacity was 82% to 170% compared with that of the control beam. Typically, beams with a high area of strengthening material exhibit an enhanced ultimate load-carrying capacity.

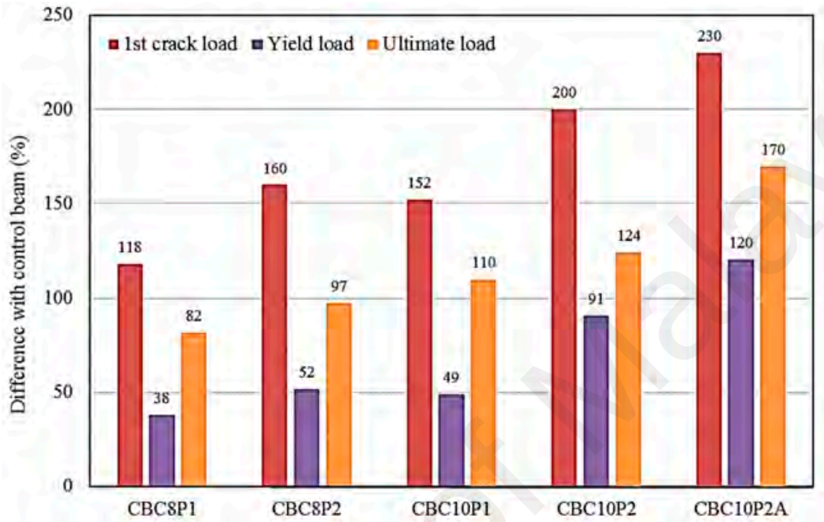

Figure 3. Percentile increment of the first crack, yield, and ultimate load-carrying capacities of combined externally bonded and near-surface mounted (CEBNSM)-strengthened beams compared with the control beam.

3.2. Load–Deflection Diagram

The load–deflection relationship of the control and strengthened RC beams is depicted in Figure 4. The unstrengthened RC beam showed the typical behaviour, with crack and yield point followed by a nonlinear portion at the post-yield stage. All of the CEBNSM-strengthened RC beams exhibited a trilinear response up to the ultimate load. The first segment of the curve moved in a linear manner with minor deflection until the first crack appeared. For all the strengthened beams, this technique contributed to the increment of the first crack load.

The second segment was the post-crack to yield stage of the internal reinforcement of the beams. Strengthened beams exhibited a considerable stiffness improvement in this stage compared with the control beam. At this stage, the internal steel reinforcement and the strengthening materials exhibited the tensile stresses of the beam. The average pre-yield stiffness increment of the strengthened beam was 36% compared with the control beam. The CBC8P2-strengthened beam showed a maximum 50% more pre-yield stiffness compared to the control beam. With the prevention of the further expansion of flexural cracks, the CFRP bar contributed to the enhancement of the moment of inertia of the cracked section.

Polymers **2016**, *8*, 261 8 of 23
Polymers **2016**, *8*, 261 8 of 23

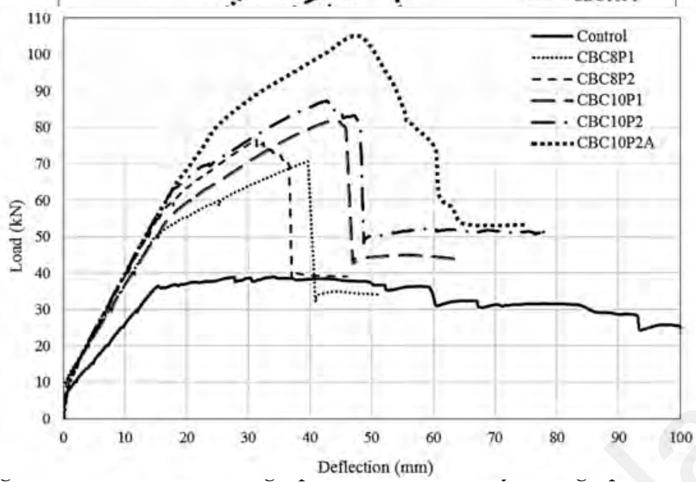

Figure 4. Load–deflection diagram of tested beams.

The third stage of the load–deflection graph continued from yielding up to failure. This segment exhibited better improvement in terms of strength and stiffness. In this post-yield stage, most of the tension stresses are resisted by the NSM reinforcement and the EBR CFRP fabric because of the yielding of the tension steel. The strengthened beams exhibited 183% more average pre-ultimate stiffness increment than that of the control beam. CBC8P2-strengthened beam showed a maximum post-yield stiffness of approximately 116% more than that of the control beam. The anchored CBC10P2A-strengthened beams exhibited 93% more stiffness increment than that of the control beam. The post-peak response of the load–deflection curve of strengthened beams was characterized by a sudden drop in load carrying capacity, regardless of the FRP fracture (flexural failure) or premature (debonding) failure.

Figure 5 shows the deflection reduction of the CEBNSM-strengthened beams at 15, 36.29, and 38.95 kN loads with respect to the control beam. The last two loads were the yield and ultimate loads of the control beam. A 15 kN load was added for better comparison, which was the first crack load for most of the strengthened beams. The aforementioned figure clearly showed that the deflection was reduced at these load levels. However, at 38.95 kN load, the difference was more pronounced than that of the other load levels. At the ultimate load stage, the deflection reduction was 69%, 71%, 68%, 72% and 73% for the CBC8P1-, CBC8P2-, CBC10P1-, CBC10P2-, and CBC10P2A-strengthened beams, respectively.

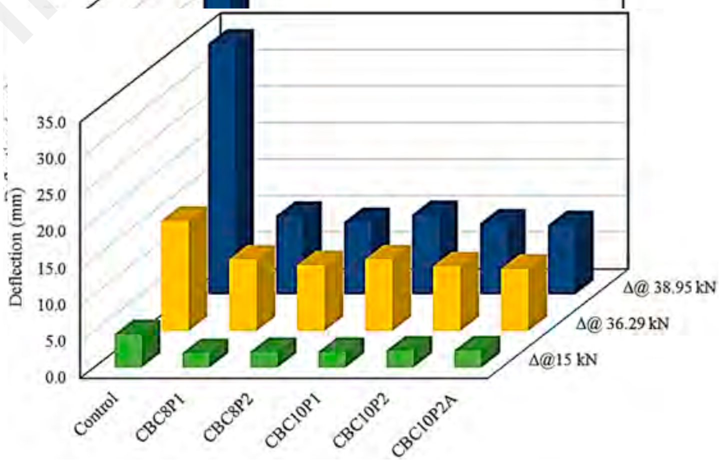

Figure 5. Deflection reduction of CEBNSM-strengthened beams.

Polymers **2016**, *8*, 261 9 of 23

3.3. Failure Modes

Figure 6 illustrates the failure modes of the control beam (a) and the CEBNSM-strengthened beams (b–f). Except for the CBC10B2-strengthened beam, all of the CEBNSM-strengthened beams without anchorage showed EBR CFRP fabric fracture at the bottom tensile mid-span area, which was a manifestation of flexural failure modes. The 8 and 10 mm-diameter CFRP bars inside the NSM groove with a single layer of CFRP fabric showed a CFRP fracture at the middle, except for the CBC10B2-strengthened beam, which demonstrated debonding failure.

(**a**)

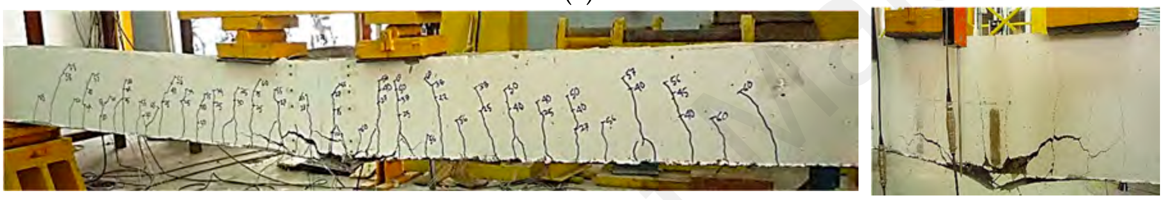

(**b**)

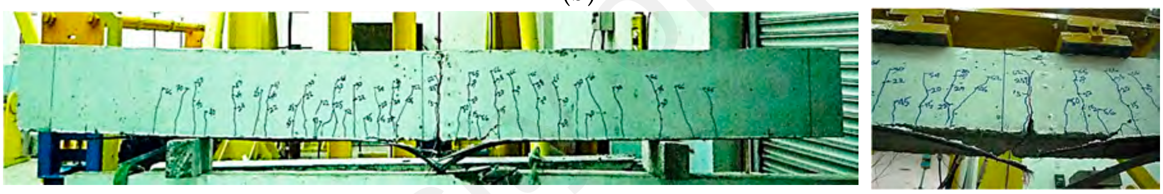

(**c**)

(**d**)

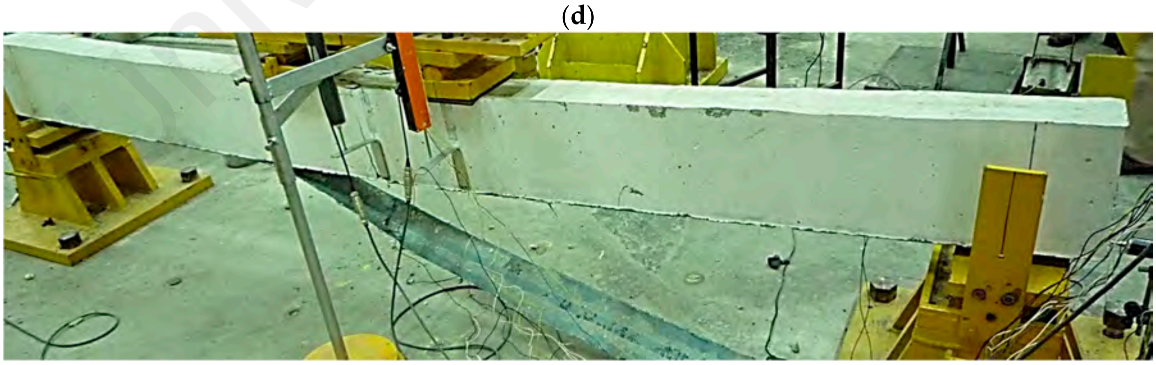

(**e**)

Figure 6. *Cont.*

Polymers **2016**, *8*, 261 10 of 23

(**f**)

Figure 6. Failure modes of the control beam and the strengthened RC beams with close-up pictures at failure locations. (**a**) Control beam; (**b**) CBC8P1 beam; (**c**) CBC8P2 beam; (**d**) CBC10P1 beam; (**e**) CBC10P2 beam; (**f**) CBC10P2A beam.

The CBC10P2-strengthened beam exhibited the premature debonding failure. After the yielding of the internal reinforcement, a cracking noise was detected like those detected from other CEBNSM-strengthened beams. At this stage, the CFRP fabric was stretched under high tensile strain, which was the maximum at the mid-span. Numerous new micro-cracks developed at the interface of the fabric and concrete cover, which expanded. At the maximum moment zone, the primary flexural crack widened and, at some point, the CFRP fabric could not maintain its curvature with the beam. Afterwards, the fabric lost its compatibility with the concrete surface and, with a bursting sound, the debonding initiated. The failure process was quick, and no sign of NSM failure was observed. Afterwards, the load was resisted only by the NSM reinforcement, which maintained an almost invariable load increment with increasing deflection. A concrete crushing failure was marked at this stage, and the machine was stopped.

Another beam was assessed with the same strengthening arrangement as the CBC10P2-strengthened beam, with two layers of U-CFRP wrap at the CFRP fabric cut-off location. Afterwards, the beam was called CBC10P2A. The beam survived against the debonding failure and showed the concrete crushing failure after steel bar yielding.

It can be seen that the CFRP fabric has a large influence on the failure mode experienced by CEBNSM-strengthened beams. The CFRP fabric was placed at the beam soffit; thus, it experienced the maximum tensile stress at the centre point of the mid-span. The NSM reinforcement was covered with concrete and was placed at least 8 mm away from the extreme bottom fibre. Consequently, the CFRP fabric played a dominant role in contributing to the ultimate flexural capacity as well as the failure modes. When maximum tensile strain in fabric reached closer to the rupture strain of the CFRP before attaining the maximum strain in concrete, the beam failed due to rupture of the CFRP fabric. Before that, the reinforcing steel in the tension area reached the plastic range.

3.4. Cracking Behaviour

During the test, cracking was clearly visualised into two different stages, which were the crack formation phase and the crack stabilisation phase. A digital crack microscope (DinoLite) was used to measure cracks at the steel bar level within the maximum moment region and was stored in a laptop. The cracks were documented after the appearance of the first crack and the subsequent crack formation at different load levels. Depending on the strengthening scheme and bond properties of concrete and internal steel, various crack spacing and widths were monitored for different beams. After the crack stabilisation period, new crack formations were stopped, whereas existing cracks were widened to maintain the same crack spacing.

3.4.1. Crack Spacing

Crack spacing is a major parameter associated with crack width and deflection. Crack spacing is influenced by the concrete cover, strengthening scheme, internal bar spacing, bond properties, and strain distribution of different internal structural components.

3.4.1. Crack Spacing

Crack spacing is a major parameter associated with crack width and deflection. Crack spacing is influenced by the concrete cover, strengthening scheme, internal bar spacing, bond properties, and strain distribution of different internal structural components.

According to the strain compatibility, the minimum crack (s_{r0}) spacing can be expressed as the nearest point to a present crack at which a fresh crack can develop, where the concrete again reaches the tensile strength (Equation (1)). It can be expressed as

$$s_{r0} = \frac{f_{ctm}\varnothing_s}{4\tau_{bm}\rho_{ef}} = \left(\frac{f_{ctm}A_{c,eff}}{\tau_{bm}\sum u}\right) \tag{1}$$

where f_{ctm} = mean tensile strength of concrete; $\varnothing_s$ = nominal diameter of reinforcement; τ_{bm} = average bond stress along the disturbed zone; ρ_{ef} = effective reinforcement ratio; $A_{c,eff}$ = effective concrete area in tension; and $\sum u$ = (sum of) perimeter(s) of reinforcing bar(s).

According to [38,39], crack spacings were supposed to fluctuate between $s_{r.min} = s_{r0}$ and $s_{r,max} = 2s_{r0}$. Various researchers proposed different values of average (mean) crack spacing, which varied from 1.33 to 1.54 times the minimum value (Equations (2) and (3)), whilst maximum crack spacing can be expressed as $s_{r,max} = 2s_{r,min}$.

$$\frac{s_{r,min}}{s_{r,mean}} = 0.67 \textit{ to } 0.77 \tag{2}$$

$$\frac{s_{r,max}}{s_{r,mean}} = 1.33 \textit{ to } 1.54 \tag{3}$$

The minimum, mean, and maximum crack spacings were determined based on the recorded data shown in Table 4. The maximum and mean crack spacings of CEBNSM-strengthened beams were comparatively lower than that of the control beam, although the number of cracks was greater. This information affirmed the better energy dissipation in the CEBNSM-strengthened beams.

Table 4. Experimental crack spacing and analysis.

Beam No.	$S_{r.max}$ (mm)	$S_{r.min}$ (mm)	$S_{r.mean}$ (mm)	No. cracks
CB	140	75	109	21
CBC8P1	85	45	64	39
CBC8P2	110	50	77	31
CBC10P1	95	50	70	38
CBC10P2	90	48	65	34
CBC10P2A	110	60	70	33

$S_{r.max}$ denotes the maximum crack spacing, $S_{r.min}$ denotes the minimum crack spacing and $S_{r.mean}$ denotes the mean crack spacing.

Table 4 shows the maximum, minimum, and average crack spacings, along with the number of cracks that appeared on the tested beams. The minimum, maximum, and mean crack spacings of the strengthened beams were observed to be 45, 110, and 69 mm, respectively. The average crack spacing of CEBNSM-strengthened beams maintained a range between 64 and 77 mm, whereas the average crack spacing of the control beam was 109 mm. The number of cracks that appeared on the strengthened beam was almost the same, and its average was approximately 35, compared with 21 cracks on the control beam. The CBC8P1-strengthened beam exhibited the highest number of cracks (39 cracks), whereas the CBC8P2-strengthened beam showed the minimum number of cracks (31 cracks). The strengthened beams displayed many cracks with small width, whereas the unstrengthened beam had fewer cracks with large width. Owing to beam deformation due to the applied loads, the strengthening material in strengthened beams creates a tensile force that equalises the internal bending forces so that less deformation occurs compared to the unstrengthened beam [40].

Figure 7 shows the ratios of minimum-to-average and maximum-to-average crack spacings of the CEBNSM-strengthened RC beams. The experimental result shown in Figure 7 reveals the average maximum and minimum crack spacing ratio as 1.41 $S_{r.max}$ and 0.73 $S_{r.min}$, which complies with the limit suggested in Equations (2) and (3). Moreover, the ratio of the average $S_{r.max}$ and $S_{r.min}$ was 1.94, which was close to the findings of Borosnyói [39].

Polymers **2016**, *8*, 261 12 of 23

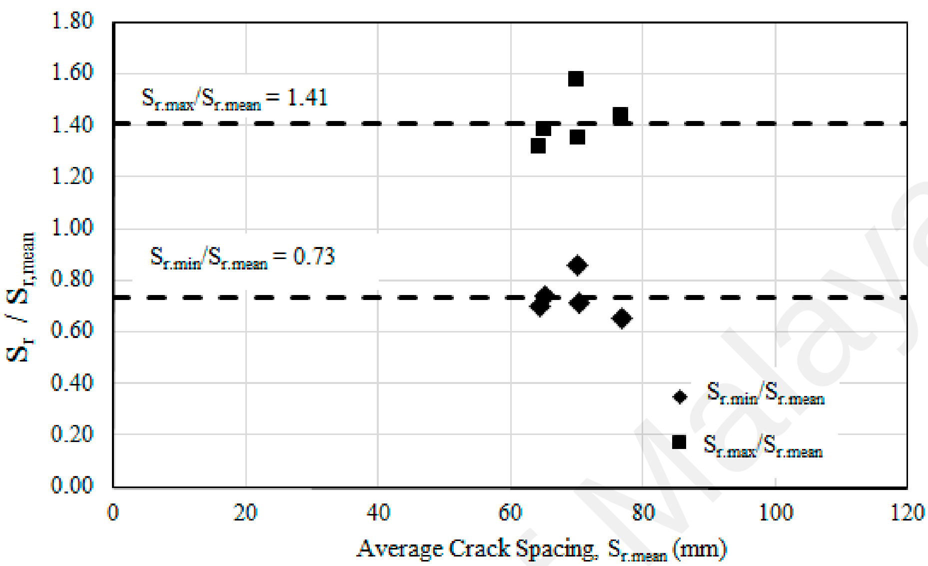

Figure 7. Relationship of maximum and minimum crack spacing against mean crack spacing.

3.4.2. Crack Width

The flexural crack width of beams was measured across the main reinforcement position in the maximum moment region at different load levels with the help of a crack-measuring microscope. For all of the beams, the cracks were measured beyond their yield load-carrying limits, which were close to their failure stage. The minimum-to-maximum range of the first crack improvement was 118% to 230% compared with the control beam. Figure 8 shows the trend of the crack width of strengthened RC beams compared with the control beam. For all cases, the strengthened beams exhibited less crack width and higher first crack load compared with the control beam. It is possible to characterize the trend of crack width into three groups, where the control beam exhibited the widest crack width. The CBC8P1-, CBC8P2-, and CBC10P1-strengthened beams showed moderate decrements in crack width, whereas the CBC10P2- and CBC10P2A-strengthened beams demonstrated the stiffest response in widening crack width compared with the control beam. Up to the yielding stage, the formation of crack width was stiffer, which widened faster beyond the region as the stiffness of the beam decreased.

If a single load is considered, then comparing the crack width of different beams would be easier. As a 35 kN load was close to the yield load of the control beam, comparing the crack width with this value would be easier. At a 35 kN load, a 0.56 mm crack width was developed in the control beam. The corresponding crack widths formed at this load were 0.17, 0.25, 0.19, 0.11, and 0.10 mm for the CBC8P1-, CBC8P2-, CBC10P1-, CBC10P2-, and CBC10P2A-strengthened beams, respectively.

The ACI-318 code included provisions for cracking control based on crack width limits of 0.4 and 0.33 mm for interior and exterior applications, respectively. A permissible crack width of between 0.4 and 0.53 mm was selected by Frosch [41]. A service load steel stress of 0.6 Fy was assumed, and simplified design curves were generated based on this assumption. Barris [38] selected and analysed the experimental FRP RC beams with a crack width of between 0.5 and 0.7 mm. Among the several code requirements, 0.33 mm [42] was the most conservative value. For comparison purposes, the load corresponding to this crack width (listed in Table 5) will be determined. The service load (60% of the ultimate load) and its corresponding crack width are presented in Table 5. Although the service

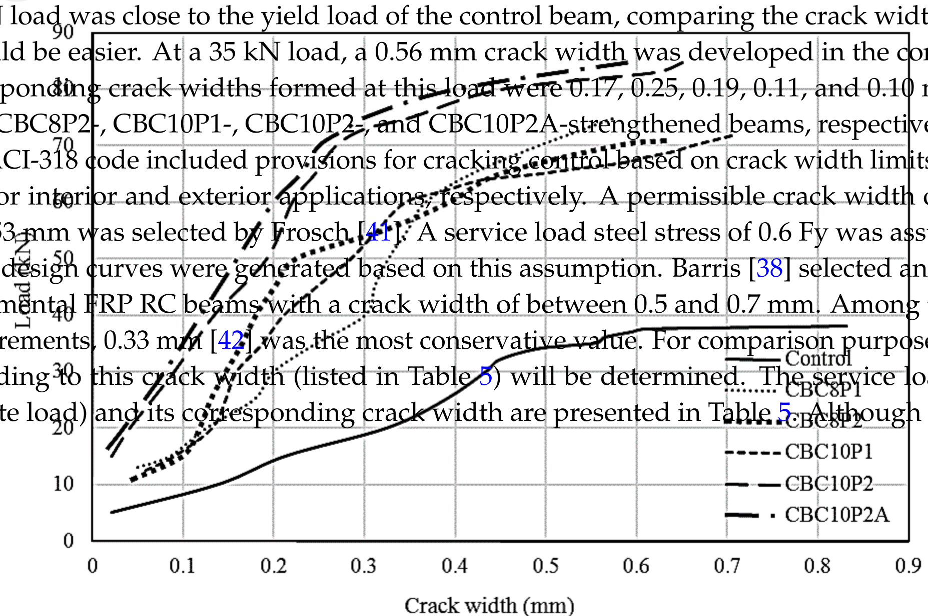

all of the beams, the cracks were measured beyond their yield load-carrying limits, which were close to their failure stage. The minimum-to-maximum range of the first crack improvement was 118% to 230% compared with the control beam. Figure 8 shows the trend of the crack width of strengthened RC beams compared with the control beam. For all cases, the strengthened beams exhibited less crack width and higher first crack load compared with the control beam. It is possible to characterize the trend of crack width into three groups, where the control beam exhibited the widest crack width. The CBC8P1-, CBC8P2-, and CBC10P1-strengthened beams showed moderate decrements in crack width, whereas the CBC10P2- and CBC10P2A-strengthened beams demonstrated the stiffest response in widening crack width compared with the control beam. Up to the yielding stage, the formation of crack width was stiffer, which widened faster beyond the region as the stiffness of the beam decreased.

load of strengthened beams was higher, their corresponding service crack width was less than that of the control beam. The average load of the strengthened beams at the 0.33 mm crack width was 63.6 kN. This mean value represented a load corresponding to an average of 75% of their corresponding ultimate load-carrying capacity.

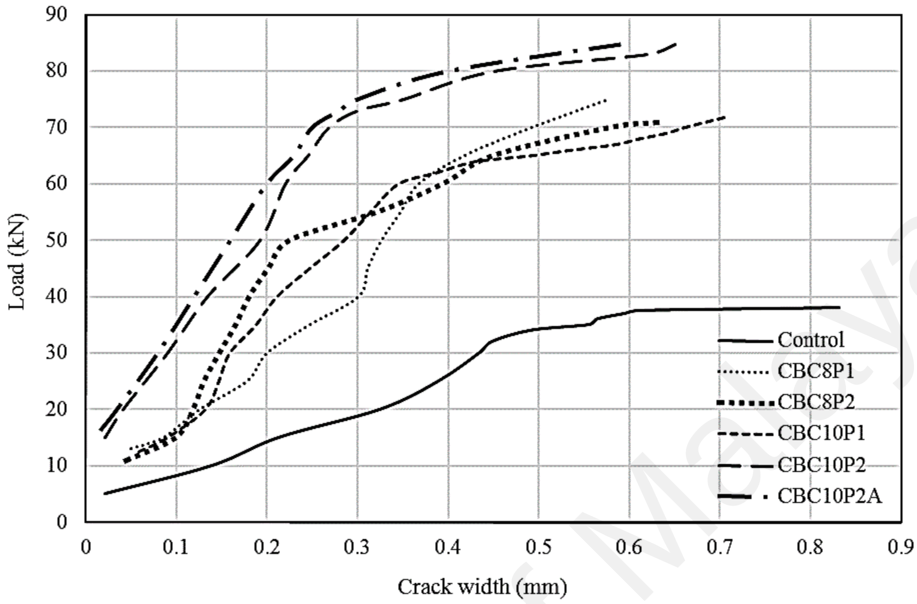

Figure 8. Crack widths of CEBNSM-strengthened beams against incremental load.

Figure 8. Crack widths of CEBNSM-strengthened beams against incremental load.

Table 5. Equivalent experimental load at w = 0.33 mm.

Beam ID	P_{cr} (kN)	P_{serv} (kN)	w_{serv} (mm)	Load (kN) at w = 0.33 mm	% of Pu
Control	5.0	23.4	0.34	22	56
CBC8P1	10.9	42.5	0.18	56	79
CBC8P2	13.0	46.1	0.31	54	70
CBC10P1	12.6	49.0	0.28	58	71
CBC10P2	15.0	52.4	0.19	74	85
CBC10P2A	16.5	63.1	0.21	76	72

P_{cr} = 1st crack load, P_{serv} = Service load (60% of the ultimate load), w_{serv} = crack width at service load.

3.5. Stiffness Assessment

Stiffness is one of the dominant characteristics of RC structures, given that the change of its value with the applied load influences the deflection and curvature of any structure. Stiffness depends significantly on the cracking, the load level, and the thickness of bonded material and adhesive. Stiffness can be characterised as the product of the modulus of elasticity and moment of inertia of a certain section. Bending stiffness is easily defined for a true homogenous material, such as steel. However, for RC, estimating bending stiffness is difficult, as it is controlled by cracking, creep, shrinkage, and load history. In the RC section, the moment of inertia is continuously changing, which is termed as the effective moment of inertia (I_{eff}) after exceeding the cracking moment (M_{cr}) instead of using the gross moment of inertia (I_g). For the full crack formation of the beam, I_{eff} should be referred to as the cracked moment of inertia (I_{cr}) of the cracked transformed section. With the formation of flexural cracks, the neutral axis also keeps changing its position, which is also a significant challenge for the appropriate estimation of bending stiffness.

The RC beam section significantly varies with the un-cracked and cracked stages because of the applied load. Bending stiffness can be estimated from the displacement data coming from the LVDTs placed along the beam length (Figure 1). By using elastic bending theory in the displacement-based equation, calculating the experimental bending stiffness using Equation (4) is possible [43].

$$(EI)_{\exp} = \frac{Pa\left(3l^2 - 4a^2\right)}{48\delta_{\exp}} \tag{4}$$

Polymers **2016**, *8*, 261 14 of 23

Here, P, l, a, and $\delta_{\exp}$ represent the applied service load, clear span of the RC beam, shear span of the beam, and the maximum mid-span experimental deflection at service load, respectively.

Another approach for the determination of bending stiffness is to evaluate the curvature of the beam at bending due to the applied experimental load. For that purpose, the moment–curvature relationship of the RC beam should be developed. Three approaches are employed to establish this relationship, as follows: (a) analyse the strain of the top compression fibre and bottom steel; (b) analyse the strain of the bottom and top steel; and (c) analyse the strain of the top fibre and CFRP bar.

$$(EI)_{\exp} = \frac{M}{\varphi} \tag{5}$$

$$\varphi = \frac{\varepsilon_c + \varepsilon_s}{d} \tag{6}$$

For the analysis, curvature and neutral axis location was determined by using the tensile and compression strain values of steel and concrete from their respective strain gauges [44]. From Figure 9 and Equations (5) and (6), the bending stiffness of the beams can be calculated. A moment–curvature relationship was developed using the extreme tension strain values from the strain gauge of the internal steel bar and the extreme compression strain gauge values from the top of the mid-span.

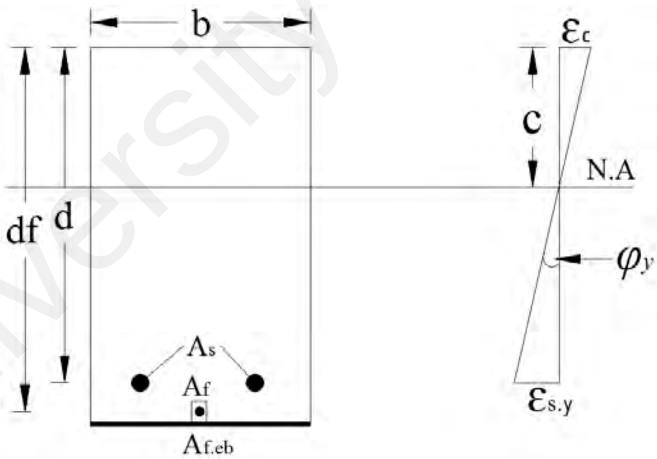

Figure 9. Cross-sectional view of the strengthened beamshowing neutral axis (NS) location and curvature. b is the width of the beam, d is the effective depth of the beam, d_f is the effective depth of the NSM reinforcement, A_s is the area of the main reinforcement, A_f is the area of the NSM reinforcement, $A_{f.eb}$ is the area of the externally bonded reinforcement, N.A is the neutral axis of the section, c is the depth of the neutral axis, ε_c is the compressive strain of the concrete, $\varepsilon_{s.y}$ is the tensile strain of the main reinforcement and φ_y is the curvature of the section.

Figure 10 depicts the moment *versus* bending stiffness diagram, where the first crack and the yield of the beams were marked in the diagram. The strain gauge of CBC10P2A-strengthened beams yielded erroneous data, which were excluded from the analysis. The overall shape of the moment *versus* bending stiffness curve was formed like an "L". The stiffness was initially high and then constantly decreased until the appearance of the first crack in the beam. Afterwards, the moment increased with almost an invariable amount of stiffness until the yielding of the beam. The stiffness again decreased with a minute change of moment increment. Then, the moment increased again with an insignificant change in stiffness.

almost an invariable amount of stiffness until the yielding of the beam. The stiffness again decreased with a minute change of moment increment. Then, the moment increased again with an insignificant change in stiffness.

Polymers **2016**, *8*, 261 15 of 23

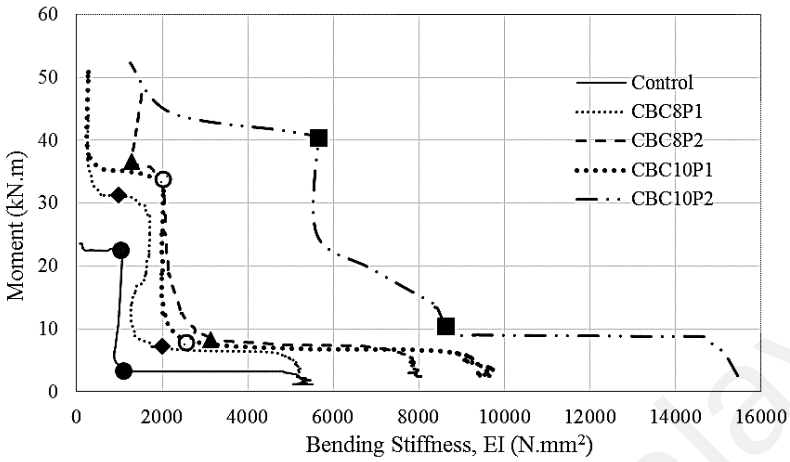

Figure 10. Bending stiffness of the strengthened beams.

For all cases, as expected, the CEBNSM-strengthened beams exhibited a superior moment–stiffness relationship compared with the control beam. The bending stiffness was initially high, as expected, because of the un-cracked stage of the beam section. The initial stiffness of the control beam was 5512 N·mm². The initial stiffness values of the strengthened beams were 5203, 8042, 9653, and 15,453 N·mm² for the CBC8P1-, CBC8P2-, CBC10P1-, and CBC10P2-strengthened beams, respectively.

With the increase in load application, the stiffness decreased and formed the knee of the "L", where the first crack appeared. This first crack stiffness of the control beam was 1,105 N·mm². The intermediate stiffness at the first crack of the CEBNSM-strengthened beams was 2008, 3142, 2553, and 8637 N·mm² for the CBC8P1-, CBC8P2-, CBC10P1-, and CBC10P2-strengthened beams, respectively. No noticeable difference in stiffness was observed after the first crack, and a radical realignment was visualised for this curve. An almost straight vertical line was formed where the moment increased with a steady rate. The CBC10P2-strengthened beam showed a gradually-decreasing stiffness with the increase in the moment capacity from the crack moment to the yield moment.

At the yield moment, the stiffness of the control beam was 1032 N·mm². The stiffness at the yield moment of the CBC series beams was 983, 1292, 2002, and 5656 N·mm² for the CBC8P1-, CBC8P2-, CBC10P1-, and CBC10P2-strengthened beams. After crossing the yield moment point, the beams showed an almost constant decrease in stiffness with a negligible moment increment. Then, the moment capacity increased again without any appreciable change in stiffness up to failure.

4. Simulation Method and Verification

4.1. Moment-Rotation Approach

The behaviour of RC beams is commonly simulated using the moment-curvature approach. The moment-curvature approach is usually capable of simulating strengthened RC beams with reasonable accuracy and with less computation needed compared to finite element modelling. However, the moment-curvature models are generally analytical models that rely heavily on empirical formulations derived specifically for the type of strengthening used on the RC beam. In order to use the moment-curvature approach for new strengthening methods such as the hybrid strengthening proposed in this paper, some recalibrations or modifications of these empirical formulations would be necessary. Yet, due to the small number of samples tested in this paper, the resulting empirical formulations may not be as accurate as needed. As such, an alternative method was used—the moment-rotation approach [45–47]. The moment-rotation approach requires no calibrations, as it is able to directly simulate the mechanisms of the RC beam—such as tension stiffening, crack formation, and crack widening—without the need for empirical formulations that are normally needed to indirectly simulate these mechanisms.

4.1.1. Tension Stiffening Analysis

formulations may not be as accurate as needed. As such, an alternative method was used—the moment-rotation approach [45–47]. The moment-rotation approach requires no calibrations, as it is able to directly simulate the mechanisms of the RC beam—such as tension stiffening, crack formation, and crack widening—without the need for empirical formulations that are normally needed to indirectly simulate these mechanisms.

Polymers **2016**, *8*, 261 16 of 23

4.1.1. Tension Stiffening Analysis

The moment-rotation approach uses the partial interaction theory to simulate the slip of reinforcements in RC beams, thus allowing the tension stiffening to be directly simulated. In this paper, the segmental method as presented by Visintin, et al. [47] will be used. Consider Figure 11a, which shows a beam segment of length $2L_{def}$ located between two flexural cracks. The slip of reinforcements would be at maximum at the location of the flexural cracks. As the bond stress acting on the reinforcements reacts against the slip of the reinforcements, the slip of the reinforcements would be gradually reduced, as the force acting on the reinforcements would be transferred to the adjacent concrete. Due to symmetry of forces, the slip of reinforcements would tend to zero at the middle of the beam segment, as shown in Figure 11b. As such, the analysis area can be reduced to length L_{def}.

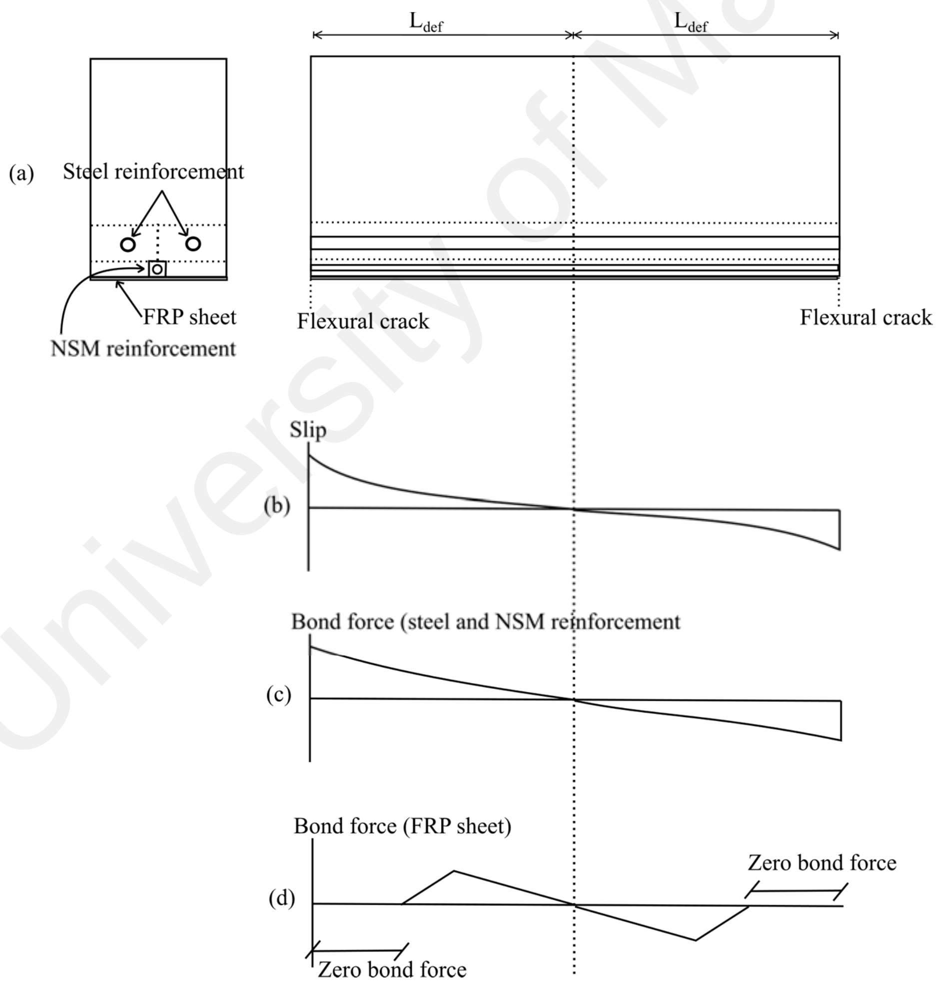

Figure 11. Tension stiffening analysis. FRP: fibre reinforced polymer; NSM: near surface mounted.

A numerical method similar to what was used by a previous researcher [48] was used to simulate the slip of steel and NSM reinforcements. The beam segment is discretized into small elements of size with length of each element (L_s) taken as 0.1 mm, where the stress and strain acting in each element is assumed to be constant due to its small size. The maximum element for the analysis, $i_{max} = L_sL_{def}$. The steel reinforcement is assumed to slip by a certain amount, and the load needed to cause this slip is assumed. The load and slip values for each element are then solved numerically and the load is adjusted until the slip is reduced to zero at the middle of the beam segment. The process is repeated until a load–slip relationship is obtained. The bond–slip model by CEB-FIP [49] was used to determine the bond force acting on the steel reinforcement.

with length of each element (L_s) taken as 0.1 mm, where the stress and strain acting in each element is assumed to be constant due to its small size. The maximum element for the analysis, $i_{max} = L_s L_{def}$. The steel reinforcement is assumed to slip by a certain amount, and the load needed to cause this slip is assumed. The load and slip values for each element are then solved numerically and the load is adjusted until the slip is reduced to zero at the middle of the beam segment. The process is repeated until a load–slip relationship is obtained. The bond–slip model by CEB-FIP [49] was used to determine the bond force acting on the steel reinforcement.

The method used to simulate the slip of NSM reinforcement is similar to the method used by Shukri, et al. [46]. The numerical procedure of the NSM reinforcement is nearly the identical to the steel reinforcement, except the bond–slip model by De Lorenzis, et al. [50] was used to determine the bond force of the NSM reinforcement:

$$\tau = \tau_{max-n}\left(\frac{\delta}{\delta_{max-n}}\right)^{\alpha} \quad for\ \delta \leqslant \delta_{max-n} \tag{7}$$

$$\tau = \tau_{max-n}\left(\frac{\delta}{\delta_{max-n}}\right)^{\alpha'} \quad for\ \delta > \delta_{max-n} \tag{8}$$

where τ is the bond stress, τ_{max-n} is the maximum bond stress, δ is the slip, and δ_{max-n} is slip corresponding to τ_{max-n}. The full list of parameters used for the bond–slip model for NSM FRP bars is provided in Table 6, where the parameters are empirically derived by De Lorenzis [50] for RC beams strengthened with NSM FRP ribbed bars, with the exception of τ_{max-n}, which was 21 MPa based on the value of bond strength given by the manufacturer of the Sikadur® 30 epoxy adhesive.

Table 6. Parameters for bond-slip of NSM FRP.

Parameter	Value
δ_{max} (mm)	0.319
τ_{max-n} (mm)	21
α	0.65
α'	−0.88

A numerical tension stiffening analysis was also applied to the FRP sheet. The bilinear bond-slip model by Lu, et al. [51] was used:

$$\tau = \tau_{max-s}\sqrt{\left(\frac{\delta}{\delta_o}\right)} \text{ for } \delta \leqslant \delta_o \tag{9}$$

$$\tau = \tau_{max-s}\left(\frac{\delta_f - \delta}{\delta_f - \delta_o}\right) \text{ for } \delta_o < \delta \ll \delta_f \tag{10}$$

$$\tau = 0 \text{ for } \delta > \delta_f \tag{11}$$

where,

$$B_w = \sqrt{\frac{2.25 - b_f/b_c}{1.25 + b_f/b_c}} \tag{12}$$

$$\tau_{max-s} = 1.5 B_w f_t \tag{13}$$

$$\delta_o = 0.0195 B_w f_t \tag{14}$$

$$\delta_f = 2G_f/\tau_{max} \tag{15}$$

$$G_t = 0.308 B_w^2 \sqrt{f_t} \tag{16}$$

Unlike the steel and NSM reinforcement, the bond between the FRP sheet and the concrete can be reduced to zero if the slip is larger than the maximum slip as determined using the bond–slip model. As more slip occurs, nearly all the bond along the beam segment will be reduced to zero. This causes the bond force for the FRP sheet to vary significantly from the bond force for steel and NSM reinforcements, as shown in Figure 11c,d. Importantly, the small amount of bond for the FRP sheet in this state causes the tension stiffening contribution of the FRP sheet to the RC beam to be very insignificant compared to the tension stiffening contribution of steel and NSM reinforcement.

A bilinear stress–strain relationship for steel reinforcement was used. For the FRP bar and sheet, a linear stress–strain relationship was used.

4.1.2. Moment-Rotation Analysis

The procedure for the moment-rotation approach prior to the occurrence of flexural cracking is similar to the moment-curvature approach. As moment M is applied, it causes a rotation θ to occur on the beam segment. A deformation profile (as shown in Figure 12a) is thus formed due to this rotation. To account for the formation of concrete wedges and the occurrence of concrete crushing, the size-dependent stress–strain relationship proposed by Chen, et al. [52] was used, which allows the concrete stress–strain relationship to be adjusted to length L_{def}. The concrete stress–strain model by Popovics [53] was used as the base model that was adjusted for concrete size:

$$\sigma_c = f_c\left(\frac{\left(\frac{\varepsilon_c}{\varepsilon_a}\right)r}{r-1+\left(\frac{\varepsilon_c}{\varepsilon_a}\right)^r}\right) \tag{17}$$

where σ_c is the concrete stress, f_c is the concrete strength, ε_c is the concrete strain. The parameters r and peak strain, ε_a are determined as:

$$r = \frac{E_c}{E_c - f_c/\varepsilon_a} \tag{18}$$

$$\varepsilon_a = 4.76 \times 10^{-6}\,(f_c) + 2.13 \tag{19}$$

where E_c is the elastic modulus of concrete. It should be noted that Equation (19) was proposed by Chen, et al. [52], based on their research. To obtain the adjusted stress–strain relationship of concrete, $\sigma_c/\varepsilon_{c\text{-}sd}$—where $\varepsilon_{c\text{-}sd}$ is the size adjusted strain—the size dependent strain for concrete is then determined as:

$$\varepsilon_{c-sd} = (\varepsilon_c - \sigma_c/E_c)\left(\frac{100}{L_{def}}\right) + \varepsilon_c \tag{20}$$

While the beam is in a state with no flexural crack, the forces acting on the reinforcements can be determined using the strain and stress profile in Figure 12b,c. The depth of neutral axis, d_{NA} is then adjusted until an equilibrium of forces is achieved and the value of moment M is then determined from forces in Figure 12d.

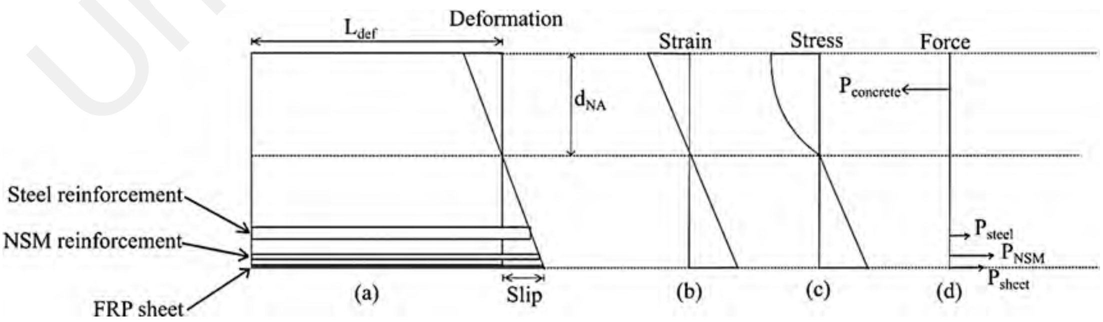

Figure 12. Moment-rotation analysis.

Further rotation will cause a larger deformation, and once the strain in the tensile region reaches the concrete cracking strain, a flexural crack is assumed to have appeared on the beam segment. The force acting on the steel reinforcement, NSM reinforcement, and FRP sheet is determined using the deformation profile in Figure 12a, and the load–slip relationships determined using the tension stiffening analysis. The neutral axis is then adjusted to achieve equilibrium of forces, and the moment M is determined. The process is repeated to obtain a moment-rotation relationship. To obtain a moment-curvature relationship, then, is just a matter of dividing the rotation by L_{def}. The load–deflection of the beam can then be determined from the moment-curvature relationship using the double integration method.

adjusted until an equilibrium of forces is achieved and the value of moment M is then determined from forces in Figure 12d.

Further rotation will cause a larger deformation, and once the strain in the tensile region reaches the concrete cracking strain, a flexural crack is assumed to have appeared on the beam segment. The force acting on the steel reinforcement, NSM reinforcement, and FRP sheet is determined using the deformation profile in Figure 12a, and the load–slip relationships determined using the tension stiffening analysis. The neutral axis is then adjusted to achieve equilibrium of forces, and the moment M is determined. The process is repeated to obtain a moment-rotation relationship. To obtain a moment-curvature relationship, then, is just a matter of dividing the rotation by L_{def}. The load–deflection of the beam can then be determined from the moment-curvature relationship using the double integration method.

The comparison between simulated and experimental load–deflection curves are as shown in Figures 13–16. It can be seen that the simulated curve follows the general shape of the experimental curves reasonably well; the tension stiffening analysis was able to simulate the beam behaviour with considerable accuracy. However, the method is currently unable to simulate the concrete cover separation failure of CEBNSM-strengthened beams with good accuracy. Further work is needed into this area.

Polymers **2016**, *8*, 261 19 of 23

separation failure of CEBNSM-strengthened beams with good accuracy. Further work is needed into this area.

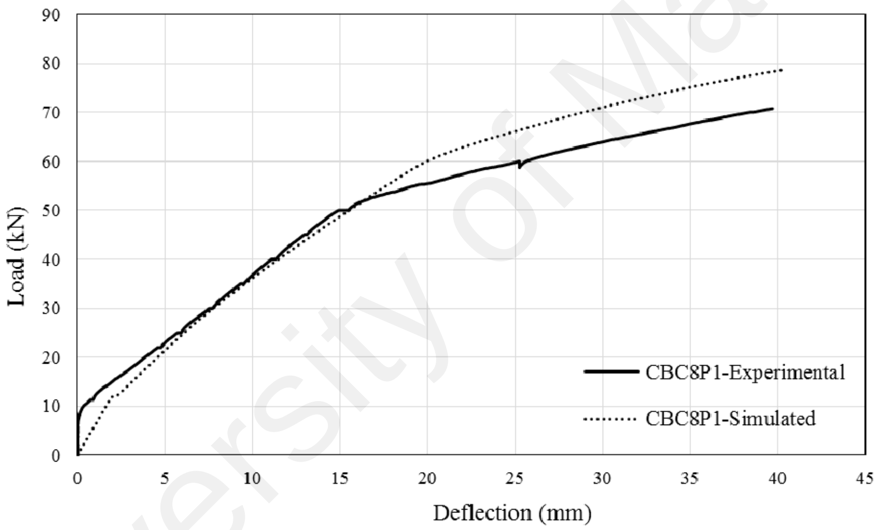

Figure 13. Experimental and Simulated output of CBC8P1.

Figure 13. Experimental and Simulated output of CBC8P1.

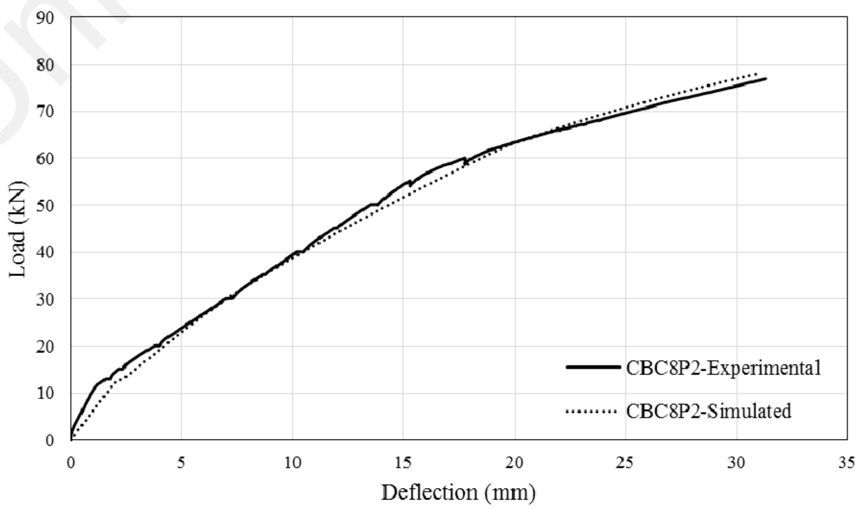

Figure 14. Experimental and Simulated output of CBC8P2.

Figure 14. Experimental and Simulated output of CBC8P2.

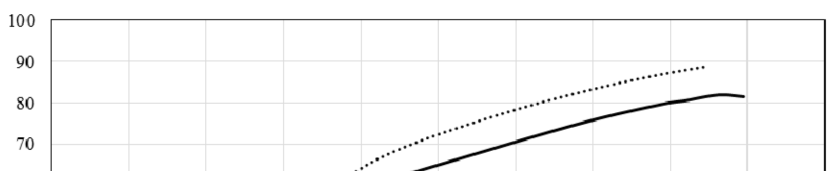

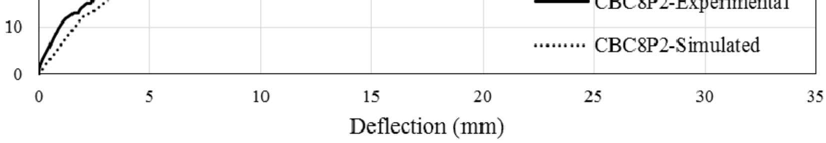

Figure 14. Experimental and Simulated output of CBC8P2.

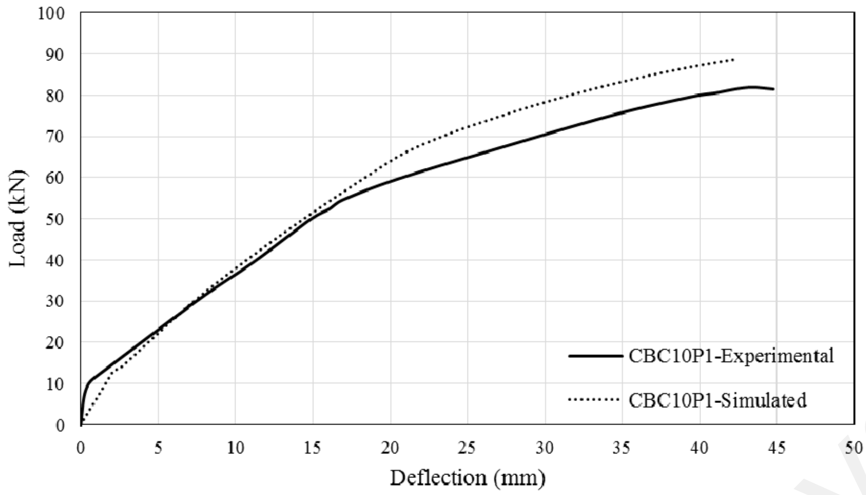

Polymers **2016**, *8*, 261 20 of 23

Figure 15. Experimental and Simulated output of CBC10P1.

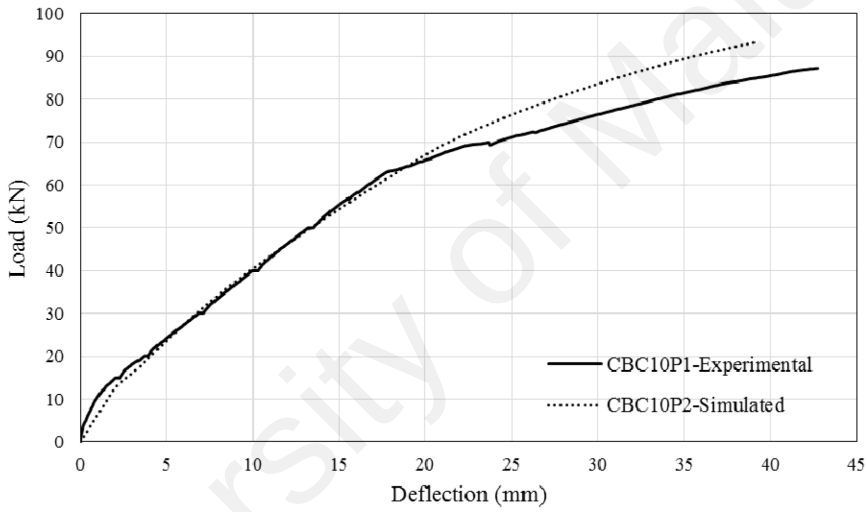

Figure 16. Experimental and Simulated output of CBC10P2.

5. Conclusions

This study introduces the CEBNSM method for strengthening RC beams, which involves strengthening beams using NSM CFRP round bar in combination with EBR CFRP fabric at the beam soffit. The effect of the variable NSM bar diameter, the thickness of the EBR CFRP fabric, and the anchorage performance was evaluated based on a four-point bending experimental test. A simulation method based on the moment-rotation approach was used to predict the deflection of the CEBNSM-strengthened RC beams. The following summary can be drawn from the experimental and analytical outcomes.

i. The first crack, yield, and ultimate load of the CEBNSM-strengthened beams significantly increased compared with the control beam. The increment of the first crack load was the highest (230%) among the three load levels, which is particularly important for serviceability performance. The maximum ultimate load-carrying capacity increased to 170% over that of the control beam.
ii. A trilinear load–deflection response was detected, whereas a considerable reduction of the deflection for all of the strengthened beams was witnessed at the ultimate stage. The stiffness of the strengthened beam significantly increased at all levels of load compared with that of the control beam.
iii. All of the strengthened beams exhibited flexural failure, except for the CBC10P2-strengthened beam, which was strengthened using a double-ply CFRP fabric with a 10 mm-diameter NSM CFRP bar. However, this debonding failure was successfully eliminated by using CFRP U-Wrap anchorage at the fabric curtailment location.
iv. The average crack spacing of the strengthened beams was 64 to 77 mm, which was smaller than

ii A trilinear load–deflection response was detected, whereas a considerable reduction of the deflection for all of the strengthened beams was witnessed at the ultimate stage. The stiffness of the strengthened beam significantly increased at all levels of load compared with that of the control beam.
iii All of the strengthened beams exhibited flexural failure, except for the CBC10P2-strengthened beam, which was strengthened using a double-ply CFRP fabric with a 10 mm-diameter NSM CFRP bar. However, this debonding failure was successfully eliminated by using CFRP U-Wrap anchorage at the fabric curtailment location.
iv The average crack spacing of the strengthened beams was 64 to 77 mm, which was smaller than that of the control beam (109 mm). The number of cracks was also more significant (average of 35 cracks) than that of the control beam (21 cracks), which affirmed the enhanced energy dissipation of the strengthened beams. Furthermore, the crack width of the strengthened beams was significantly reduced.
v The strain value of steel and concrete for the strengthened beams was less than that of the control beam. The strain values of the NSM bar and the EBR fabric showed the perfect distribution of the strain by strengthening reinforcement after the yielding of the internal steel bar.
vi The moment-rotation approach was applied to simulate the behaviour of CEBNSM-strengthened RC beams and was able to give good accuracy.

Acknowledgments: The authors gratefully acknowledge the financial support from the University of Malaya High Impact Research Grant under Account No-UM.C/HIR/MOHE/ENG/36 (Strengthening Structural Elements for Load and Fatigue).

Author Contributions: Kh Mahfuz ud Darain performed the experiments and wrote the manuscript. Mohd Zamin Jumaat suggested and supervised the work and executed the article editing. Ahmad Azim Shukri performed the analytical simulation works. M. Obaydullah, Md. Nazmul Huda and Md. Akter Hosen helped to perform the experimental works. Nusrat Hoque provided constructive suggestions about this work.

Conflicts of Interest: The authors declare no conflict of interest.

References

1. Inci, P.; Goksu, C.; Ilki, A.; Kumbasar, N. Effects of reinforcement corrosion on the performance of RC frame buildings subjected to seismic actions. *J. Perform. Constr. Facil.* **2012**, *27*, 683–696. [CrossRef]
2. Aslam, M.; Shafigh, P.; Jumaat, M.Z.; Shah, S. Strengthening of RC beams using prestressed fiber reinforced polymers—A review. *Constr. Build. Mater.* **2015**, *82*, 235–256. [CrossRef]
3. Darain, K.M.; Jumaat, M.Z.; Hossain, M.A.; Hosen, M.A.; Obaydullah, M.; Huda, M.N.; Hossain, I. Automated serviceability prediction of NSM strengthened structure using a fuzzy logic expert system. *Expert Syst. Appl.* **2015**, *42*, 376–389. [CrossRef]
4. Darain, K.M.; Shamshirband, S.; Jumaat, M.Z.; Obaydullah, M. Adaptive neuro fuzzy prediction of deflection and cracking behavior of NSM strengthened RC beams. *Constr. Build. Mater.* **2015**, *98*, 276–285. [CrossRef]
5. Ilki, A.; Bedirhanoglu, I.; Kumbasar, N. Behavior of FRP-retrofitted joints built with plain bars and low-strength concrete. *J. Compos. Constr.* **2010**, *15*, 312–326. [CrossRef]
6. Reza Aram, M.; Czaderski, C.; Motavalli, M. Effects of gradually anchored prestressed CFRP strips bonded on prestressed concrete beams. *J. Compos. Constr.* **2008**, *12*, 25–34. [CrossRef]
7. ACI 440.2R-08. In *Guide for the Design and Construction of Externally Bonded FRP Systems for Strengthening Concrete Structures*; ACI Committee 440; American Concrete Institute: Farmington Hills, MI, USA, 2008.
8. Fédération internationale du béton (fib). Externally bonded FRP reinforcement for RC structures. In *Bulletin*; fib: Lausanne, Switzerland, 2001; Volume 14, p. 138.
9. Lou, T.; Lopes, S.M.R.; Lopes, A.V. External CFRP tendon members: Secondary reactions and moment redistribution. *Compos. B Eng.* **2014**, *57*, 250–261. [CrossRef]
10. Lignola, G.P.; Prota, A.; Manfredi, G. Simplified modeling of rectangular concrete cross-sections confined by external FRP wrapping. *Polymers* **2014**, *6*, 1187–1206. [CrossRef]
11. Teng, J.; Chen, J.; Smith, S.T.; Lam, L. Behaviour and strength of FRP-strengthened RC structures: A state-of-the-art review. *Proc. ICE Struct. Build.* **2003**, *156*, 51–62. [CrossRef]

12. De Lorenzis, L.; Teng, J.G. Near-surface mounted FRP reinforcement: An emerging technique for strengthening structures. *Compos. B Eng.* **2007**, *38*, 119–143. [CrossRef]
13. Rosenboom, O.; Rizkalla, S. Behavior of prestressed concrete strengthened with various CFRP systems subjected to fatigue loading. *J. Compos. Constr.* **2006**, *10*, 492–502. [CrossRef]
14. Aram, M.R.; Czaderski, C.; Motavalli, M. Debonding failure modes of flexural FRP-strengthened RC beams. *Compos. B Eng* **2008**, *39*, 826–841. [CrossRef]
15. Martinelli, E.; Napoli, A.; Nunziata, B.; Realfonzo, R. RC beams strengthened with mechanically fastened composites: Experimental results and numerical modeling. *Polymers* **2014**, *6*, 613–633. [CrossRef]
16. Li, G.; Zhang, A.; Jin, W. Effect of shear resistance on flexural debonding load-carrying capacity of RC beams strengthened with externally bonded FRP composites. *Polymers* **2014**, *6*, 1366–1380. [CrossRef]
17. Lousdad, A.; Megueni, A.; Bouchikhi, A. Geometric edge shape based optimization for interfacial shear stress reduction in fiber reinforced polymer plate retrofitted concrete beams. *Comput. Mater. Sci.* **2010**, *47*, 911–918. [CrossRef]
18. Garden, H.; Hollaway, L.; Thorne, A. A preliminary evaluation of carbon fibre reinforced polymer plates for strengthening reinforced concrete members. *Proc. Inst. Civil Eng. Struct. Build.* **1997**, *122*, 127–142. [CrossRef]
19. Oehlers, D.J. Reinforced concrete beams with plates glued to their soffits. *J. Struct. Eng.* **1992**, *118*, 2023–2038. [CrossRef]
20. De Lorenzis, L. Strengthening of RC structures with near surface mounted FRP rods. Ph.D. Thesis, University of Lecce, Lecce, Italy, 2002.
21. Blaschko, M. Bond behaviour of CFRP strips glued into slits. In Proceedings of the 6th International Symposium on FRP Reinforcement for Concrete Structures (FRPRCS-6), Singapore, 8–10 July 2003; World Scientific: Singapore, 2003; pp. 205–214.
22. Parretti, R.; Nanni, A. Strengthening of RC members using near-surface mounted FRP composites: Design overview. *Adv. Struct. Eng.* **2004**, *7*, 469–483. [CrossRef]
23. Park, Y.; Kim, Y.H.; Lee, S.-H. Long-term flexural behaviors of GFRP reinforced concrete beams exposed to accelerated aging exposure conditions. *Polymers* **2014**, *6*, 1773–1793. [CrossRef]
24. Bencardino, F.; Condello, A. Innovative solution to retrofit RC members: Inhibiting-Repairing-Strengthening (IRS). *Constr. Build. Mater.* **2016**, *117*, 171–181. [CrossRef]
25. Bencardino, F.; Condello, A. Eco-friendly external strengthening system for existing reinforced concrete beams. *Compos. B* **2016**, *93*, 163–173. [CrossRef]
26. El-Maaddawy, T.; El Refai, A. Innovative repair of severely corroded t-beams using fabric-reinforced cementitious matrix. *J. Compos. Constr.* **2015**, *20*, 04015073. [CrossRef]
27. Rahman, M.; Jumaat, M.Z.; Rahman, M.A.; Qeshta, I.M.I. Innovative hybrid bonding method for strengthening reinforced concrete beam in flexure. *Constr. Build. Mater.* **2015**, *79*, 370–378. [CrossRef]
28. Arduini, M.; Nanni, A. Parametric study of beams with externally bonded FRP reinforcement. *ACI Struct. J.* **1997**, *94*, 493–501.
29. Kotynia, R.; Cholostiakow, S. New proposal for flexural strengthening of reinforced concrete beams using CFRP T-shaped profiles. *Polymers* **2015**, *7*, 2461–2477. [CrossRef]
30. Lim, D.H. Combinations of NSM and EB CFRP strips for flexural strengthening of concrete structures. *Mag. Concr. Res.* **2009**, *61*, 633–643. [CrossRef]
31. Maalej, M.; Bian, Y. Interfacial shear stress concentration in FRP-strengthened beams. *Compos. Struct.* **2001**, *54*, 417–426. [CrossRef]
32. British Standards Institution. *BS EN 12390–5. Testing Hardened Concrete—Part 5: Flexural Strength of Test Specimens*; British Standards Institution-BSI: CEN European Committee for Standardization: London, UK, 2009.
33. British Standards Institution. *BS EN 12390-3. Testing Hardened Concrete. Compressive Strength of Test Specimens*; British Standards Institution-BSI: London, UK, 2009; Volume 19.
34. ASTM. *A615/A615M-14: Standard Specification for Deformed and Plain Carbon-Steel Bars for Concrete Reinforcement*; ASTM International: West Conshohocken, PA, USA, 2014.
35. SikaWrap®-301C. Product Data sheet-woven carbon fibre fabric for structural strengthening. Available online: https://mys.Sika.Com/dms/.../sikawrap-301%20c%202010-12_1.pdf (accessed on 21 May 2016).
36. Sikadur®-30. Product Data sheet-adhesive for bonding reinforcement. Available online: https://mys.Sika.Com/dms/...Get/...E6dc.../sikadur-30%202011-10_1.pdf (accessed on 21 May 2016).

37. Sikadur®-330. Product Data sheet-adhesive for bonding reinforcement. Available online: https://mys.Sika.Com/dms/...Get/.../sikadur-330%202012-05_1.pdf (accessed on 21 May 2016).
38. Barris, C.; Torres, L.; Comas, J.; Mias, C. Cracking and deflections in GFRP RC beams: An experimental study. *Compos. B Eng.* **2013**, *55*, 580–590. [CrossRef]
39. Borosnyói, A. Serviceability of CFRP Prestressed Concrete Beams. Ph.D. Thesis, Budapest University of Technology and Economics, Budapest, Hungary, 2002.
40. Wight, R.; Green, M.; Erki, M. Prestressed FRP sheets for poststrengthening reinforced concrete beams. *J. Compos. Constr.* **2001**, *5*, 214–220. [CrossRef]
41. Frosch, R.J. Another look at cracking and crack control in reinforced concrete. *ACI Struct. J.* **1999**, *96*, 437–442.
42. American Concrete Institute (ACI). *Building Code Requirements for Structural Concrete (ACI 318-14) and Commentary*; ACI: Farmington Hills, MI, USA, 2011.
43. Mohammadhassani, M.; Jumaat, M.Z.B.; Maghsoudi, A.A.; Akib, S.; Jameel, M.; Najmeh, R.; Amin, M.; Hamid, S.; Esmaeil, H.R.; Farhad, G. Bending stiffness and neutral axis depth variation of high strength concrete beams in seismic hazardous areas: Experimental investigation. *Int. J. Phys. Sci.* **2011**, *6*, 482–494.
44. Hosen, M.A.; Jumaat, M.Z.; Alengaram, U.J.; Islam, A.; bin Hashim, H. Near surface mounted composites for flexural strengthening of reinforced concrete beams. *Polymers* **2016**, *8*, 67. [CrossRef]
45. Oehlers, D.; Visintin, P.; Zhang, T.; Chen, Y.; Knight, D. Flexural rigidity of reinforced concrete members using a deformation based analysis. *Concr. Aust.* **2012**, *38*, 50–56.
46. Shukri, A.A.; Darain, K.M.; Jumaat, M.Z. The tension-stiffening contribution of NSM cFRP to the behavior of strengthened RC beams. *Materials* **2015**, *8*, 4131–4146. [CrossRef]
47. Visintin, P.; Oehlers, D.; Wu, C.; Haskett, M. A mechanics solution for hinges in RC beams with multiple cracks. *Eng. Struct.* **2012**, *36*, 61–69. [CrossRef]
48. Muhamad, R.; Ali, M.M.; Oehlers, D.J.; Griffith, M. The tension stiffening mechanism in reinforced concrete prisms. *Adv. Struct. Eng.* **2012**, *15*, 2053–2069. [CrossRef]
49. CEB-FIP. *CEB-FIP Model Code 2010*; Ernst & Sohn: Berlin, Germany, 2013.
50. De Lorenzis, L. Anchorage length of near-surface mounted fiber-reinforced polymer rods for concrete strengthening—Analytical modeling. *ACI Struct. J.* **2004**, *101*, 375–386.
51. Lu, X.; Teng, J.; Ye, L.; Jiang, J. Bond–slip models for FRP sheets/plates bonded to concrete. *Eng. Struct.* **2005**, *27*, 920–937. [CrossRef]
52. Chen, Y.; Visintin, P.; Oehlers, D.; Alengaram, U. Size-dependent stress–strain model for unconfined concrete. *J. Struct. Eng.* **2013**, *140*, 04013088. [CrossRef]
53. Popovics, S. A numerical approach to the complete stress–strain curve of concrete. *Cem. Concr. Res.* **1973**, *3*, 583–599. [CrossRef]

5.2 Research paper 5: Simulating intermediate crack debonding on RC beams strengthened with hybrid methods

Published in *Latin American Journal of Solids and Structures*

Article history:

Received 6 March 2018

Accepted 31 May 2018

Original Article

Latin American Journal of Solids and Structures
www.lajss.org

Simulating Intermediate Crack Debonding on RC Beams Strengthened with Hybrid Methods

Abstract

The externally bonded (EB) and the near-surface mounted (NSM) are two well-known methods for strengthening reinforced concrete (RC) beams. Both methods are unfortunately prone to fail prematurely through debonding when the amount of strengthening reinforcement provided is high. In response to this, a hybrid method that combines the EB and NSM method was introduced. The method allows the amount of reinforcement needed for EB and NSM methods to be reduced; this, in theory, should lower the interfacial stresses, thus reducing the possibility of debonding failures. While debonding failure can be prevented, certain amounts of debonding would still occur through the interfacial crack (IC) debonding mechanism which can affect the strength and stiffness of hybrid strengthened beams even if it does not directly cause failure. This paper presents a method to simulate IC debonding of hybrid strengthened beams using the moment-rotation approach. The proposed method allows a better prediction of maximum load and stiffness of the beams. The method is also less dependent on empirical formulations compared to the commonly used moment-curvature approach; this allows the method to be applicable to all material and shape of hybrid strengthening reinforcement, assuming correct material models are used. The proposed method was then used to perform parametric studies; among the important findings is the length of IC debonding tend to increase when FRP sheet with higher elastic modulus is used, thus negating most of the benefit from the higher modulus.

Keywords

Externally bonded; fibre reinforced polymers; near-surface mounted; numerical analysis; partial-interaction; reinforced concrete.

Ahmad Azim Shukri[a]
Mohd Fazaulnizam Shamsudin[b]
Zainah Ibrahim[a*]
U. Johnson Alengaram[a]
Huzaifa Hashim[a]

[a] Department of Civil Engineering, Faculty of Engineering, University of Malaya, Kuala Lumpur, Malaysia. E-mail: ahmadazimshukri@gmail.com, zainah@um.edu.my, johnson@um.edu.my, huzaifahashim@um.edu.my.

[b] Faculty of Engineering, The University of Nottingham, University Park, Nottingham, NG7 2RD United Kingdom. E-mail: zackzaul@gmail.com

*Corresponding author

http://dx.doi.org/10.1590/1679-78254948

Received: 06 March, 2018
In Revised Form: March 11, 2018
Accepted: May 31, 2018
Available Online: June 05, 2018

1 INTRODUCTION

There are generally two types of strengthening methods available for reinforced concrete (RC) structural members in flexure: the externally bonded (EB) method (Barros et al., 2017; Ceroni et al., 2008; Chen et al., 2016; Fabrics et al., 2003; Maalej, 2005; Pesic, 2005; Tam et al., 2016; Toutanji et al., 2006) and the near-surface mounted (NSM) method (Badawi and Soudki, 2009; Capozucca et al., 2016; Capozucca and Magagnini, 2016; Kreit et al., 2011; Pachalla and Prakash, 2017; Seo et al., 2016). The EB method uses either fibre reinforced polymer (FRP) plates or sheets that are attached on the soffit of RC beams using epoxy adhesive. The NSM method involves making a groove on the soffit of RC beams and inserting either FRP bars or strips into the grooves and filling them with epoxy adhesive.

Both of these methods are prone to one or more types of debonding failures. An EB strengthened RC beam can fail prematurely due to either critical diagonal crack (CDC) debonding, interfacial crack (IC) debonding or end debonding (Narayanamurthy et al., 2012). On the other hand, NSM strengthened RC beams tend to fail prematurely only from end debonding through concrete cover separation (Zhang and Teng, 2014). While the NSM method is less prone to IC and CDC debonding failures, the probability of concrete cover separation failure is significantly high and the failure occurs in nearly all experimental tests in the literature (Zhang and Teng, 2014). To reduce the possibility of concrete cover separation, several rules were introduced with regard to the use of NSM method. One of them is the requirement of sufficient clear spacing and edge clearance for the NSM reinforcements. This causes difficulty to apply the NSM method on beams with small widths.

In response to this, a new method was proposed. The method is a hybrid between the EB method and the NSM method. The main purpose of the hybrid method is to reduce the amount of strengthening reinforcement needed by EB and NSM method individually, thus reducing the thickness of the FRP sheet needed as well as reducing the number of NSM grooves needed. The theory is that the reduction of strengthening reinforcement reduces the interfacial stresses, thus reducing the possibility of concrete cover separation debonding failures for both EB and NSM strengthening used in the hybrid method.

There are at least two earlier research on the hybrid method. The first research by Rahman et al. (2015) introduced a hybrid strengthening method using EB steel plates and NSM steel bars. The use of steel instead of FRP was intended to increase the ductility of the strengthened beam, as steel is much more ductile than FRP. However, the increase in ductility was barely noticeable from the experimental results due to the concrete cover separation failure that occurred on all the tested strengthened beams. Furthermore, the concrete cover separation debonding failure that occurred shows that the proposed method was unable to give the supposed higher resistance against debonding failures. Due to the poor performance of steel bars and plates, Darain et al. (2016) used carbon FRP (CFRP) bars and sheets to apply hybrid strengthening on RC beams. The results show that the use of CFRP gives much better result compared to steel bars and plates as none of the beams tested failed due to concrete cover separation. Most of the beams failed due to fracture of FRP sheet, though one of the beams experienced end debonding at the epoxy-FRP interface; this type of failure is rare and can be prevented by proper application of epoxy adhesive (Narayanamurthy et al., 2012). As the hybrid method is very new, various aspects of it remain unknown, among them the effect of IC debonding. It is well known that IC debonding is particularly prevalent on EB strengthened beams and can result in loss of an EB strengthened beam's strength even if it does not directly cause the beam's failure.

Conducting further experimental works, while necessary, is costly and time consuming. As an alternative method of study, this paper intends to apply the moment-rotation (M/θ) approach to simulate and study the effect of IC debonding on hybrid strengthened RC beams. The M/θ approach (Darain et al., 2016; Knight et al., 2014b; Oehlers et al., 2012, 2013, 2015; Shukri et al., 2015, 2016; Shukri and Jumaat, 2016; Visintin et al., 2012a, 2012b; Visintin et al., 2013a, 2013b) is a relatively new simulation method, which applies the partial interaction theory (Gupta and Maestrini, 1990; Haskett et al., 2008; Muhamad et al., 2011) to simulate various mechanics of RC beams, such as the formation of flexural cracks, widening of flexural cracks, tension stiffening and concrete wedge formation. The advantage that the M/θ approach has over conventional moment-curvature approach is the fact that it can readily simulate these mechanics without resorting to empirical formulations, such as the use of Branson's equation in the moment-curvature approach to simulate tension stiffening, although it should be noted that empirical formulations are still required in terms of material models, such as stress-strain relationships and bond stress-slip relationships. Apart from this, however, the M/θ approach presented in this paper should be applicable to any material type and shape of hybrid strengthening used as long as the correct material models are used.

In this paper, a new method for tension stiffening simulation for hybrid strengthened RC beams will be presented. The proposed method presents an improvement to the method used by Darain et al. (2016) as it allows for a better simulation of IC debonding, specifically the loss of strength that is caused by IC debonding of FRP sheets used in the hybrid strengthening method. The proposed method was validated against published experimental results. This is followed by a parametric study performed using the proposed method.

2 TENSION STIFFENING SIMULATION

For RC beams without any flexural cracks, there exists perfect bonding between the steel reinforcements and the concrete adjacent to them. Once flexural cracks occur, this perfect bonding no longer applies; causing the steel reinforcements to slip from the concrete. The partial interaction theory has been applied by many researchers as the basis to form a numerical simulation of the slip of steel reinforcement mentioned above (Gupta and Maestrini, 1990; Haskett et al., 2008; Muhamad et al., 2011; Shukri et al., 2015; Shukri and Jumaat, 2016; Visintin et al., 2012a, 2012b). It has also been shown that this tension stiffening simulation is also applicable to FRP reinforcements, such as NSM FRP bars (Darain et al., 2016; Shukri et al., 2015, 2016; Shukri and Jumaat, 2016) and FRP sheets (Darain et al., 2016; Oehlers et al., 2013, 2015).

The tension stiffening simulation has also been successfully applied on hybrid strengthened beams (Darain et al., 2016), where a tension stiffening simulation based on the multiple crack segmental analysis (Shukri et al., 2015; Visintin et al., 2012a) was applied on the steel bars, CFRP bars, and CFRP sheets respectively.

In the multiple crack segmental analysis, the length of primary crack is first determined, allowing the area of analysis to be reduced to half of the primary crack length, L_{def} as shown in Figure 1(a) due to the symmetry of forces where S_{cr} is the primary crack length. From Figure 1(a), the load applied to the beam segmental causes a rotation θ. The reinforcements slip by δ_r, δ_b and δ_s for the steel bar, FRP bar, and FRP sheet respectively. The slips are gradually reduced the further away from the crack face due to the transfer of load from the steel and FRP reinforcements to the adjacent concrete through bond stress. A numerical analysis is then performed to determine the value of loads P_r, P_b, and P_s that causes these slips by applying the boundary condition of slip being reduced to zero at the centre of the beam section, as shown in Figure 1(b). With regard to the FRP sheet, a bilinear bond stress-slip such as the one proposed by Lu et al. (2005) is usually applied. In the bilinear model, as shown in Figure 2, the bond stress is reduced to zero at δ_f. This loss of bond allows the multiple crack segmental analysis to simulate IC debonding (Darain et al., 2016). As shown in Figure 1(b) and Figure 1(c), when the slip for FRP sheet is increased higher than δ_f, the bond stress is reduced to zero and the area is considered to have debonded.

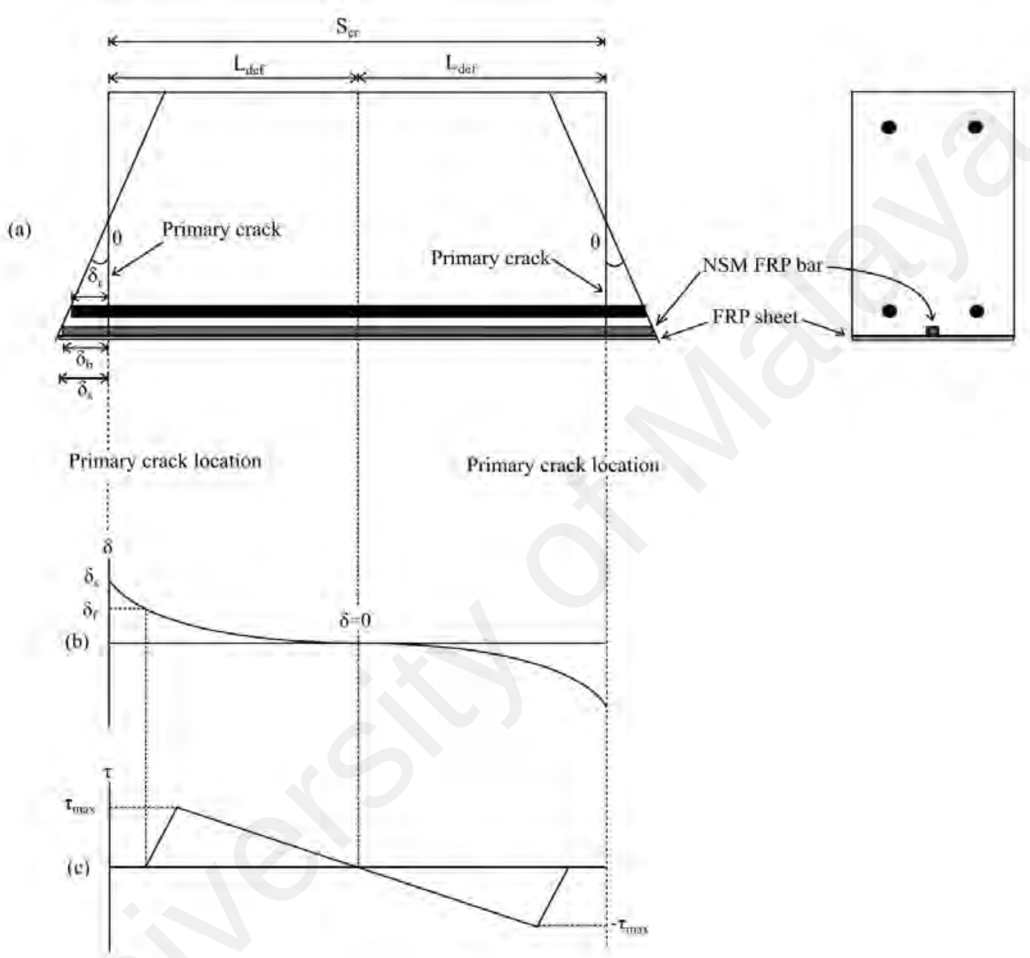

Figure 1. Multiple crack segmental analysis (a) RC beam segment; (b) Slip distribution for FRP sheet; (c) Bond stress distribution for FRP sheet.

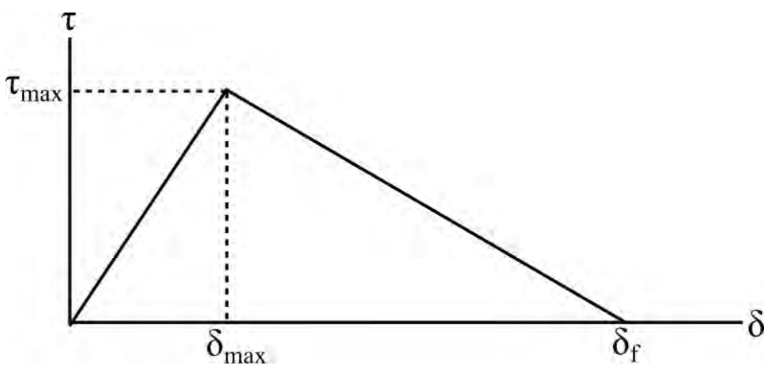

Figure 2. Bond stress-slip model for FRP sheet.

The multiple crack segmental analysis allows for an accurate simulation of tension stiffening in hybrid strengthened RC beams. However, the resulting equilibrium of forces in the multiple crack segmental analysis does not limit the force in the FRP strengthening reinforcements (Oehlers et al., 2015). This greatly affects the accuracy of the simulation as the loss of strength due to IC debonding is not taken into account; this was reflected in the simulated results of Darain et al. (2016), where multiple crack analysis was applied and the simulated results over-predict most of the ultimate load. In response to this, in this paper, a single crack segmental analysis will be used to form a tension stiffening simulation for the FRP sheets and bars.

The single crack segmental analysis is focused on the flexural crack forming in the maximum moment region, as shown in Figure 3(a). The load applied to the beam causes a rotation θ which in turn causes slips δ_r, δ_b and δ_s for the steel bar, FRP bar, and FRP sheet respectively. Numerical analysis is then applied to determine the values of loads P_r, P_b, and P_s that causes these slips. The single crack segmental analysis does not limit the tension stiffening analysis to half-crack length L_{def}; the numerical analysis is continued until the slip is reduced to zero at L_{end}, which can be any distance from the crack face. When a slip of FRP sheet is higher than δ_f, the bond stress is reduced to zero, as shown in Figure 3(b) and Figure 3(c). Unlike in the multiple crack analysis, the equilibrium of forces in the single crack analysis causes the debonded section to occur while the applied load on the FRP sheet remains constant at P_{IC}, which is the load at which IC debonding starts occurring.

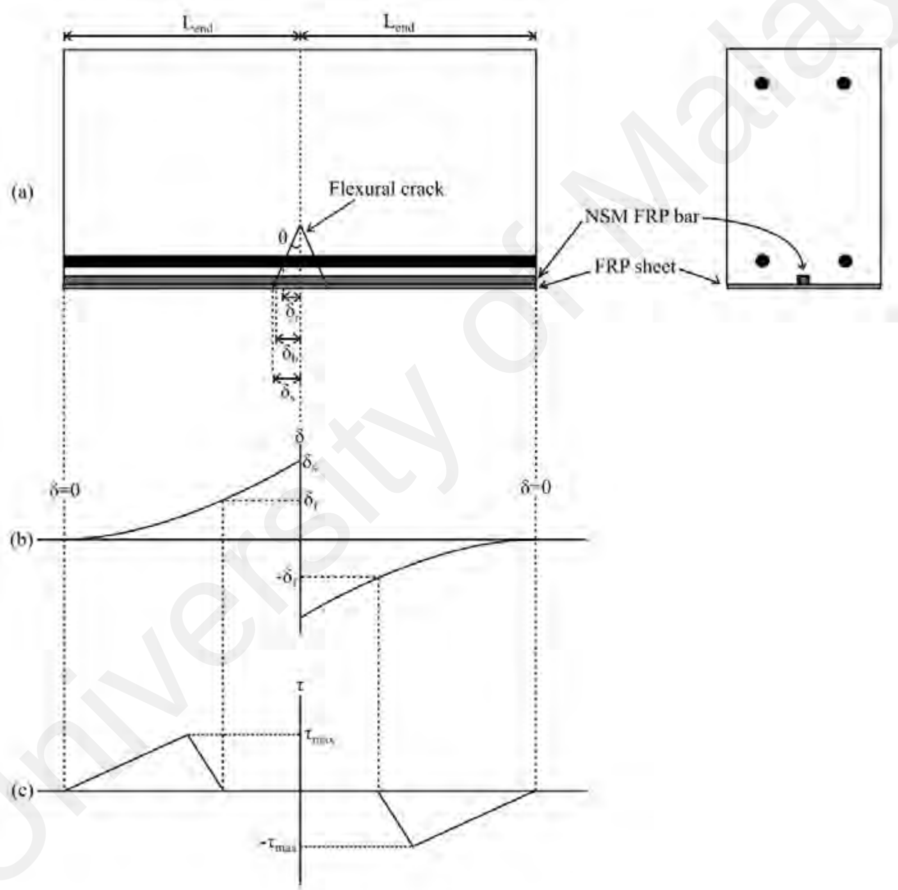

Figure 3. Single crack segmental analysis (a) RC beam segment; (b) Slip distribution for FRP sheet; (c) Bond stress distribution for FRP sheet.

The numerical procedure required for the single crack analysis is as shown below, along with a flowchart in Figure 4:

1. The beam geometry and material properties are determined:
   a. Area of EB/NSM/steel reinforcement, A_r.
   b. Area of concrete adjacent to the EB/NSM/steel reinforcement, A_c. More information on determining the A_c is available elsewhere (Darain et al., 2016; Shukri et al., 2015; Shukri and Jumaat, 2016).
   c. Perimeter of EB/NSM/steel reinforcement, L_{per}.
   d. Compressive strength of concrete, f_c.
   e. Elastic modulus of concrete, E_c.

f. Yield strength of steel reinforcement, σ_y.
g. Ultimate strength of EB/NSM/steel reinforcement, σ_f.
h. Ultimate load of EB/NSM/steel reinforcement, $P_{r\_max}=A_r\sigma_f$
i. Elastic modulus of EB/NSM/steel reinforcement, E_y.
j. Strain hardening modulus of steel reinforcement, E_h.

2. The beam is divided into small segments where the length, L_s=0.1mm. The analysis will start at the crack face, with the following boundary conditions:
   a. Slip of reinforcement, $\Delta_r = \delta(1) = 0.01$ mm.
   b. $P_c(1) = 0$
   c. The value of $P_r(1)$ is assumed.
3. The rest of the procedure will determine the forces and strains acting on each beam segment; a dummy variable 'i' is introduced to identify the beam segment being solved.
4. The bond stress, $\tau(i)$ acting on the EB/NSM/steel reinforcement is determined.
5. The bond force is determined as $B(i) = \tau(i)L_sL_{per}$. The strain of the EB/NSM/steel reinforcement is determined as $\varepsilon_r = P_r(i)A_r/E_r$. The change in slip for the reinforcement from this beam segment to the next segment is determined as $\Delta\delta = (\varepsilon_r - \varepsilon_c)L_s$. It should be noted that for the EB reinforcements, it is assumed that the area of concrete is thin enough to be negligible; the change in slip is thus $\Delta\delta = \varepsilon_r L_s$.
6. The values of boundary conditions for the next beam segment are determined. Note that the values of $P_c(i + 1)$ and ε_c are only calculated for NSM/steel reinforcements:
   a. $\delta(i + 1) = \delta(i) + \Delta\delta$
   b. $P_r(i + 1) = P_r(i) - B(i)$
   c. $P_c(i + 1) = P_c(i) + B(i)$
   d. $\varepsilon_c = P_c(i + 1)A_c/E_c$
7. The condition $\delta(i + 1)/\delta(1) < 0.01$, which represents a 99% reduction from $\delta(1)$ is checked.
8. If the condition in procedure 7 is not met, another condition is checked, which is $P_r(i + 1) < 0$.
9. If the condition in procedure 8 is also not met, the analysis will move on to the next beam segment. The dummy variable i is updated by 1 and procedure 3–8 is repeated.
10. If the condition in procedure 8 is met, the assumed value of applied load $P_r(1)$ is too low and the procedure 2–7 will be repeated with a higher value of assumed $P_r(1)$.
11. If $P_r(1)>P_{r\_max}$, the EB/NSM/steel reinforcement has fractured and failed.
12. If condition 11 is not met, the slip $\delta(1)$ and the corresponding $P_r(1)$ is then recorded and a larger value of $\delta(1)$ is set. The analysis is then repeated starting from procedure 3.
13. If condition 11 is met, the analysis can be stopped and the load-slip $(P_r(1)/\delta(1))$ relationship is recorded.

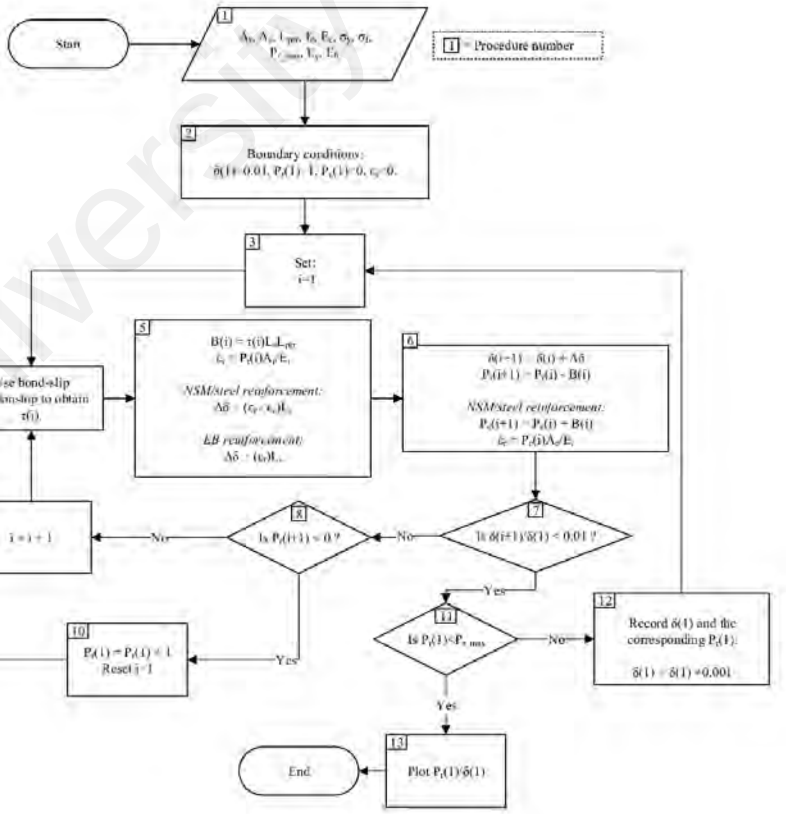

Figure 4. Single crack tension stiffening analysis procedure.

The numerical procedure for multiple crack analysis is not presented here, however the full procedure can be found in Shukri and Jumaat (2016).

3 MOMENT-ROTATION SIMULATION

The M/θ simulation is performed within the range of length L_{def}, which is determined using the tension stiffening simulation (Shukri and Jumaat, 2016). Consider Figure 4, where a beam section of length L_{def} is rotated by θ degree due to moment M. Prior to flexural cracking, the forces that cause deformation on the beam as shown in Figure 5(a) can be determined from the stress-strain relationships of each material. The depth of neutral axis d_{na} is then adjusted until equilibrium of forces is achieved; the actual value of moment M which causes rotation θ is then determined.

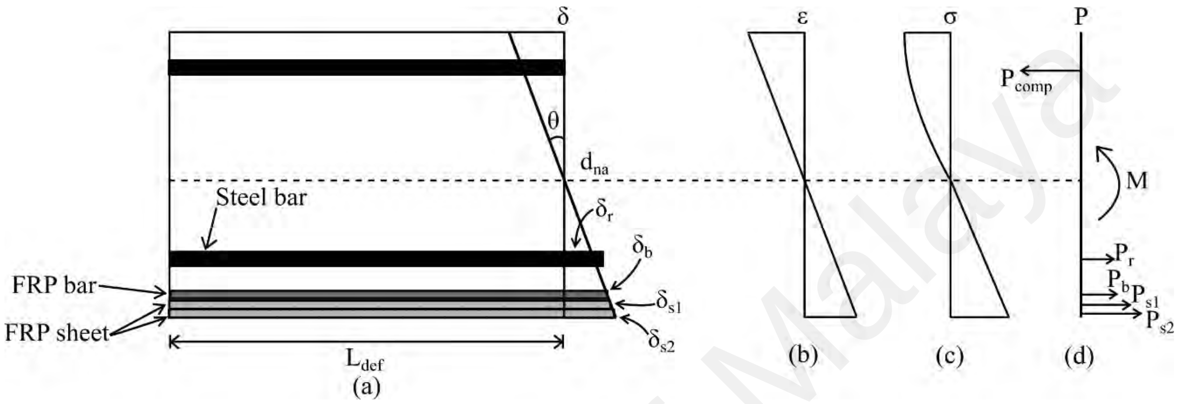

Figure 5. Moment-rotation analysis (a) Beam segment and deformation profile; (b) Strain profile; (c) Stress profile; (d) Force profile.

When flexural cracking occurs, a slip of reinforcements occurs such that the strains of reinforcement are no longer constant along length L_{def}. The forces acting on the steel and FRP reinforcements must then be determined using the load-slip (P_r/δ_r) relationship obtained from the tension stiffening simulation, where the slip is determined from the deformation profile in Figure 5(a). It should be noted that where more than one FRP sheet is used, the slip and the resulting load for each slip must be determined separately as shown in Figure 5(a) and Figure 5(d). The neutral axis d_{na} is then adjusted to obtain the equilibrium of forces and the actual value of is determined. The process is repeated for different values of θ in order to obtain an M/θ relationship. The moment-curvature can be obtained by dividing the values of θ with L_{def}. The load-deflection relationship of hybrid strengthened RC beams can then be determined using the commonly used double integration method.

4 VALIDATION OF PROPOSED METHOD

The proposed method was validated against the published experimental results of Darain et al. (2016). The experimental results are from four RC beams strengthened with the hybrid method made up of carbon FRP (CFRP) bars and CFRP sheets. A single CFRP bar was used for each beam, with a diameter of either 8mm or 10mm; the size of the NSM groove on the beam is twice the diameter of the bar used. The beams used either a single or two plies of CFRP sheets used had 0.17mm thickness. Further details on the beams and the materials used are given in Table 1 and Table 2.

Table 1: Beam details.

Beam Designation	EB reinforcement	NSM reinforcement
CBC8P1	One ply of CFRP sheet	One 8 mm CFRP bar
CBC8P2	Two ply of CFRP sheet	One 8 mm CFRP bar
CBC10P1	One ply of CFRP sheet	One 10 mm CFRP bar
CBC10P2	Two ply of CFRP sheet	One 10 mm CFRP bar

Table 2: Material properties.

Material	Property	Value (MPa)
Concrete	Compressive strength	50.1
	Tensile strength	5.5
	Elastic modulus	33260
Steel bar	Yield stress	529
	Ultimate strength	587
	Elastic modulus	200000
CFRP bar	Ultimate strength	2400
	Elastic modulus	165
CFRP sheet	Ultimate strength	4900
	Elastic modulus	230000

5 MATERIAL MODELS

Several material models were used in this paper, which will be mentioned only in brief to keep the paper short. Further details on the material models can be found in the reference given. The material models are only used as input for the tension stiffening and moment-rotation simulations; they can be replaced with other models if deemed appropriate (Knight et al., 2014a).

A bilinear stress-strain relationship with strain hardening was used for the steel reinforcements, while a linear stress-strain relationship was used for the CFRP bars. For the tension stiffening simulation, the bond-slip model by CEB-FIP (1993) was used for the steel reinforcement while the bond-slip model by De Lorenzis (2004) was used to determine the bond force of the NSM reinforcement. The maximum bond stress, τ_{max} was obtained using the bond strength model by Hassan and Rizkalla (2004). For the tension stiffening analysis of FRP sheet, the bilinear bond-slip model by Lu et al. (2005) was used. For concrete in compression, the stress-strain model by Popovics (1973) was used in conjunction with the size-dependent stress-strain method by Chen et al. (2014).

6 COMPARISONS OF SIMULATED AND EXPERIMENTAL RESULTS

A summary of the simulated results is given in Table 3. The proposed method was able to predict the maximum loads very well, where the deviation is found to be within 4% of the experimental value. The accuracy of the simulated deflection at maximum load is also good, apart from the simulated value for beam CBC8P2 which was found to be 20% higher than the experimental value. The simulated yield loads overpredict the experimental values, with a deviation between 12-16%. The use of the single crack analysis as the basis of the tension stiffening simulation may be the cause of this, as the single crack analysis is known to be less accurate at predicting tension stiffening effect compared to the multiple crack analysis. The simulated length of IC debonding is also given in Table 3, although its accuracy cannot be verified in this case. The length of IC debonding is affected by the amount of strengthening reinforcement provided. The use of two FRP sheets can be seen to give a shorter length of IC debonding compared to when only one FRP sheet is used. A similar effect can be seen when a larger size of NSM FRP bar is used, although the change to the length of IC debonding is negligible when compared to FRP sheets.

Table 3: Summary of simulated and experimental results

Beam	Results	P_y (kN)	P_{max} (kN)	Δ_{max} (mm)	L_{IC} (mm)
CBC8P1	Simulated	59.40	69.80	41.75	483.60
	Experimental	52.51	70.66	39.50	-
	Simulated/Experimental	1.13	0.99	1.06	-
CBC8P2	Simulated	67.40	76.40	37.40	428.80
	Experimental	59.11	76.71	31.18	-
	Simulated/Experimental	1.14	1.00	1.20	-
CBC10P1	Simulated	64.40	78.00	46.34	469.00
	Experimental	57.64	81.66	42.96	-
	Simulated/Experimental	1.12	0.96	1.08	-
CBC10P2	Simulated	72.80	84.20	42.06	421.40
	Experimental	62.59	86.98	42.64	-
	Simulated/Experimental	1.16	0.97	0.99	-

Note: P_y=yield load; P_{max}=maximum load; Δ_{max}=deflection at maximum load; L_{IC}=length of IC debonding.

A comparison between simulated and experimental load-deflection results are also given in Figure 6. The simulated load-deflection using the method proposed Darain et al. (2016) is also included in Figure 6; their simulated results were obtained using the multiple crack analysis and hence is incapable of simulating IC debonding. Its inclusion in Figure 6 is meant to show the benefit of simulating IC debonding as opposed to ignoring it. It can be seen that the method proposed in this paper is able to follow the general shape of the experimental load-deflection curve relatively well compared to the simulation using the method by Darain et al. (2016) which tends to overpredict the load-deflection capacity of hybrid strengthened RC beams, especially after steel yielding. However, the previous simulation method by Darain et al. (2016) was found to be better at predicting the pre-yield stiffness of the beams, which as mentioned before can be attributed to the multiple crack analysis being better at simulating tension stiffening (Oehlers et al., 2015). However, the new method proposed in this paper is better at predicting the failure load of the hybrid strengthened beams.

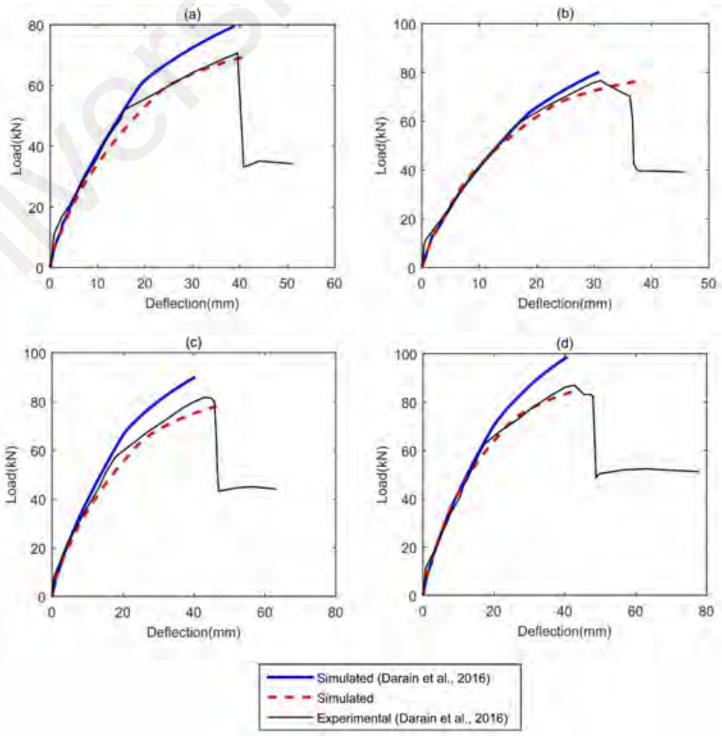

Figure 6. Comparison of load-deflection results (a) Beam CBC8P1; (b) Beam CBC8P2; (c) Beam CBC10P1; (d) Beam CBC10P2.

7 PARAMETRIC STUDY

The proposed simulation method was used to perform several parametric studies. The details of the simulated beams used for the parametric study is similar to beam CBC10P1, apart from the list of properties listed in Table 4. Four test groups were used for the parametric studies. Test groups n-e and s-e were used to study the effect of the elastic modulus of NSM FRP bars ($E_{r\text{-}nsm}$) and FRP sheets ($E_{r\text{-}sheet}$) respectively; test groups n-t and s-t, on the other hand, were used to determine the effect of the bond strength of NSM FRP bars ($\tau_{max\text{-}nsm}$) and FRP sheets ($\tau_{max\text{-}sheet}$) respectively.

Table 4: Properties of simulated hybrid strengthened RC beams.

Test Group	Beam	$E_{r\text{-}nsm}$ (GPa)	$E_{r\text{-}sheet}$ (GPa)	$\tau_{max\text{-}nsm}$ (GPa)	$\tau_{max\text{-}sheet}$ (GPa)
n-e	n-e-50	50	230	9.31	6.78
	n-e-100	100	230	9.31	6.78
	n-e-150	150	230	9.31	6.78
	n-e-200	200	230	9.31	6.78
s-e	s-e-50	165	50	9.31	6.78
	s-e-100	165	100	9.31	6.78
	s-e-150	165	150	9.31	6.78
	s-e-200	165	200	9.31	6.78
n-t	n-t-5	165	230	5	6.78
	n-t-10	165	230	10	6.78
	n-t-15	165	230	15	6.78
	n-t-20	165	230	20	6.78
s-t	s-t-5	165	230	9.31	5
	s-t-10	165	230	9.31	10
	s-t-15	165	230	9.31	15
	s-t-20	165	230	9.31	20

Note: $E_{r\text{-}nsm}$=elastic modulus of NSM FRP bar; $E_{r\text{-}sheet}$=elastic modulus of FRP sheet; $\tau_{max\text{-}nsm}$=bond strength of NSM FRP bar; $\tau_{max\text{-}sheet}$=bond strength of FRP sheet.

The summary of the simulated results for test groups n-e and s-e is given in Table 5, while Figure 7 and Figure 8 shows the load-deflection results for test group n-e and s-e respectively. All the beams failed through concrete crushing, which in this paper is taken as the concrete strain of 0.003. The yield load (P_y) and maximum load (P_{max}) of the hybrid strengthened beams were found to increase as the values of $E_{r\text{-}nsm}$ and $E_{r\text{-}sheet}$ are increased.

Table 5: Summary of simulated results for test group n-e and s-e

Test group	Beam	E_r (N/mm2)	P_y (kN)	P_{max} (kN)	Δ_{max} (mm)	L_{IC} (mm)
n-e	n-e-50	$E_{r\text{-}nsm}$=50	54.8	64.2	43.9	494.4
	n-e-100	100	59.8	70	42.6	439.8
	n-e-150	150	63.8	74.4	41.3	403
	n-e-200	200	66.8	77.8	40.5	377
s-e	s-e-50	$E_{r\text{-}sheet}$=50	59.8	71.8	43.3	184.4
	s-e-100	100	62.2	73	42.4	262.8
	s-e-150	150	63.2	74	42.0	322.4
	s-e-200	200	63.8	74.6	41.1	368

Note: E_r=Elastic modulus; $E_{r\text{-}nsm}$=elastic modulus of NSM FRP bar; $E_{r\text{-}sheet}$=elastic modulus of FRP sheet; P_y=yield load; P_{max}=maximum load; Δ_{max}=deflection at maximum load; L_{IC}=length of IC debonding.

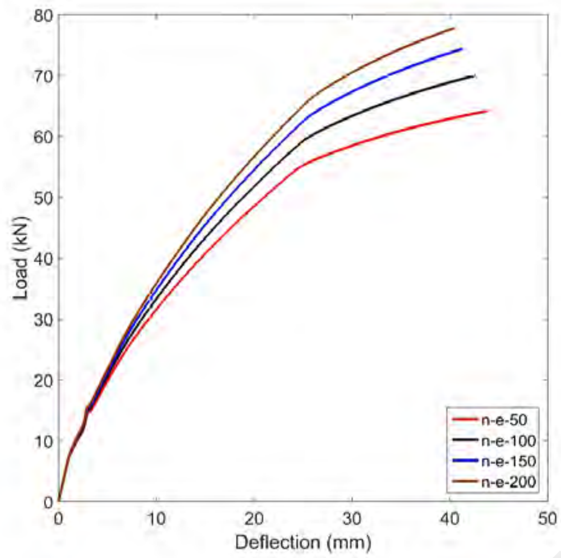

Figure 7. Load-deflection results of test group n-e.

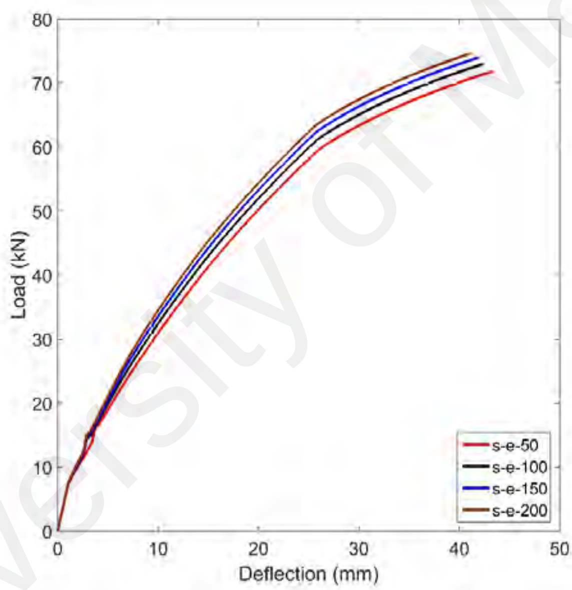

Figure 8. Load-deflection results of test group s-e.

In Figure 9, a plot of E_r against the length of IC debonding, L_{IC} is presented. It should be noted that the value of E_r for test group n-e and s-e refer to $E_{r\text{-}nsm}$ and $E_{r\text{-}sheet}$ respectively. The L_{IC} was found to decrease when higher $E_{r\text{-}nsm}$ was used. On the other hand, as the $E_{r\text{-}sheet}$ is increased, the L_{IC} also increases. This contrasting IC debonding behaviour inevitably affects the load-deflection relationships of the beams as well. As shown in Figure 7, since the L_{IC} decreases for higher $E_{r\text{-}nsm}$, a significant increase in the stiffness and maximum load for beams in test group n-e can be seen. However, for beams in test group s-e, as shown in Figure 8, since L_{IC} will also increase when higher $E_{r\text{-}sheet}$ is used, the increase in stiffness and the maximum load becomes minimal.

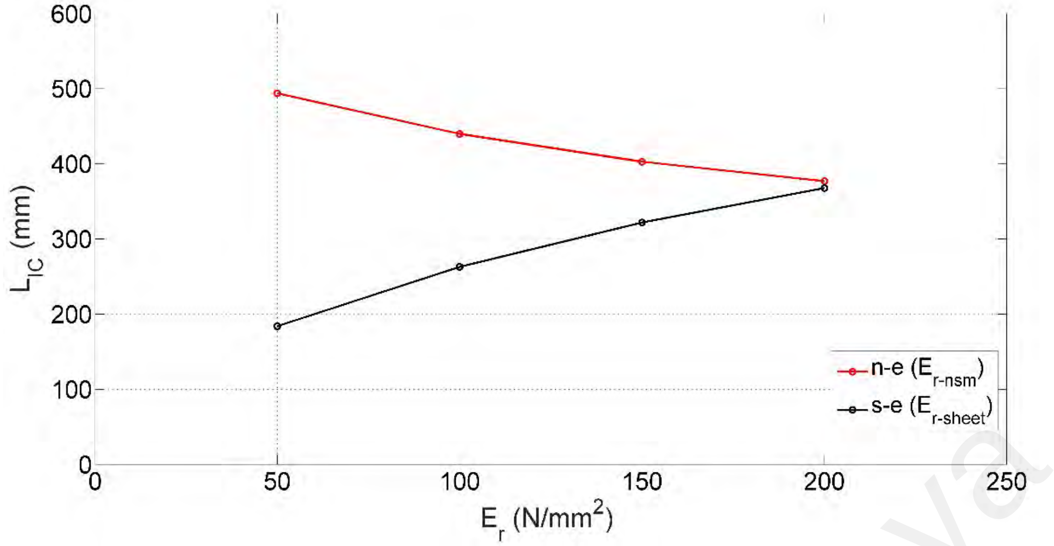

Figure 9. Comparison of simulated IC debonding length for test group n-e and s-e.

A summary of the results for test groups n-t and s-t is given in Table 6; the load-deflection results are shown in Figure 10 and Figure 11. Similar to before, all beams failed by concrete crushing. From Table 6, it can be seen that higher values of $\tau_{max-nsm}$ and $\tau_{max-sheet}$ causes the P_y and P_{max} to increase. However, the overall increase is much lower when compared to the increase seen in the parametric study of elastic modulus, which suggests that while $\tau_{max-nsm}$ and $\tau_{max-sheet}$ are important for tension stiffening, changes in their values does not impact the behaviour of hybrid strengthened beams to a significant degree.

Table 6: Summary of simulated results for test group n-t and s-t

Test group	Beam	τ_{max} (N/mm^2)	P_y (kN)	P_{max} (kN)	Δ_{max} (mm)	L_{IC} (mm)
n-t	n-t-5	$\tau_{max-nsm}$=5	62.2	74	41.9	395.6
	n-t-10	10	64.6	75.4	41.0	395.6
	n-t-15	15	66.8	76.4	39.6	384.4
	n-t-20	20	68.8	77.4	38.5	377
s-t	s-t-5	$\tau_{max-sheet}$=5	65.4	75.2	41.3	376.6
	s-t-10	10	65.6	75.2	41.1	412.8
	s-t-15	15	66.2	76.2	40.4	346.6
	s-t-20	20	67.2	77.2	39.5	298.6

Note: τ_{max}=bond strength; $\tau_{max-nsm}$=bond strength of NSM FRP bar; $\tau_{max-sheet}$=bond strength of FRP sheet; P_y=yield load; P_{max}=maximum load; Δ_{max}=deflection at maximum load; L_{IC}=length of IC debonding.

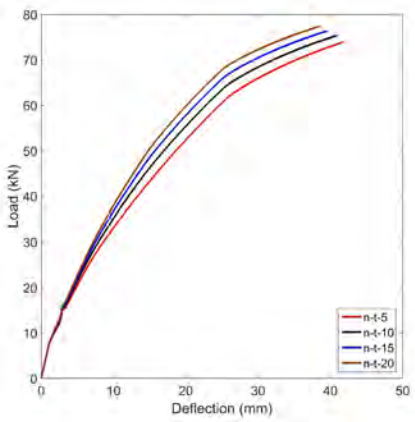

Figure 10. Load-deflection results of test group n-t.

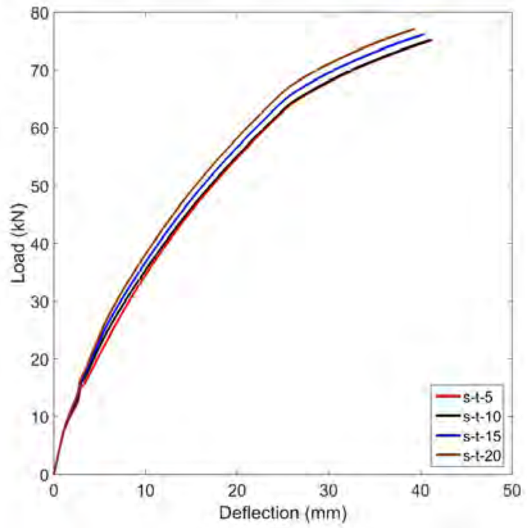

Figure 11. Load-deflection results of test group s-t.

A plot of L_{IC} against τ_{max} for test group n-t and s-t is given in Figure 12. The L_{IC} was found to reduce for higher values of $\tau_{max\text{-}nsm}$. The result of L_{IC}-$\tau_{max\text{-}sheet}$ curve shows a similar trend, apart from a slight increase in L_{IC} for beam s-t-10, which uses $\tau_{max\text{-}sheet} = 10$ N/mm^2. This slight increase in L_{IC} is related to the bond stress and slip of the FRP sheet. Consider Figure 13(b) and Figure 13(c), which shows the slip and bond stress distribution of the FRP sheet for beams s-t-5, s-t-10 and s-t-15. At the same amount of initial slip δ_1, the beam with a higher $\tau_{max\text{-}sheet}$ such as beam s-t-15 will have a shorter hinge span (L_{end}) due to a quicker transfer of force from the FRP sheet to the concrete. However, the transfer of force for beam s-t-10 is not high enough; this causes beam s-t-5 and s-t-10 to have an almost similar L_{end}. As the L_{end} is the same, the summation of bond stresses τ_{sum} for both beams should be similar. However, beam s-t-10 have a higher $\tau_{max\text{-}sheet}$ than beam s-t-5. This results in beam s-t-10 having a longer L_{IC} in order to have the same τ_{sum} as beam s-t-5. This situation does not occur in beam s-t-15, which have a high enough $\tau_{max\text{-}sheet}$ to cause it to have a significantly shorter L_{end} compared to the other two beams. The L_{IC} for beam s-t-15 is also the shortest of the three beams. The most significant effect of a longer L_{IC} is the reduction of the strength and stiffness for beam s-t-10. This can be seen in Figure 11, where the load-deflection curve for s-t-5 and s-t-10 is almost identical despite beam s-t-10 having a higher $\tau_{max\text{-}sheet}$.

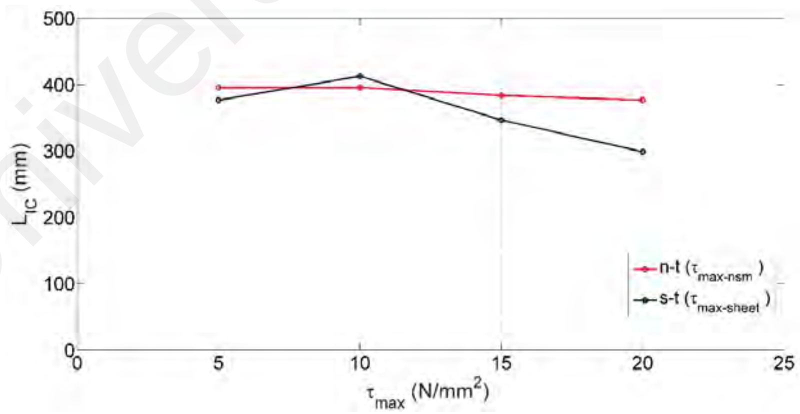

Figure 12. Comparison of simulated IC debonding length for test group n-t and s-t.

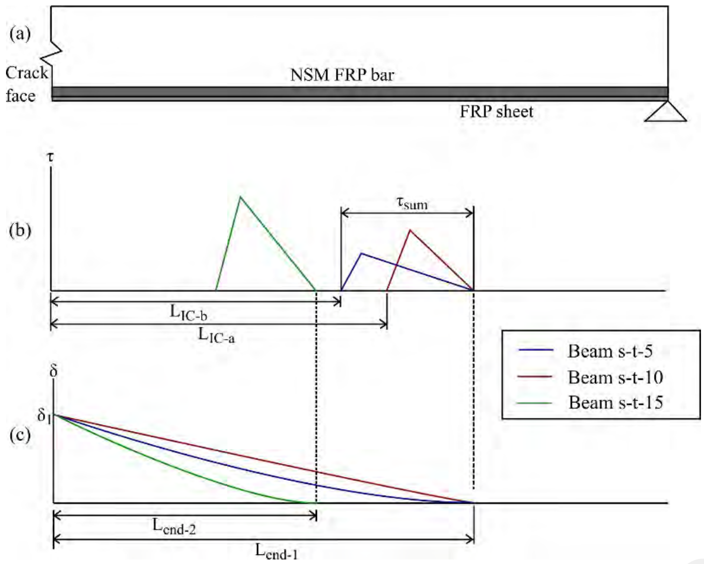

Figure 13. Distribution of slip and bond stress of FRP sheet (a) Beam detail; (b) Bond stress distribution for FRP sheet; (c) Slip distribution for FRP sheet.

8 CONCLUSIONS

An improvement to the method presented by Darain et al. (2016) for simulating the behaviour of hybrid strengthened RC beams was proposed, which can correctly simulate the effect of IC debonding. Several conclusions were made based on the work done:

- The proposed method was able to simulate the behaviour of hybrid strengthened beams with good accuracy. The single crack analysis was found to be important in simulating the loss of stiffness due to IC debonding in hybrid strengthened RC beams.
- The simulated maximum load was found to be within 4% of the experimental value.
- On the other hand, the simulated maximum deflection was found to be less accurate with deviation from the experimental value from 1% to 20%.
- The simulated yield load was found to deviate from experimental values from 12-16% due to the use of the single crack analysis as the basis of the tension stiffening simulation, as the single crack analysis is known to be less accurate at predicting tension stiffening effect compared to the multiple crack analysis.
- Increasing the elastic modulus of NSM FRP bar increases the stiffness and maximum load of the hybrid strengthened beam while decreasing the length of IC debonding.
- Increasing the elastic modulus of FRP sheet, on the other hand, increases the length of IC debonding; as such while the stiffness and maximum load of the hybrid strengthened beam still increase, the amount is less significant compared to increasing the elastic modulus of NSM FRP bar.
- Increasing the bond strength of NSM FRP bar and FRP sheet slightly increases the stiffness and maximum load of hybrid strengthened beams.

While the proposed method is perhaps too complicated to be used in general design, it is hoped that it can be used to perform further studies on the hybrid strengthening method similar to the parametric study presented in this paper. The proposed method should be applicable to hybrid strengthened beams using any type of material and shape of FRP reinforcement, assuming the correct material models (in particular the bond stress-slip model) are used.

Acknowledgement

This study was funded by the University of Malaya, Grand Challenge - SUS (Sustainability Science) Grant, project number GC003A-15SUS.

References

Badawi M and Soudki K (2009) Flexural strengthening of RC beams with prestressed NSM CFRP rods - Experimental and analytical investigation. Construction and Building Materials 23(10): 3292–3300.

Barros JAO, Rezazadeh M, Laranjeira JPS, et al. (2017) Simultaneous flexural and punching strengthening of RC slabs according to a new hybrid technique using U-shape CFRP laminates. Composite Structures 159: 600–614.

Capozucca R and Magagnini E (2016) Vibration of RC beams with NSM CFRP with unbonded/notched circular rod damage. Composite Structures 144: 108–130.

Capozucca R, Domizi J and Magagnini E (2016) Damaged RC beams strengthened with NSM CFRP rectangular rods under vibration in different constrain conditions. Composite Structures 154: 660–683.

CEB-FIP (1993) CEB-FIP model code 1990. London, UK: Thomas Telford Ltd.

Ceroni F, Pecce M, Matthys S, et al. (2008) Debonding strength and anchorage devices for reinforced concrete elements strengthened with FRP sheets. Composites Part B: Engineering 39(3): 429–441.

Chen GM, Zhang Z, Li YL, et al. (2016) T-section RC beams shear-strengthened with anchored CFRP U-strips. Composite Structures 144: 57–79.

Chen Y, Visintin P, Oehlers D, et al. (2014) Size-Dependent Stress-Strain Model for Unconfined Concrete. Journal of Structural Engineering 140(4): 4013088.

Darain KM ud, Jumaat M, Shukri AA, et al. (2016) Strengthening of RC Beams Using Externally Bonded Reinforcement Combined with Near-Surface Mounted Technique. Polymers 8(7): 261.

De Lorenzis L (2004) Anchorage length of near-surface mounted fiber-reinforced polymer rods for concrete strengthening - Analytical modeling. ACI Structural Journal 101(3): 375–386.

Fabrics H, Cedex V, Cedex R, et al. (2003) Experimental analysis of flexural behaviour of externally bonded CFRP reinforced concrete structures. 36(May): 238–241.

Gupta AK and Maestrini SR (1990) Tension Stiffness Model for Reinforced Concrete Bars. Journal of Structural Engineering 116(3): 769-790.

Haskett M, Oehlers DJ and Mohamed Ali MS (2008) Local and global bond characteristics of steel reinforcing bars. Engineering Structures 30(2): 376–383.

Hassan TK and Rizkalla SH (2004) Bond mechanism of near-surface-mounted fiber-reinforced polymer bars for flexural strengthening of concrete structures. ACI Structural Journal 101(6): 830–839.

Knight D, Visintin P, Oehlers DJ, et al. (2014a) Short-Term Partial-Interaction Behavior of RC Beams with Prestressed FRP and Steel. Journal of Composites for Construction 18(1): 4013029.

Knight D, Visintin Phillip, Oehlers DJ, et al. (2014b) Simulating RC beams with unbonded FRP and steel prestressing tendons. Composites Part B: Engineering 60: 392–399.

Kreit A, Al-Mahmoud F, Castel A, et al. (2011) Repairing corroded RC beam with near-surface mounted CFRP rods. Materials and Structures 44(7): 1205–1217.

Lu XZ, Teng JG, Ye LP, et al. (2005) Bond-slip models for FRP sheets/plates bonded to concrete. Engineering Structures 27(6): 920–937.

Maalej M (2005) Analysis and design of FRP externally-reinforced concrete beams against debonding-type failures. Materials and Structures 34(241): 418–425.

Muhamad R, Mohamed Ali MS, Oehlers D, et al. (2011) Load-slip relationship of tension reinforcement in reinforced concrete members. Engineering Structures 33(4): 1098–1106.

Narayanamurthy V, Chen JF, Cairns J, et al. (2012) Plate end debonding in the constant bending moment zone of plated beams. Composites Part B: Engineering 43(8): 3361–3373.

Oehlers D, Visintin P, Zhang T, et al. (2012) Flexural rigidity of reinforced concrete members using a deformation based analysis. Concrete in Australia 38(4): 50–56.

Oehlers DJ, Visintin P, Haskett M, et al. (2013) Flexural ductility fundamental mechanisms governing all RC members in particular FRP RC. Construction and Building Materials 49: 985–997.

Oehlers DJ, Visintin P and Lucas W (2015) Flexural Strength and Ductility of FRP-Plated RC Beams: Fundamental Mechanics Incorporating Local and Global IC Debonding. Journal of Composites for Construction 20(2): 4015046.

Pachalla SKS and Prakash SS (2017) Efficient near surface mounting CFRP strengthening of pretensioned hollow-core slabs with opening – An experimental study. Composite Structures, Elsevier Ltd 162: 28–38.

Pesic N (2005) Flexural analysis and design of reinforced concrete beams with externally bonded FRP reinforcement. Materials and Structures 38(276): 183–192.

Popovics S (1973) A numerical approach to the complete stress-strain curve of concrete. Cement and Concrete Research 3(5): 583–599.

Rahman M, Jumaat MZ, Rahman MA, et al. (2015) Innovative hybrid bonding method for strengthening reinforced concrete beam in flexure. Construction and Building Materials, Elsevier Ltd 79: 370–378.

Seo S, Sung M and Feo L (2016) Flexural analysis of RC beam strengthened by partially de-bonded NSM FRP strip. Composites Part B, Elsevier Ltd 101: 21–30.

Shukri AA and Jumaat MZ (2016) Simulating concrete cover separation in RC beams strengthened with near-surface mounted reinforcements. Construction and Building Materials 122: 1–11.

Shukri AA, Darain KM ud and Jumaat MZ (2015) The Tension-Stiffening Contribution of NSM CFRP to the Behavior of Strengthened RC Beams. Materials 8(7): 4131–4146.

Shukri AA, Hosen MA, Muhamad R, et al. (2016) Behaviour of precracked RC beams strengthened using the side-NSM technique. Construction and Building Materials 123: 617–626.

Tam B, Si A and Limam A (2016) Numerical modelling of reinforced concrete beams repaired by TRC composites. Composite Structures 152: 779–790.

Toutanji H, Zhao L and Zhang Y (2006) Flexural behavior of reinforced concrete beams externally strengthened with CFRP sheets bonded with an inorganic matrix. Engineering Structures 28(4): 557–566.

Visintin P, Oehlers DJ, Wu C., et al. (2012a) A mechanics solution for hinges in RC beams with multiple cracks. Engineering Structures 36: 61–69.

Visintin P, Oehlers DJ, Wu Chengwing, et al. (2012b) The reinforcement contribution to the cyclic behaviour of reinforced concrete beam hinges. Earthquake Engineering & Structural Dynamics 41: 1591–1608.

Visintin P, Oehlers DJ, Muhamad R, et al. (2013a) Partial-interaction short term serviceability deflection of RC beams. Engineering Structures 56: 993–1006.

Visintin P, Oehlers D and Haskett M (2013b) Partial-interaction time dependent behaviour of reinforced concrete beams. Engineering Structures 49: 408–420.

Zhang SS and Teng JG (2014) Finite element analysis of end cover separation in RC beams strengthened in flexure with FRP. Engineering Structures 75: 550–560.

CHAPTER 6 - DESIGN PROCEDURE FOR NSM AND SNSM STRENGTHENED RC BEAMS

This chapter presents the research paper "Concrete cover separation of reinforced concrete beams strengthened with near-surface mounted method: Mechanics based design approach". In this paper, the methodology and results from studies done in chapters 3, 4 and 5 will be used to obtain closed form solutions for crack spacing and load-slip relationships, which will be used to obtain a design procedure for NSM strengthened beams. The proposed design procedure is much simpler than the full simulation for general design purpose and as such is difficult to use. The proposed procedure allows the designed NSM strengthened beam to be safe from CCS debonding, which is the primary mode of failure for NSM strengthened beams.

The details of the research papers contained in this chapter along with the statement of contribution of authors is as follows:

1) Shukri, A. A., Ibrahim, Z., & Hashim, H. (2019). Concrete cover separation of reinforced concrete beams strengthened with near-surface mounted method: Mechanics based design approach. *Advances in Structural Engineering*, 22, 1739–1754.
    a. Statement of contribution: Ahmad Azim Shukri (author) performed the simulations and wrote the paper, Zainah Ibrahim (co-author) supervised the research and checked the paper, Huzaifa Hashim (co-author) checked the paper.

6.1 Research paper 6: Concrete cover separation of reinforced concrete beams strengthened with near-surface mounted method: Mechanics based design approach

Published in *Advances in Structural Engineering*

Article history:

Published 23 January 2019

Original Research

Advances in Structural Engineering

Advances in Structural Engineering
2019, Vol. 22(7) 1739–1754

DOI: 10.1177/1369433218824922
journals.sagepub.com/home/ase
SAGE

Concrete cover separation of reinforced concrete beams strengthened with near-surface mounted method: Mechanics based design approach

Ahmad Azim Shukri, Zainah Ibrahim and Huzaifa Hashim

Abstract

The primary mode of premature failure for near-surface mounted strengthened beams is the concrete cover separation. Due to its complexity, most of the prediction methods for concrete cover separation tend to be empirical based, which can limit their usage to specific near-surface mounted strengthening configurations. In response to that, this article presents a mechanics-based design which uses the moment-rotation approach and the global energy balance approach which is less reliant on empirical formulations, as the mechanics of reinforced concrete beam such as tension stiffening and propagation of concrete cover separation debonding crack are directly simulated rather than empirically derived. The proposed design procedure was validated against published experimental results of reinforced concrete beams strengthened with near-surface mounted carbon fibre–reinforced polymer bars, near-surface mounted carbon fibre–reinforced polymer strips or side-near-surface mounted carbon fibre–reinforced polymer bars and show good accuracy. As it is less reliant on empirical formulations, the proposed design procedure should be applicable to various near-surface mounted reinforcement configurations and materials.

Keywords

fibre-reinforced polymer, fracture mechanics, moment-rotation, near-surface mounted, partial interaction, reinforced concrete

Introduction

Structural reinforced concrete (RC) members can require strengthening to compensate for deficiencies in either flexural or shear strength. The reasons for structural strengthening are varied; most structures require strengthening to compensate for strength loss due to ageing, while some structures were damaged in some ways that result in loss of strength. The focus of this article is the near-surface mounted (NSM) method (Badawi and Soudki, 2009; Bilotta et al., 2011; Capozucca and Bossoletti, 2014; Galati and De Lorenzis, 2009; Sharaky et al., 2017; Wu et al., 2014), which is a type of flexural strengthening for RC beams or slabs. The NSM method involves drilling grooves within the concrete cover and placing an NSM reinforcement within it, after which the groove is filled with epoxy adhesive. Currently, there are also several new derivative methods based on the NSM method, such as the side-NSM (SNSM) method (Sharaky et al., 2017; Shukri et al., 2016a) where the NSM reinforcement is placed at the sides of the beam to allow NSM strengthening to be applied on beams with small width or with beam soffits which are inaccessible and the partially bonded NSM (Choi et al., 2011; Seo et al., 2016) where the high moment area of the NSM is left unbonded to increase ductility.

The main problem of the NSM method is its vulnerability to concrete cover separation (CCS) failure. The CCS involves a debonding crack which appears at the location of NSM reinforcement curtailment, which then propagates towards the higher moment area of the beam. It is a type of premature mode of failure, which means that NSM-strengthened beams that failed by CCS will have failed well below the design strength.

Department of Civil Engineering, Faculty of Engineering, University of Malaya, Kuala Lumpur, Malaysia

Corresponding authors:
Ahmad Azim Shukri and Zainah Ibrahim, Department of Civil Engineering, Faculty of Engineering, University of Malaya, 50603 Kuala Lumpur, Malaysia.
Emails: ahmadazimshukri@gmail.com; zainah@um.edu.my

There has not been much research done on CCS failure on NSM-strengthened beams, likely due to the presence of a large number of parameters involved. Several methods to predict or simulate CCS have been proposed using the finite element method (Al-Mahmoud et al., 2010; Zhang and Teng, 2014) or using the concrete tooth model (De Lorenzis and Nanni, 2003). Recently, Teng et al. (2016) proposed a strength model for NSM carbon fibre–reinforced polymer (CFRP) strips derived using finite element study while an analytical design approach was proposed by Rezazadeh et al. (2016), which was derived using concrete fracture mechanic. Most of these methods can be highly empirical, such as in terms of predicting crack spacing. Empirical methods that are formulated around a specific shape or material type of NSM reinforcement are only accurate within the regime of testing used to formulate them, which can limit their usage.

In response to all these problems, this article proposes a mechanics-based approach to design, which can prevent CCS failure while being less reliant on empirical means. An example of this can be seen in the work of Shukri and Jumaat (2016), where the moment-rotation (M/θ) approach (Knight et al., 2014; Mo et al., 2016; Oehlers et al., 2012; Shukri et al., 2015, 2016b; Visintin et al., 2013; Visintin and Oehlers, 2016, 2017) was used in conjunction with the global energy balance approach (GEBA) (Achintha and Burgoyne, 2013, 2011; Guan and Burgoyne, 2014) to simulate CCS failure. The M/θ approach is a mechanics-based method that applies the partial interaction theory (Gupta and Maestrini, 1990; Haskett et al., 2008; Muhamad et al., 2012; Visintin et al., 2013) to directly simulate concrete cracking, crack widening, and tension stiffening of RC beams. The GEBA, on the other hand, applies the fracture mechanics of concrete to predict whether the CCS debonding crack will propagate and cause failure. The proposed method by Shukri and Jumaat (2016) shows that the use of these two mechanics-based methods allows the CCS failure of NSM-strengthened beams to be predicted with good accuracy and applicable to various types of NSM reinforcement material and shape due to lower reliance on empirical means. However, it was not made for general design purpose and as such is difficult to use. Hence, in this article, closed-form solutions for crack spacing and load–slip relationships will be used to formulate a simpler design procedure based on the M/θ-GEBA method, which is then validated against published experimental results.

Fundamental theories

In this section, the fundamental theories used in the M/θ approach and GEBA will be presented. The aim of this article is to introduce a design procedure, hence only a brief description of the M/θ approach and GEBA that is relevant to this article are given while references to the original research are provided.

M/θ approach

The M/θ approach used is a segmental simulation focused on the behaviour of cracked RC beam, as shown in Figure 1(a), which feature an NSM-strengthened RC beam section with cross-section as shown in Figure 1(b). The spacing between these primary cracks is designated S_{cr}, and due to symmetry of forces within the RC beam segment, it is possible to only consider half the crack spacing, L_{def}, for analysis purpose.

Slip occurs along L_{def} between the steel and NSM reinforcements and adjacent concrete, causing a cumulative slip of δ_r and δ_f at the crack face, respectively; this occurrence can be idealized as prism with a reinforcement and its adjacent concrete as shown in Figure 2, where slip of steel reinforcement (δ_r) is shown as example. The size of the prisms is as shown in Figure 1(b), where c_r refers to the distance from the centroid of the steel reinforcement to beam soffit and c_f refers to the distance from the centroid of the NSM reinforcement to the beam soffit.

The bond stress, τ, gradually transfers load P_r onto the adjacent concrete, causing both P_r and δ_r to reduce the further it gets from the crack face. Using the boundary condition of $\delta_r = 0$ at length L_{def}, the stresses and strains within the prism can be solved to determine the force P_r which causes the slip δ_r, which allows the load–slip (P-δ) relationship to be obtained as shown in Figure 3. This procedure is called the partial interaction tension stiffening analysis (Haskett et al., 2008; Muhamad et al., 2011, 2012); the benefit of this analysis is the resulting load–slip relationship has directly accounted for the effects of tension stiffening through the use of bond stress–slip relationship, such that other empirical indirect methods, such as the commonly used Branson's equation (Branson, 1968), are not needed.

From Figure 3, it can be seen that there is an initial linear portion OA with stiffness K (Zhang et al., 2017), such that the P_r-δ_r and P_f-δ_r relationship can be written as $P_r = K_r\delta_r$ and $P_f = K_f\delta_f$, respectively. This assumption should be correct for steel reinforcements prior to steel yielding and for NSM FRP reinforcements, which do not yield. Closed-form solutions based on this theory have been proposed (Visintin and Oehlers, 2016; Zhang et al., 2017) and will be used extensively in this article.

GEBA

The GEBA is a fracture mechanics-based method where the primary assumption is that CCS debonding

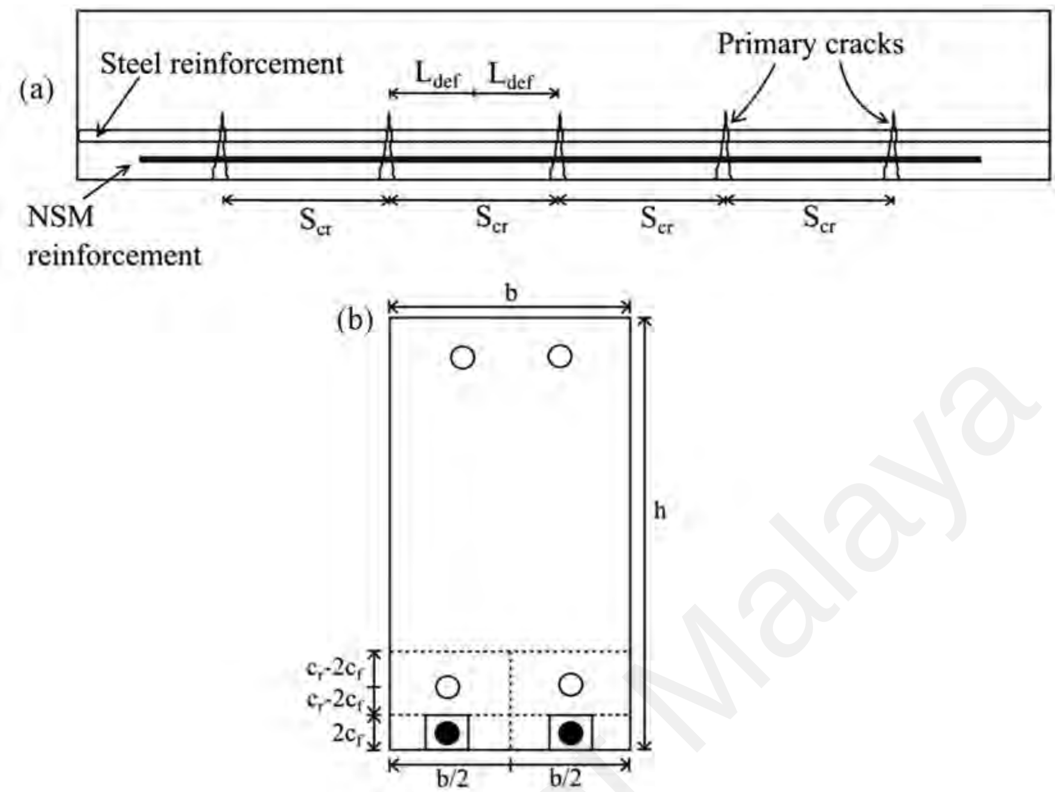

Figure 1. RC beam: (a) NSM-strengthened beam segment and (b) cross-section of NSM-strengthened beam.

cracks will always appear on strengthened RC beams, causing a debonded length L_d as shown in Figure 4. It is then only a matter of determining whether there is enough energy for the debonding crack to propagate and cause failure. When the GEBA is applied on beams strengthened with FRP sheet (Achintha and Burgoyne, 2011) or NSM (Shukri et al., 2018; Shukri and Jumaat, 2016), it is usually assumed that the debonding crack starts to propagate at an angle of 45° to the beam axis until it reaches the shear link; with this assumption, L_d is considered equal to the concrete cover's depth as shown in Figure 4(a). It was stated by Achintha and Burgoyne (2013) that the actual direction of the crack may be slightly varied from 45°, but it should not have a significant effect on the results. On the other hand, for SNSM-strengthened beams, the experimental studies on SNSM-strengthened beams (Hosen et al., 2015; Sharaky et al., 2017; Shukri et al., 2016a) had shown that the shear crack starts to propagate horizontally as it reaches the SNSM reinforcement, such that $L_d = 0$ as shown in Figure 4(b).

As the GEBA is concerned with the start of the fracture process, mode II effects of concrete fracture such as aggregate interlock are not relevant; hence, the focus of the GEBA is mainly on mode I (Achintha and Burgoyne, 2008). For the fundamental procedure of the GEBA, consider the NSM-strengthened beam section as shown in Figure 4, with a CCS debonding crack already present at location L_a where moment M_a is acting. It is assumed that the debonding crack will propagate instantaneously, such that M_a remains the same as the change from strengthened to unstrengthened section due to CCS debonding occurs, as shown in Figure 5. The strain energy available at L_a that can cause the debonding crack to propagate, designated as W_a, can be determined from the difference between the moment–curvature (M/χ) relationship of the NSM-strengthened section $(M/\chi)_s$ and the unstrengthened section $(M/\chi)_u$. The method to determine fracture energy available for debonding (G_a) is presented in section 'CCS prediction'.

Design procedure for CCS

The proposed mechanics-based design procedure will be presented in this section, while a flowchart is given in Figure 6 as an overview. A preliminary design for the NSM strengthening is first made. Assuming the maximum moment that the beam needs to withstand is known, the maximum moment at L_a, M_a is known. The rotation at the strengthened and unstrengthened section due to moment M_a is then determined and the

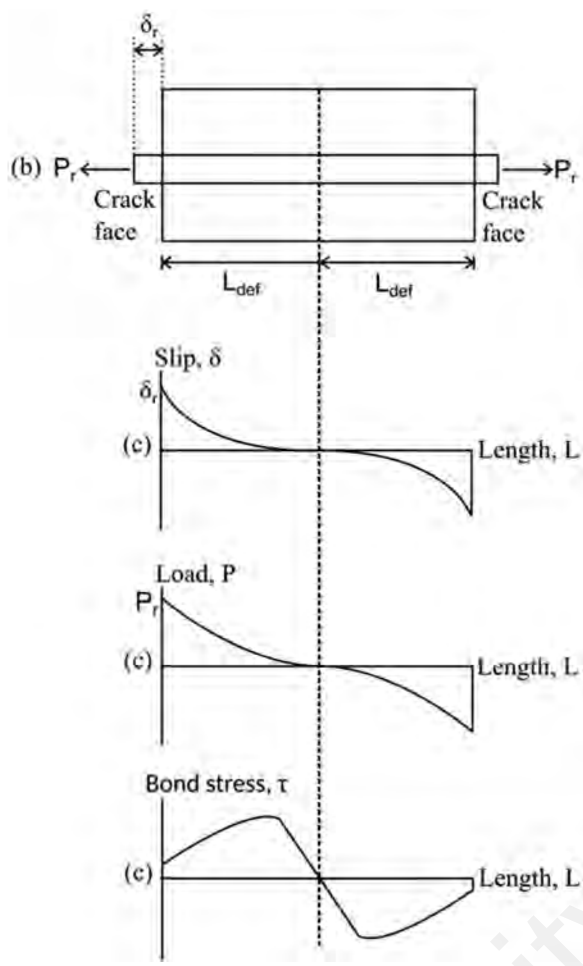

Figure 2. Partial interaction tension stiffening analysis of steel reinforcement.

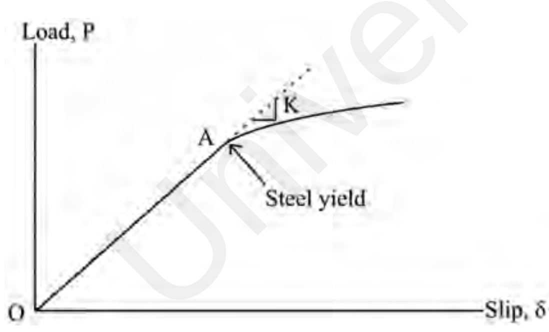

Figure 3. Load–slip relationship of steel or NSM reinforcement.

GEBA is used to determine if the debonding crack will propagate. If the beam is predicted to fail by CCS, the design for the NSM strengthening is changed and the procedure is repeated. Once a suitable design for NSM strengthening is determined, the flexural strength of the NSM-strengthened beam is then determined.

The proposed design procedure is applicable for both virgin and cracked RC beams. It has been shown that the crack spacing near the support of the beams is usually similar regardless of whether the beam is virgin or cracked prior to NSM strengthening (Shukri et al., 2018), which allows the method for CCS prediction presented in Figure 6 to be used as it is for both types of beams. Furthermore, it was shown that the difference in ultimate load between virgin and cracked NSM-strengthened RC beam to be negligible when the failure is by flexure rather than CCS (Shukri et al., 2016a, 2018).

Primary crack spacing and load–slip stiffness

The primary crack spacing, S_{cr}, and the length of deformation, L_{def}, can be defined through the mechanically derived equation by Sturm et al. (2018)

$$S_{cr} = \alpha\left(\frac{2^{\alpha}(1+\alpha)}{\lambda_2(1-\alpha)^{1+\alpha}}\right)^{\frac{1}{1+\alpha}}\left(\frac{f_{ct}}{E_c}\left(\frac{E_cA_c}{E_rA_r}+1\right)\right)^{\frac{1-\alpha}{1+\alpha}} \quad (1)$$

where

$$\lambda_2 = \frac{\tau_{max}}{\delta_1^{\alpha}}\beta \quad (2)$$

$$\beta = L_{per}\left(\frac{1}{E_rA_r}+\frac{1}{E_cA_c}\right) \quad (3)$$

$$L_{def} = \frac{S_{cr}}{2} \quad (4)$$

where f_{ct} is the tensile strength of concrete, L_{per} is the total perimeter of a single tensile steel reinforcement of area A_r contained within the tension stiffening prism as shown in Figure 2. A_{cr} is the area of adjacent concrete in the tension stiffening prism, which can be determined using Figure 1(b). The variables α, δ_1 and τ_{max} are the ascending branch of the non-linear bond stress–slip relationship by CEB-FIP (1993) where $\alpha = 0.4$, $\delta_1 = 1$ mm and $\tau_{max} = 1.25\sqrt{f_c}$.

Having determined the S_{cr}, the load–slip stiffness parameter for the steel reinforcement, K_r can be determined as

$$K_r = \frac{2E_rA_r}{S_{cr}c_2} \quad (5)$$

where E_r is the elastic modulus of steel and c_2

$$c_2 = 1.08\left(\frac{A_r}{A_{cr}}\right)^{0.105} \quad (6)$$

The coefficient c_2 allows for the effect of bond and was determined using semimechanical means by Zhang et al. (2017) using a numerical tension stiffening

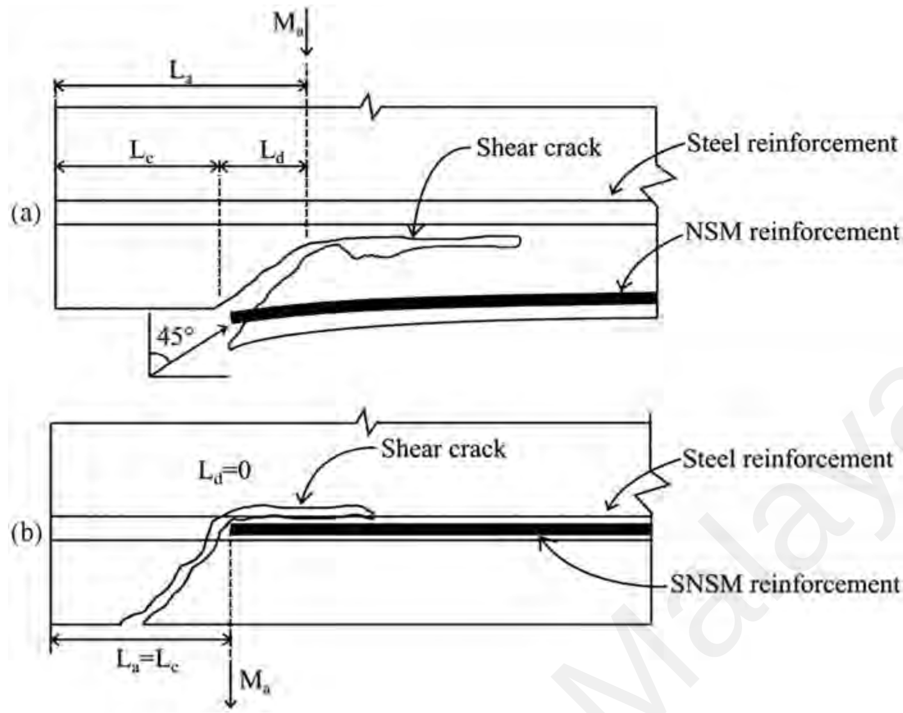

Figure 4. Initial debonded length of NSM- and SNSM-strengthened beams: (a) NSM strengthened beam; (b) SNSM strengthened beam.

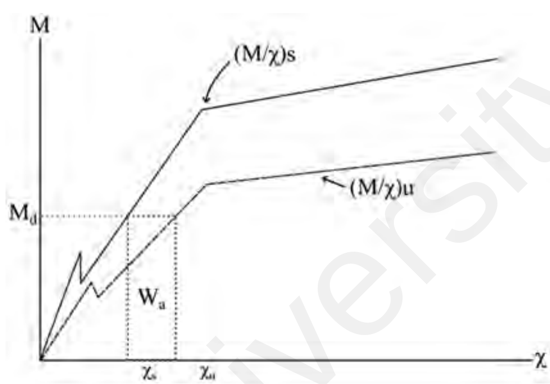

Figure 5. Moment–curvature relationship of strengthened and unstrengthened beam section.

analysis shown in Figure 2 to perform parametric study, from which c_2 was extracted. Since it was derived for steel reinforcement, it is unsuitable for NSM reinforcements. Hence, a parametric study was performed in this research to extract c_2 for NSM CFRP bar and NSM CFRP strip.

Parametric study for c_2. The objective of this brief parametric study is to obtain the relationship between A_f/A_{cf} and c_2; A_f is the area of NSM reinforcement and A_{cf} is the area of adjacent concrete for the tension stiffening prism containing the NSM reinforcement. Three types of NSM reinforcement configuration will be used:

- NSM CFRP bar with ratio of groove to bar diameter of 2;
- NSM CFRP bar with ratio of groove to bar diameter of 1.5;
- NSM CFRP strip with ratio of groove height to width of 2.75.

The NSM reinforcement configurations above were chosen as they are commonly used in the literature. The bond stress–slip relationship by De Lorenzis (2004) and Zhang et al. (2013) were used for NSM CFRP bar and NSM CFRP strip, respectively. The material properties used in the parametric study were fixed and are shown in Table 1. The S_{cr} of a NSM-strengthened beam is assumed to be controlled by the steel reinforcement and not the NSM reinforcement (Shukri et al., 2015; Shukri and Jumaat, 2016); hence, for this parametric study of NSM reinforcements, the S_{cr} is fixed to the value given in Table 1.

The full numerical procedure for the partial interaction tension stiffening analysis, as illustrated in Figure 2, has been shown in multiple published research papers (Haskett et al., 2008; Muhamad et al., 2011; Shukri et al., 2015, 2016b; Shukri and Jumaat, 2016) and so will not be repeated again here. The results of the parametric study are shown in Figures 7

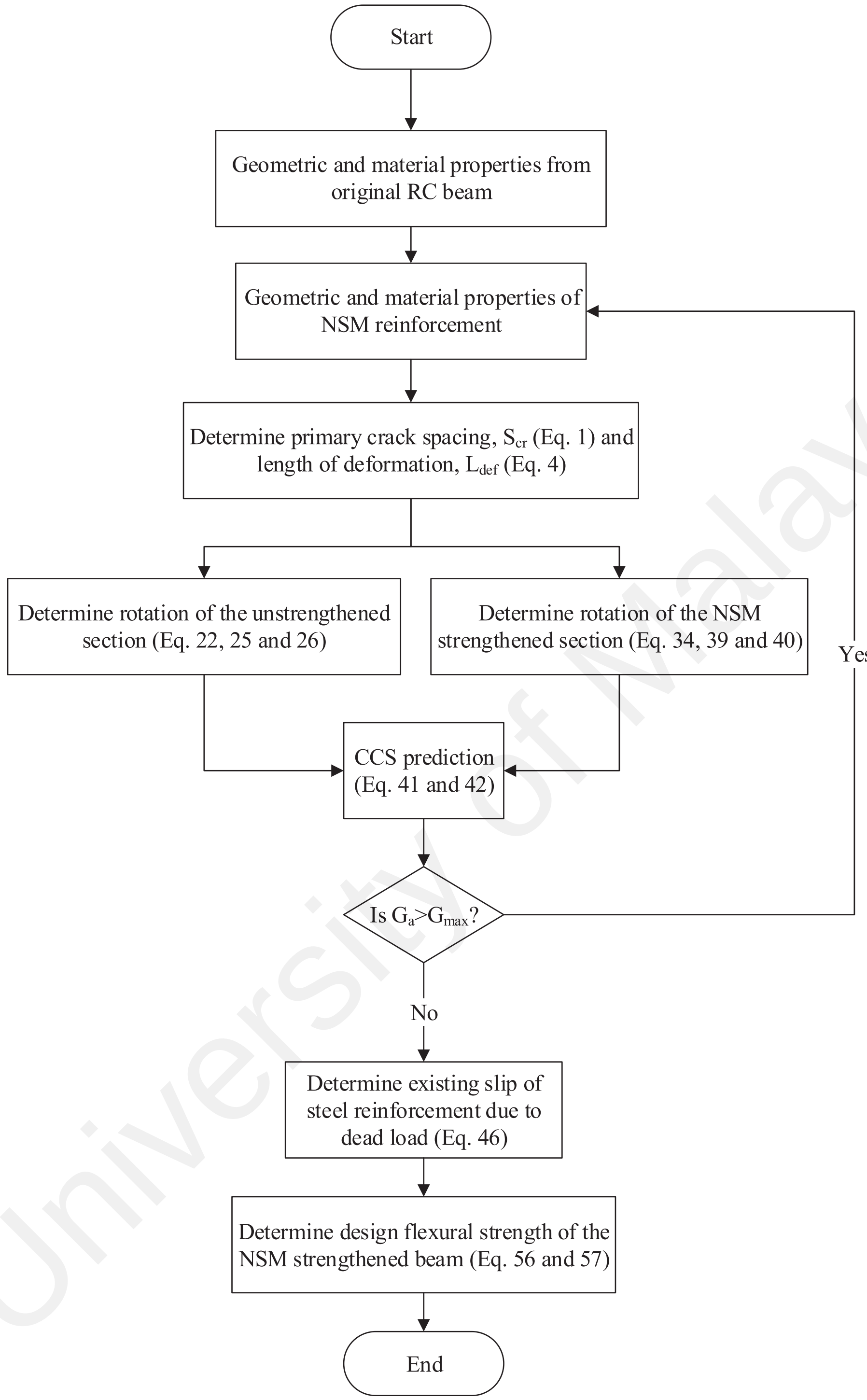

Figure 6. Design procedure for NSM-strengthened beams.

to 9, where c_{2b2} is the coefficient of bond for NSM CFRP bar with ratio of groove to bar diameter of 2, $c_{2b1.5}$ is the coefficient of bond for NSM CFRP bar with ratio of groove to bar diameter of 1.5 and c_{2s} is the coefficient for NSM CFRP strip. From the results, it can be seen that the bond effect coefficient c_2 decreases when A_f/A_{cf} increases.

Extracting the coefficients from the parametric study results using a linear relationship yield

$$c_{2b2} = -0.529\left(\frac{A_f}{A_{cf}}\right) + 0.884 \qquad (7)$$

Table 1. Fixed properties for parametric study.

Properties	Value
Concrete compressive strength, f_c (N/mm^2)	35
Concrete elastic modulus, E_c (N/mm^2)	27,800
Concrete tensile strength, f_t (N/mm^2)	3.2
Epoxy adhesive tensile strength, f_{et} (N/mm^2)	27
Yield strength of steel reinforcement, σ_y (N/mm^2)	500
Elastic modulus of steel reinforcement, E_r (N/mm^2)	200,000
Elastic modulus of NSM reinforcement, E_f (N/mm^2)	165,000
Primary crack spacing, S_{cr} (mm)	142.9

NSM: near-surface mounted.

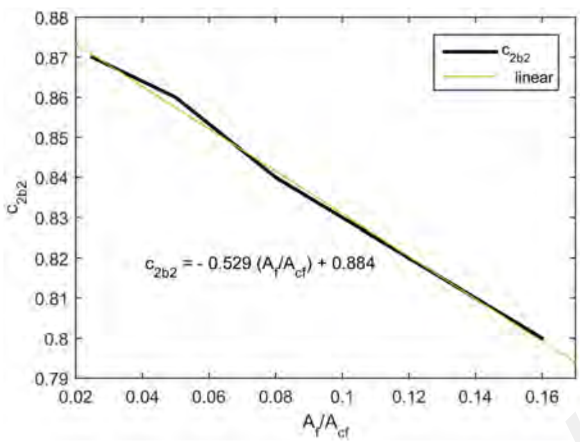

Figure 7. Parametric study for NSM CFRP bars with ratio of groove to bar diameter of 2.

$$c_{2b1.5} = -\,0.586\left(\frac{A_f}{A_{cf}}\right) + 0.862 \tag{8}$$

$$c_{2s} = -\,1.645\left(\frac{A_f}{A_{cf}}\right) + 1.367 \tag{9}$$

The stiffness parameter for NSM CFRP bar can then be determined as

$$K_f = \frac{2E_fA_f}{S_{cr}c_{2b2}} \tag{10}$$

where E_f, A_f and A_{cf} are the elastic modulus of the NSM reinforcement, area of a single NSM reinforcement and area of adjacent concrete area within the tension stiffening prism of the NSM reinforcement, which can be determined using Figure 1(b). The coefficient c_{2b2} in equation (10) can be changed to either $c_{2b1.5}$ or c_{2bs} according to the NSM reinforcement configuration used. If some other NSM material or NSM configuration is used, to obtain the relevant coefficient c_2 is only a matter of performing a numerical parametric study similar to what is shown here.

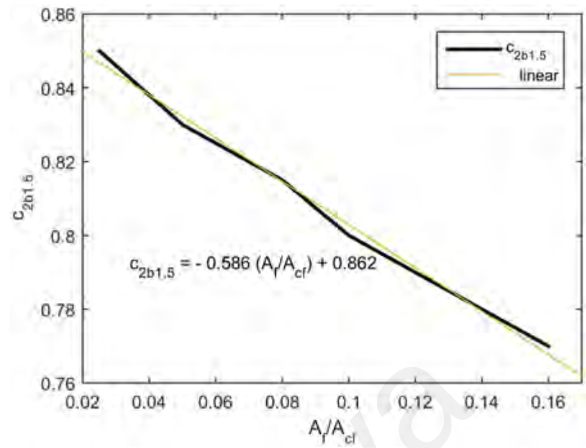

Figure 8. Parametric study for NSM CFRP bars with ratio of groove to bar diameter of 1.5.

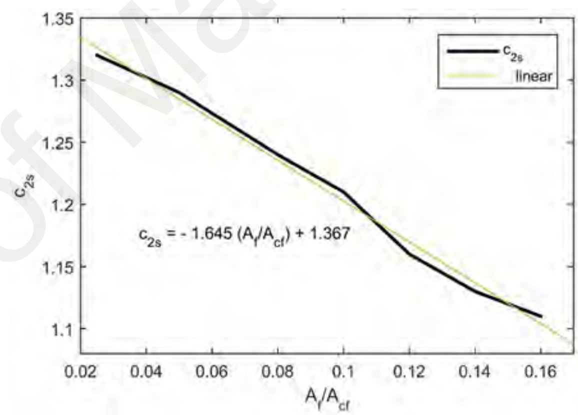

Figure 9. Parametric study for NSM CFRP strips with ratio of groove height to width of 2.75.

Depth of neutral axis for unstrengthened RC beam section

Having determined the K_r and K_f, the load acting on a single steel and NSM reinforcement for a given slip can be determined as

$$P_r = K_r\delta_r \tag{11}$$

$$P_f = K_f\delta_f \tag{12}$$

Let n_r be the number of total steel reinforcement used in the RC beam. From equation (11), the sum of forces acting on all the steel reinforcements can be simplified as

$$P_rn_r = \delta_r\alpha_1 \tag{13}$$

where

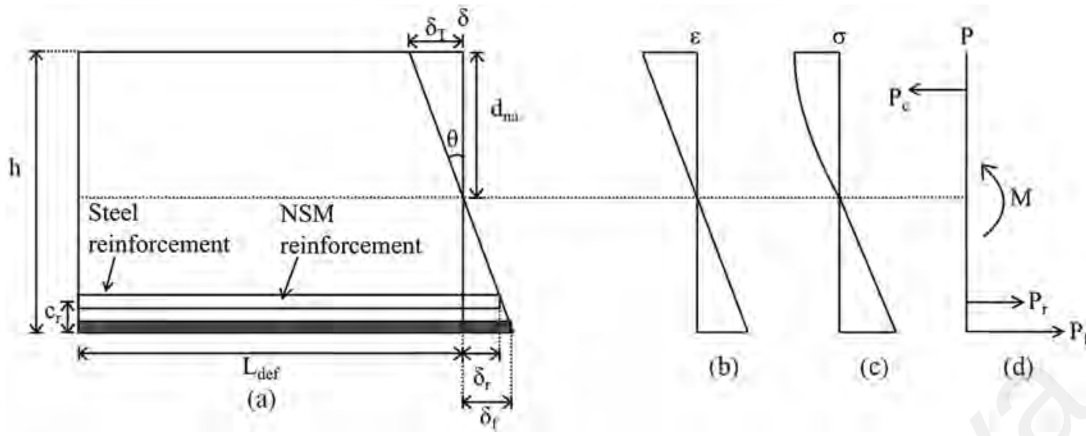

Figure 10. Moment-rotation of NSM-strengthened beam section: (a) beam section of length L_{def} and deformation profile, (b) strain profile, (c) stress profile and (d) forces acting on the beam section.

$$\alpha_1 = K_f n_r \tag{14}$$

Now consider the equation of equilibrium of the unstrengthened section

$$P_c = P_r n_r \tag{15}$$

where P_c is the compressive force of concrete. Assuming a triangular-shaped concrete stress and inserting equation (13) into equation (15) leads to

$$E_c\left(\frac{\delta_T}{L_{def}}\right)\left(\frac{bd_{na-u}}{2}\right) = \delta_r\alpha_1 \tag{16}$$

where E_c is the elastic modulus of concrete, δ_T is the deformation of the topmost section of the beam and $d_{na\text{-}u}$ is the depth of neutral axis for the unstrengthened section. From Figure 10(a), the relationship between the rotation and the slips and deformations of a strengthened beam is

$$\tan\theta = \frac{\delta_r}{h - d_{na} - c_r} = \frac{\delta_f}{h - d_{na} - c_f} = \frac{\delta_T}{d_{na}} \tag{17}$$

where h is the height of the beam and d_{na} is the depth of neutral axis. From equation (17), the relationship between the slip of reinforcement and concrete deformation at the topmost section of the beam for the unstrengthened section can be written as

$$\delta_r = \frac{\delta_T}{d_{na-u}}(h - d_{na-u} - c_r) \tag{18}$$

Inserting equation (18) into equation (16) leads to

$$E_c\left(\frac{\delta_T}{L_{def}}\right)\left(\frac{bd_{na-u}}{2}\right) = \frac{\delta_T}{d_{na-u}}(h - d_{na-u} - c_r)\alpha_1 n_r \tag{19}$$

To simplify equation (19), let

$$\alpha_2 = \frac{E_c b}{2L_{def}} \tag{20}$$

Replacing equation (20) into equation (19) yields

$$\delta_T d_{na-u}\alpha_2 = \frac{\delta_T}{d_{na-u}}(h - d_{na-u} - c_r)\alpha_1 \tag{21}$$

Solving equation (21) for $d_{na\text{-}u}$ gives

$$d_{na-u} = \sqrt{\frac{\alpha_1^2}{4\alpha_2^2} - \frac{c_r\alpha_1 - h\alpha_1}{\alpha_2}} - \frac{\alpha_1}{2\alpha_2} \tag{22}$$

Rotation of unstrengthened RC beam section

Since a triangular-shaped concrete stress was assumed, the lever arm for the steel reinforcement in the unstrengthened section, Z_{ru}, is

$$Z_{ru} = h - \frac{d_{na-u}}{3} - c_r \tag{23}$$

The equation of moment for the unstrengthened beam section is

$$M_a = P_r n_r Z_{ru} \tag{24}$$

Inserting equation (13) into equation (24) and rearranging leads to

$$\delta_{ru} = \frac{M_a}{\alpha_1 Z_{ru}} \tag{25}$$

where δ_{ru} is the slip of steel reinforcement for the unstrengthened beam section. From equation (17), the rotation of the unstrengthened section can be determined as

$$\theta_u = \tan^{-1}\frac{\delta_{ru}}{h - d_{na-u} - c_r} \tag{26}$$

Depth of neutral axis for strengthened beam section

From equation (17), the following relationships can be obtained

$$\delta_{rs} = \frac{\delta_T}{d_{na-s}}(h - d_{na-s} - c_r) \tag{27}$$

$$\delta_f = \frac{\delta_T}{d_{na-s}}\left(h - d_{na-s} - c_f\right) \tag{28}$$

where $d_{na\text{-}s}$ is the depth of neutral axis for the strengthened section of the RC beam. The equilibrium equation for the strengthened beam section is

$$P_c = P_r n_r + P_f n_f \tag{29}$$

where P_f is the force acting on the NSM reinforcement and n_f is the number of NSM reinforcement. Similar to equation (13), total NSM FRP force $P_f n_f$ can be written as

$$P_f n_f = \delta_f \alpha_3 \tag{30}$$

where

$$\alpha_3 = K_f n_f \tag{31}$$

Assuming a triangular shape for the concrete stress and inserting equations (13), (27), (28) and (30) into equation (29) gives

$$\begin{aligned} E_c\left(\frac{\delta_T}{L_{def}}\right)\left(\frac{bd_{na-s}}{2}\right) &= \left(\frac{\delta_T}{d_{na-s}}\right)(h - d_{na-s} - c_r)\alpha_1 \\ &+ \left(\frac{\delta_{Ts}}{d_{na-s}}\right)\left(h - d_{na-s} - c_f\right)\alpha_3 \end{aligned} \tag{32}$$

Replacing equation (20) in equation (32) and simplifying it gives

$$\alpha_2 d_{na-s}^2 = (h - d_{na-s} - c_r)\alpha_1 + \left(h - d_{na-s} - c_f\right)\alpha_3 \tag{33}$$

Solving equation (33) for $d_{na\text{-}s}$ gives

$$d_{na-s} = \sqrt{\frac{(\alpha_1 + \alpha_3)^2}{4\alpha_2{}^2} - \frac{c_r\alpha_1 - h\alpha_1 + c_f\alpha_3 - h\alpha_3}{\alpha_2}} - \frac{\alpha_1 + \alpha_3}{2\alpha_2} \tag{34}$$

Rotation of strengthened beam section

Since a triangular-shaped concrete stress was assumed, the lever arms for the steel and NSM reinforcements in the strengthened section can be written as

$$Z_{rs} = h - \frac{d_{na-s}}{3} - c_r \tag{35}$$

$$Z_{fs} = h - \frac{d_{na-f}}{3} - c_f \tag{36}$$

where Z_{rs} and Z_{fs} are the lever arm for the steel and NSM reinforcement in the strengthened beam section, respectively. The equation for moment in the strengthened beam section is

$$M_a = P_r n_r Z_{rs} + P_f n_f Z_{fs} \tag{37}$$

From equation (17), the following relationship can be obtained

$$\delta_f = \frac{\delta_{rs}}{h - d_{na} - c_r}\left(h - d_{na} - c_f\right) \tag{38}$$

where δ_f and δ_{rs} are the slips of NSM and steel reinforcement in the strengthened section, respectively. Replacing equations (13), (30) and (38) into equation (37) and solving for δ_{rs} leads to

$$\delta_{rs} = \frac{M_a}{\alpha_1 Z_{rs} + \left(\frac{h - d_{na} - c_f}{h - d_{na} - c_r}\right)\alpha_3 Z_{fs}} \tag{39}$$

From equation (17), the rotation of the strengthened section can be determined as

$$\theta_s = \tan^{-1}\frac{\delta_{rs}}{h - d_{na} - c_r} \tag{40}$$

CCS prediction

The fracture strength of concrete can be determined using any appropriate model. Here, the CEB-FIP model (CEB-FIP, 1993) will be used

$$G_{max} = G_{fo}\left(\frac{S_a}{10}\right)^{0.7} \tag{41}$$

where S_a is maximum aggregate size used in the concrete in millimetres and G_{fo} is the base value for concrete fracture strength and can be taken as 0.037 for aggregate of size 20 mm. The fracture energy of the NSM-strengthened beam due to moment M_a can be determined as

$$G_a = \frac{W_a}{b_f \Delta_L} \tag{42}$$

where Δ_L is the propagation of CCS debonding crack, b_f is the total width of the tension stiffening prism for NSM reinforcements, which as shown in Figure 1(b) can be taken as the width of the beam (b) if two or more NSM reinforcement is used, or half the width of beam if only one NSM reinforcement is used (Shukri et al., 2015) and

$$W_a = \frac{M_a}{(\chi_s - \chi_u)} \tag{43}$$

$$\chi_s = \frac{\theta_s}{L_{def}} \tag{44}$$

$$\chi_u = \frac{\theta_u}{L_{def}} \tag{45}$$

If $G_a > G_{max}$, the beam is predicted to fail by CCS. Assuming this occurs, to redesign the NSM-strengthened beam is only a matter of changing the properties and configuration of the NSM strengthening, such as diameter of the NSM reinforcement (which results in a smaller A_f) and number of NSM reinforcement (n_f). The design procedure is then repeated starting from section 'Depth of neutral axis for strengthened beam section'.

With regard to the value of Δ_L, as the GEBA is concerned with the start of the fracture process, the value Δ_L used is usually a very small value. Previous researchers had used Δ_L = 1 mm in their research (Achintha and Burgoyne, 2008; Shukri et al., 2018; Shukri and Jumaat, 2016). It was also noted that values of Δ_L <1 mm can cause numerical convergence problem (Achintha and Burgoyne, 2008). In this article, Δ_L = 1 mm will be used based on a sensitivity analysis of Δ_L that will be presented in section 'Sensitivity analysis for Δ_L'

Existing slip due to dead load

The dead load on RC beams prior to strengthening can affect the serviceability condition of the beam. Assuming that the moment due to existing permanent action (dead load), M_p, can be determined by the design engineer, equations derived for the unstrengthened beam section can be used to determine the slip of steel reinforcement due to permanent action

$$\delta_p = \frac{M_p}{\alpha_1 Z_{ru}} \tag{46}$$

The lever arm should remain the same, as the equation used to obtain it and to obtain the depth of neutral axis is independent of applied load. Note that the equation above assumes a triangular shape for concrete stress. The existing crack width prior to strengthening would be equal to $2\delta_p$.

Design flexural strength of NSM-strengthened beam

The design flexural strength of NSM-strengthened beam will be limited by the concrete crushing. For simplicity, several assumptions are used:

1. A rectangular concrete stress block is assumed.
2. The concrete strain will be limited to 0.0035 to adhere to Eurocode 2 requirement.
3. The strain hardening of the steel reinforcements will be ignored.
4. Compression bars will be ignored.

The assumptions used are common in design practice. Since the concrete strain will be limited to 0.0035, the following relationship is obtained

$$\frac{\delta_T}{L_{def}} = 0.0035 \tag{47}$$

The equilibrium equation at ultimate limit state is

$$P_c = P_y n_r + P_f n_f \tag{48}$$

where P_y is the load at which the steel reinforcement yields. From equation (17)

$$\delta_{fd} = \frac{\delta_T}{d_{na-d}}\left(h - d_{na-d} - c_f\right) \tag{49}$$

where $d_{na\text{-}d}$ is the depth of neutral axis for the design strength of the NSM-strengthened beam and δ_{fd} is the slip of the NSM reinforcement at ultimate limit state. Inserting equation (47) into equation (49) yields

$$\delta_{fd} = \frac{0.0035L_{def}}{d_{na-d}}\left(h - d_{na-d} - c_f\right) \tag{50}$$

Replacing equations (30) and (50) into equation (48) and expanding yields

$$(\alpha_c f_c)(\beta_c b d_{na-d}) = \sigma_r E_r n_r + \left(\frac{\delta_T}{d_{na-d}}\right)\left(h - d_{na-d} - c_f\right)\alpha_3 \tag{51}$$

where concrete stress is assumed to be equal to f_c at concrete strain of 0.0035, while α_c and β_c are ratio of equivalent concrete stress and equivalent concrete stress block height, respectively. From Eurocode 2, α_c = 0.85 and β_c = 0.8 for $f_c \leqslant 50$ MPa. Equation (51) can be simplified into

$$\alpha_4 d_{na-d}^2 = \alpha_5 d_{na-d} + \left(h - d_{na-d} - c_f\right)\alpha_6 \tag{52}$$

where

$$\alpha_4 = f_c b \tag{53}$$

$$\alpha_5 = \sigma_r E_r n_r \tag{54}$$

$$\alpha_6 = 0.0035 L_{def} \alpha_3 \tag{55}$$

Solving equation (52) for $d_{na\text{-}d}$

$$d_{na-d} = \sqrt{\frac{(\alpha_6 - \alpha_5)^2}{4{\alpha_4}^2} - \frac{c_f \alpha_6 - h\alpha_6}{\alpha_4}} - \frac{\alpha_6 - \alpha_5}{2\alpha_4} \tag{56}$$

With $d_{na\text{-}d}$ known, the slip of the NSM FRP bar, δ_f, can be determined using equation (49). The design flexural moment of the NSM-strengthened beam can be determined as

$$M_d = \sigma_r E_r n_r Z_{rd} + K_f \delta_{fd} Z_{fd} \tag{57}$$

where Z_{rd} and Z_{fd} are the lever arm for steel and NSM reinforcements at ultimate limit state, respectively, and are determined as

$$Z_{rd} = h - \frac{\beta_c d_{na-d}}{2} - c_r \tag{58}$$

$$Z_{fd} = h - \frac{\beta_c d_{na-d}}{2} - c_f \tag{59}$$

It is also possible to determine the crack width of the beam at ultimate limit state. From equation (17)

$$\delta_{rd} = \frac{\delta_T}{d_{na-d}}(h - d_{na-d} - c_r) \tag{60}$$

Inserting equation (47) into equation (60) yields

$$\delta_{fd} = \frac{0.0035 L_{def}}{d_{na-d}}\left(h - d_{na-d} - c_f\right) \tag{61}$$

where δ_{rd} is the slip of steel reinforcement due to applied load. The crack width, Δ_r, of the beam is then determined as twice the slip due to permanent action and applied load

$$\Delta_r = 2\left(\delta_p + \delta_{rd}\right) \tag{62}$$

Validation

The proposed design procedure was validated using published experimental results (Al-Mahmoud et al., 2010; Barros et al., 2007; Ceroni, 2010; Sharaky et al., 2015; Shukri et al., 2015, 2016a; Teng et al., 2006) that failed by either CCS or flexure. In the validation process, the experimental and predicted failure mode will first be compared by determining the available fracture energy (G_a) and the fracture strength (G_{max}). Comparisons between predicted and experimental moment of resistance at failure will also be given for beams that failed by flexure.

The geometric and material properties of the beam that are necessary to apply the design procedure are given in Tables 2 and 3. The beams were strengthened using NSM CFRP bars (Al-Mahmoud et al., 2010; Ceroni, 2010; Sharaky et al., 2015; Shukri et al., 2015), NSM CFRP strips (Barros et al., 2007; Teng et al., 2006) or with side-NSM CFRP bars (Shukri et al., 2016a). As the use of SNSM method only changes the

Table 2. Geometric and loading properties of beams.

Reference	Beam	h (mm)	b (mm)	n_r	c_r (mm)	n_f	c_f (mm)	L_a (mm)	M_a (kNm)
Shukri et al. (2015)	A2	250	125	2	41	1	12	77	5.13
Shukri et al. (2015)	A1	250	125	2	41	1	12	127	8.31
Ceroni (2010)	A10	180	100	2	30	2	7.5	215	5.45
Sharaky et al. (2015)	F2C1	280	160	2	44	2	8	230	13.48
Al-Mahmoud et al. (2010)	S-C (FPT) (270)	280	150	2	42	2	6	80	5.34
Al-Mahmoud et al. (2010)	S-C (FPT) (210)	280	150	2	42	2	6	380	20.82
Teng et al. (2006)	B2900	300	150	2	44	1	11	80	3.99
Teng et al. (2006)	B1800	300	150	2	44	1	11	622	28.52
Teng et al. (2006)	B1200	300	150	2	44	1	11	922	29.09
Teng et al. (2006)	B500	300	150	2	44	1	11	1272	30.40
Barros et al. (2007)	NSM S1	170	120	2	38.5	1	7.5	80	3.16
Barros et al. (2007)	NSM S2	170	120	2	39.5	2	7.5	80	3.71
Shukri et al. (2016a)	SNC8	250	125	2	39	2	39	50	3.55
Shukri et al. (2016a)	SNC10	250	125	2	39	2	39	50	4.42
Shukri et al. (2016a)	SNC12	250	125	2	39	2	39	50	4.33
Shukri et al. (2016a)	PSNC8	250	125	2	39	2	39	50	3.54
Shukri et al. (2016a)	PSNC10	250	125	2	39	2	39	50	4.28
Shukri et al. (2016a)	PSNC12	250	125	2	39	2	39	50	4.24

h: beam height; b: beam width; n_r: number of tensile reinforcement bars; n_f: number of FRP bars/strips; c_r: distance from beam soffit to centre of tensile reinforcement bars; c_f: distance from beam soffit to centre of FRP bars/strips; L_a: distance from end of beam to the location of curtailment of FRP bars/strips.

Table 3. Material properties.

Reference	Beam	f_c (N/mm^2)	σ_y (N/mm^2)	E_r (kN/mm^2)	E_f (kN/mm^2)
Shukri et al. (2015)	A2	35.63	520	200	165
Shukri et al. (2015)	A1	35.63	520	200	165
Ceroni (2010)	A10	26.88	441	200	109
Sharaky et al. (2015)	F2C1	30.5	455	200	158
Al-Mahmoud et al. (2010)	S-C (FPT) (270)	36.1	600	200	146
Al-Mahmoud et al. (2010)	S-C (FPT) (210)	36.1	600	200	146
Teng et al. (2006)	B2900	44	532	200	131
Teng et al. (2006)	B1800	44	532	200	131
Teng et al. (2006)	B1200	44	532	200	131
Teng et al. (2006)	B500	44	532	200	131
Barros et al. (2007)	NSM S1	44.2	788	200	159
Barros et al. (2007)	NSM S2	44.2	788	200	159
Shukri et al. (2016a)	SNC8	40 (cube)	520	200	124
Shukri et al. (2016a)	SNC10	40 (cube)	520	200	124
Shukri et al. (2016a)	SNC12	40 (cube)	520	200	124
Shukri et al. (2016a)	PSNC8	40 (cube)	520	200	124
Shukri et al. (2016a)	PSNC10	40 (cube)	520	200	124
Shukri et al. (2016a)	PSNC12	40 (cube)	520	200	124

f_c: concrete strength; σ_y: yield strength of steel; E_r: elastic modulus of steel; E_f: elastic modulus of FRP bar/strip.

Table 4. Predicted and experimental result comparison.

Reference	Beam	G_a/G_{max}	FM_e	FM_d	M_e (kNm)	M_d (kNM)	M_d/M_e
Shukri et al. (2015)	A2	0.82	CCS	F	50.0	49.3	0.99
Shukri et al. (2015)	A1	2.15	CCS	CCS	49.1	–	–
Ceroni (2010)	A10	2.39	CCS	CCS	22.3	–	–
Sharaky et al. (2015)	F2C1	1.70	CCS	CCS	515.7	–	–
Al-Mahmoud et al. (2010)	S-C (FPT) (270)	0.17	F	F	53.4	55.4	1.04
Al-Mahmoud et al. (2010)	S-C (FPT) (210)	2.52	CCS	CCS	32.9	–	–
Teng et al. (2006)	B2900	0.13	F	F	59.9	57.3	0.96
Teng et al. (2006)	B1800	6.61	CCS	CCS	55.0	–	n/a
Teng et al. (2006)	B1200	6.88	CCS	CCS	37.9	–	n/a
Teng et al. (2006)	B500	7.51	CCS	CCS	28.7	–	n/a
Barros et al. (2007)	NSM S1	1.69	CCS	CCS	11.8	–	n/a
Barros et al. (2007)	NSM S2	1.47	CCS	CCS	13.9	–	n/a
Shukri et al. (2016a)	SNC8	0.60	F	F	46.2	37.7	0.82
Shukri et al. (2016a)	SNC10	1.08	F	CCS	57.5	–	n/a
Shukri et al. (2016a)	SNC12	1.14	CCS	CCS	56.2	–	–
Shukri et al. (2016a)	PSNC8	0.59	F	F	46.0	37.7	0.82
Shukri et al. (2016a)	PSNC10	1.01	F	CCS	55.6	–	n/a
Shukri et al. (2016a)	PSNC12	1.09	CCS	CCS	55.1	–	n/a

G_a: predicted fracture energy; G_{max}: fracture strength; FM_e: experimental failure mode; FM_d: predicted failure mode; M_e: experimental maximum moment at failure; M_d: predicted maximum moment at failure; CCS: concrete cover separation failure mode; F: flexural failure mode α; n/a: not applicable.

lever arm of the NSM reinforcement, the proposed design procedure can be used without any changes. The maximum size of aggregates in concrete, S_a, was assumed to be 20 mm if not specified in the original research paper. Referring to Table 2, the moment M_a is the moment at the length L_a corresponding to the reported experimental failure load, P_{max}, of each beam.

The result of the validation is given in Table 4, where the calculated G_{max}, G_a, failure mode, experimental maximum moment (M_e) and maximum moment obtained using the design procedure (M_d) are presented. It should be noted that M_d is only given when it is predicted that the beam fails by flexure. From Table 4, it can be seen that the proposed design procedure was able to correctly predict the CCS failure mode of the beams apart from beam A2, SNC10 and PSNC10. In the case of beam A2, the predicted failure mode is flexure, whereas the actual failure mode is

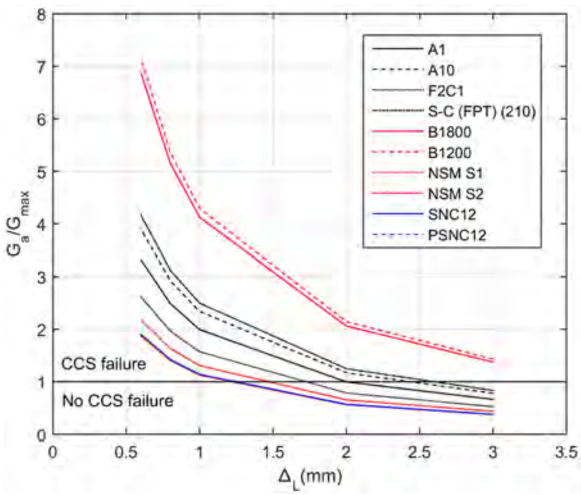

Figure 11. Sensitivity analysis for Δ_L.

CCS. The ratio of M_d/M_e, however, is very close, at 0.99, which shows that while the beam was reported to fail by CCS, the loss of strength due to the premature debonding is negligible. For the case of beams SNC10 and PSNC10, the predicted failure mode was CCS, while the actual failure mode was flexure. The ratio of G_a/G_{max} for beam SNC10 shows that the fracture strength was only very slightly exceeded, hence the incorrect predicted failure mode can be due to difference in the calculated and actual fracture energy, G_{max}, which is not uncommon due to the variable nature of concrete.

Sensitivity analysis for Δ_L

A sensitivity analysis was conducted using the properties of nearly all the beams in the used in the validation process that failed by CCS with the result as shown in Figure 11. As all the beams had experimentally failed by CCS, the G_a/G_{max} should be more than 1. Where G_a/G_{max} is less than 1, it shows that the value of Δ_L used failed to provide a correct prediction of CCS failure for the beam.

It can be seen from Figure 11 that $\Delta_L = 1$ mm was able to give an accurate assessment of CCS failure for all beams. Values of $\Delta_L < 1$ mm were also able to correctly predict the CCS failure; however, it should be noted that when $\Delta_L < 1$ mm, the resulting G_a can be considerably higher. This can cause a very conservative design, as the design engineer may have to greatly reduce the amount of NSM reinforcement provided in order to ensure that $G_a < G_{max}$ and prevent CCS failure. Hence, the value of $\Delta_L = 1$ mm is suggested as it gives a reasonable balance between accuracy and conservativeness.

Conclusion

In this research article, a mechanics-based design procedure was proposed. The proposed design procedure uses the M/θ approach and the GEBA to predict the behaviour of NSM-strengthened RC beams and the CCS failure mode. Several conclusions can be made based on this study:

- Published experimental results of beams strengthened with NSM CFRP bars, NSM CFRP strips or SNSM CFRP bars were used to validate the proposed design procedure and good correlation was found between the experimental and predicted results.
- The proposed design approach should be more versatile compared to other existing design approach as it is less reliant on empirical formulations. Hence, it can easily be applicable to most types of NSM reinforcement material and configurations. The design approach can also accommodate any new innovations in terms of the NSM strengthening material or configurations. The coefficient of bond c_2 for those new NSM material or configuration can be determined using a similar approach described in this article.

Declaration of Conflicting Interests

The author(s) declared no potential conflicts of interest with respect to the research, authorship and/or publication of this article.

Funding

The author(s) disclosed receipt of the following financial support for the research, authorship and/or publication of this article: Financial support from the Fundamental Research Grant Scheme (FRGS), Ministry of Education Malaysia (project number FP004-2014B) is gratefully acknowledged.

ORCID iD

Ahmad Azim Shukri https://orcid.org/0000-0001-5471-5317

References

Achintha M and Burgoyne CJ (2008) Fracture mechanics of plate debonding: experimental. *Journal of Composites for Construction* 12(4): 396–404.

Achintha M and Burgoyne C (2013) Fracture energy of the concrete-FRP interface in strengthened beams. *Engineering Fracture Mechanics* 110: 38–51.

Achintha M and Burgoyne CJ (2011) Fracture mechanics of plate debonding: validation against experiment. *Construction and Building Materials* 25(6): 2961–2971.

Al-Mahmoud F, Castel A, François R, et al. (2010) RC beams strengthened with NSM CFRP rods and modeling of peeling-off failure. *Composite Structures* 92(8): 1920–1930.

Badawi M and Soudki K (2009) Fatigue behavior of RC beams strengthened with NSM CFRP rods. *Journal of Composites for Construction* 13(5): 415–421.

Barros JAO, Dias SJE and Lima JLT (2007) Efficacy of CFRP-based techniques for the flexural and shear strengthening of concrete beams. *Cement and Concrete Composites* 29(3): 203–217.

Bilotta A, Ceroni F, Di Ludovico M, et al. (2011) Bond efficiency of EBR and NSM FRP systems for strengthening concrete members. *Journal of Composites for Construction* 15(5): 757–772.

Branson DE (1968) Design procedures for computing deflections. *ACI Journal* 65(9): 730–735.

Capozucca R and Bossoletti S (2014) Static and free vibration analysis of RC beams with NSM CFRP rectangular rods. *Composites Part B: Engineering* 67: 95–110.

CEB-FIP (1993) *CEB-FIP Model Code 1990*. London: Thomas Telford Ltd.

Ceroni F (2010) Experimental performances of RC beams strengthened with FRP materials. *Construction and Building Materials* 24(9): 1547–1559.

Choi HT, West JS and Soudki KA (2011) Partially bonded near-surface-mounted CFRP bars for strengthened concrete T-beams. *Construction and Building Materials* 25(5): 2441–2449.

De Lorenzis L (2004) Anchorage length of near-surface mounted fiber-reinforced polymer rods for concrete strengthening – analytical modeling. *ACI Structural Journal* 101(3): 375–386.

De Lorenzis L and Nanni A (2003) Proposed design procedure of NSM FRP reinforcement for strengthening of RC beams. In: *Proceedings of the 6th international symposium on FRP reinforcement for concrete structures, Singapore*, pp. 1455–1451. Available at: https://pdfs.semanticscholar.org/f71d/27f4c87dd157bd99b5250055999b797880b8.pdf

Galati D and De Lorenzis L (2009) Effect of construction details on the bond performance of NSM FRP bars in concrete. *Advances in Structural Engineering* 12(5): 683–700.

Guan GX and Burgoyne CJ (2014) Comparison of moment-curvature models for fiber-reinforced polymer plate-end debonding studies using global energy balance approach. *ACI Structural Journal* 111(1): 27–36.

Gupta AK and Maestrini SR (1990) Tension stiffness model for reinforced concrete bars. *Journal of Structural Engineering* 116(3): 769–790.

Haskett M, Oehlers DJ and Mohamed Ali MS (2008) Local and global bond characteristics of steel reinforcing bars. *Engineering Structures* 30(2): 376–383.

Hosen MA, Jumaat MZ and Islam ABMS (2015) Side Near Surface Mounted (SNSM) technique for flexural enhancement of RC beams. *Materials & Design* 83: 587–597.

Knight D, Visintin P, Oehlers DJ, et al. (2014) Simulation of RC beams with mechanically fastened FRP strips. *Composite Structures* 114: 99–106.

Mo KH, Visintin P, Alengaram UJ, et al. (2016) Prediction of the structural behaviour of oil palm shell lightweight concrete beams. *Construction and Building Materials* 102: 722–732.

Muhamad R, Mohamed Ali MS, Oehlers D, et al. (2011) Load-slip relationship of tension reinforcement in reinforced concrete members. *Engineering Structures* 33(4): 1098–1106.

Muhamad R, Mohamed Ali MS, Oehlers DJ, et al. (2012) The tension stiffening mechanism in reinforced concrete prisms. *Advances in Structural Engineering* 15(12): 2053–2069.

Oehlers D, Visintin P, Zhang T, et al. (2012) Flexural rigidity of reinforced concrete members using a deformation based analysis. *Concrete in Australia* 38(4): 50–56.

Rezazadeh M, Barros JAO and Ramezansefat H (2016) End concrete cover separation in RC structures strengthened in flexure with NSM FRP: Analytical design approach. *Engineering Structures* 128: 415–427.

Seo S, Sung M and Feo L (2016) Flexural analysis of RC beam strengthened by partially de-bonded NSM FRP strip. *Composites Part B* 101: 21–30.

Sharaky IA, Reda RM, Ghanem M, et al. (2017) Experimental and numerical study of RC beams strengthened with bottom and side NSM GFRP bars having different end conditions. *Construction and Building Materials* 149: 882–903.

Sharaky IA, Torres L and Sallam HEM (2015) Experimental and analytical investigation into the flexural performance of RC beams with partially and fully bonded NSM FRP bars/strips. *Composite Structures* 122: 113–126.

Shukri AA and Jumaat MZ (2016) Simulating concrete cover separation in RC beams strengthened with near-surface mounted reinforcements. *Construction and Building Materials* 122: 1–11.

Shukri AA, Darain KMU and Jumaat MZ (2015) The tension-stiffening contribution of NSM CFRP to the behavior of strengthened RC beams. *Materials* 8(7): 4131–4146.

Shukri AA, Hosen MA, Muhamad R, et al. (2016a) Behaviour of precracked RC beams strengthened using the side-NSM technique. *Construction and Building Materials* 123: 617–626.

Shukri AA, Shamsudin MF, Ibrahim Z, et al. (2018) Parametric study for concrete cover separation failure of retrofitted SNSM strengthened RC beams. *Mechanics of Advanced Materials and Structures*. Epub ahead of print 11 June. DOI: 10.1080/15376494.2018.1482034

Shukri AA, Visintin P, Oehlers DJ, et al. (2016b) Mechanics model for simulating RC hinges under reversed cyclic loading. *Materials* 9(4): E305.

Sturm AB, Visintin P, Oehlers DJ, et al. (2018) Time-dependent tension-stiffening mechanics of fiber-reinforced and ultra-high-performance fiber-reinforced concrete. *Journal of Structural Engineering* 144(8): 4018122.

Teng JG, De Lorenzis L and Wang B (2006) Debonding failures of RC beams strengthened with near surface mounted CFRP strips. *Journal of Composites for Construction* 10: 92–106.

Teng JG, Zhang S and Chen JF (2016) Strength model for end cover separation failure in RC beams strengthened with near-surface mounted (NSM) FRP strips. *Engineering Structures* 110: 222–232.
Visintin P and Oehlers DJ (2016) Mechanics-based closed-form solutions for moment redistribution in RC beams. *Structural Concrete* 17(3): 377–389.
Visintin P and Oehlers DJ (2017) Fundamental mechanics that govern the flexural behaviour of reinforced concrete beams with fibre-reinforced concrete. *Advances in Structural Engineering* 21(7): 1088–1102.
Visintin P, Oehlers DJ, Muhamad R, et al. (2013) Partial-interaction short term serviceability deflection of RC beams. *Engineering Structures* 56: 993–1006.
Wu G, Dong Z-Q, Wu Z-S, et al. (2014) Performance and parametric analysis of flexural strengthening for RC beams with NSM-CFRP bars. *Journal of Composites for Construction* 18(4): 04013051.
Zhang SS and Teng JG (2014) Finite element analysis of end cover separation in RC beams strengthened in flexure with FRP. *Engineering Structures* 75: 550–560.
Zhang SS, Teng JG and Yu T (2013) Bond–slip model for CFRP strips near-surface mounted to concrete. *Engineering Structures* 56: 945–953.
Zhang T, Visintin P and Oehlers DJ (2017) Partial-interaction tension-stiffening properties for numerical simulations. *Advances in Structural Engineering* 20(5): 812–821.

Appendix 1

Notation

A_{cf}	area of concrete in the tension stiffening prism for NSM reinforcement
A_{cr}	area of concrete in the tension stiffening prism for steel reinforcement
A_r	area of a single steel reinforcement
b	width of RC beam
c_2	coefficient of bond for steel reinforcement
$c_{2b1.5}$	coefficient of bond for NSM CFRP bar with ratio of groove to bar diameter of 2
c_{2b2}	coefficient of bond for NSM CFRP bar with ratio of groove to bar diameter of 1.5
c_{2s}	coefficient of bond for NSM CFRP strip
c_f	distance from beam soffit to the centre of NSM reinforcement
c_r	distance from beam soffit to the centre of steel reinforcement
d_{na}	depth of neutral axis from top of RC beam
$d_{na\text{-}d}$	depth of neutral axis from top of RC beam for NSM strengthened beam at ultimate limit state
$d_{na\text{-}s}$	depth of neutral axis from top of RC beam for NSM strengthened beam section
$d_{na\text{-}u}$	depth of neutral axis from top of RC beam for unstrengthened beam section
E_c	modulus of elasticity for concrete
E_f	modulus of elasticity for NSM reinforcement
E_r	modulus of elasticity for steel reinforcement
f_c	compressive strength of concrete
f_{ct}	tensile strength of concrete
G_a	available fracture energy for propagation of concrete cover separation debonding crack
G_{fo}	fracture strength of concrete
G_{max}	fracture strength of concrete
h	height of RC beam
K	stiffness of load–slip relationship
K_f	stiffness of load–slip relationship for NSM reinforcement
K_r	stiffness of load–slip relationship for steel reinforcement
L_a	distance from beam support to the end of the initial bonded length
L_c	distance from beam support to the start of the initial bonded length
L_d	initial debonded length
L_{def}	length of deformation
L_{per}	perimeter of steel reinforcement
M	moment applied on RC beam
M_a	moment at L_a for unstrengthened beam section
M_d	moment of NSM strengthened beam at ultimate limit state
M_p	moment due to permanent action
n_f	number of NSM reinforcement
n_r	number of steel reinforcement
P	force acting on beam reinforcement
P_c	force acting on concrete
P_f	force acting on steel reinforcement
P_f	force acting on NSM reinforcement
P_r	force acting on steel reinforcement
P_y	force acting on steel reinforcement at steel yield
S_a	maximum size of aggregate used in concrete
S_{cr}	primary crack spacing
W_a	bending strain energy of beam at the location of debonding crack
Z_{fd}	lever arm for the NSM reinforcement at ultimate limit state
Z_{fs}	lever arm for the NSM reinforcement at the strengthened section of the beam
Z_{rd}	lever arm for the steel reinforcement at ultimate limit state
Z_{rs}	lever arm for the steel reinforcement at the strengthened section of the beam
Z_{ru}	lever arm for the steel reinforcement at the unstrengthened section of the beam

α_c	ratio of equivalent concrete stress
α	parameter controlling shape of CEB-FIP bond stress-slip model
β_c	ratio of equivalent concrete stress block height
δ	slip of beam reinforcement
δ_1	slip corresponding to bond strength for CEB-FIP bond stress–slip relationship
δ_f	slip of NSM reinforcement
δ_{fd}	slip of NSM reinforcement at ultimate limit state
δ_p	slip of steel reinforcement due to permanent action
δ_r	slip of steel reinforcement
δ_{rd}	slip of steel reinforcement at ultimate limit state
δ_{rs}	slip of reinforcement in the strengthened section of the beam
δ_{ru}	slip of reinforcement in the unstrengthened section of the beam
δ_T	deformation of concrete at topmost section of beam due to compression for unstrengthened beam section
Δ_L	progression of concrete cover separation debonding crack
Δ_r	crack width due to permanent action and applied load
θ_d	rotation of NSM strengthened beam section at ultimate limit state
θ_s	rotation of NSM strengthened beam section
θ_u	rotation of unstrengthened beam section
τ_{max}	bond strength of steel reinforcement
χ	curvature of RC beam
χ_s	curvature for NSM strengthened beam section
χ_u	curvature for unstrengthened beam section

CHAPTER 7 - DISCUSSION

The previous chapters had presented and validated the moment-rotation (M/θ) approach for simulating NSM strengthened RC beams. In this chapter, the research will be complemented by a study on the accuracy of the proposed M/θ approach compared other existing simulation methods by other researchers in section 7.1. The purpose of the comparison study is to determine the weaknesses in the proposed M/θ approach compared to other simulation methods.

The identified weaknesses for the M/θ approach will be detailed in section 7.2 of this chapter. Furthermore, a list of errors in the research papers which were not detected prior to publication will be listed in section 7.2. Finally, section 7.3 will present a concluding remark which will summarize the cumulative effect of the research papers, the significance of the findings and the knowledge claim in the thesis.

7.1 Comparison with other simulation methods

A comparison of the performance of the moment-rotation (M/θ) approach simulation was done by comparing it against the simulations performed by other researchers. A total of two types of simulation methods will be used for the comparison study of NSM strengthened beam simulation, which are from the works of Almusallam, Elsanadedy, Al-Salloum, & Alsayed (2013) and Sharaky et al. (2015), where the former used finite element method and the latter used analytical method. Additionally, the finite element method by Chen et al. (2010) will be used to perform a comparison study of EB strengthened beam in order to check the accuracy of the method to simulate IC debonding as presented in paper 5 of this thesis. A brief summary of the methods used by the researchers will first be given. This will be followed by a comparison of the load-deflection relationship from the M/θ approach, from the simulation method proposed by other researchers and from the experimental result.

7.1.1 Comparison with FEM (Almusallam et al. (2013)) for NSM strengthened beams

In this section, simulation performed using the M/θ approach as presented in paper 1 of this thesis will be compared with the simulation by Almusallam et al. (2013), where finite element modelling (FEM) was used to simulate the behaviour of NSM strengthened beams. The 8-node reduced integration solid hexahedron elements were used to model both the concrete and the epoxy adhesive. The authors stated that the biggest advantage of using solid elements with one-point integration is its substantial savings in computing time, although its disadvantage is the need to control the zero energy modes known as hourglass modes. These modes have periods that are much shorter than the periods of the structural response, and they are often observed to be oscillatory. The authors stated that they used three-dimensional algorithms in the LS-DYNA software in order to control the hourglass modes.

The longitudinal steel and GFRP bars and the transverse ties were modeled using 2-node Hughes–Liu beam elements (Hughes & Liu, 1981) due to its compatibility with the solid elements, as the element is based on a degenerated solid element formulation. Perfect bond was assumed between the tensile steel reinforcements and the adjacent concrete, between the NSM reinforcements and the epoxy adhesive and between the epoxy adhesive and concrete.

The material model type 159, MAT_CSCM_CONCRETE was employed to model the concrete volume. It is a smooth or continuous cap model available in LS-DYNA for solid elements, with a smooth intersection between the shear yield surface and the hardening cap. The material model type 24, MAT_PIECEWISE_ LINEAR_PLASTICITY was utilized to model steel bars, GFRP bars and epoxy adhesive as it is suited to model elasto-plastic materials with an arbitrary stress versus strain curve and an arbitrary strain rate dependency. The authors used the erosion option to include failure to the material models. It is not a material or physics-based property although it can imitate concrete spalling phenomena and produce graphical plots to represent the actual events.

Three beams were used for the purpose of this comparison, where two of the beams were strengthened with NSM steel bars and the other beam was strengthened with NSM GFRP bar. The geometry and material properties of the beam are given in Table 7.1 and Table 7.2 respectively; these are also available in the research paper in Chapter 3, although it is repeated here for ease of reference.

Table 7.1 Beam geometric properties.

Ref	Beam designation	b (mm)	d (mm)	L (mm)	L_a (mm)	M_{NSM}	N_{NSM}	FM
Almusallam et al. (2013)	RW1S	150	200	2000	0	Steel bar	1	CC
Almusallam et al. (2013)	RW1Ø14S	150	200	2000	0	Steel bar	1	CC
Almusallam et al. (2013)	RW1F	150	200	2000	0	GFRP bar	1	F

Note: b=width of beam; d=depth of beam; L=length of beam; L_a=distance of NSM to the nearest support; M_{NSM}=material for NSM reinforcement; N_{NSM}=number of NSM reinforcement bar/strip; FM=failure mode; CC= concrete crushing; F=fracture of NSM reinforcement.

Table 7.2 Beam material properties.

Ref	Beam designation	f_c (N/mm^2)	E_y (N/mm^2)	σ_y (N/mm^2)	E_f (N/mm^2)	σ_f (N/mm^2)
Almusallam et al. (2013)	RW1S	36.6	200000	408	200000	408
Almusallam et al. (2013)	RW1Ø14S	36.6	200000	408	200000	550
Almusallam et al. (2013)	RW1F	36.6	200000	408	40000	743

Note: f_c=concrete compressive strength (cylinder); E_y=steel elastic modulus; σ_y=steel yield strength; E_f=FRP modulus; σ_f=FRP tensile strength.

The comparison of load-deflection relationships obtained from the M/θ simulation, Almusallam et al (2013) and experimental result are shown in Figure 7.1, while a summary of the results are given in Table 7.3. Both the M/θ approach and the FEM by Almusallam et al (2013) were able to give load-deflection curves that followed the general shape of the experimental load-deflection curve well. For beam RW1S, it was found that the M/θ approach underpredict the load response slightly, although the yield load was correctly predicted. The FEM simulation was found to predict the load response better, although it slightly overpredicts the yield load. Both methods were able to predict the failure load at high accuracy, with the deviation from the experimental value of 2.7% and 2.1% for the M/θ approach and the FEM respectively. The FEM was able to predict the deflection at failure well with 3.5% deviation from experimental value, while the M/θ approach had a deviation of -22.3%. This was found to be due to the fact that the M/θ approach had predicted the beam would fail by NSM steel reinforcement fracture, whereas the experimental result show that the beam failed by concrete crushing; the FEM was able to correctly predict the concrete crushing failure. This error by the M/θ approach was attributed to the bond stress-slip model used, where since there is no study on the bond behaviour of NSM steel encased in epoxy, the bond stress-slip model for NSM CFRP bar had to be used.

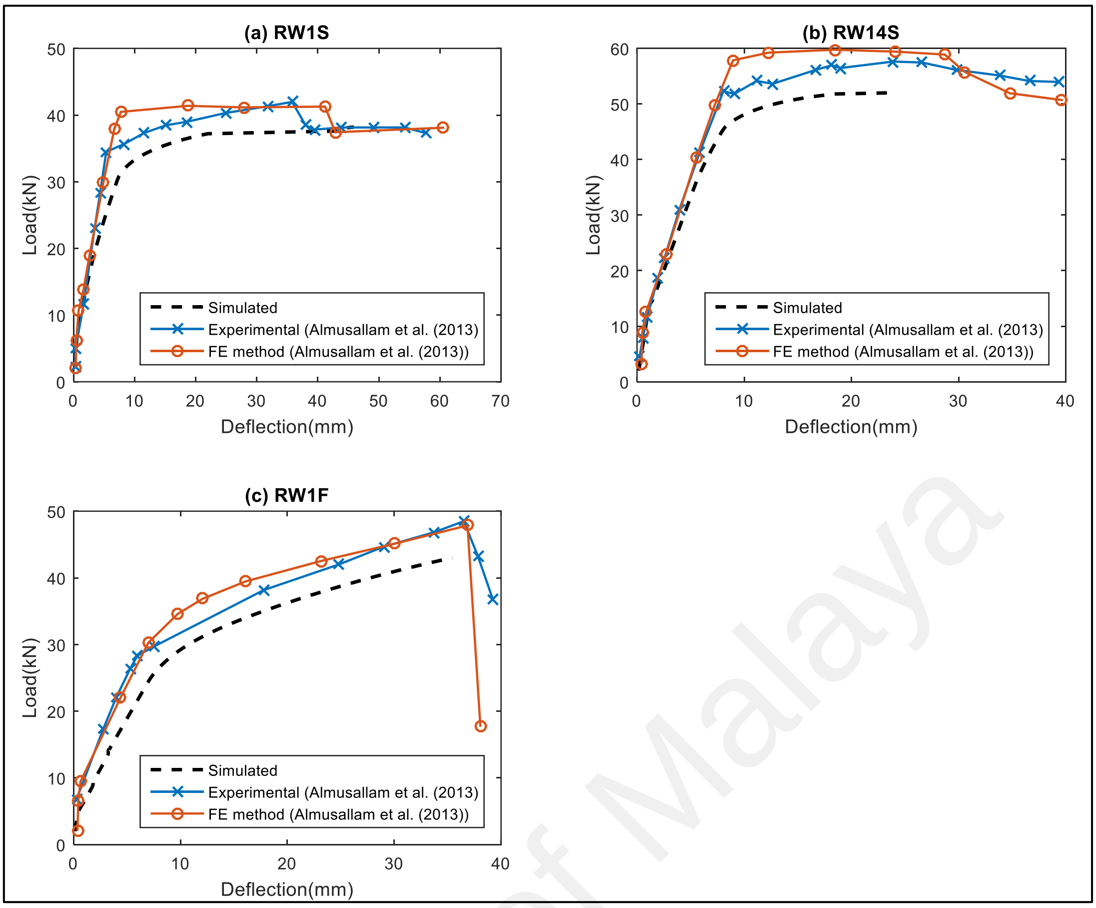

Figure 7.1 Comparison of load-deflection relationship from M/θ simulation, simulation by Almusallam et al. (2013) and experimental result.

Table 7.3 Summary of simulated and experimental load-deflection curves.

Beam	P_e	P_1	ΔP_1 (%)	P_2	ΔP_2 (%)	D_e	D_1	ΔD_1 (%)	D_2	ΔD_2 (%)	FM	SFM1	SFM2
RW1S	37.2	38.2	2.7	38.0	2.1	59.0	45.9	-22.3	61.1	3.5	CC	F	
RW1Ø14S	54.0	52.0	-3.6	50.4	-6.6	39.3	23.6	-39.9	39.9	1.7	CC	F	
RW1F	48.5	42.6	-12.1	47.4	-2.2	36.5	35.9	-1.8	35.9	-1.6	F	F	

Note: P_e=experimental failure load; P_1=simulated failure load using M/θ approach; ΔP_1=percentage difference between simulated failure load using M/θ approach and the experimental failure load; P_2=simulated failure load using FEM; ΔP_2=percentage difference between simulated failure load using FEM and the experimental failure load; D_e= experimental deflection at failure; D_1= simulated deflection at failure using M/θ approach; ΔD_1=percentage difference between simulated deflection at failure using M/θ approach and the experimental failure load; D_2= simulated deflection at failure using FEM; ΔD_2=percentage difference between simulated deflection at failure using FEM and the experimental failure load; FM=failure mode; CCS=concrete cover separation; ID=interfacial debonding; CC= concrete crushing; F=fracture of NSM reinforcement; CS=concrete splitting; SFM1=simulated failure load using M/θ approach; SFM2=simulated failure load using FEM.

The M/θ approach was found to underpredict the load response for beam RW14S as well, although the yield load was correctly simulated and the deviation of the simulated failure load from the experimental failure load was quite small at -3.6%. The deviation for deflection at failure however was much larger, at -39.9%. From Table 7.3, it can be seen that M/θ approach predicted the beam would fail by fracture of NSM steel reinforcement, whereas the concrete crushing failure was the actual failure mode. The incorrect simulation of the NSM steel reinforcement strain is again attributed to the use of the bond stress-slip model for NSM CFRP bar due to the lack of any study in the literature on the bond performance of NSM steel reinforcement encased in epoxy. The FEM was to slightly overpredict the load response of beam RW13S, although the deviation of failure load and deflection at failure are quite small at -6.6% and 1.7% respectively. However, once again the FEM overpredicts the yield load of the beam.

The simulated results from the M/θ approach was found to underpredict the load response of beam RW1F, with the deviation between simulated and experimental failure load at -12.1%. However, the deflection at failure was correctly predicted, with deviation of only -1.8%. This is attributed to using the proper bond stress-slip model for the NSM GFRP bar in beam RW1F which was proposed by Laura De Lorenzis (2004), while the simulated results for the other two beams clearly shows the error that would result from an unsuitable bond stress-slip model. The FEM was found to slightly overpredict the load-response again, although this time the simulated yield load was accurate. The deviation for failure load and deflection at failure was -2.2% and -1.6% respectively.

7.1.2 Comparison with analytical method (Sharaky et al. (2015)) for NSM strengthened beams

In this section, the simulation using M/θ approach as presented in paper 1 of this thesis will be compared with the simulation by Sharaky et al. (2015), where an analytical model was used to simulate NSM strengthened beams. The assumptions used are:

1. There is linear distribution of strain along the depth of the beam.
2. Small deformations.
3. Concrete does not carry tensile stresses after cracking.
4. Shear deformations are not considered.
5. There is perfect bond between the steel reinforcement and adjacent concrete, between NSM reinforcement and epoxy, and between epoxy and adjacent concrete.

The incremental deformation method proposed by Ross, Jerome, Tedesco and Hughes (1999) was used to determine the sectional strains and stresses:

$$C_t = \begin{cases} 0.5\varepsilon_{cf}\dfrac{(h-c)^2}{c}E_{csc}b, & 0 \le f_{ct} < f_r \\ 0, & otherwise \end{cases} \tag{7.1}$$

$$F_s = \begin{cases} \varepsilon_s E_s A_s, & 0 \le \varepsilon_s < \varepsilon_y \\ f_y A_s, & \varepsilon_y \le \varepsilon_s < \varepsilon_{su} \end{cases} \tag{7.2}$$

$$F_f = \begin{cases} \varepsilon_f E_f A_f, & 0 \le \varepsilon_f < \varepsilon_{fu} \\ 0, & \varepsilon_f > \varepsilon_{fu} \end{cases} \tag{7.3}$$

$$F_{sc} = -\varepsilon_{sc} E_s A_{sc} \tag{7.4}$$

$$C_c = \alpha f_c b c \tag{7.5}$$

$$\alpha = \begin{cases} \dfrac{\varepsilon_{cf}}{\varepsilon_0} - \dfrac{\varepsilon_{cf}^2}{3\varepsilon_0^2}, & 0 \le \varepsilon_{cf} < \varepsilon_0 \\ 1 + \dfrac{\varepsilon_{cf}}{\varepsilon_0}\left(1 - \dfrac{\varepsilon_{cf}}{3\varepsilon_0} - \dfrac{\varepsilon_0^2}{3\varepsilon_{cf}^2} - \dfrac{0.15}{0.004 - \varepsilon_0}\left(\dfrac{\varepsilon_{cf}}{2} - \varepsilon_0\right)\right), & \varepsilon_0 \le \varepsilon_{cf} < 0.003 \end{cases} \quad (7.6)$$

$$E_{csc} = E_c\left(1 - \frac{\varepsilon_{cf}}{\varepsilon_0}\right) \quad (7.7)$$

Where C_t is the tensile force in concrete, ε_{cf} is the concrete strain, E_{csc} is the instant concrete modulus, f_{ct} is the concrete tensile stress, f_r is the ultimate concrete tensile stress, F_s is the tensile force in steel reinforcement, ε_s is the steel strain, E_s is the steel modulus of elasticity, ε_y is the steel yield strain, f_y is the steel yield stress, A_s is the area of tensile steel, ε_{su} is the ultimate steel strain, F_f is the tensile force in NSM FRP reinforcement, ε_f is the FRP strain, E_f is FRP modulus of elasticity, A_f is the area of NSM FRP reinforcement, ε_{fu} is the ultimate FRP strain, F_{sc} is the compressive force in steel, ε_{sc} is steel compressive strain, A_{sc} is the area of compression steel, C_c is the compressive force in concrete, b is the beam width, h is the beam depth, α is the mean stress factor used to convert the nonlinear stress-strain relationship of concrete into an equivalent rectangular stress-strain curve, ε0 is concrete strain at its ultimate stress, f_c is the stress in concrete corresponding to concrete strain ε_{cf} determined using the following equation:

$$f_c = \begin{cases} f_c''\left(2\dfrac{\varepsilon_{cf}}{\varepsilon_0} - \dfrac{\varepsilon_{cf}^2}{\varepsilon_0^2}\right), & 0 \le \varepsilon_{cf} < \varepsilon_0 \\ f_c''\left(1 - \dfrac{0.15}{0.004 - \varepsilon_0}(\varepsilon_{cf} - \varepsilon_0)\right), & \varepsilon_0 \le \varepsilon_{cf} < 0.003 \end{cases} \quad (7.8)$$

Where,

$$\varepsilon_0 = 2\frac{f_c}{E_c} \quad (7.9)$$

$$f_c'' = 0.92 f_{cu} \quad (7.10)$$

For the purpose of predicting the peeling loads of concrete cover separation, the method proposed by Oehlers and Moran (1990) and Deric John Oehlers (1992) was used:

$$M_{dbf} = \frac{E_c I_{trcc} f_r}{0.901 E_f t_f} \tag{7.11}$$

Where M_{bdf} is the flexural debonding moment at the end of the plate, I_{trcc} is the cracked moment of inertia of the concrete section transformed to concrete. Another method was also used to predict NSM reinforcement concrete splitting and epoxy splitting failure using the equations presented by Hassan & Rizkalla (2004):

$$f_{FRP1} = \frac{4 L_b \mu f_r}{G_1 d_b} \tag{7.12}$$

$$f_{FRP2} = \frac{4 L_b \mu f_r}{G_2 d_b} \tag{7.13}$$

Where f_{FRP1} is the tensile strength of NSM FRP reinforcement for concrete splitting failure, f_{FRP2} is the tensile strength of NSM FRP reinforcement for epoxy splitting failure, μ is the coefficient for friction and G_1 and G_2 are coefficient functions of the ratio between the adhesive cover to the NSM FRP bar diameter and the ratio of the groove width to the NSM FRP bar diameter.

Three beams were used for the purpose of this comparison, where two of the beams were strengthened with NSM GFRP bars and the other beam was strengthened with NSM CFRP bar. The geometry and material properties of the beam are given in Table 7.4 and Table 7.5 respectively.

Table 7.4 Beam geometric properties.

Ref	Beam designation	b (mm)	d (mm)	L (mm)	L_a (mm)	M_{NSM}	N_{NSM}	FM
Sharaky et al. (2015)	F2C1	160	280	2400	200	CFRP bar	2	CCS
Sharaky et al. (2015)	F1G2	160	280	2400	200	GFRP bar	1	CS
Sharaky et al. (2015)	F2G1	160	280	2400	200	GFRP bar	2	ID

b=width of beam; d=depth of beam; L=length of beam; L_a=distance of NSM to the nearest support; M_{NSM}=material for NSM reinforcement; N_{NSM}=number of NSM reinforcement bar/strip; FM=failure mode; CCS=concrete cover separation; ID=interfacial debonding; CS=concrete splitting.

Table 7.5 Beam material properties.

Ref	Beam designation	f_c (N/mm^2)	E_y (N/mm^2)	σ_y (N/mm^2)	E_f (N/mm^2)	σ_f (N/mm^2)
Sharaky et al. (2015)	F2C1	30.5	200000	540	170000	2350
Sharaky et al. (2015)	F1G2	30.5	200000	540	64000	1350
Sharaky et al. (2015)	F2G1	30.5	200000	540	64000	1350

Note: f_c=concrete compressive strength (cylinder); E_y=steel elastic modulus; σ_y=steel yield strength; E_f=FRP modulus; σ_f=FRP tensile strength.

The comparison of load-deflection relationships obtained using the M/θ approach, using the analytical model and from experimental result is shown in Figure 7.2. A summary of the results is also given in Table 7.6

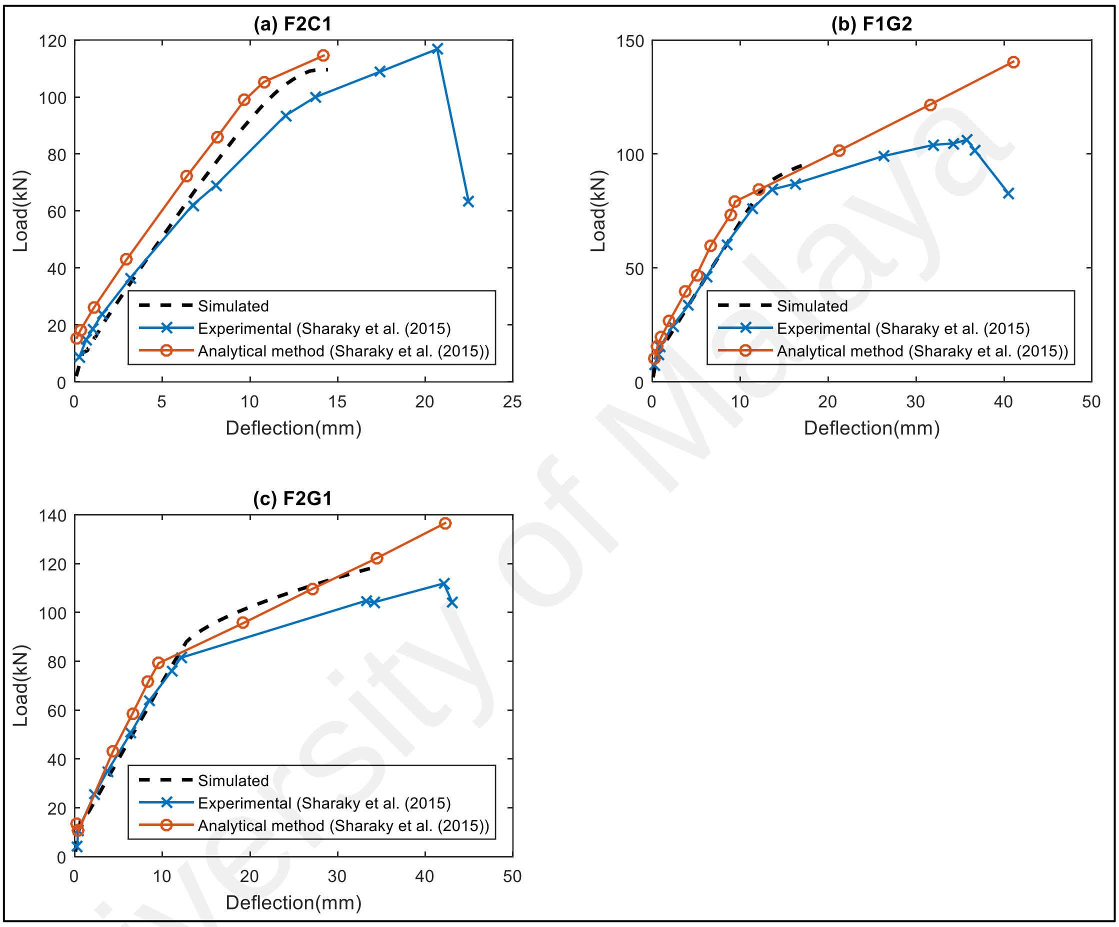

Figure 7.2 Comparison of load-deflection relationship from M/θ simulation, simulation by Sharaky et al. (2015) and experimental result.

Table 7.6 Summary of simulated and experimental load-deflection curves.

Beam	P_e	P_1	ΔP_1 (%)	P_2	ΔP_2 (%)	D_e	D_1	ΔD_1 (%)	D_2	ΔD_2 (%)	FM	SFM1	SFM2
F2C1	116.8	109.6	-6.2	114.5	-1.9	20.7	14.5	-30.1	14.2	-31.3	CCS	CCS	
F1G2	106.2	96.0	-9.6	140.5	32.3	35.8	17.9	-49.9	41.0	14.7	CS	F	
F2G1	111.8	118.6	6.0	136.5	22.1	42.1	34.7	-17.7	42.3	0.4	ID	CCS	

Note: P_e=experimental failure load; P_1=simulated failure load using M/θ approach; ΔP_1=percentage difference between simulated failure load using M/θ approach and the experimental failure load; P_2=simulated failure load using analytical model; ΔP_2=percentage difference between simulated failure load using analytical model and the experimental failure load; D_e= experimental deflection at failure; D_1= simulated deflection at failure using M/θ approach; ΔD_1=percentage difference between simulated deflection at failure using M/θ approach and the experimental failure load; D_2= simulated deflection at failure using analytical model; ΔD_2=percentage difference between simulated deflection at failure using analytical model and the experimental failure load; FM=failure mode; CCS=concrete cover separation; ID=interfacial debonding; F=fracture of NSM reinforcement; CS=concrete splitting, SFM1=simulated failure load using M/θ approach; SFM2=simulated failure load using analytical model.

Beam F2C1 was reported to fail by concrete cover separation. Both the M/θ approach and the analytical model were able to simulate this failure correctly, with the deviation of simulated and experimental failure load at -6.2% and -1.9% for the M/θ approach and the analytical model respectively. However both methods show high deviation for the deflection at failure, with -30.1% and -31.3% for the M/θ approach and the analytical model respectively. From Figure 7.2(a), it can be seen that the flexural stiffness of both M/θ approach and analytical model are identical and higher than the flexural stiffness shown in the experimental result. Hence the error can be attributed to the possibility that the elastic modulus of the CFRP bar used in the experimental test was actually lower than what was reported by Sharaky et al. (2015). This error is common in experimental tests.

For beam F1G2, the simulated load-deflection curve using the M/θ approach was found to be more accurate at simulating the tension stiffening effect, whereas the analytical model overpredicts the tension stiffening effect. However, the M/θ approach had a very high deviation for deflection at failure at -49.9%. The deviation for failure load on the other hand was only -9.6%. That, combined with the fact the prior to steel yielding the accuracy was very high, leads to the error being attributed to the wrong material property being used, where that the strain hardening modulus used in the simulation was higher than the actual strain hardening modulus of the steel reinforcement. This caused a higher load response for a given deflection for the load-deflection relationship past the steel yielding, leading to failure by fracture of GFRP bar to occurr at a lower deflection than it should. The M/θ approach also failed to simulate the concrete splitting failure, although this should be expected as it is not capable of simulating that failure type. The analytical model was able to predict the concrete splitting failure, but is highly inaccurate as the deviation between simulated and experimental failure load and deflection at failure was 32.3% and 14.7% respectively.

The M/θ approach was found to simulate the tension stiffening of beam F2G1 accurately, whereas the analytical method overpredicts it slightly. However, both methods overpredicts the load response after steel reinforcement had yielded, which again is attributed to the strain hardening modulus used for the steel reinforcement as being higher than the actual value in the experimental test. The deviation of simulated and experimental failure load for the M/θ approach and analytical model to be 6% and 22.1% respectively. Despite the good accuracy of the M/θ approach, it should be noted that it cannot predict the interfacial debonding failure that occurred on the beam. The analytical model was able to simulate that failure mode, however as can be seen its accuracy is low. Despite that, the analytical model managed to get a good accuracy in terms of deflection at failure, with deviation between simulated and experimental value at 0.4%. On the other hand the M/θ approach had a deviation of -17.7% for the simulated and experimental deflection at failure, which can be attributed to the incorrect value of strain hardening modulus as mentioned previously, which causes a higher load response for a given deflection, hence causing failure to be simulated at a much lower deflection than it should.

7.1.3 Comparison with FEM and IC debonding (Chen et al. (2011)) for EB strengthened beams

In this section, the simulation using M/θ approach as presented in paper 5 of this thesis will be compared with the simulation by Chen et al. (2011), where finite element modelling (FEM) was used to simulate IC debonding of FRP plated RC beams. This comparison study will be done using experimental results of EB FRP strengthened beams as there are very few experimental results for hybrid strengthened beam available in the literature.

The smeared crack approach was used by Chen et al. (2011) for the FEM, where cracked concrete is treated as a continuum and the deterioration of concrete is captured using a constitutive relationship, hence smearing crack over the continuum. The plane stress element CPS4 in ABAQUS was used to model the concrete while the steel and FRP were modelled using truss elements. The bonds between steel-concrete and FRP-concrete interfaces were modelled using the interfacial element COH2D4 in ABAQUS. The bond stress-slip curve for the EB FRP was assumed to unload linearly through the origin to simulate the softening related to IC debonding. It was also assumed that FRP-concrete bond in normal and shear directions were insignificant, thus only bond parallel to the FRP-concrete interface was considered.

The experimental results of EB FRP strengthened RC beams from Matthys (2000) and Brena, Bramblett, Wood, & Kreger (2003) will be used. Two of the beams were strengthened using FRP plates while another two uses FRP sheets. The geometry and material properties of the beam are given in Table 7.7 and Table 7.8 respectively. The comparison of load-deflection relationships obtained using the M/θ approach, using the FEM and from experimental result is shown in Figure 7.3. A summary of the results is also given in Table 7.9

Table 7.7 Beam geometric properties.

Ref	Beam designation	b (mm)	d (mm)	L (mm)	L_a (mm)	M_{NSM}	N_{NSM}	FM
Brena et al. (2003)	D2	203	406	3000	128	FRP plate	1	IC
Brena et al. (2003)	C2	203	406	3000	128	FRP sheet	2	IC
Matthys (2000)	BF8	200	2400	3000	70	FRP plate	1	IC
Matthys (2000)	BF9	200	2400	3000	70	FRP sheet	2	IC

Note: b=width of beam; d=depth of beam; L=length of beam; L_a=distance of NSM to the nearest support; M_{NSM}=type of FRP material; N_{NSM}=number of FRP sheet/plate; FM=failure mode; IC=intermediate crack debonding; CC= concrete crushing.

Table 7.8 Beam material properties.

Ref	Beam designation	f_c (N/mm^2)	E_y (N/mm^2)	σ_y (N/mm^2)	E_f (N/mm^2)	σ_f (N/mm^2)
Brena et al. (2003)	D2	35.1	200000	440	155000	2400
Brena et al. (2003)	C2	35.1	200000	440	62000	760
Matthys (2000)	BF8	39.4	200000	590	159000	3200
Matthys (2000)	BF9	33.7	200000	590	233000	3500

Note: f_c=concrete compressive strength (cylinder); E_y=steel elastic modulus; σ_y=steel yield strength; E_f=FRP modulus; σ_f=FRP tensile strength.

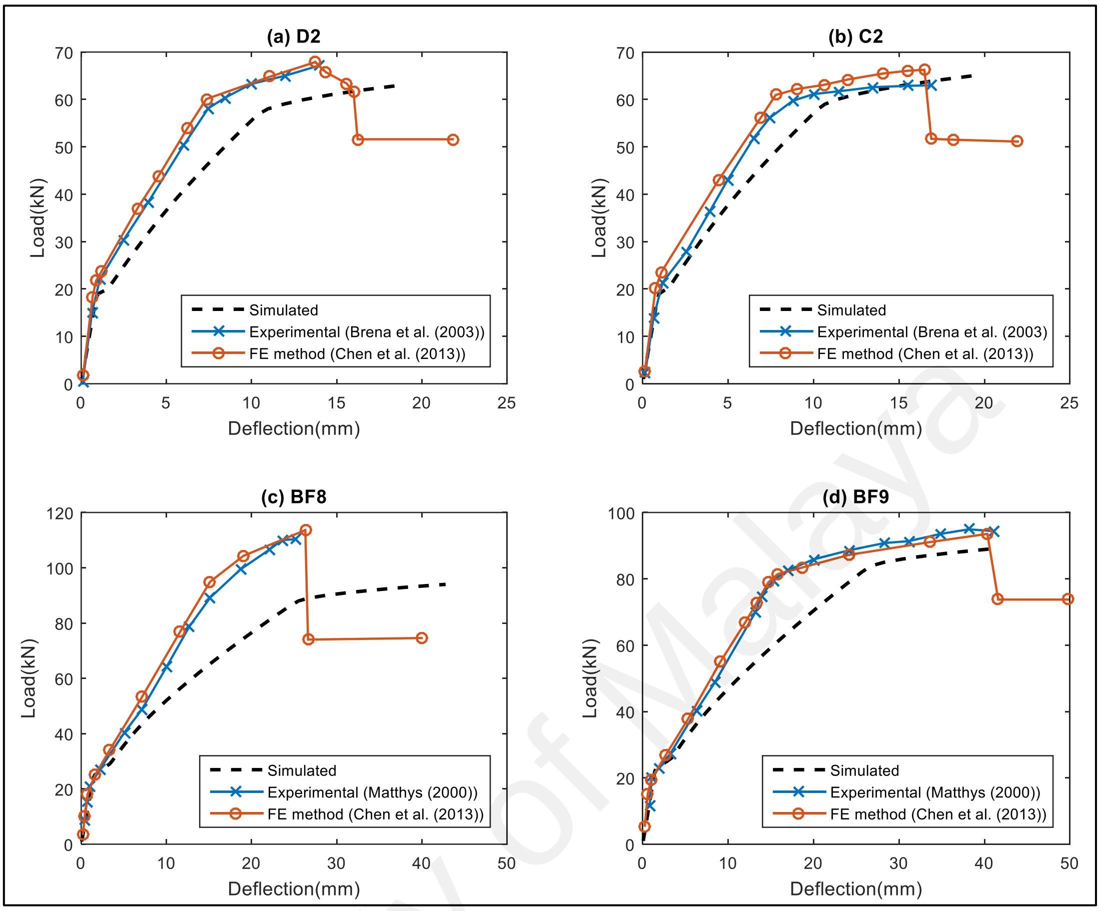

Figure 7.3 Comparison of load-deflection relationship from M/θ simulation, simulation by Chen et al. (2011) and experimental result.

Table 7.9 Summary of simulated and experimental load-deflection curves.

Beam	P_e	P_1	ΔP_1 (%)	P_2	ΔP_2 (%)	D_e	D_1	ΔD_1 (%)	D_2	ΔD_2 (%)	FM	SFM1	SFM2
D2	67.1	63	-6.1	67.9	1.1	13.9	18.75146	34.6	13.8	-1.3	IC	IC	IC
C2	63	65	3.2	66.2	5.2	16.9	19.32784	14.6	16.5	-2.3	IC	IC	IC
BF8	110.3	94	-14.8	113.6	3.0	25.2	42.77392	69.6	26.3	4.3	IC	IC	IC
BF9	94.4	89	-5.7	93.6	-0.9	41.2	40.60253	-1.3	40.3	-2.0	IC	IC	IC

Note: P_e=experimental failure load; P_1=simulated failure load using M/θ approach; ΔP_1=percentage difference between simulated failure load using M/θ approach and the experimental failure load; P_2=simulated failure load using finite element; ΔP_2=percentage difference between simulated failure load using analytical model and the experimental failure load; D_e= experimental deflection at failure; D_1= simulated deflection at failure using M/θ approach; ΔD_1=percentage difference between simulated deflection at failure using M/θ approach and the experimental failure load; D_2= simulated deflection at failure using analytical model; ΔD_2=percentage difference between simulated deflection at failure using analytical model and the experimental failure load; FM=failure mode; IC=intermediate crack debonding; CC= concrete crushing; SFM1=simulated failure load using M/θ approach; SFM2=simulated failure load using analytical model.

From Figure 7.3, the FEM simulation was much more accurate than the simulation with M/θ approach. The M/θ approach for EB strengthened beam used single crack analysis presented by Oehlers et al. (2015) in order to simulate IC debonding, which as shown in paper 5 is less accurate in simulating the tension stiffening of RC beams compared to the multiple crack analysis. It was found that the M/θ approach simulation for beams D2 and BF8, which were strengthened with EB FRP plates, were a lot worse in terms of tension stiffening accuracy than the simulation for beams C2 and BF9, which were strengthened with EB FRP sheets. However, all the simulated results using M/θ approach was able to predict the failure load relatively well, which shows that despite the inaccuracy in tension stiffening caused by the single crack analysis, it still manages to simulate the IC debonding failure correctly.

The lowest accuracy for the M/θ approach in terms of failure load was observed for beam BF8 which was strengthened with EB FRP plate; the deviation between simulated and experimental failure load was -14.8%. It can be concluded that more research is needed in order to improve the accuracy of the IC debonding failure for EB strengthened beams.

7.2 Limitations and errors

This section will list the limitations of the current M/θ approach:

1. The accuracy of the M/θ approach is dependent on the accuracy of the bond stress-slip model used. Assuming a beam uses a novel type of reinforcement, the bond properties of that reinforcement would need to be studied first before the M/θ approach can be used to simulate its behaviour. Incorrect bond stress-slip properties can have an impact on the accuracy of the M/θ approach, as shown in the comparison study in section 7.1.1 where the lack of appropriate bond stress-slip model for NSM steel bars caused a drop in terms of accuracy.

2. Errors due to incorrect values of material property values can be magnified in the M/θ approach, as demonstrated in section 7.1.2 where an incorrect strain hardening modulus greatly reduces the accuracy of the simulated deflection at failure.
3. In terms of accuracy, it was found that finite element modelling can currently simulate the load-deflection behaviour of NSM strengthened beams better than M/θ approach, although this thesis did not do a comprehensive comparison between the two. Furthermore, the finite element model used in the comparison study of this thesis did not include the simulation of concrete cover separation. On the other hand, the comparison between the M/θ approach and an analytical model show that the M/θ approach can give better accuracy.
4. The comparison study using EB strengthened beams show that the accuracy of IC debonding simulation is low for beams strengthened with EB FRP sheets and extremely low for beams strengthened with FRP plates. This is due to the use of single crack analysis instead of multiple crack analysis, although the predicted failure loads were reasonably accurate due to the single crack analysis' ability to capture IC debonding failure.
5. The M/θ approach used in this thesis only considers the primary crack, while secondary and tertiary cracks are ignored for simplicity.
6. The M/θ approach requires the bond stress-slip relationship for a reinforcement type to be studied first before it can be reliably used.
7. Currently the M/θ approach presented in this thesis have only been validated against a small number of specimens.

There are also some errors in the research papers, which were not detected prior to publication. The errors are as shown below:

1. In paper 1 page 5, the equation $B(i) = T(i)L_{per}$ should have been $B(i) = T(i)L_{per}L_s$.
2. In paper 2 page 620, the k_e is the stiffness for the elasto-cracked state of the beam rather than the elastic state.
3. In paper 2 page 623, the symbols s and s_m should have been δ and δ_{max}.
4. In paper 2, Dinolite digital microscope was used to measure the crack width with accuracy up to 0.001mm.
5. In paper 5, Table 5, the P_{serv}=service load (60% of the yield load).
6. In paper 5, the results in Figure 10 contain errors possibly caused by incorrect strain gauge readings and should thus be disregarded.
7. In paper 6, Barros et al. (2017) presented a strengthening technique that combines NSM and ETS methods with a new type of CFRP reinforcement rather than EB strengthening.

7.3 Concluding remarks

This section will attempt to summarize the cumulative effect of the research papers, the significance of the findings and the knowledge claim in the thesis.

This research extends the M/θ approach to allow for analysis and simulation of NSM-based strengthening methods. Unlike the moment-curvature approach, the M/θ approach does not use the linear strain profile, although it is still subject to the Euler-Bernoulli theorem of plane sections remaining plane. The M/θ approach applies the partial interaction theory to simulate the slip of reinforcements, which in turn allows the mechanics of tensile cracking, crack widening and tension stiffening to be simulated. Hence, the M/θ approach obviates the need for empiricisms in simulating the mechanics of RC beams, making it generic and unbound by testing regimes of empirical derivations. The extension of M/θ approach presented in this thesis allows for a more direct simulation of NSM-based strengthened RC beams, which can promote further research and better design guidelines by removing the need for costly and time-consuming structural tests for both existing and novel NSM-based strengthening methods.

With regard to the extension that this research brings to the existing knowledge on M/θ approach, the research shows how a strong bond strengthening method such as the NSM method can be simulated by considering the size of tension stiffening prisms. This research also shows how the concrete cover separation can be simulated by incorporating the use of the global energy balance approach (GEBA), which again involves an understanding of how the debonding process changes the tension stiffening analysis.

This research also show examples on how the extended M/θ approach can be applied as a research tool for NSM-based strengthening methods. Additionally, the studies on NSM-based methods serves as further validation on the accuracy and versatility of the extended M/θ approach, where derivatives of the NSM method can be simulated with minimal new considerations needed.

The example applications of the M/θ approach on NSM-based methods themselves have significant research values. The example application on side-NSM (SNSM) method presents a study on parameters that affect concrete cover separation in SNSM strengthened beams. The study also presents the difference in behaviour in SNSM strengthened virgin beams and SNSM retrofitted beams, the latter which has tensile cracks already on the beam prior to being strengthened, thus being more representative of real world situation where RC beams are likely to have tensile cracks due to service load. These studies are novel and has never been done previously. The second example application presented in this thesis is the study on hybrid strengthened RC beams. The research shows how the extended M/θ approach can also be used to simulate IC debonding if the situation requires it. The research presents a parametric study on IC debonding of hybrid strengthened beams.

The design procedure (which is based on the extended M/θ approach) proposed in this thesis can be used by design engineers to design NSM strengthened beams that is safe from concrete cover separation failures. Despite all this however, the M/θ approach have some limitations which were determined from comparison studies performed against other simulation method. The limitations are as presented in section 7.2.

CHAPTER 8 - CONCLUSION

Based on the study conducted in this thesis, the following conclusions can be made:

- The moment-rotation (M/θ) approach and the global energy balance approach (GEBA) were combined to allow the simulation of the behaviour and concrete cover separation failure of NSM strengthened beams. The proposed method is more versatile compared to existing methods as it requires significantly less empirical formulations when simulating NSM strengthened RC beams as the mechanics of the beam such as crack formation, crack widening and tension stiffening are simulated directly. The proposed method was validated against published experimental results. Comparison between simulated and experimental load-deflection curves shows that the method is able to give good accuracy.
- The M/θ-GEBA method was applied on SNSM strengthened beams, where it was shown that the method is also applicable to SNSM method with some minor changes. A parametric study was then conducted, where the differences between virgin and retrofitted SNSM strengthened beams were studied, the former which represents beams tested in labs and the latter representing beams in real world situations. Among the conclusion of the parametric study are:
  - SNSM retrofitted strengthened beams was found to have approximately 3 – 4% lower failure load compared to virgin SNSM strengthened beams when concrete cover separation is a factor.
  - In cases where concrete cover separation failure did not occur or less pronounced, the failure load was found higher in SNSM retrofitted beams by up to 1% due to approximately 15 – 19% higher flexural stiffness of

retrofitted beams than virgin beams due to longer crack spacing of the retrofitted beams.

  - There is only a slight difference in failure load of SNSM retrofitted beams compared to virgin SNSM strengthened beams, although the small difference is negligible.
  - There is a considerable difference in the flexural stiffness of virgin and retrofitted beams that should not be neglected.
  - It was found that retrofitted and virgin beam conditions do not affect the failure mode of the SNSM strengthened beams.

- The extended M/θ approach was applied in the simulation and parametric study of hybrid strengthened beams, where NSM strengthening are used in conjunction with EB strengthening. It was also shown how the IC debonding, which has been noted to occur on NSM strengthened beams albeit rarely, can be simulated using the single crack analysis method. A parametric study was then conducted on hybrid strengthening method with the following conclusions made:
  - Increasing the elastic modulus of NSM FRP bar increases the rigidity and maximum load of the hybrid strengthened beam while decreasing the length of IC debonding.
  - Increasing the elastic modulus of FRP sheet on the other hand increases the length of IC debonding; as such while the rigidity and maximum load of the hybrid strengthened beam still increase, the amount is less significant compared to increasing the elastic modulus of NSM FRP bar.
  - Increasing the bond strength of NSM FRP bar and FRP sheet slightly increases the rigidity and maximum load of hybrid strengthened beams.
- A design procedure for NSM strengthened beams was also introduced, which was made using closed form solutions derived using the M/θ-GEBA method.

- The coefficient of bond, c_2 for NSM CFRP strips and NSM CFRP bars with ratio of groove to bar diameter of 2 or 1.5 were determined by performing a parametric study using numerical partial interaction tension stiffening analysis.
- Published experimental results of beams strengthened with either NSM CFRP bars, NSM CFRP strips or SNSM CFRP bars were used to validate the proposed design procedure and good correlation was found between the experimental and predicted results.
- As the proposed design procedure is less reliant on empirical formulations, it should be applicable to other types of NSM reinforcement material and configuration as well, with the coefficient of bond c_2 determined using a similar approach used in this paper.

- For future research work, it is proposed that:
  - The M/θ approach should be used to perform simulation on NSM strengthened beams using novel strengthening materials such as basalt FRP.
  - The bond stress-slip of NSM steel should be studied and proper bond stress-slip models should be proposed for it.
  - Further research on SNSM strengthening method be done to determine its performance under fatigue and cyclic loading.
  - Methods to reduce IC debonding for the hybrid strengthening method should be explored.
  - A study should be done to improve the accuracy of EB strengthened beams using the M/θ approach.

REFERENCES

Achintha, M., & Burgoyne, C. (2013). Fracture energy of the concrete-FRP interface in strengthened beams. *Engineering Fracture Mechanics*, *110*, 38–51.

Achintha, M., & Burgoyne, C. J. (2011). Fracture mechanics of plate debonding: Validation against experiment. *Construction and Building Materials*, *25*, 2961–2971.

Achintha, P., & Burgoyne, C. (2009). Moment-curvature and strain energy of beams with external fiber-reinforced polymer reinforcement. *ACI Structural Journal*, *106*, 21–29.

Achintha, P., & Burgoyne, C. J. (2008). Fracture Mechanics of Plate Debonding : Experimental. *Journal of Composites for Construction*, *12*, 396–404.

Achintha, P. M. M. (2009). *Fracture analysis of debonding mechanism for FRP plates*. University of Cambridge. Retrieved from http://eprints.soton.ac.uk/209479/

Al-Mahmoud, F., Castel, A., François, R., & Tourneur, C. (2010). RC beams strengthened with NSM CFRP rods and modeling of peeling-off failure. *Composite Structures*, *92*, 1920–1930.

Al-Sulaimani, G. J., Kaleemullah, M., & Basunbul, I. A. (1990). Influence of corrosion and cracking on bond behavior and strength of reinforced concrete members. *Structural Journal*, *87*, 220–231.

Almusallam, A. A., Al-Gahtani, A. S., & Aziz, A. R. (1996). Effect of reinforcement corrosion on bond strength. *Construction and Building Materials*, *10*, 123–129.

Almusallam, T. H., Elsanadedy, H. M., Al-Salloum, Y. a., & Alsayed, S. H. (2013). Experimental and numerical investigation for the flexural strengthening of RC beams using near-surface mounted steel or GFRP bars. *Construction and Building Materials*, *40*, 145–161.

Aydin, H., Gravina, R. J., & Visintin, P. (2018). A partial-interaction approach for extracting FRP-to-concrete bond characteristics from environmentally loaded flexural tests. *Composites Part B: Engineering*, *132*, 214–228.

Badawi, M., & Soudki, K. (2009). Flexural strengthening of RC beams with prestressed NSM CFRP rods - Experimental and analytical investigation. *Construction and Building Materials*, *23*, 3292–3300.

Barros, J.A.O., & Fortes, A. S. (2005). Flexural strengthening of concrete beams with CFRP laminates bonded into slits. *Cement and Concrete Composites*, *27*, 471–480.

Barros, J.A.O., Rezazadeh, M., Laranjeira, J. P. S., Hosseini, M. R. M., Mastali, M., & Ramezansefat, H. (2017). Simultaneous flexural and punching strengthening of RC slabs according to a new hybrid technique using U-shape CFRP laminates. *Composite Structures*, *159*, 600–614.

Barros, Joaquim A O, Dias, S. J. E., & Lima, J. L. T. (2007). Efficacy of CFRP-based techniques for the flexural and shear strengthening of concrete beams. *Cement and Concrete Composites*, *29*, 203–217.

Branson, D. E. (1968). Design procedures for computing deflections. *ACI Journal*, *65*, 730–735.

Brena, S. F., Bramblett, R. M., Wood, S. L., & Kreger, M. E. (2003). Increasing flexural capacity of reinforced concrete beams using carbon fiber-reinforced polymer composites. *Structural Journal*, *100*, 36–46.

Capozucca, R., Domizi, J., & Magagnini, E. (2016). Damaged RC beams strengthened with NSM CFRP rectangular rods under vibration in different constrain conditions. *Composite Structures*, *154*, 660–683.

Capozucca, R., & Magagnini, E. (2016). Vibration of RC beams with NSM CFRP with unbonded/notched circular rod damage. *Composite Structures*, *144*, 108–130.

CEB-FIP. (1993). *CEB-FIP model code 1990: Design code*. Thomas Telford.

Ceroni, F. (2010). Experimental performances of RC beams strengthened with FRP materials. *Construction and Building Materials*, *24*, 1547–1559.

Ceroni, Francesca, Pecce, M., Matthys, S., & Taerwe, L. (2008). Debonding strength and anchorage devices for reinforced concrete elements strengthened with FRP sheets. *Composites Part B: Engineering*, *39*, 429–441.

Chahrour, A., & Soudki, K. (2005). Flexural response of reinforced concrete beams strengthened with end-anchored partially bonded carbon fiber-reinforced polymer strips. *Journal of Composites for Construction*, *9*, 170–177.

Chen, G. M., Teng, J. G., & Chen, J. F. (2010). Finite-Element Modeling of Intermediate Crack Debonding in FRP-Plated RC Beams. *Journal of Composites for Construction*, *15*, 339–353.

Chen, G. M., Zhang, Z., Li, Y. L., Li, X. Q., & Zhou, C. Y. (2016). T-section RC beams shear-strengthened with anchored CFRP U-strips. *Composite Structures*, *144*, 57–79.

Chen, Y., Visintin, P., Oehlers, D., & Alengaram, U. J. (2014). Size-Dependent Stress-Strain Model for Unconfined Concrete. *Journal of Structural Engineering*, *140*, 04013088.

Choi, H. T., West, J. S., & Soudki, K. a. (2011). Partially bonded near-surface-mounted CFRP bars for strengthened concrete T-beams. *Construction and Building Materials*, *25*, 2441–2449.

Cruz, J. S., & Barros, J. (2004). Modeling of bond between near-surface mounted CFRP laminate strips and concrete. *Computers & Structures*, *82*, 1513–1521.

De Lorenzis, Laura. (2004). Anchorage length of near-surface mounted fiber-reinforced polymer rods for concrete strengthening - Analytical modeling. *ACI Structural Journal*, *101*, 375–386.

De Lorenzis, Laura, Lundgren, K., & Rizzo, A. (2004). Anchorage Length of Near-Surface Mounted Fiber-Reinforced Polymer Bars for Concrete Strengthening - Experimental Investigation and Numerical Modeling. *ACI Structural Journal*, *101*, 269–278.

De Lorenzis, Laura, & Teng, J. G. (2007). Near-surface mounted FRP reinforcement: An emerging technique for strengthening structures. *Composites Part B: Engineering*, *38*, 119–143.

Guan, G. X., & Burgoyne, C. J. (2014). Comparison of Moment-Curvature Models for Fiber- Reinforced Polymer Plate-End Debonding Studies Using Global Energy Balance Approach. *ACI Structural Journal*, *111*, 27–36.

Haskett, M., Oehlers, D. J., & Mohamed Ali, M. S. (2008). Local and global bond characteristics of steel reinforcing bars. *Engineering Structures*, *30*, 376–383.

Haskett, M., Oehlers, D. J., Mohamed Ali, M. S., & Sharma, S. K. (2011). Evaluating the shear-friction resistance across sliding planes in concrete. *Engineering Structures*, *33*, 1357–1364.

Haskett, M., Oehlers, D. J., Visintin, P., & S, M. A. M. (2011). Using shear-friction properties to simulate concrete softening in reinforced concrete flexural members.

Hassan, T. K., & Rizkalla, S. H. (2004). Bond mechanism of near-surface-mounted fiber-reinforced polymer bars for flexural strengthening of concrete structures. *ACI Structural Journal*, *101*, 830–839.

Hassan, T., & Rizkalla, S. (2003). Investigation of Bond in Concrete Structures Strengthened with Near Surface Mounted Carbon Fiber Reinforced Polymer Strips. *Journal of Composites for Construction*, *7*, 248–257.

Hosen, M. A., Jumaat, M. Z., & Islam, a. B. M. S. (2015). Side Near Surface Mounted (SNSM) technique for flexural enhancement of RC beams. *Materials & Design*, *83*, 587–597.

Hosen, M. A., Jumaat, M. Z., Islam, A. B. M. S., Kamruzzaman, M., Huda, N., & Soeb, M. R. (2015). Eliminating concrete cover separation of NSM strengthened beam by CFRP end anchorage. *Structural Engineering and Mechanics*, *56*. doi:10.12989/sem.2015.56.6.899

Hughes, T. J. R., & Liu, W. K. (1981). Nonlinear finite element analysis of shells-part II. two-dimensional shells. *Computer Methods in Applied Mechanics and Engineering*, *27*, 167–181.

Hutchinson, J. W., & Suo, Z. (1991). Mixed mode cracking in layered materials. In *Advances in applied mechanics* (Vol. 29, pp. 63–191). Elsevier.

Jung, W., Park, Y., Park, J., Kang, J., & You, Y. (2005). Experimental investigation on flexural behavior of RC beams strengthened by NSM CFRP reinforcements. *ACI Special Publication*, 795–806.

Knight, D., Visintin, P., Oehlers, D. J., & Mohamed Ali, M. S. (2014a). Simulating RC beams with unbonded FRP and steel prestressing tendons. *Composites Part B: Engineering*, *60*, 392–399.

Knight, D., Visintin, P., Oehlers, D. J., & Mohamed Ali, M. S. (2014b). Simulation of RC beams with mechanically fastened FRP strips. *Composite Structures*, *114*, 99–106.

Kreit, A., Al-Mahmoud, F., Castel, A., & François, R. (2011). Repairing corroded RC beam with near-surface mounted CFRP rods. *Materials and Structures*, *44*, 1205–1217.

Lee, H. Y., Jung, W. T., & Chung, W. (2017). Flexural strengthening of reinforced concrete beams with pre-stressed near surface mounted CFRP systems. *Composite Structures*, *163*, 1–12.

Lorenzis, L De, & Nanni, A. (2002). Bond between near-surface mounted fiber-reinforced polymer rods and concrete in structural strengthening. *ACI Structural Journal*, *99*, 123–133.

Lorenzis, L De, & Nanni, A. (2003). Proposed design procedure of NSM FRP reinforcement for strengthening of RC beams. *Proceedings, 6th International Symposium on Frp Reinforcement for Concrete Structures, Singapore*, 1455–1.

Lu, X. Z., Teng, J. G., Ye, L. P., & Jiang, J. J. (2005). Bond-slip models for FRP sheets/plates bonded to concrete. *Engineering Structures*, *27*, 920–937.

Maalej, M. (2005). Analysis and design of FRP externally-reinforced concrete beams against debonding-type failures. *Materials and Structures*, *34*, 418–425.

Matthys, S. (2000). Structural behaviour and design of concrete members strengthened with externally bonded FRP reinforcement. Ghent University.

Mattock, A. H. (1974). Shear transfer in concrete having reinforcement at an angle to the shear plane. *Special Publication*, *42*, 17–42.

Mo, K. H., Visintin, P., Alengaram, U. J., & Jumaat, M. Z. (2016). Prediction of the structural behaviour of oil palm shell lightweight concrete beams. *Construction and Building Materials*, *102*, 722–732.

Monti, G., Renzelli, M., & Luciani, P. (2003). FRP adhesion in uncracked and cracked concrete zones. In *Proceedings of the Sixth International Symposium on FRP Reinforcement for Concrete Structures (FRPRCS-6)* (Vol. 1, pp. 183–192). World Scientific.

Muhamad, R., Mohamed Ali, M. S., Oehlers, D., & Hamid Sheikh, A. (2011). Load-slip relationship of tension reinforcement in reinforced concrete members. *Engineering Structures*, *33*, 1098–1106.

Muhamad, R., Mohamed Ali, M. S., Oehlers, D. J., & Griffith, M. (2012). The tension stiffening mechanism in reinforced concrete prisms. *Advances in Structural Engineering*, *15*, 2053–2069.

Nakaba, K., Kanakubo, T., Furuta, T., & Yoshizawa, H. (2001). Bond behavior between fiber-reinforced polymer laminates and concrete. *ACI Structural Journal*, *98*, 359–367.

Narayanamurthy, V., Chen, J. F., Cairns, J., & Oehlers, D. J. (2012). Plate end debonding in the constant bending moment zone of plated beams. *Composites Part B: Engineering*, *43*, 3361–3373.

Neubauer, U., & Rostasy, F. S. (1999). Bond failure of concrete fiber reinforced polymer plates at inclined cracks-experiments and fracture mechanics model. In *Fourth International Symposium on Fiber Reinforced Polymer Reinforcement for Reinforced Concrete Structures*.

Oehlers, D., Visintin, P., Zhang, T., Chen, Y., & Knight, D. (2012). Flexural rigidity of reinforced concrete members using a deformation based analysis. *Concrete in Australia*, *38*, 50–56.

Oehlers, Deric J., Visintin, P., Haskett, M., & Sebastian, W. M. (2013). Flexural ductility fundamental mechanisms governing all RC members in particular FRP RC. *Construction and Building Materials*, *49*, 985–997.

Oehlers, Deric J., Visintin, P., & Lucas, W. (2015). Flexural Strength and Ductility of FRP-Plated RC Beams: Fundamental Mechanics Incorporating Local and Global IC Debonding. *Journal of Composites for Construction*, *20*, 04015046.

Oehlers, Deric John. (1992). Reinforced concrete beams with plates glued to their soffits. *Journal of Structural Engineering*, *118*, 2023–2038.

Oehlers, Deric John, Mohamed Ali, M. S., Haskett, M., Lucas, W., Muhamad, R., & Visintin, P. (2011). FRP-Reinforced Concrete Beams: Unified Approach Based on IC Theory. *Journal of Composites for Construction*, *15*, 293–303.

Oehlers, Deric John, & Moran, J. P. (1990). Premature failure of externally plated reinforced concrete beams. *Journal of Structural Engineering*, *116*, 978–995.

Omran, H. Y., & El-Hacha, R. (2012). Nonlinear 3D finite element modeling of RC beams strengthened with prestressed NSM-CFRP strips. *Construction and Building Materials*, *31*, 74–85.

Oudah, F., & El-Hacha, R. (2012). Fatigue behavior of RC beams strengthened with prestressed NSM CFRP rods. *Composite Structures*, *94*, 1333–1342.

Pachalla, S. K. S., & Prakash, S. S. (2017). Efficient near surface mounting CFRP strengthening of pretensioned hollowcore slabs with opening – An experimental study. *Composite Structures*, *162*, 28–38.

Peng, H., Zhang, J., Cai, C. S., & Liu, Y. (2014). An experimental study on reinforced concrete beams strengthened with prestressed near surface mounted CFRP strips. *Engineering Structures*, *79*, 222–233.

Pesic, N. (2005). Flexural analysis and design of reinforced concrete beams with externally bonded FRP reinforcement. *Materials and Structures*, *38*, 183–192.

Popovics, S. (1973). A numerical approach to the complete stress-strain curve of concrete. *Cement and Concrete Research*, *3*, 583–599.

Quattlebaum, J. B., Harries, K. a., & Petrou, M. F. (2005). Comparison of Three Flexural Retrofit Systems under Monotonic and Fatigue Loads. *Journal of Bridge Engineering*, *10*, 731–740.

Rahman, M., Jumaat, M. Z., Rahman, M. A., & Qeshta, I. M. I. (2015). Innovative hybrid bonding method for strengthening reinforced concrete beam in flexure. *Construction and Building Materials*, *79*, 370–378.

Rasheed, H. a., Harrison, R. R., Peterman, R. J., & Alkhrdaji, T. (2010). Ductile strengthening using externally bonded and near surface mounted composite systems. *Composite Structures*, *92*, 2379–2390.

Reda, R. M., Sharaky, I. A., Ghanem, M., Seleem, M. H., & Sallam, H. E. M. (2016). Flexural behavior of RC beams strengthened by NSM GFRP Bars having different end conditions. *Composite Structures*, *147*, 131–142.

Rezazadeh, M., Barros, J. A. O., & Ramezansefat, H. (2016). End concrete cover separation in RC structures strengthened in flexure with NSM FRP: Analytical design approach. *Engineering Structures*, *128*, 415–427.

Ross, C. A., Jerome, D. M., Tedesco, J. W., & Hughes, M. L. (1999). Strengthening of reinforced concrete beams with externally bonded composite laminates. *Structural Journal*, *96*, 212–220.

Savoia, M., Ferracuti, B., & Mazzotti, C. (2003). Nonlinear bond-slip law for FRP-concrete interface. In *Proc. of 6th international symposium on FRP reinforcement for concrete structures. Singapore: World Scientific Publications* (pp. 163–172).

Seo, S., Sung, M., & Feo, L. (2016). Flexural analysis of RC beam strengthened by partially de-bonded NSM FRP strip. *Composites Part B*, *101*, 21–30.

Sharaky, I. A., Reda, R. M., Ghanem, M., Seleem, M. H., & Sallam, H. E. M. (2017). Experimental and numerical study of RC beams strengthened with bottom and side NSM GFRP bars having different end conditions. *Construction and Building Materials*, *149*, 882–903.

Sharaky, I. A., Torres, L., & Sallam, H. E. M. (2015). Experimental and analytical investigation into the flexural performance of RC beams with partially and fully bonded NSM FRP bars/strips. *Composite Structures*, *122*, 113–126.

Shukri, A. A., Darain, K. M. ud, & Jumaat, M. Z. (2015). The Tension-Stiffening Contribution of NSM CFRP to the Behavior of Strengthened RC Beams. *Materials*, *8*, 4131–4146.

Smith, S. ., & Teng, J. . (2002). FRP-strengthened RC beams. I: review of debonding strength models. *Engineering Structures*, *24*, 385–395.

Tam, B., Si, A., & Limam, A. (2016). Numerical modelling of reinforced concrete beams repaired by TRC composites. *Composite Structures*, *152*, 779–790.

Teng, J. G., Zhang, S. ., & Chen, J. F. (2016). Strength model for end cover separation failure in RC beams strengthened with near-surface mounted (NSM) FRP strips. *Engineering Structures*, *110*, 222–232.

Toutanji, H., Zhao, L., & Zhang, Y. (2006). Flexural behavior of reinforced concrete beams externally strengthened with CFRP sheets bonded with an inorganic matrix. *Engineering Structures*, *28*, 557–566.

Visintin, P., & Oehlers, D. J. (2016). Mechanics-based closed-form solutions for moment redistribution in RC beams. *Structural Concrete*, *17*, 377–389.

Visintin, P., Oehlers, D. J., Muhamad, R., & Wu, C. (2013). Partial-interaction short term serviceability deflection of RC beams. *Engineering Structures*, *56*, 993–1006.

Visintin, P., Oehlers, D. J., Wu, C., & Haskett, M. (2012). A mechanics solution for hinges in RC beams with multiple cracks. *Engineering Structures*, *36*, 61–69.

Walraven, J. C., & Reinhardt, H. W. (1981). Theory and experiments on the mechanical behaviour of cracks in plain and reinforced concrete subjected to shear loading. *Heron*, *26*.

Zaman, A., Gutub, S. A., & Wafa, M. A. (2013). A review on FRP composites applications and durability concerns in the construction sector. *Journal of Reinforced Plastics and Composites*, *32*, 1966–1988.

Zhang, S. S., & Teng, J. G. (2014). Finite element analysis of end cover separation in RC beams strengthened in flexure with FRP. *Engineering Structures*, *75*, 550–560.

Zhang, S. S., Teng, J. G., & Yu, T. (2013). Bond–slip model for CFRP strips near-surface mounted to concrete. *Engineering Structures*, *56*, 945–953.

Zhang, S. S., Yu, T., & Chen, G. M. (2017). Reinforced concrete beams strengthened in flexure with near-surface mounted (NSM) CFRP strips: Current status and research needs. *Composites Part B: Engineering*, *131*, 30–42.